Disclaimer

This course material may contain copyrighted material the use of which has not been specifically authorized or licensed by the copyright owner. This material is used here for teaching purposes constituting a fair use as provided by Swiss copyright law (URG Art. 19 Abs. 1 lit. B).

The content of this presentation is meant for use as part of the course «Thin Films and Small Scale Mechanics» offered at Empa Thun. It is intended solely for the use of the registered course participants. Distribution to individuals who are not registered course participants is prohibited. If you are not a registered course participant, you are hereby notified that any review, dissemination, distribution, duplication or other use is strictly forbidden.

Ch. 6: Small Scale Mechanical Testing

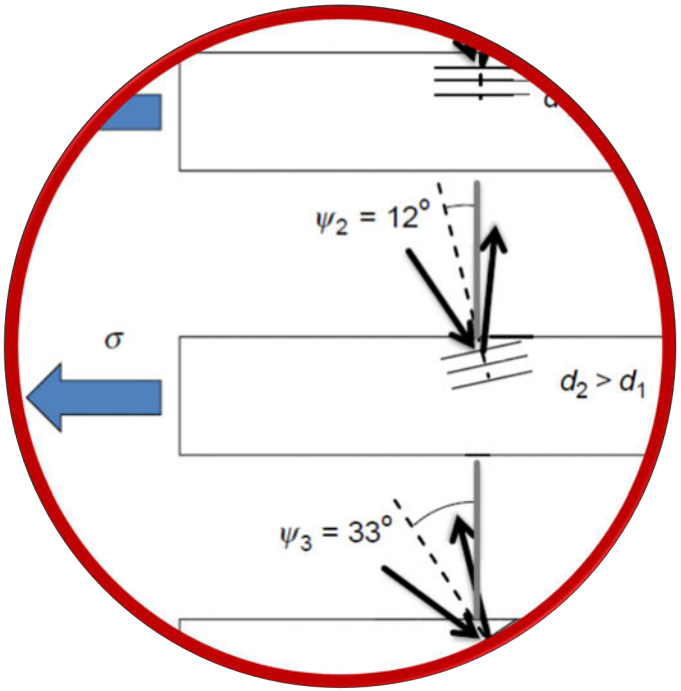

Sample fabrication techniques

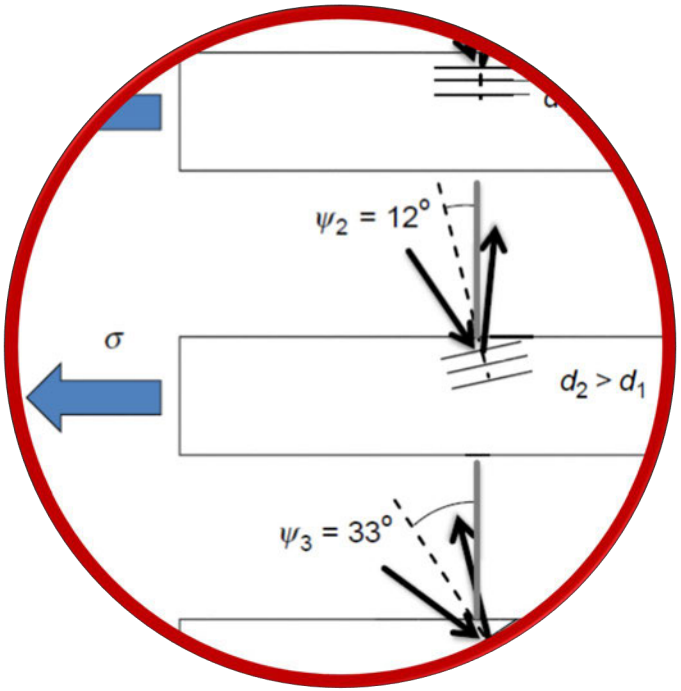

Focused ion beam

FIB applications examples

Micromechanical specimen fabrication

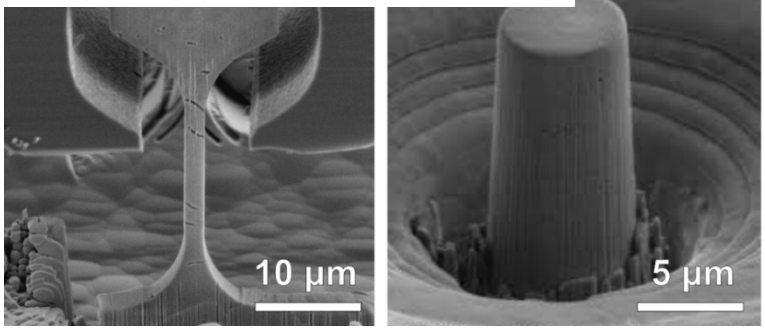

Casari et al., *Acta. Biomat.,* **120** (2021); Schwiedrzik et al., *Nat. Mat.,* **13** (2014)

FIB tomography + HR-EBSD

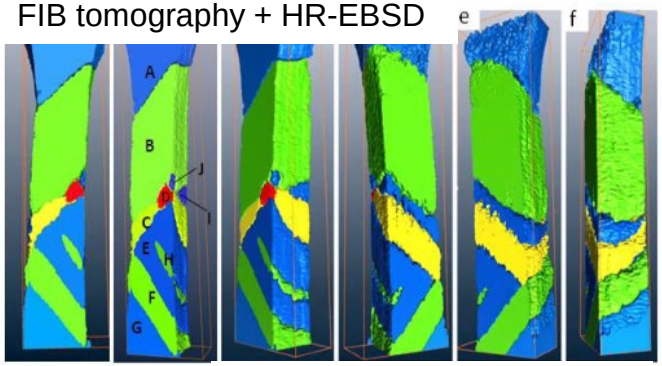

Della Ventura et al., *Mater. Des.,* **197** (2014)

3D nano structuring

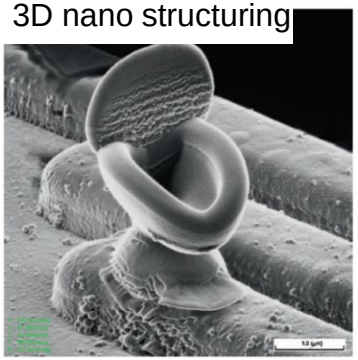

Image from Seiko instruments

TEM lamella preparation

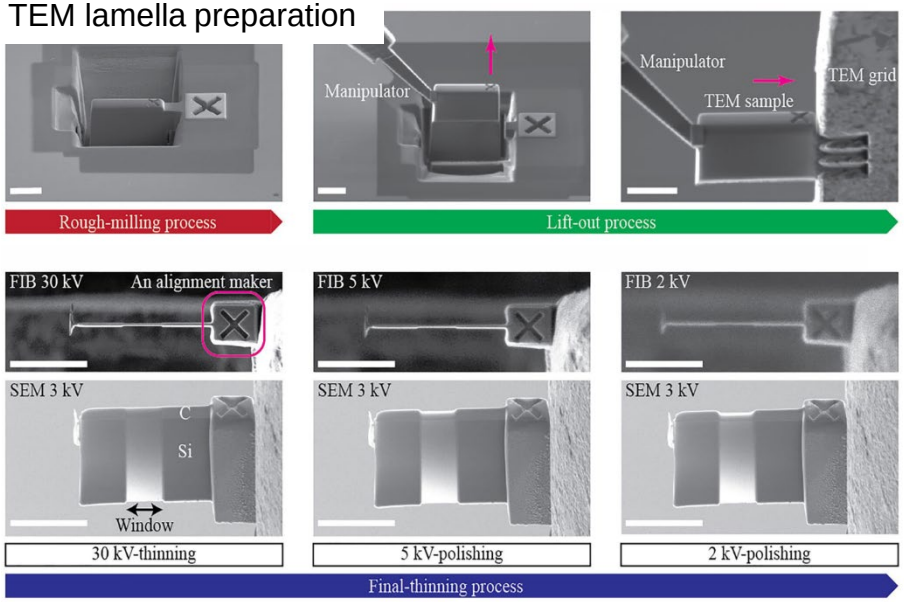

Tsurusawa et al., Sci. Rep., **11** (2014)

Ion channeling imaging

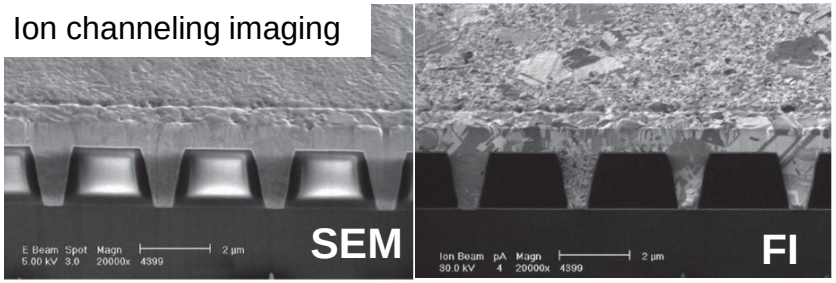

TOF-SIMS

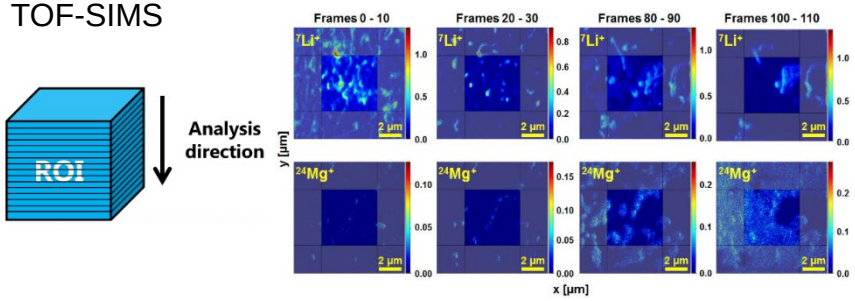

Priebe et al. EUFN Workshop poster (2018)

A quick overview on FIB

Schematic of a liquid-metal ion source (LMIS)

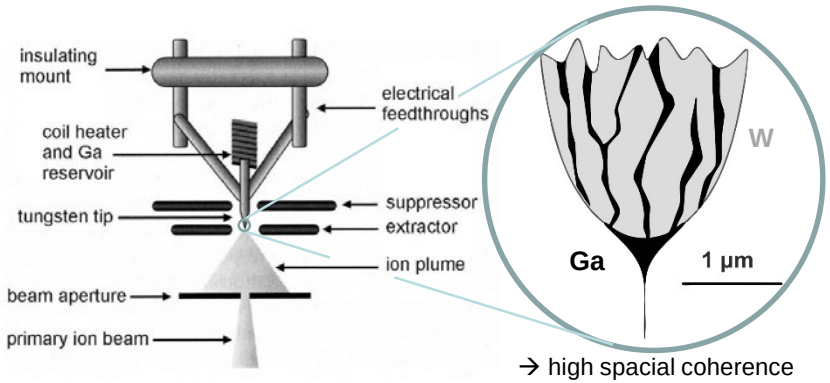

→ high spacial coherence

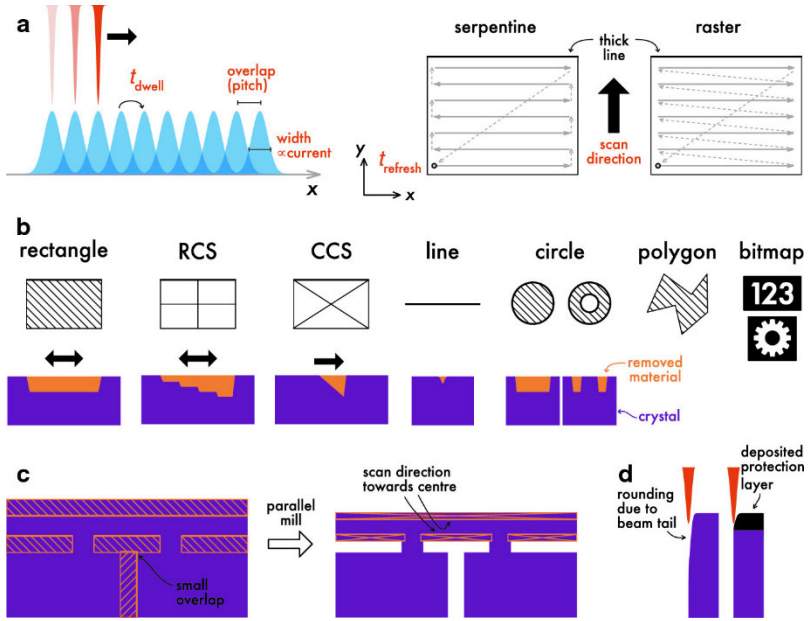

Standard milling

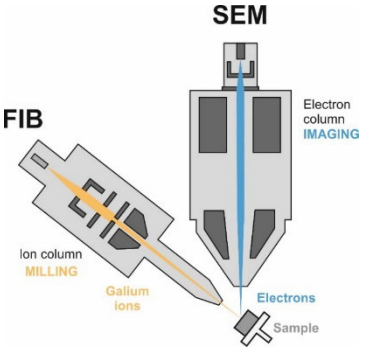

Gas induced deposition & etching

e.g. Pt, C, W

e.g. Cl_2, XeF_2

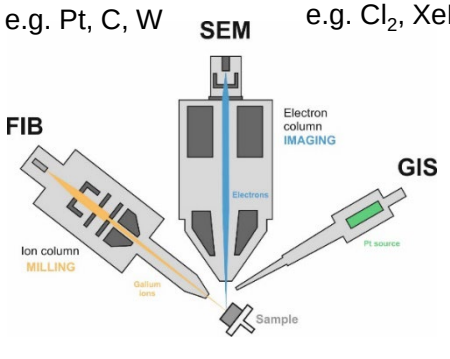

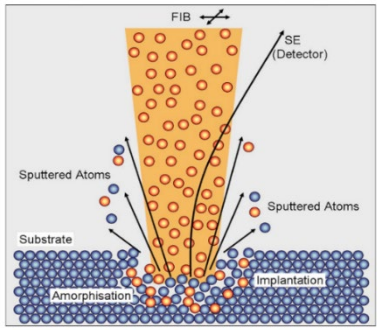

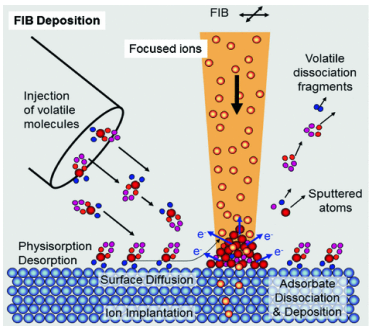

Utke et al., *J. Vac. Sci. Technol.* B 26 (2008)

Parameters we can control

- Dwell time
- Dose
- Spacing
- Beam irradiation path

Different FIB types and ion sources

Liquid metal ion source (LMIS)

- Typically Ga
- High stablility
- Alloy sources: Au, Bi, Si, ...
  Current range: 1 pA - 100 nA

Inductively coupled plasma (ICP)

- Typically Xe
- Current range: 100 pA – 1 µA

Gas field ionization source (GFIS)

- Typically He or Ne
- High spatial resolution (<0.35 nm)
- Imagin insulating samples
- Current range: 0.1 pA – 100 pA

Bassim et al., *MRS Bulletin* (2014)

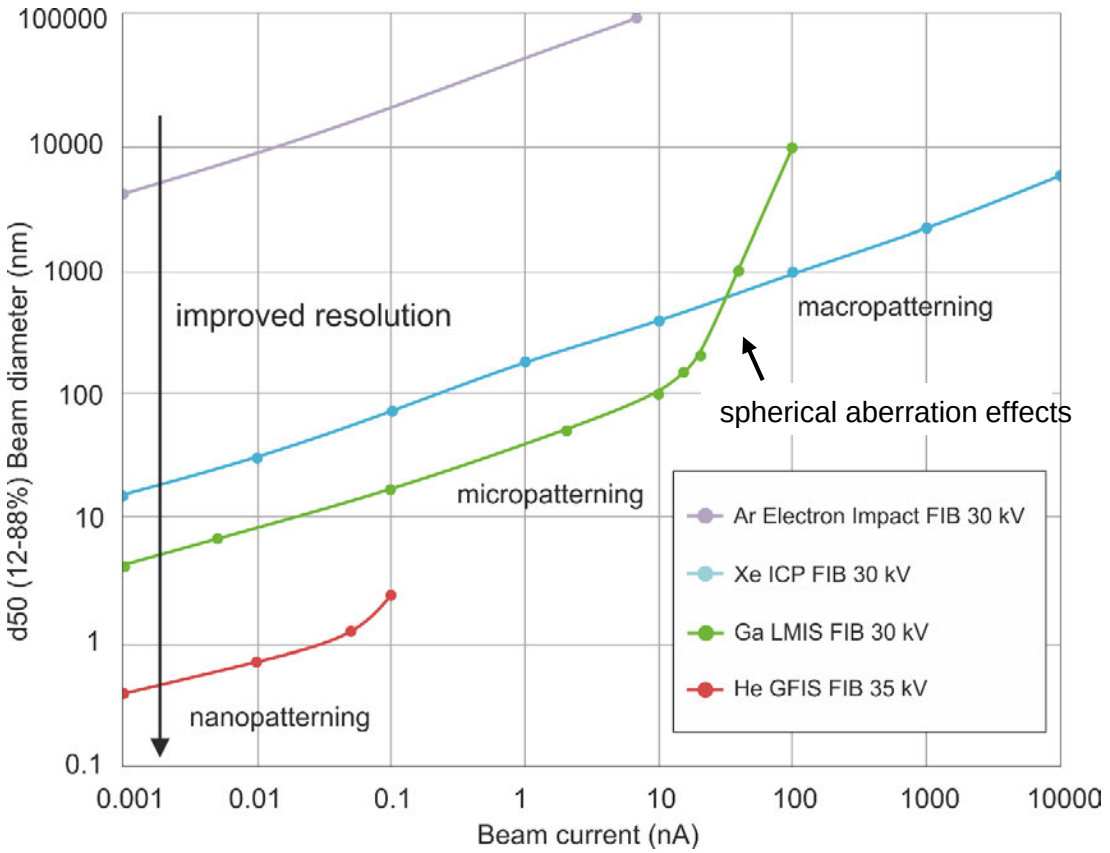

Collision cascade model

Ion-solid interaction

- Surface atoms can be ejected (sputtering /milling)
- Ca. 30 ps process
- Relaxation after first ca. 10 ps
- Implanted ions
- Amorphization
- Electrical damage zone
- 30 kV Ga+ on Si: ca. 30 nm
- Different possible sources: Ga, Xe, H, etc…

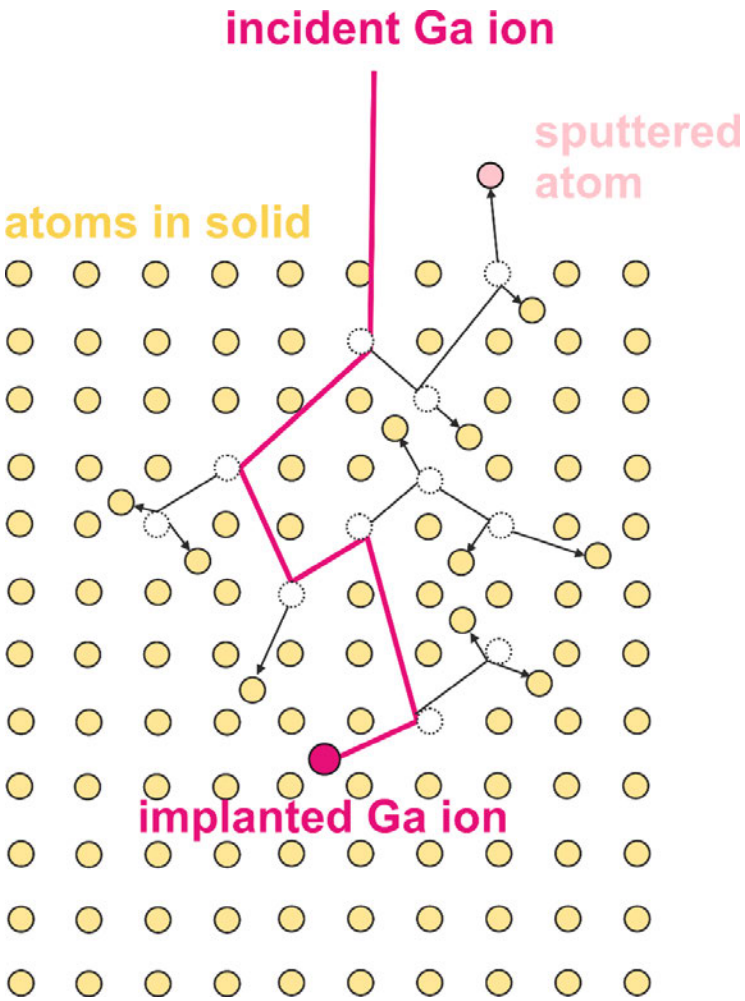

Milling at an edge

Edge effect

- **Increased sputter yield** (ca. 8x)
- Topographic effect (corner will mill even faster)
- Scan strategy matters
- Line-by-line milling is efficient
- Redeposition becomes significant

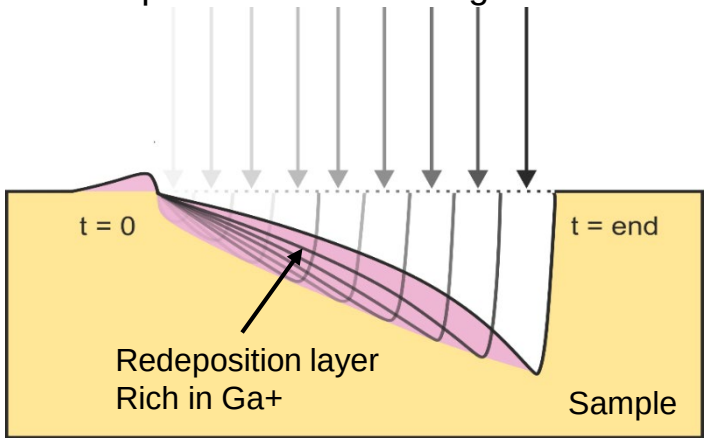

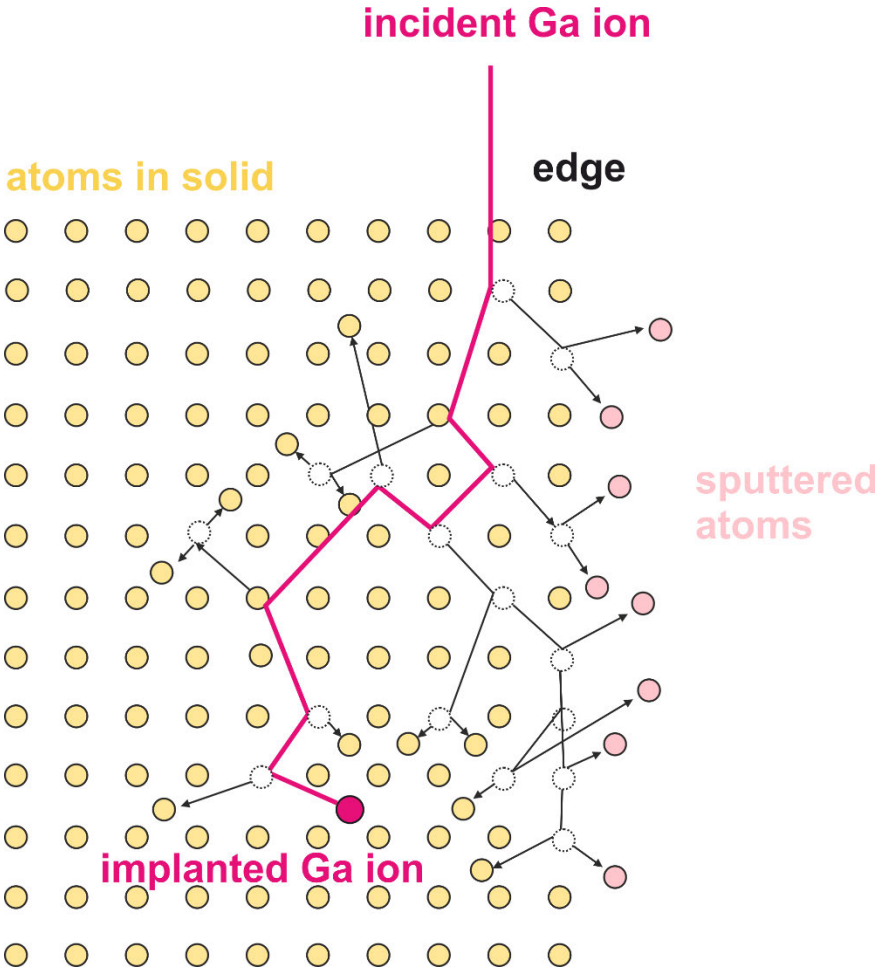

Tangential irradiation: increased sputtering rate

Sputter yield and sputter rate

Sputtering by 30 kV Ga^+ normal incidence

Element	Sputter yield* Y (-)	Sputter rate** S ($\mu m^3/nC$)
C	1.69	0.18
Al	3.47	0.29
Si	2.78	0.24
Ti	2.28	0.46
Cr	5.15	0.10
Au	15.75	1.50
W	7.59	0.12

Max efficiency for an incident angle of 75-80°

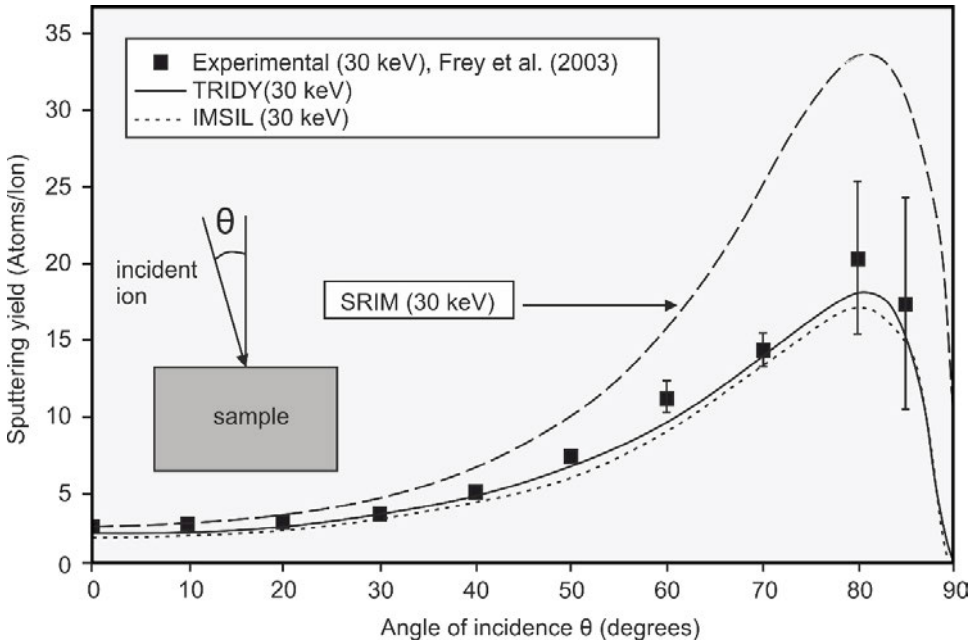

Sputtering yield *Y*: atoms sputtered per incoming ion

Sputtering rate *S*: volume removed per dose

* SRIM data from: , Lucille A. Giannuzzi and Fred A. Stevie, Introduction to focused ion beams, Springer, 2005.

** Ivo Utke, Stanislav Moshkalev, Phillipp Russell, Nanofabrication using focused ion and electron beams, Oxford University Press, 2012.

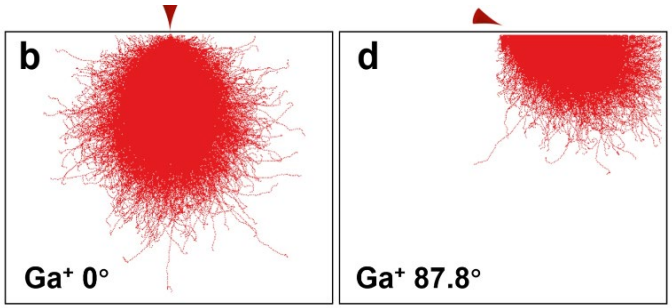

Liu et al., *Sci. Rep.*, **10** (2020)

Deposition induced by FIB

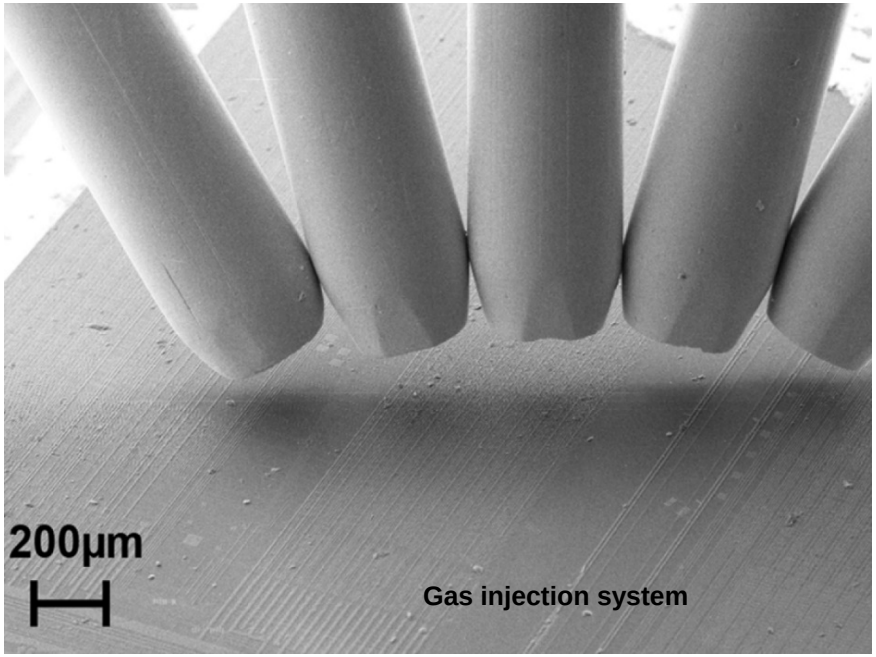

Deposited species is not pure: lots of Ga and C

Deposition without surface damage only by eBeam dep

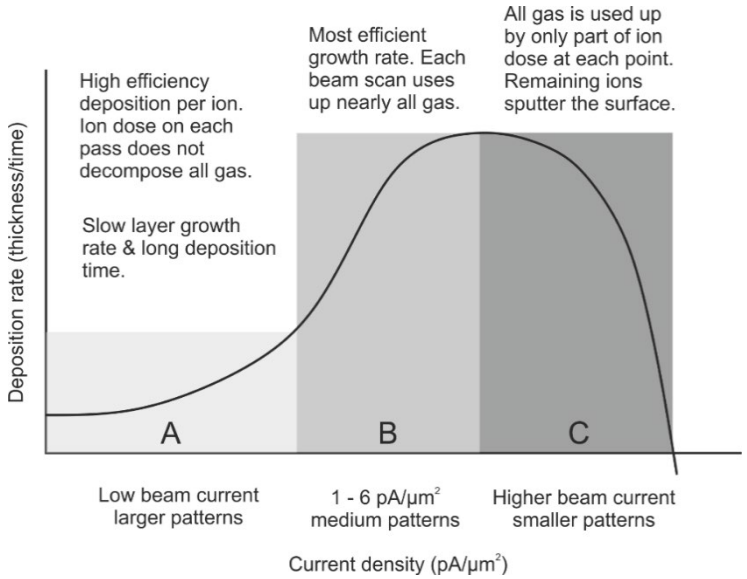

Good parameters for Ga+ ion Pt deposition

- Ion probe current = Area * 5 pA/µm² (i-dep)
- Pixel fill factor = 40 - 70 %
- Short dwell time (0.2 µs for Pt)

Good parameters for e- Pt deposition

- Electron probe current 2000 pA @ 5 kV (e-dep)

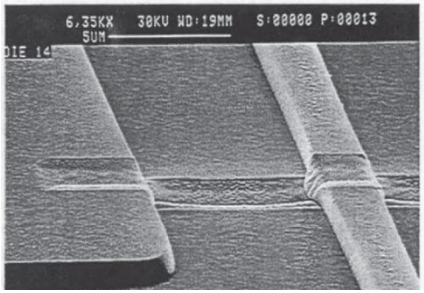

Bad parameters

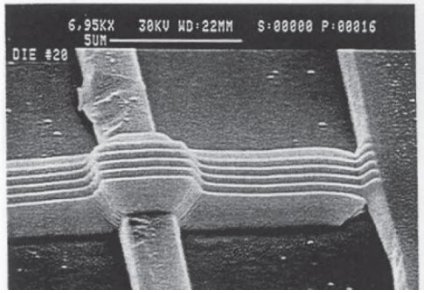

Good parameters

Beam profile

Shorubalko et al., *J. Nanotechnol.* **8** (2017)

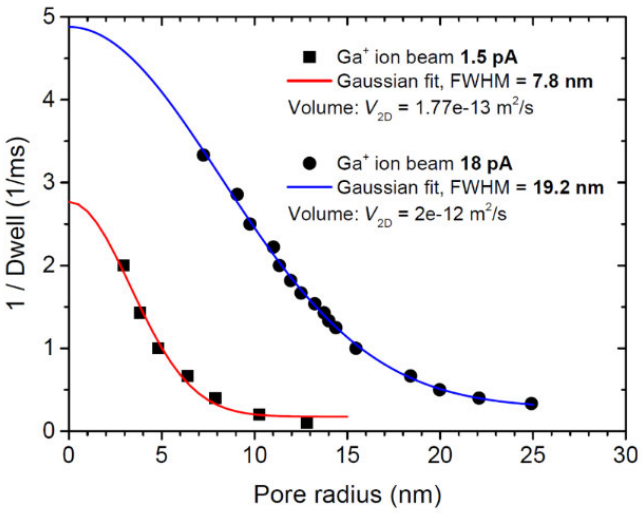

Beam traces

- Electromagnetic lenses → high current → **spherical aberration**
- Rounding of the milled edges
- Circle of less confusion at high currents lead to a better result than Gauss optimum

Gierak et al. *Semicond. Sci. Technol.* **24** 2009

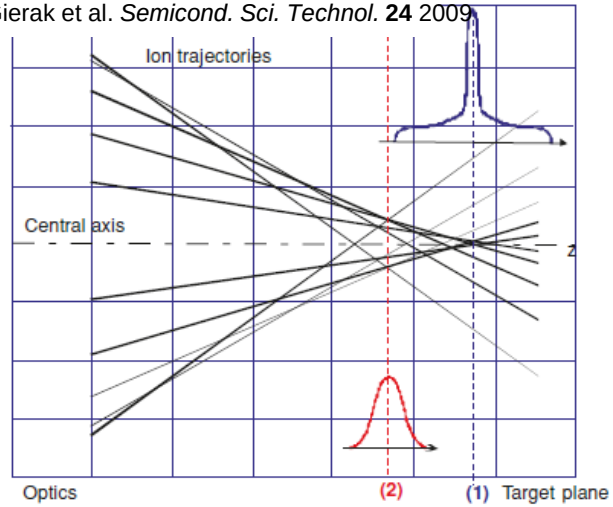

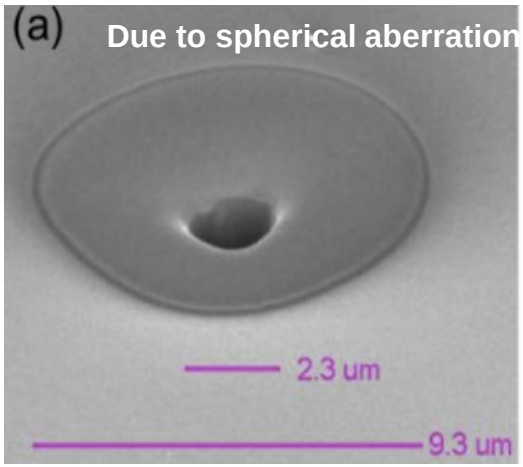

27 nA no defocus

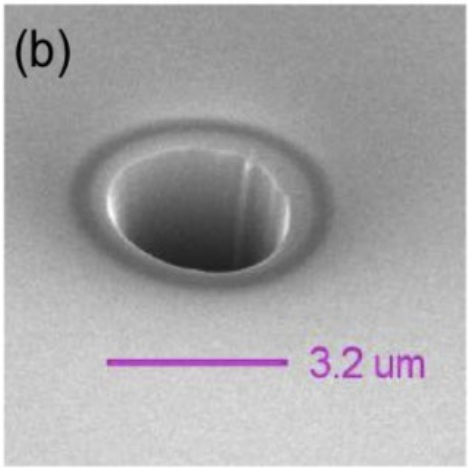

27 nA defocus

Two main milling strategies

Layer-by-layer

- Form a parallel floor
- Imaging
- Delayering
- Low redeposition but much slower

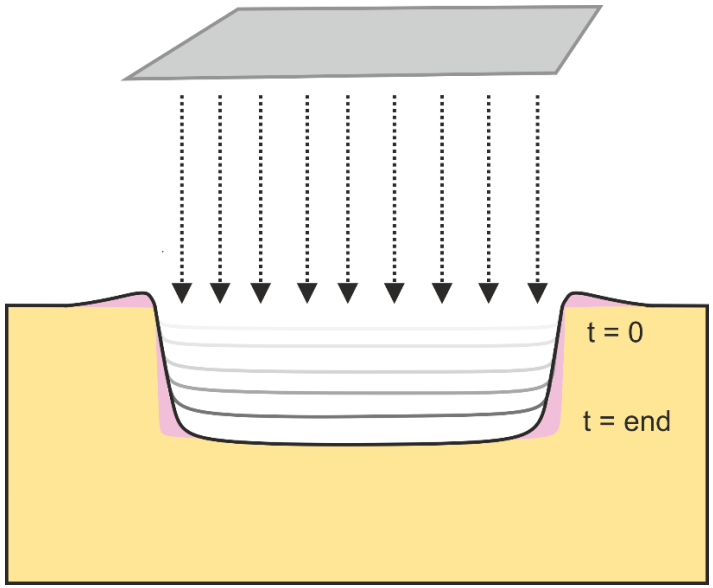

Layer-by-layer cut

Line-by-line (polishing)

- Tilted floor: shallow to deep
- Used for cutting (cross sections /polishing)
- Fast removal of large volumes
- Redeposition on floor and sides

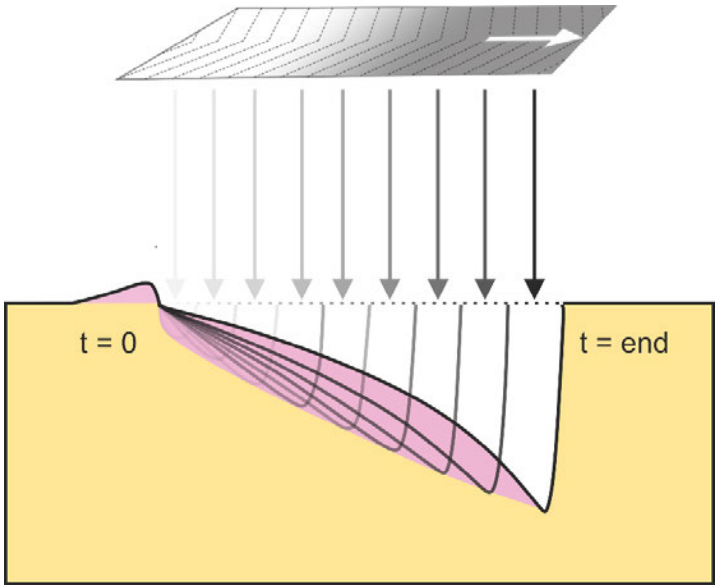

Line-by-cut (polishing)

Aspect ratio and tapering

Redeposition limits the milling aspect ratio

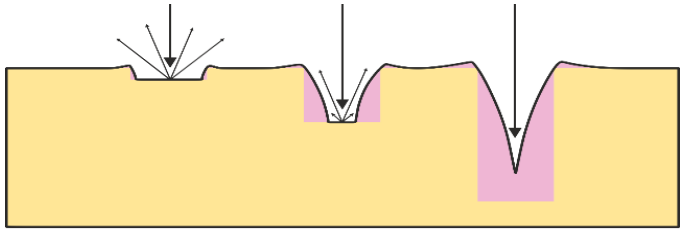

When the rate of redeposition equals the rate of sputtering: dynamic equilibrium (V-shaped trench).

- Generally maximum aspect ratio holes ~ 5:1
- Can be improved to ~ 10:1 with gas enhanced etching
- For small holes with size below 100 nm maximum aspect ratio of 1:1.

Fu et al. *Nanotechnology* **18** (2007)

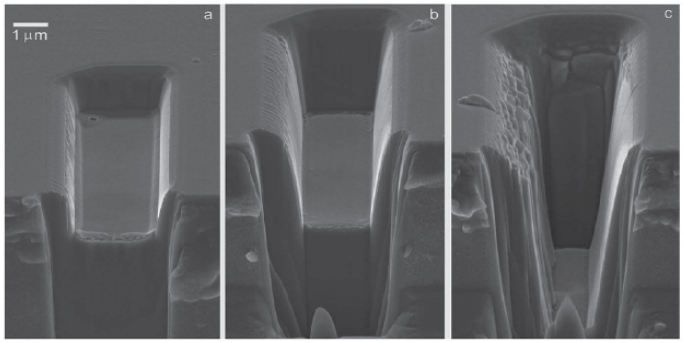

(100) Si milled at normal incidence by applying: (a) single fluence, (b) double fluence, and (c) triple fluence of Ga' ions at 25 keV.

Sidewall tapering

- Material dependent
- Typical values ~ 1-4°
- Some extreme cases e.g. Zn ~ 14°

Solution: overtilt to compensate (if possible)

Fei et al. *J. Appl. Mech.*, **79** (2012)

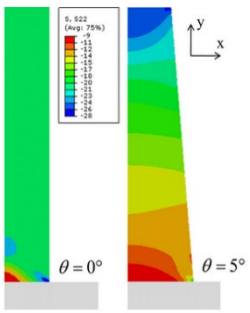

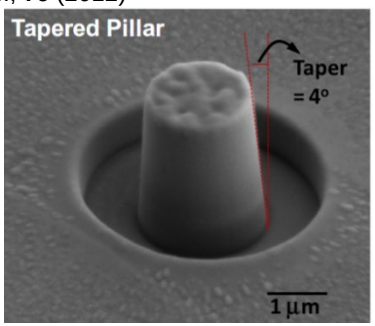

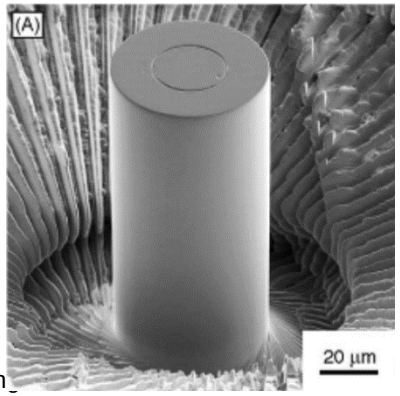

Inhomogeneous axial stress during micromechanical testin

Amorphization layer

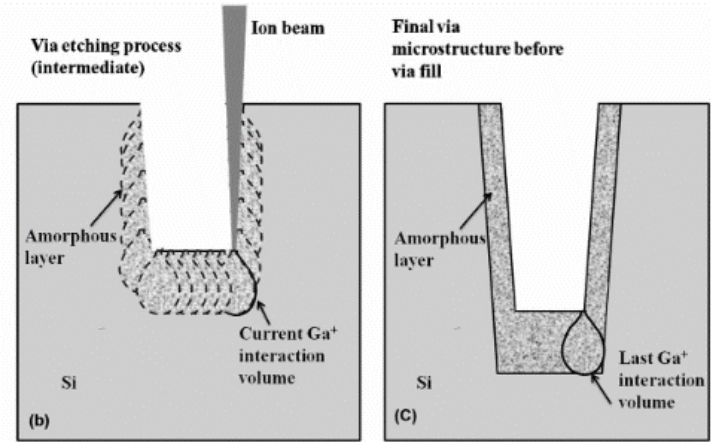

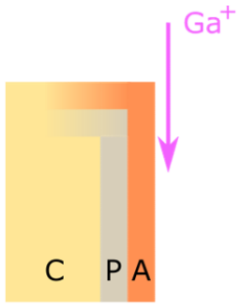

Damage zones in a crystalline solid C

A = amorphized

P = point defects

Reducing the amorphous layer

- Low kV milling
- Larger ion
- Lower angles

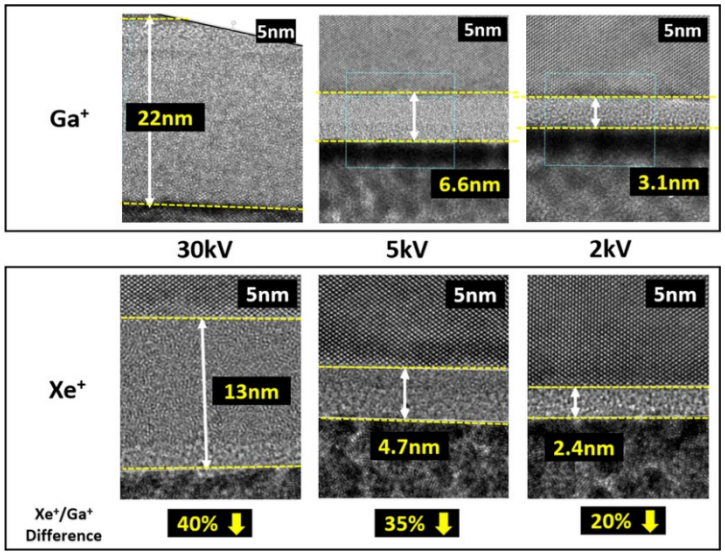

Burnett et al., *Ultramicroscopy* **161** (2016):

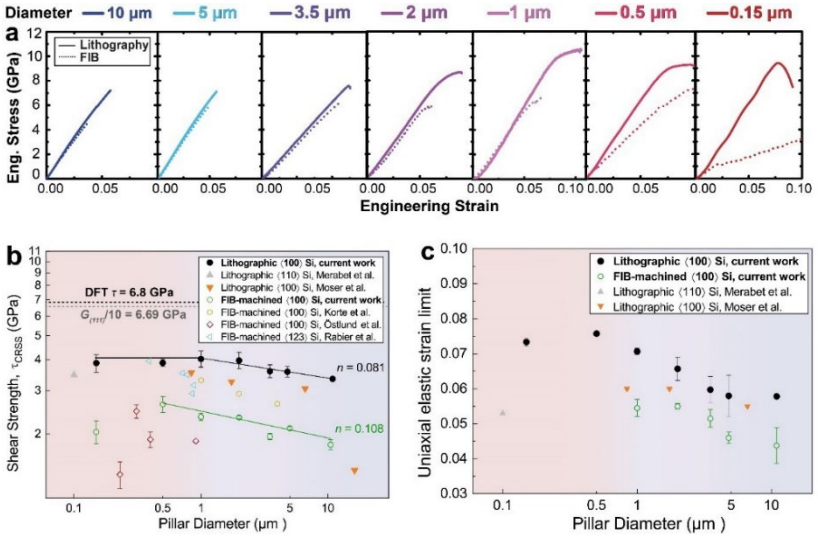

Does FIB induced damage influence the material behavior?
Something to keep in mind…

Amorphization on EBSD imaging

Matteson et al. *J. Electron. Mater.* 31 (2002)

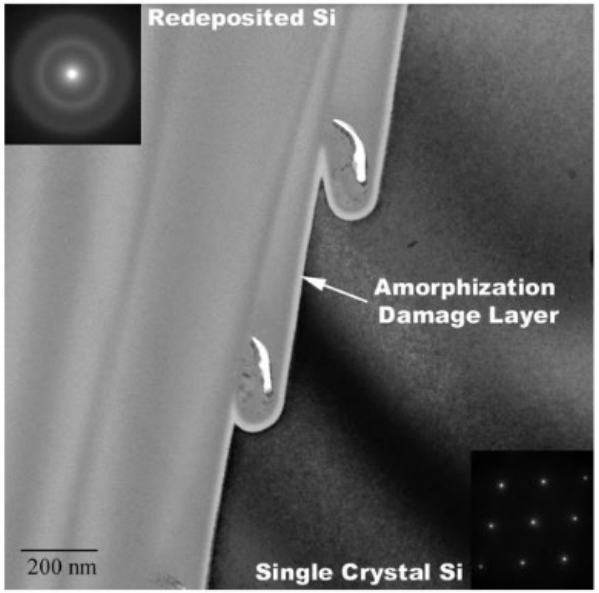

a

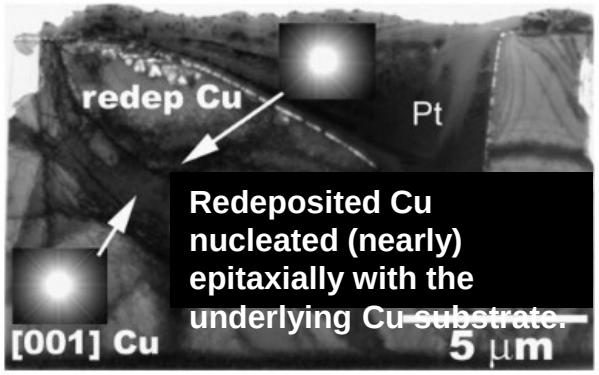

b

Amorphous layer thickness

- ion energy (low kV: **thin layer**)
- angle of incidence (tan: **small**)
- ion species
- target material

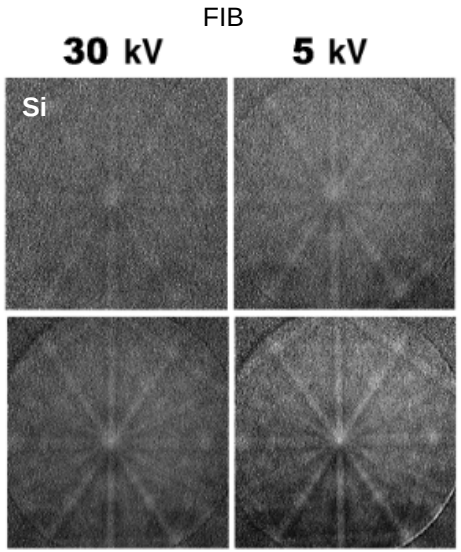

Metastable phase

Formation depends on complexity and size of the unit cell

Not always amorphous?

Small unit-celled, as well as broad phase field materials are more difficult to amorphize.

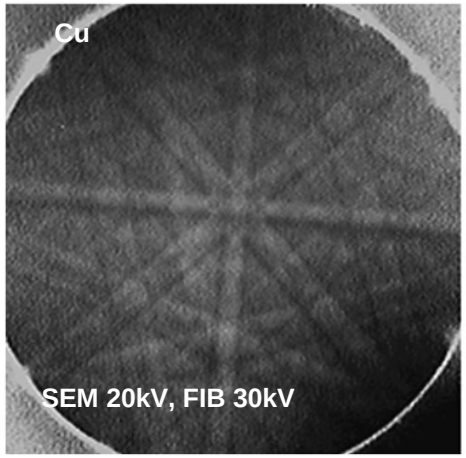

Local heating

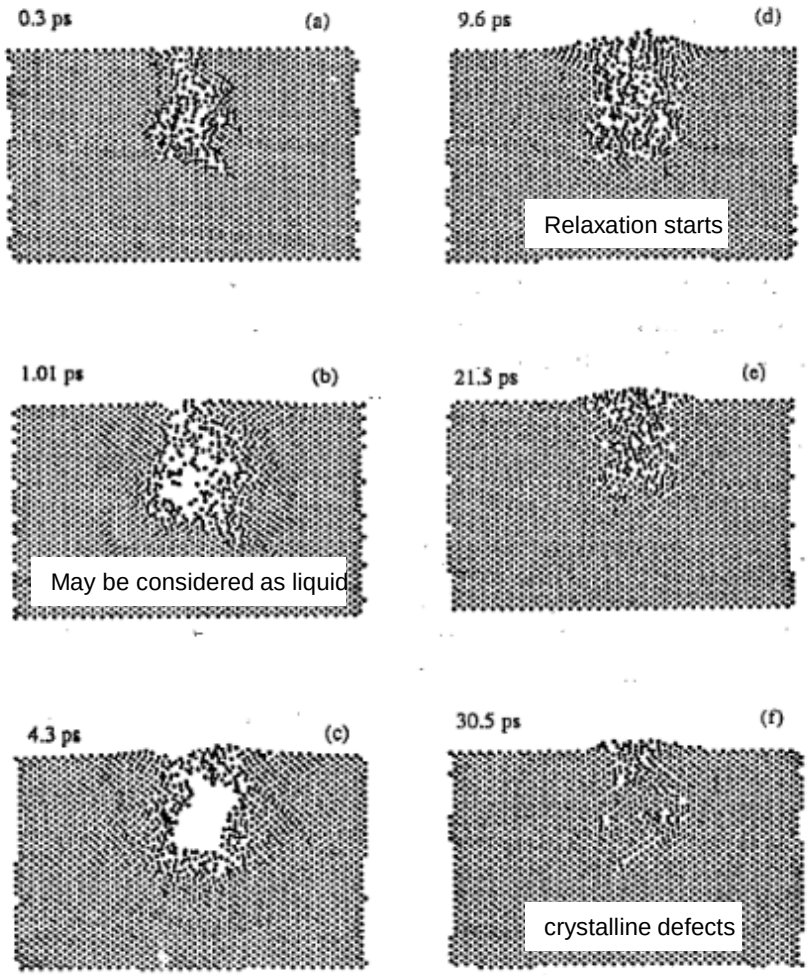

MD simulation Au particle 10 keV on a (100) Au surface
Averback and Ghaly, *J. Appl. Phys.*. 76 (1994)

- Heating **restricted** to the region defined by the **collision cascade** (a few tens of nm)
- If low dwell time < 5 us → most likely negligible for most materials.
- Be aware of polymers and low melting point materials (e.g. GaAs bleeding → reduce current)

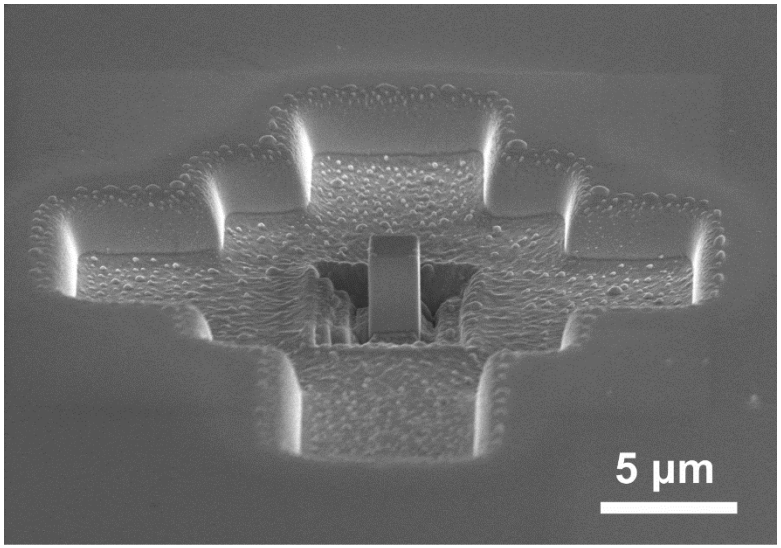

GaAs micropillar showing sings of bleeding due to local heating during milling

Curtaining

Curtaining (aka waterfall effect)

Milled face shows lines (more / less material was removed)

Irregular non flat surface: bad for quantitative image analysis

- Porous materials
- Rough surfaces
- Height steps (e.g. gates in semiconductors)
- Composites of hard and soft material
- Low kV milling

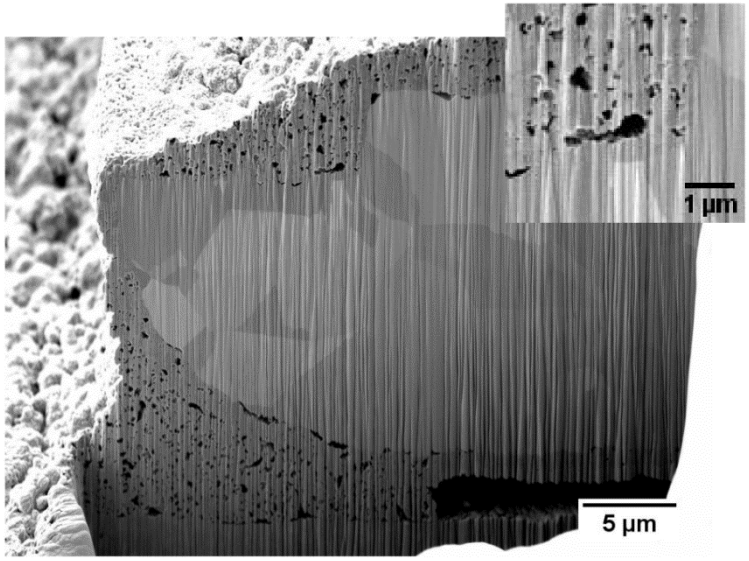

Porous ceramic on Ni: strong curtaining due to rough surface

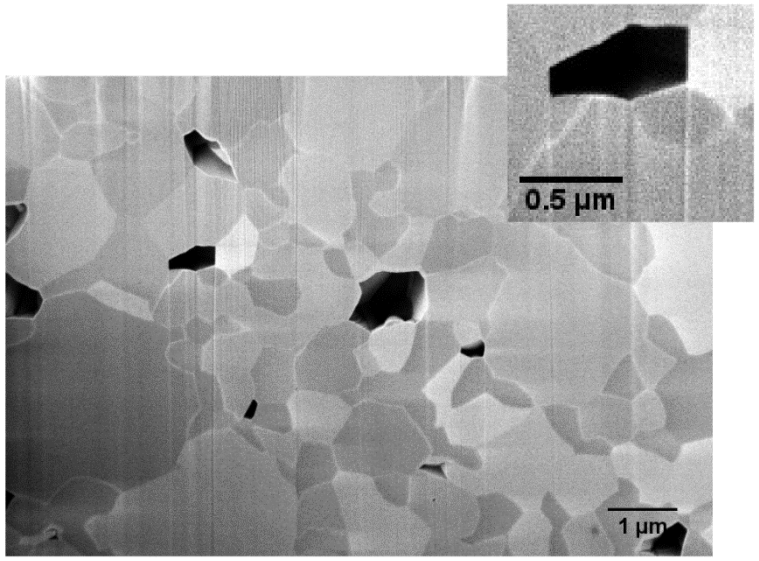

Porous cermet: mild curtaining due to pores

Curtaining is created by **spatial variation of the sputter rate** of the sample and **the modulation of the current density by forward scattering of the ions**.

How to reduce curtaining?

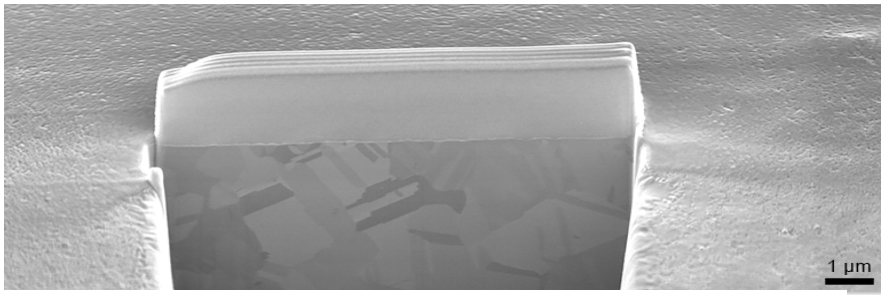

Thick protection layer

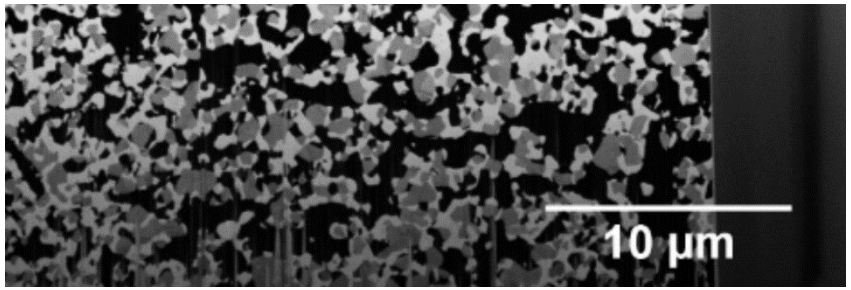

Resin infiltration

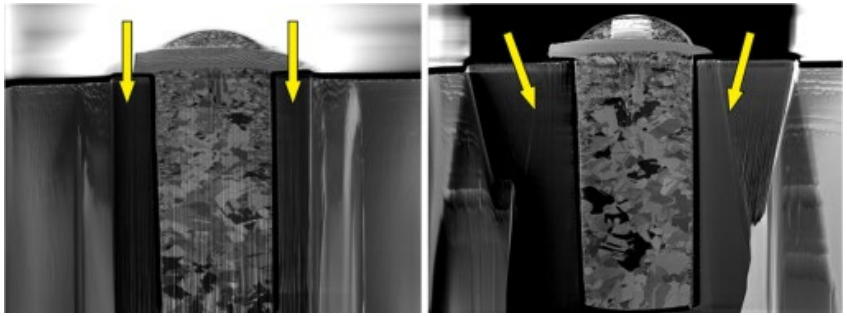

Rocking stage, sample rocking

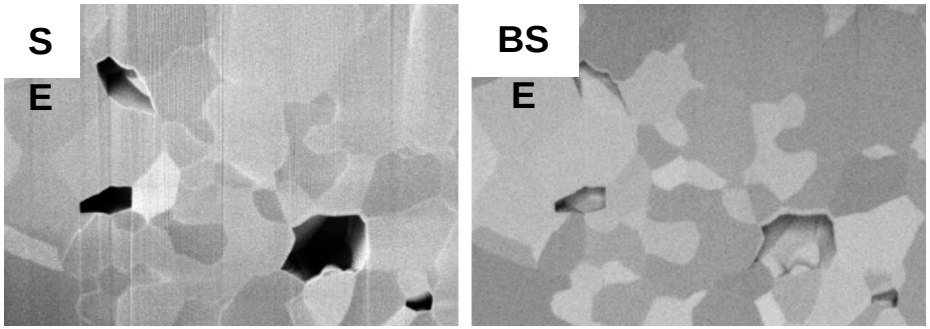

Hide it: BSE signal or post processing

1. Thick and dense FIB-deposited protective layer (W or Pt)
2. Stage rocking/tilting the specimen in the image axis
3. Increase the minimum dose
4. Resin infiltration
5. Backscattered electrons
6. Postrocessing

Rippling and how to avoid it?

Ion rippling

- Self organization
- Instability of process
- Material dependent
  (silicate rocks are bad Al and Si are fine)
- Ion dependent (size of ion vs atoms in solid)
- Current density dependent
- Mostly see it in Xe PFIB

Solution

- Thick protection cap will help
- However masking works best

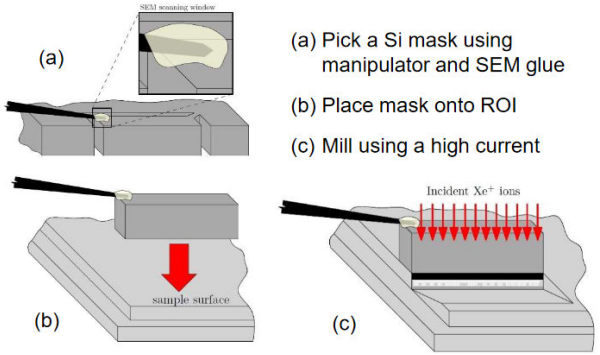

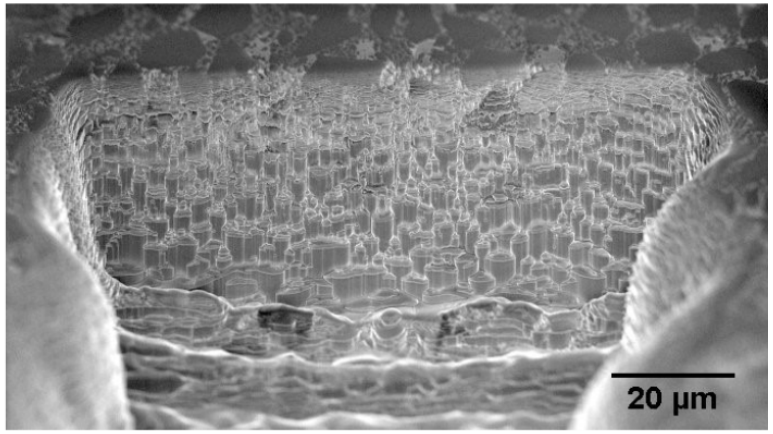

Massive ion rippling in SiC sample, microstructure completely obscured.

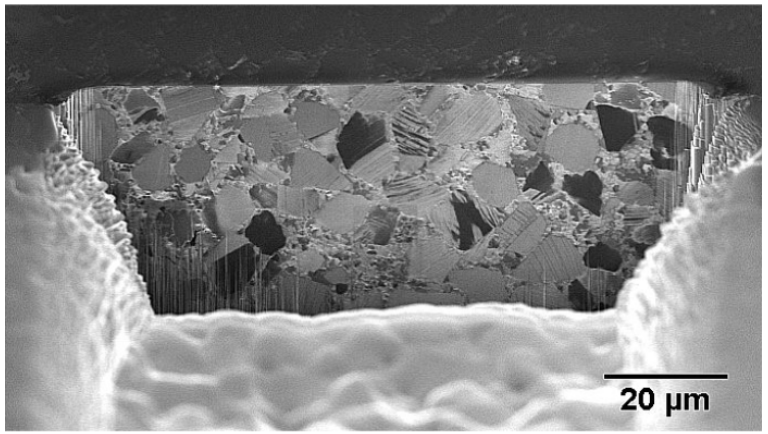

Cross section polished using Si mask, microstructure clearly visible.

Examples of TEM lamella prep.

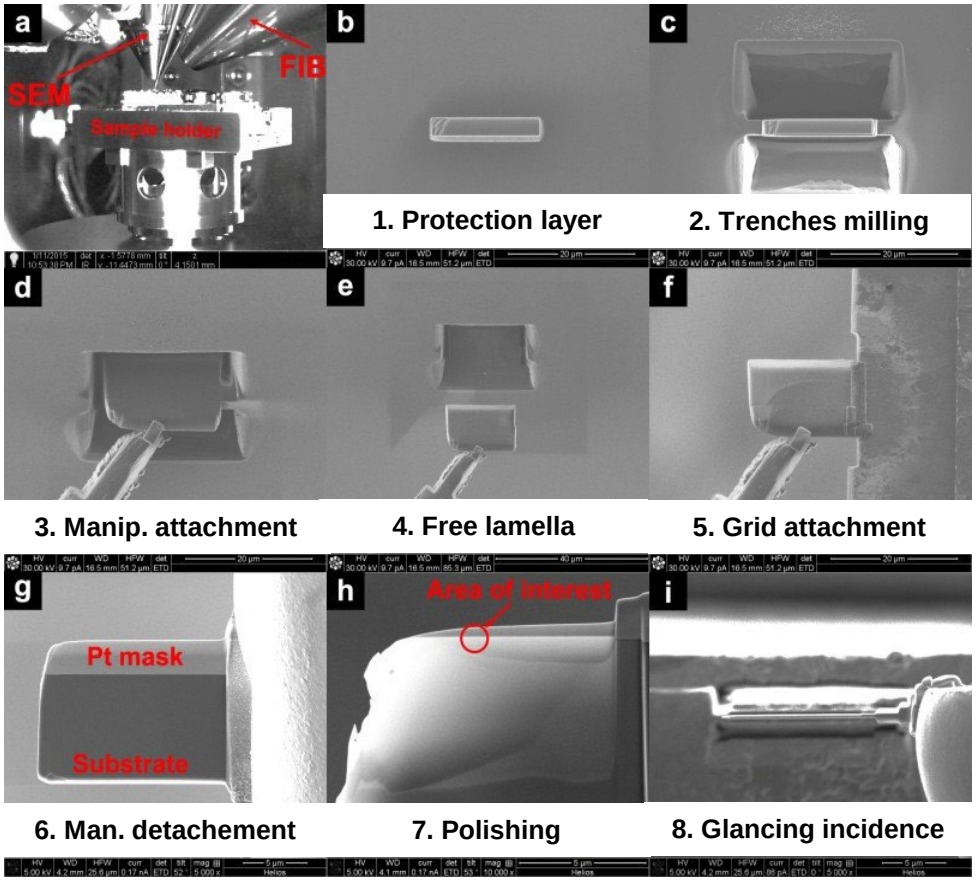

Trenches milling

Mostly work at 30 kV (most materials behave ok)

Leave a few µm from ROI at high currents (beam traces)

Sequentially reduce current e.g. 10 nA, 2nA, 200 pA

2 µm lamella ok to lift-out

Keep in mind the aspect ratio (tall lamella → larger trench)

Polishing and thinning

30 kV 1nA (1 µm thickness) → 100 pA (100 nm thickness)

Overtilt to keep the surface parallel (most cases ± 2°- 3°)

Grazing incidence 2-5 kV +/- 5-7° (1 - 3 min)

Pt. Deposition

First perform e-beam deposition (5 kV, 2000 pA)

Ion deposition 10-15 kV will be denser

Thick is good!

- Ion current = Area x 5 pA/µm^2
- Pixel fill factor = 40 - 70 %
- Short dwell time (0.2 µs for Pt)

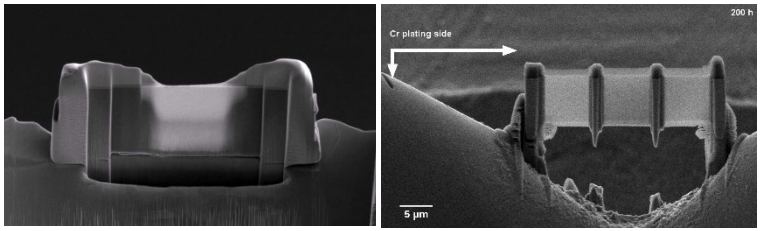

You can also attach the lamella on top of the grid instead of the side

Final tricks and tips

General tips:

- Small currents for high precision
- Large currents for speed
- Polishing for faster milling rate
- Defocus on high currents
- Tilt sample into beam for perpendicular cut
- Short dwell time for high control of shape/depth
- Long dwell time for hard materials /speed
- Several passes for nanopatterning to avoid redeposition
- Well tuned beam (e.g. dose and dwell time for GIS)

Pitfalls and possible solutions:

- **Damaged layer and ions implantation** → low kV
- **Tapering** → overtitling, reduce current
- **Curtaining** → protection cap, stage rocking
- **Redeposition** → Several milling steps, reactive gas

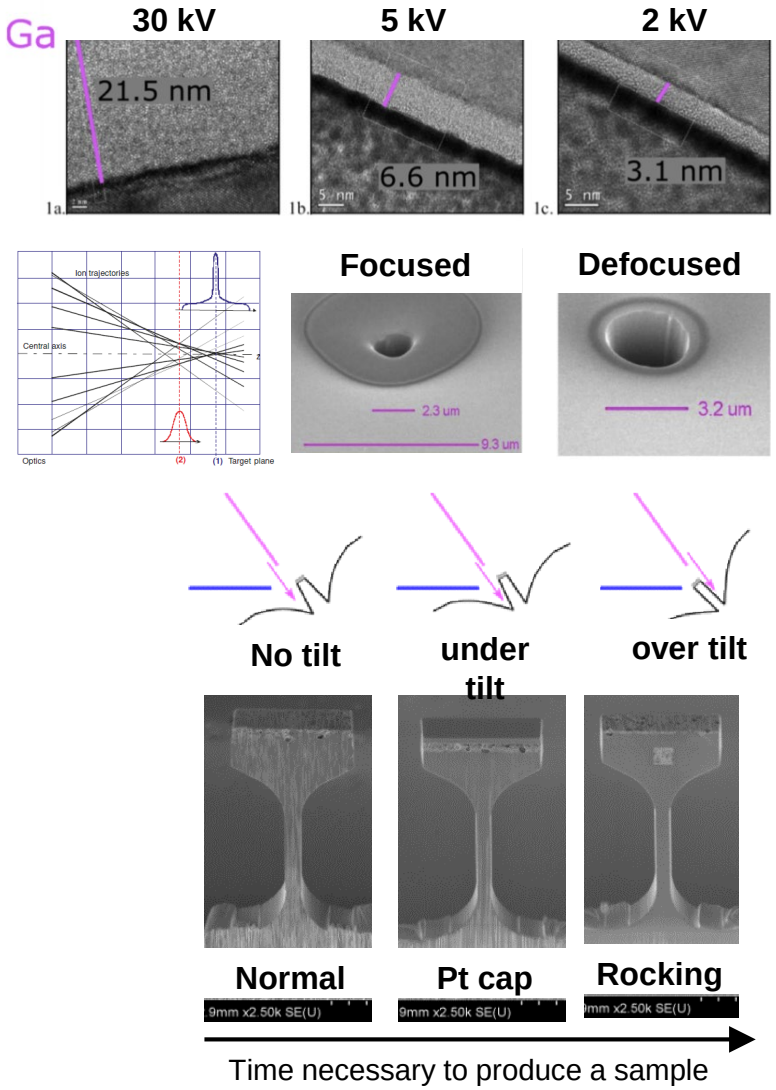

Brief History of LASER

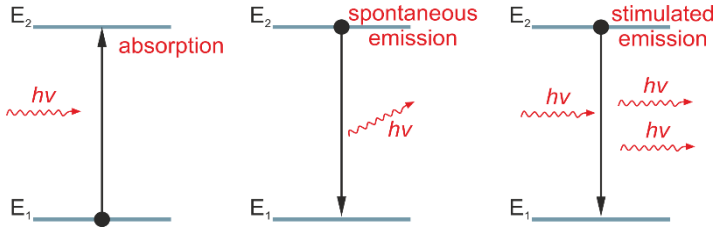

1917 *Zur Quantentheorie der Strahlung* (***Albert Einstein***)
→ stimulated emission of electromagnetic radiation

1928 **Rudolf Ladenburg** first observed stimulated emission

1950s **Charles Townes** (Columbia University) → *MASER:*
"microwave amplification by the stimulated emission of radiation."

Gordon Gould (PhD @ CU) → **LASER**

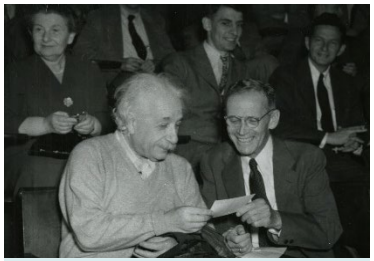

Albert Einstein and Rudolf Ladenburg
(Princeton Symposium, 1950)

1964 Nobel Prize in Physics

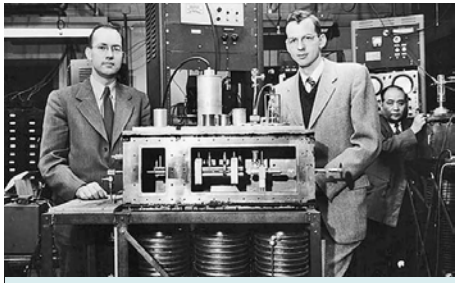

Charles Townes and Gordon Gould

Nikolay Basov

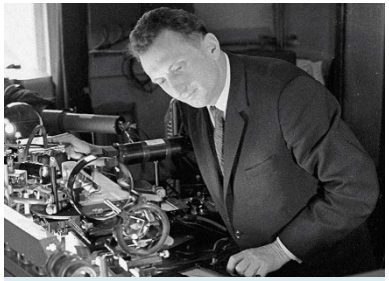

Aleksandr Prokhorov

1960s Hughes Research Laboratories in Malibu/ Bell Labs (New Jersey)/ General Electric Research and Development Center in Schenectady (New York) / …

"… a solution looking for a problem"

Laser Applications

- Scientific
- Industrial
- Medical
- Military
- Commercial

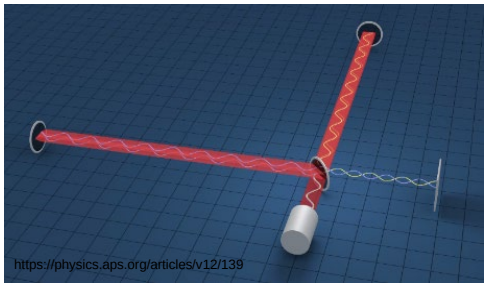

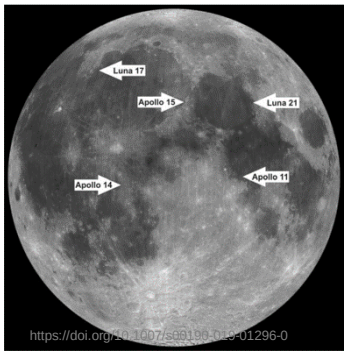

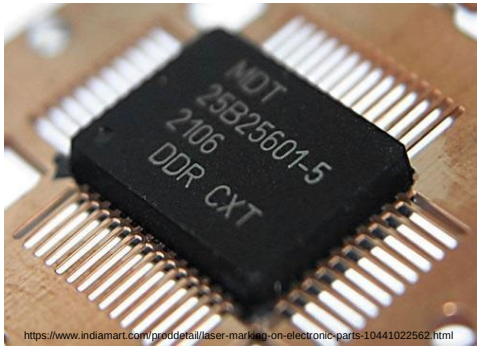

Laser Physics

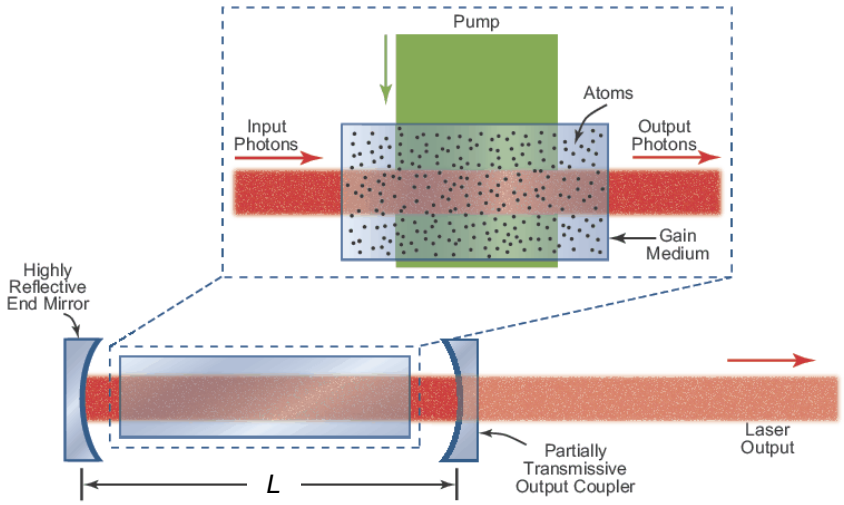

- **Optical resonator**
- **Pump** (optical/electrical/gas)
- **Gain medium**

  Solid: doped crystals (Nd:YAG, Ti:Al_2O_3), semi-conductors (InGaAs)

  Gas: HeNe, N, Ar, CO_2

  Liquid: dye solutions (rhodamine 6G)

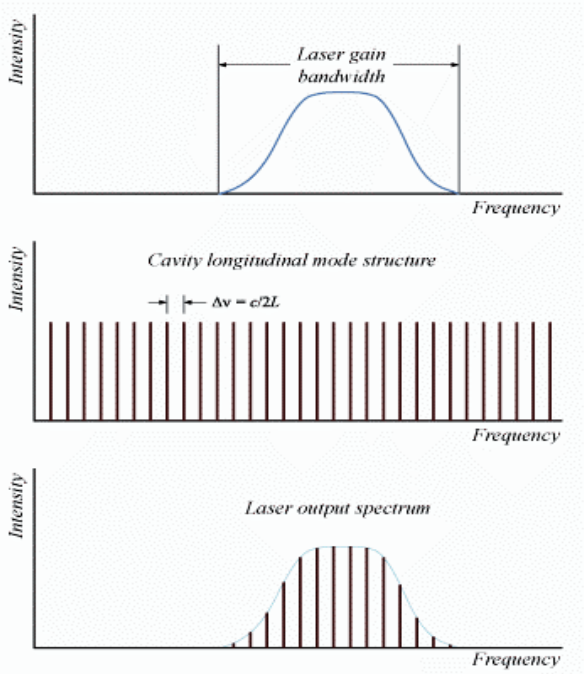

- Wavelength, λ
- Gain Bandwidth, B
- Output Power, P

Images modified from *newport.com* and *wikipedia.org/wiki/Mode_locking*

Laser Physics

- Continuous laser
- Pulsed laser (0.5 to 500 ns)
- Ultrashort pulsed laser (5 fs to 100 ps)

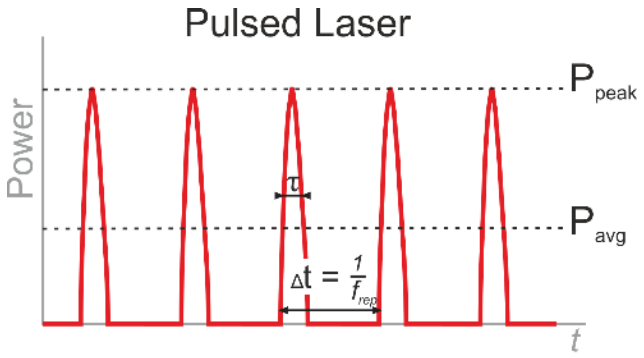

Gaussian laser beam profile

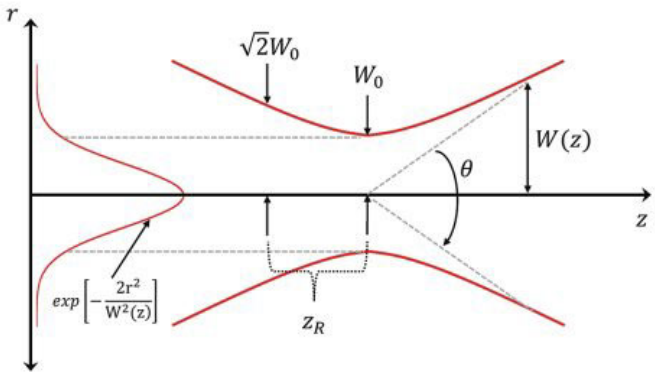

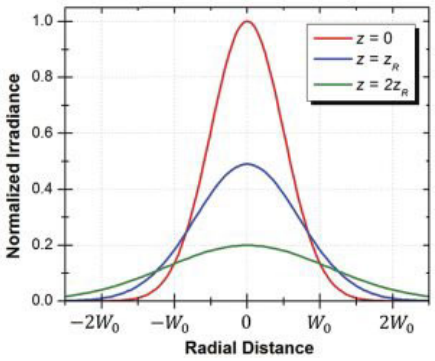

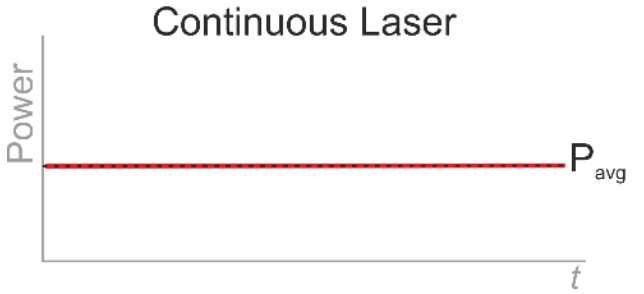

w_0 – *beam waist radius*

$$E_{pulse} = \frac{P_{avg}}{f_{rep}} \; [J]$$

$$P_{peak} = \frac{E_{pulse}}{\tau} \; [W]$$

Images modified from *newport.com*

Laser Ablation Principles

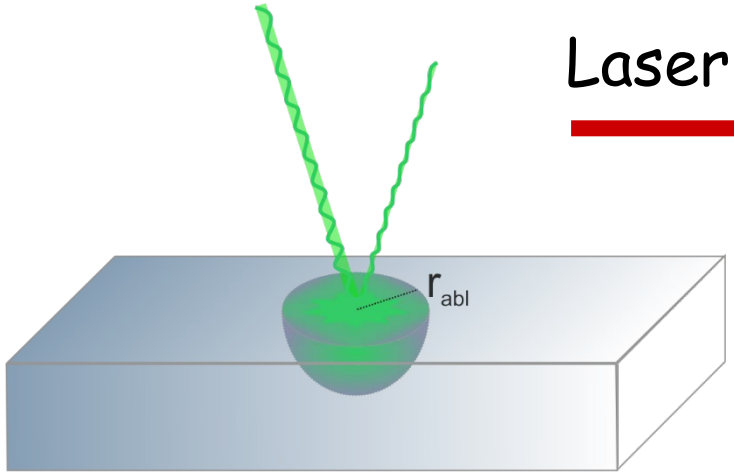

Laser-Induced Damage ↔ **Fluence** $[J/cm^2]$

$$F_0^{peak} = 2\frac{E_{pulse}}{\pi\omega_0^2}$$

$$F(r) = F_0^{peak}\exp(-\frac{2r^2}{\omega_0^2})$$

$$F_{th} = F_0^{peak}\exp(-\frac{2r_{th}^2}{\omega_0^2})$$

Ablation rate [nm/pulse]: $h_a = \alpha_{eff}^{-1}\ln\left(\frac{F_0^{av}}{F_{th}^{N\geq 1}}\right)$ [1]

Ablation "crater" diameter: $D^2 = 2w_0^2\ln\left(\frac{F_0^{peak}}{F_{th}}\right)$

$F_0^{avg} = \frac{1}{2}F_0^{peak}$, α_{eff}^{-1} $-$ *effective optical penetration depth*

Fs-laser ablation properties of borosilicate glass [2]

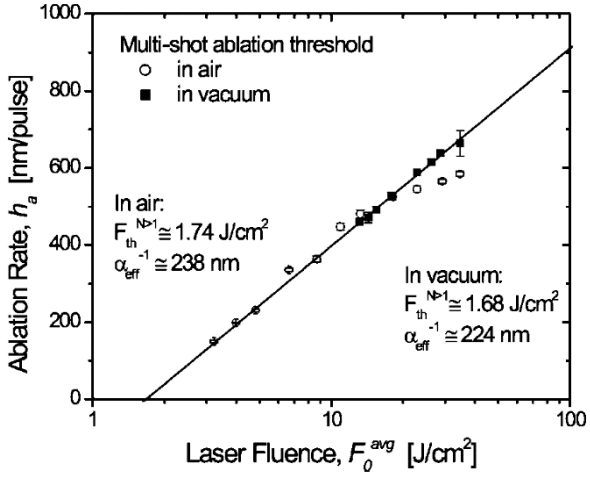

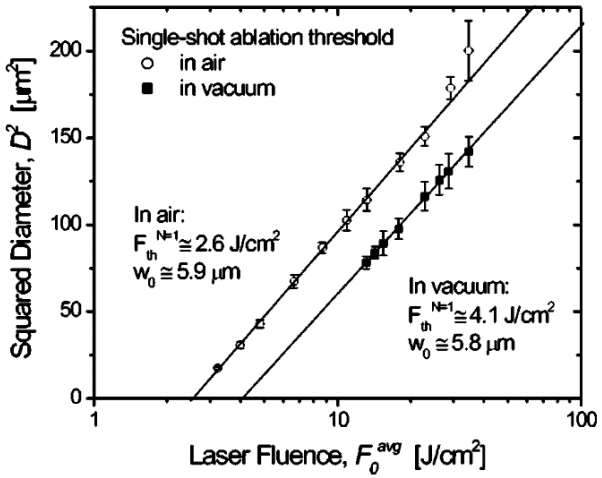

[1] Preuss, et al. Appl. Phys. (1995). DOI:10.1007/BF01538207
[2] Ben Yakar and Byer, J. Appl. Phys (2004). DOI:10.1063/1.1787145

Laser Ablation Principles

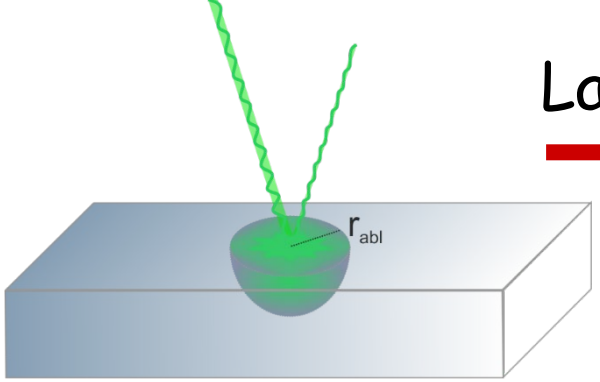

Interaction mechanisms x fs-laser ablation [3]

1) absorption of laser energy through photon-electron coupling (~ fs)
2) energy distribution to the lattice through electron-phonon coupling (~10 ps)
3) normal energy diffusion into the material through phonon-phonon collision

Laser-Induced Heat accumulation: **Two-temperature model (TTM)** [4]

$$C_e \frac{\partial T_e}{\partial t} = \nabla \cdot (k_e \nabla T_e) - g(T_e - T_p) + Q^*(x,y,z,t),$$

$$C_p \frac{\partial T_p}{\partial t} = \nabla \cdot (k_p^* \nabla T_p) + g(T_e - T_p)$$

[5] ablated volume ↔ isolated mechanism ($T_e = T_p = T$)

$$(C_e + C_p)\frac{\partial T}{\partial t} = \nabla \cdot (k_e + k_p)\nabla T + Q(x,y,z,t)$$

[5] Bulk heat capacity: $(C_e + C_p) = \rho c$
Bulk thermal conductivity $(k_e + k_p) = k$

$$\rho c \frac{\partial T}{\partial t} = \nabla \cdot k \nabla T + Q(x,y,z,t)$$

$e - \text{electron} / p - phonon$
$C, k - heat\ capacity\ and\ thermal\ conductivity$
$g - electron - phonon\ coupling$
$Q(x,y,z,t) - energy\ absorption\ rate (spatial\ and\ temporal):$
$Q(x,y,z,t) = S(x,y,z) \cdot T(t)$
$* - terms\ that\ vary\ between\ dielectrics\ and\ Me$

FEM of temperature distribution during laser ablation extraction of mineralized tissue micropillar (final diameter ~12 µm) [5]

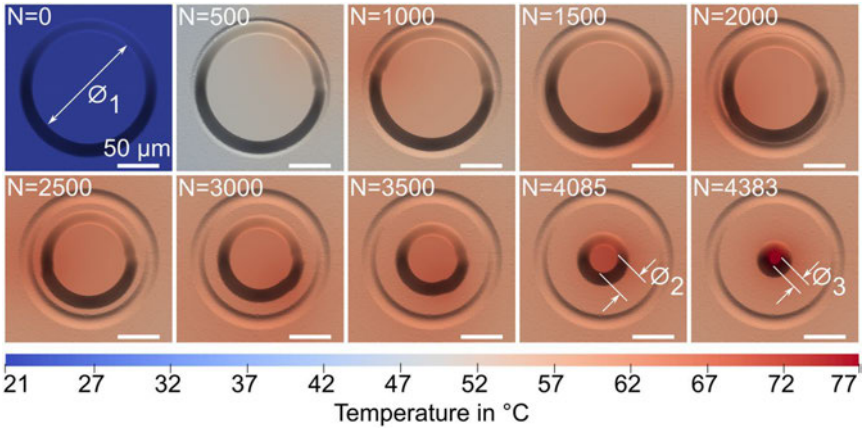

[3] Du, et al. Opt Commun (2010). DOI:10.1016/j.optcom.2009.12.038
[4] Anisimov et al. JETP Lett (1974) Bib:1974JETP...39..375A
[5] McPhee et al. Sci Rep (2021) DOI:10.1038/s41598-021-89181-9

Laser Ablation for micropillar fabrication

Heat impact during laser ablation extraction of mineralised tissue micropillars [5]
(anticlockwise inward spiral pattern)

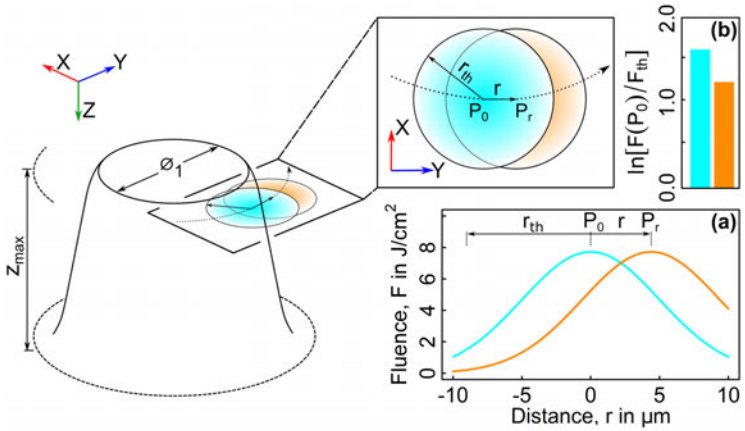

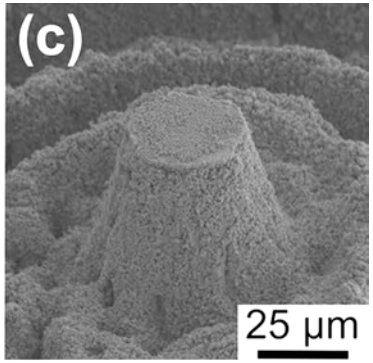

Micropillar fabrication on bovine cortical bone by direct-write femtosecond laser ablation [6]

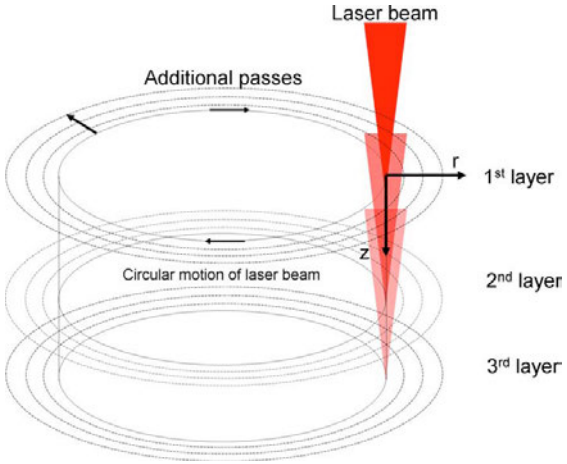

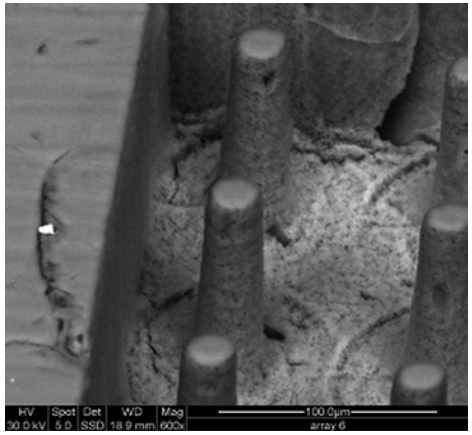

[5] McPhee et al. Sci Rep (2021) DOI:10.1038/s41598-021-89181-9
[6] Lim et al. J. of Biomedical Optics (2009) DOI:10.1117/1.3268444

Micropillar compression

Scanning ablation @ALPS BFH :

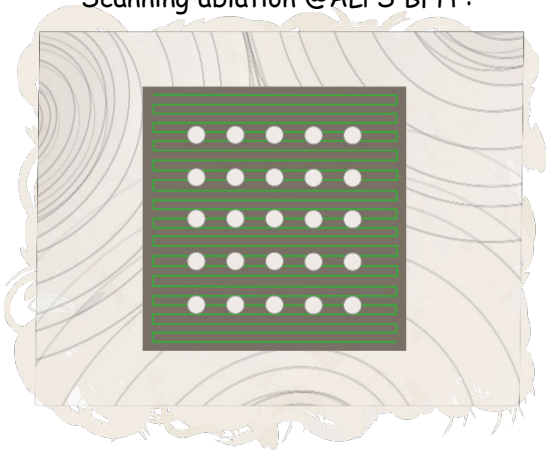

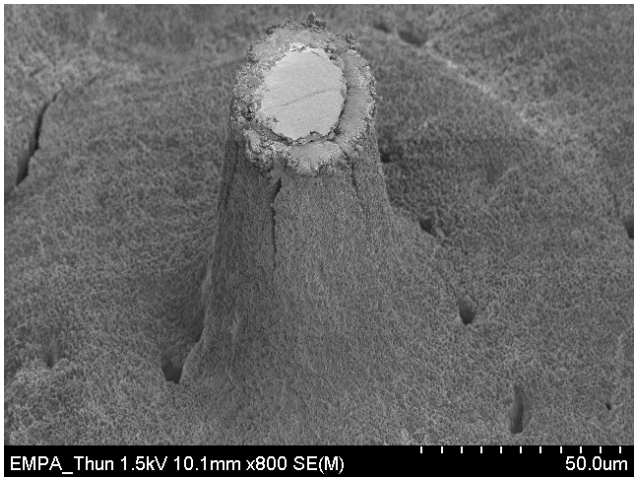

- λ = 515 nm
- frep = 3kHz
- F^{peak} = 5.14 J/cm^2

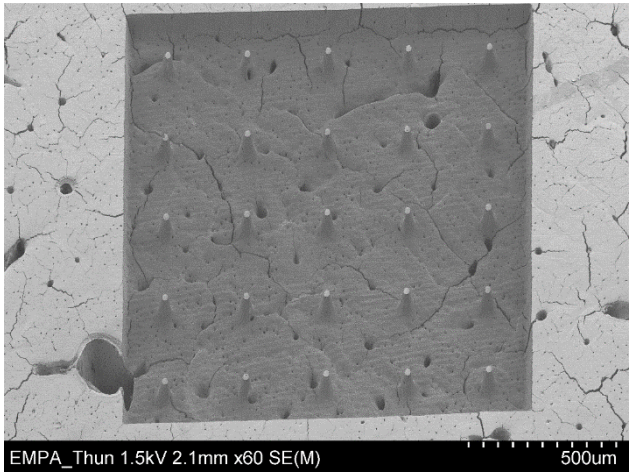

FEM of micropillar compression with different geometries

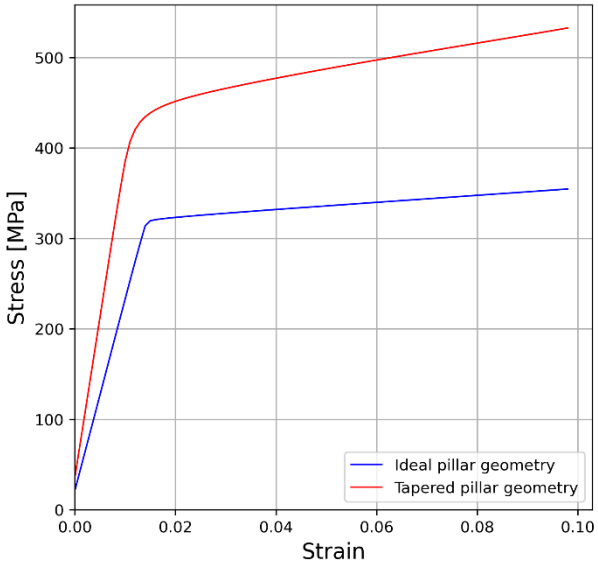

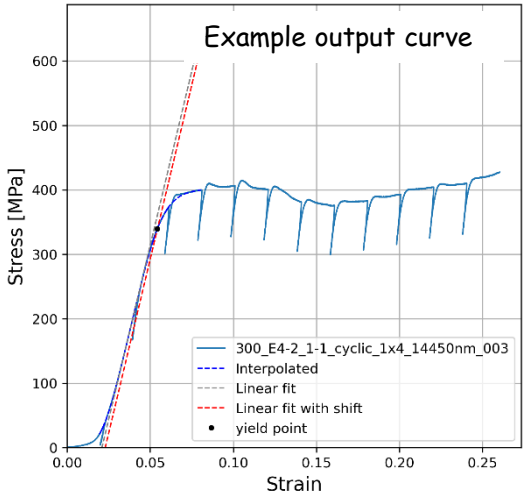

Laser Ablation for micropillar fabrication

	Ga^+FIB	PFIB	Fs-Laser
Removal rate (Si)	~18 $\mu m^3/s$ 1x	~675 $\mu m^3/s$ 38x faster	~265000 $\mu m^3/s$ 15000x faster
Spot size	50nm	100nm-10µm	10-20µm

Comparison of 3D volumes milled within the same amount of time with FIB, Plasma FIB, and femtosecond laser

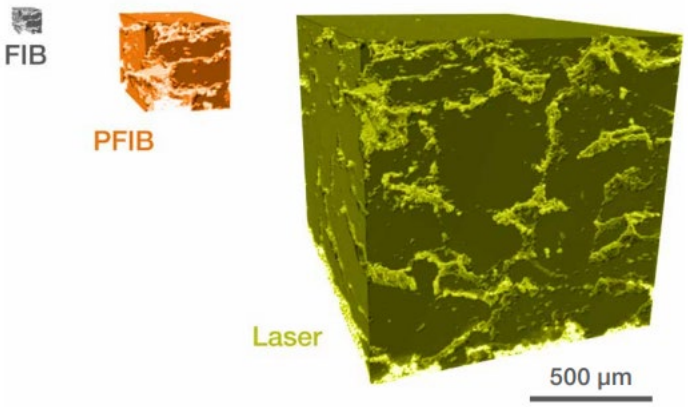

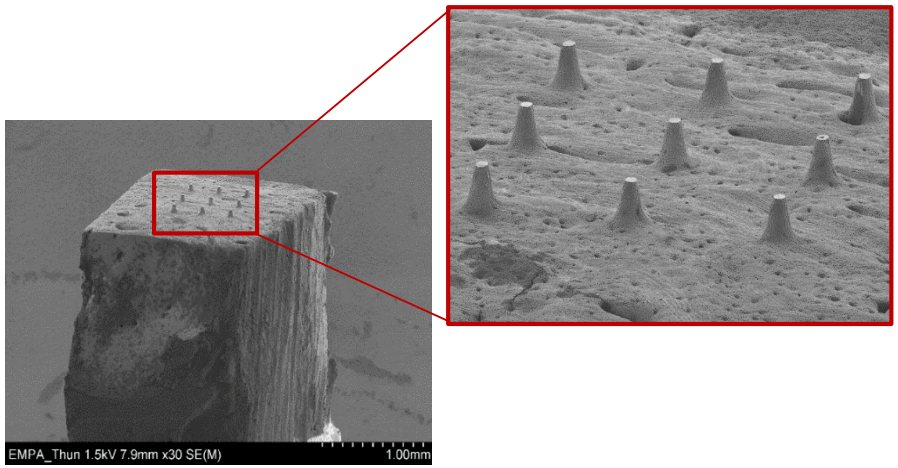

Surface damage

Spiral :

1W@5kHz

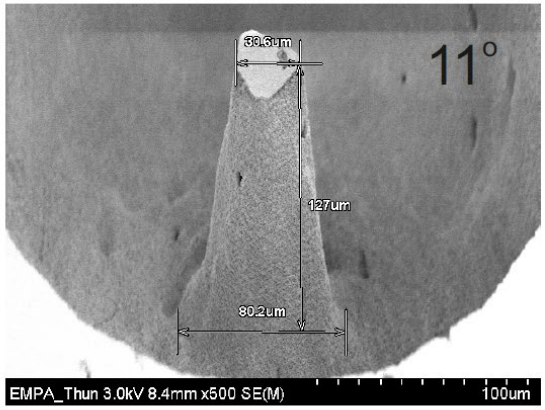

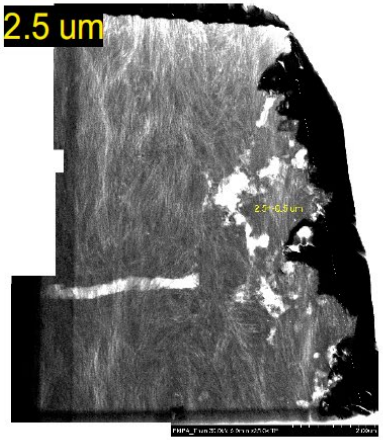

Bitmap:

2W@3kHz

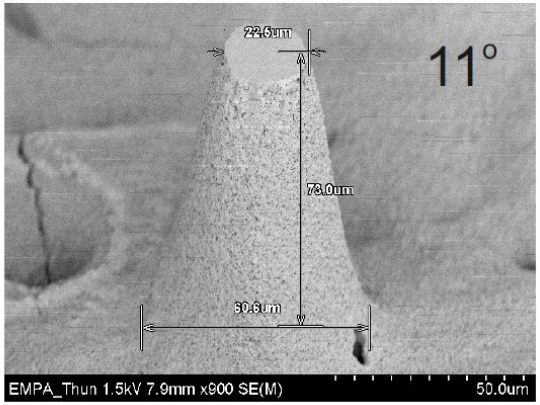

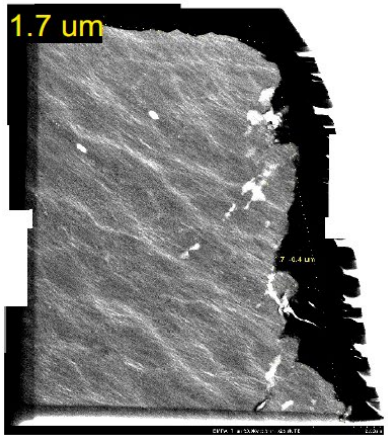

Laser Ablation for micropillar fabrication

take-home message:

- Choosing laser system for ablation (CW/pulsed)
- ★ Ultrashort pulsed laser (<100 ps)
- Choosing laser parameters for ablation (λ, τ, f_{rep}, F^{pulse}, N)
- Ways to improve micropillar geometry (focal height adjustment, beam waist radius, beam profile)

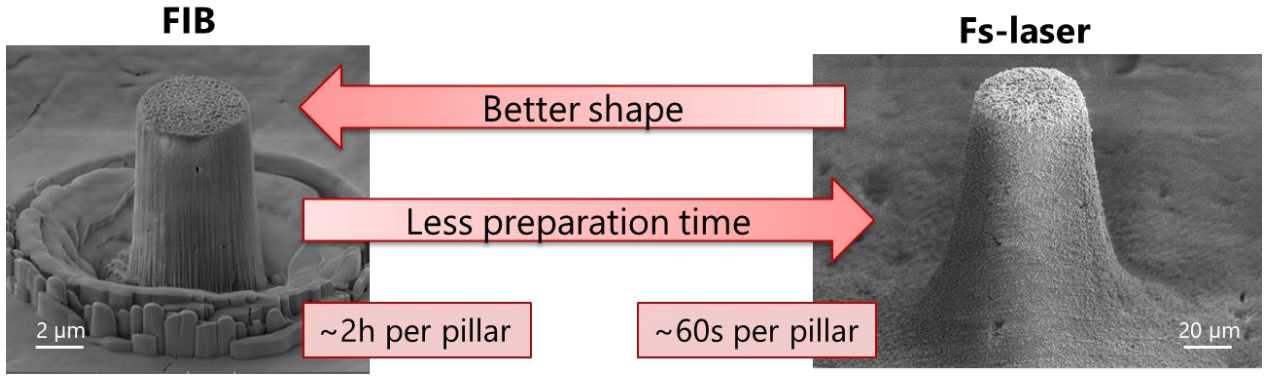

Lithography for 3D nanoscale metamaterials

Basic idea

All about integrated electronic circuits

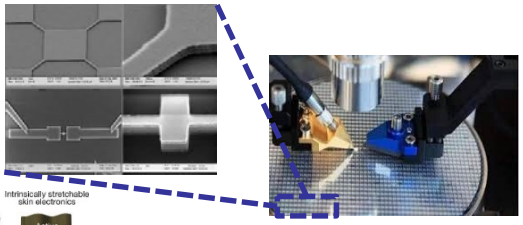

3 basic ingredients:
-light
-mask
-resist

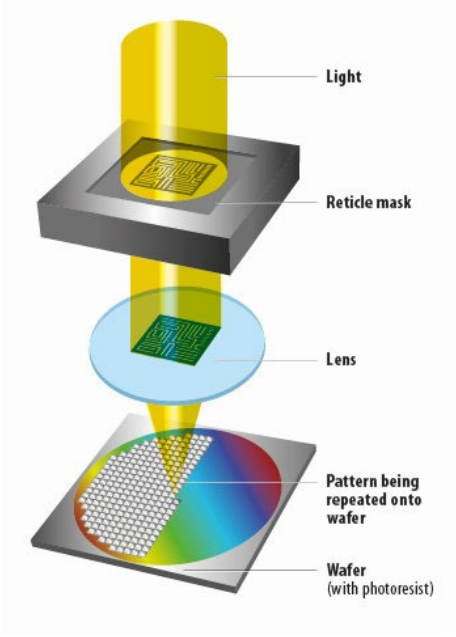

Categories

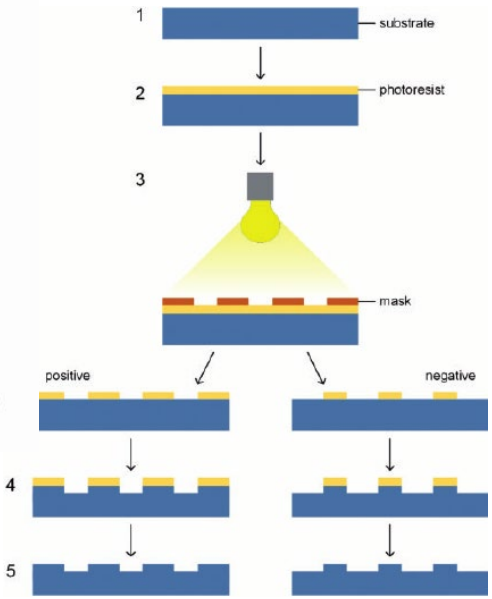

Applications

Bio-electronics

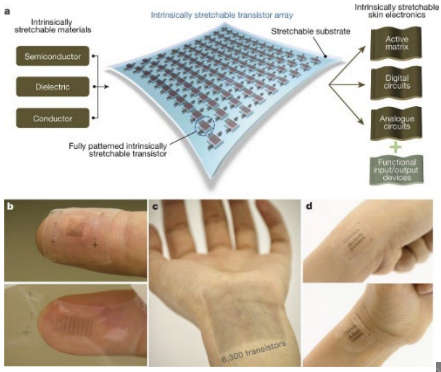

Photonic structures
Devices that guide light instead of electrons

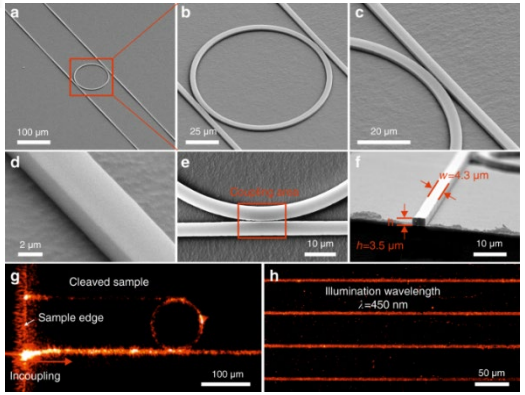

How it works

Chemistry

Photo-initiator

UV light

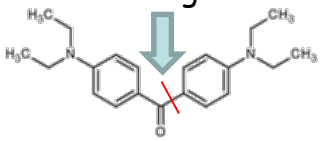

Free radicals attack monomers

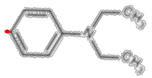

Solution mix

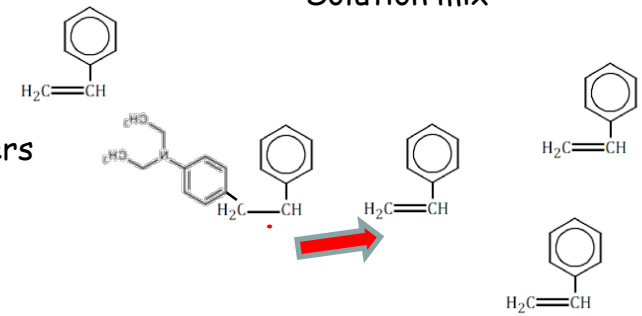

Monomer Polymer

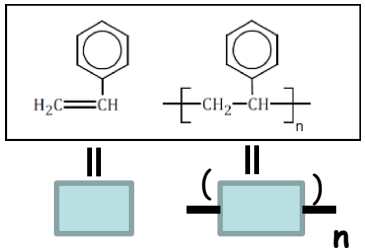

UV light

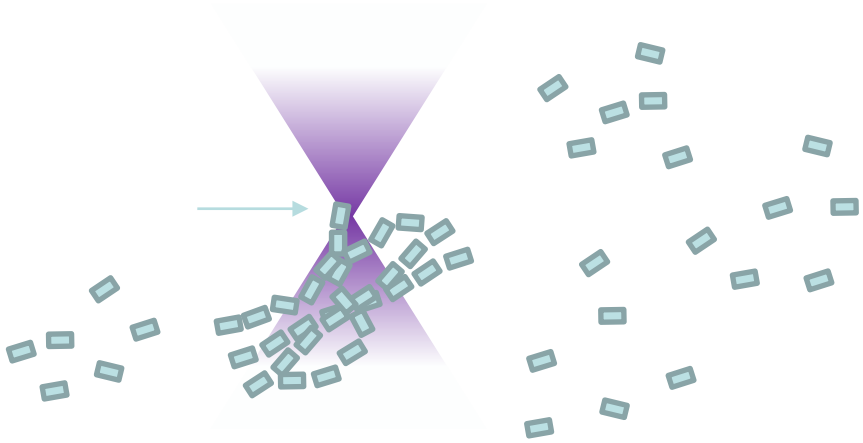

High quality patterns

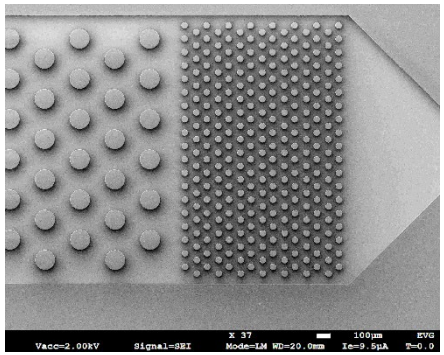

Drawbacks

-2D patterns only

-Mask required for different patterns, increases the cost

-Resolution: diffraction limited $d = \frac{\lambda}{2n\sin\theta} = \frac{\lambda}{2NA}$

λ=500nm can be focused only down to 250nm

-Limited variety of designs

-Limited Opto-mechanics

Single photon *vs* multiphoton

Volumetric Direct Laser Writing (DLW)

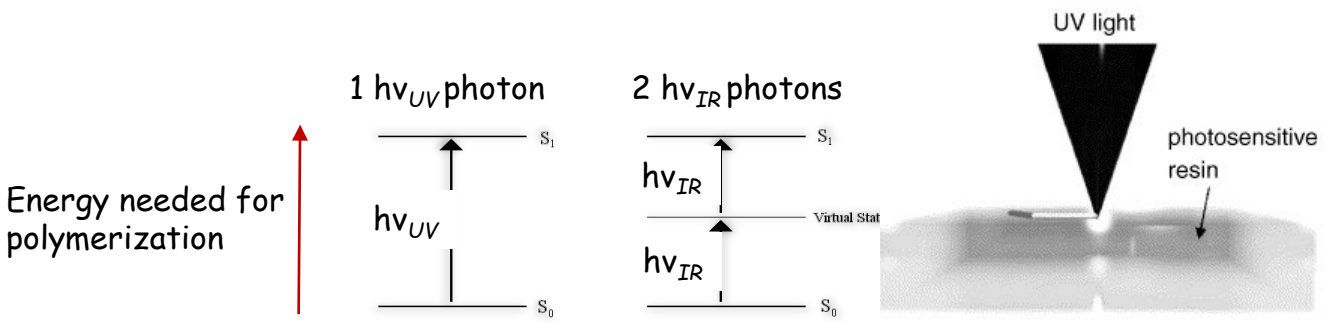

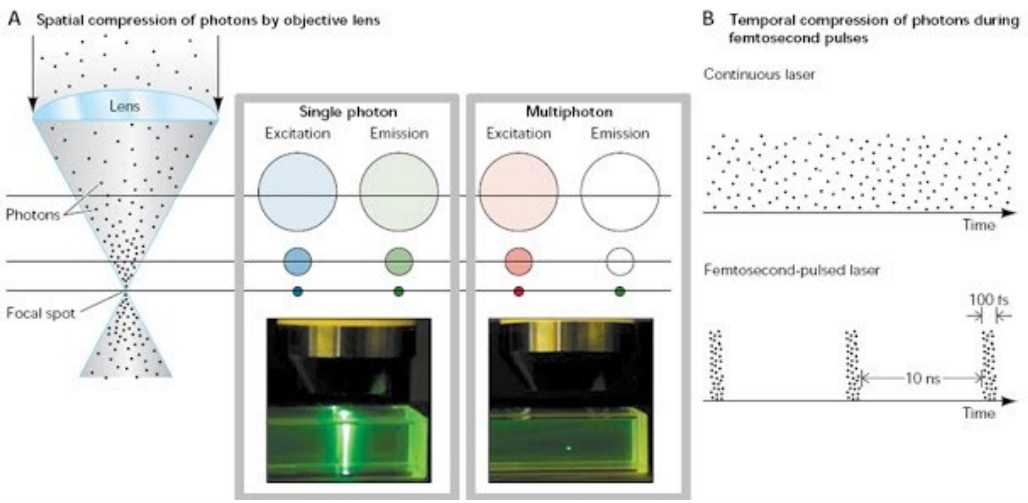

<u>Essential and potential</u>

-Ultrafast laser (pulses shorte than virtual state lifetime)

-3D patterns

-Resolution around 50nm

-Maskless

-Big variety of designs

-Rich Opto-mechanics

Setup/instrumentation

Setup

Ti: Sapphire Femtosecond Laser (800nm,75MHz, <20fs)

Direct Laser Writing

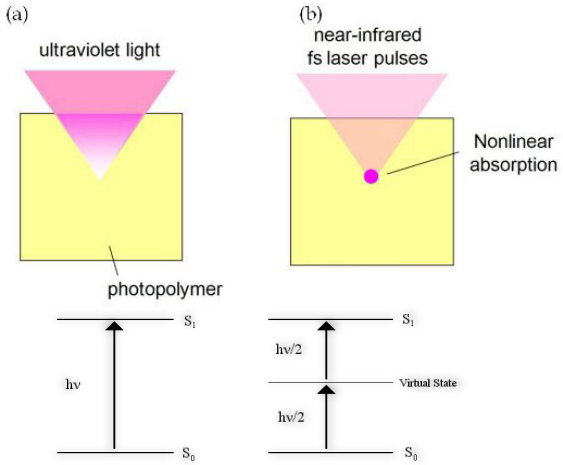

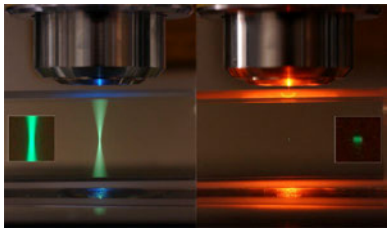

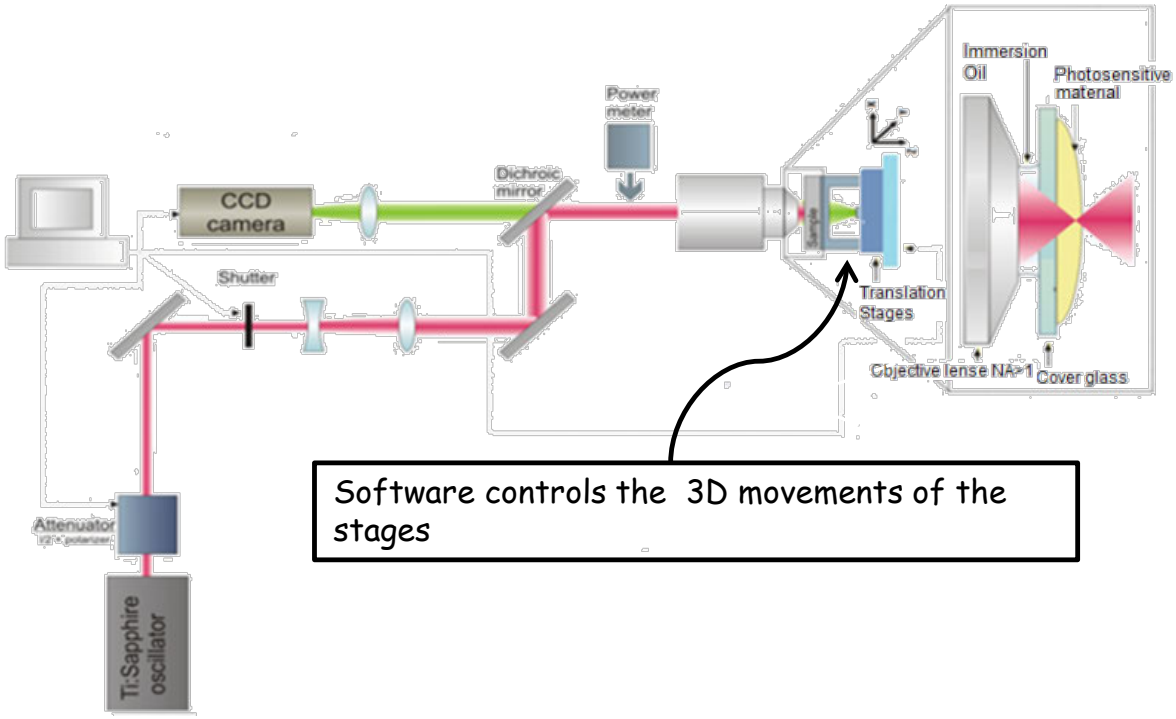

Fabrications steps

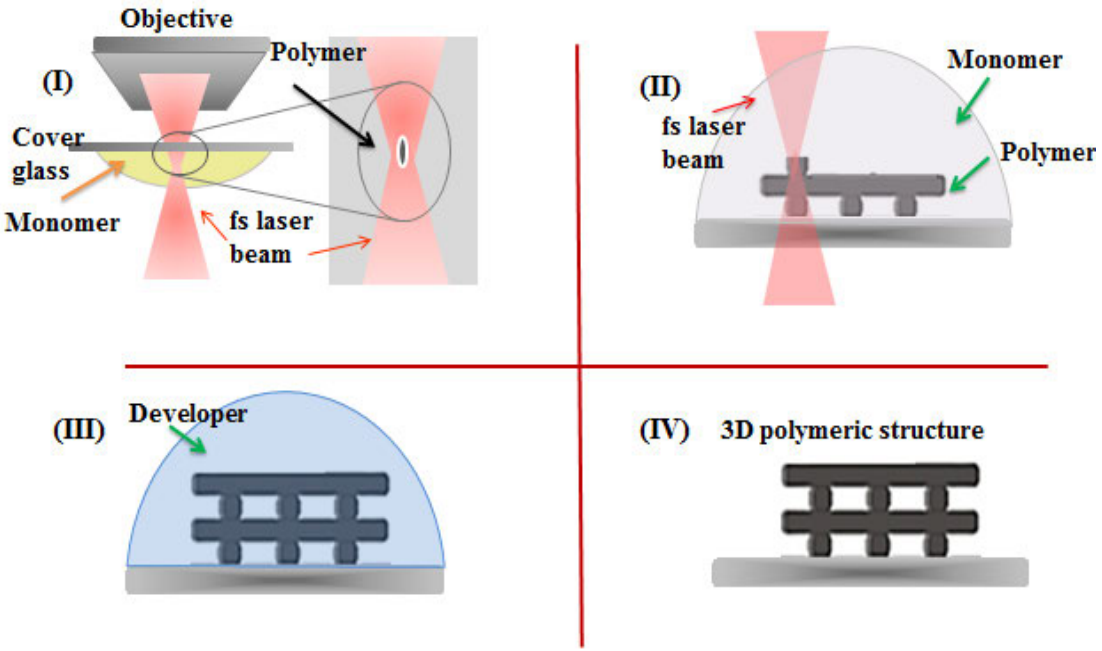

Possibilities

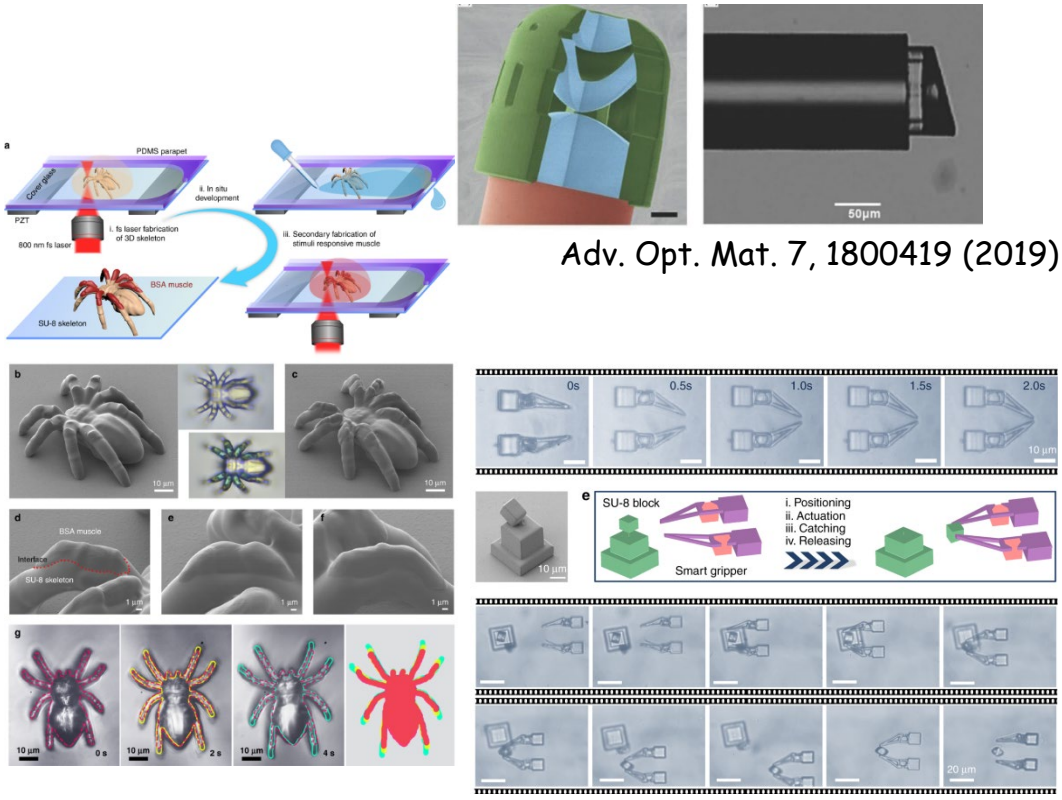

Adv. Opt. Mat. 7, 1800419 (2019)

Nature Commun. 11, 4536 (2020)

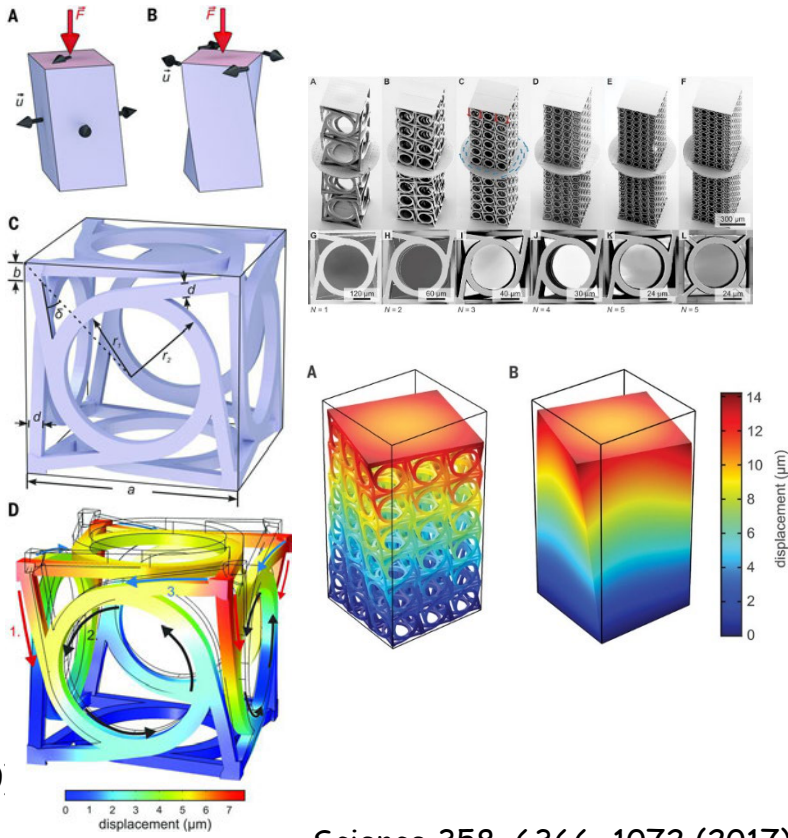

Science 358, 6366, 1072 (2017)

Actuation:
Photo, Thermal, pH, hydrophobic/ hydrophilic, abnormal mechanics

Improve/Advance materials

Selective plating of polymeric structures (binding of Au/Ag nanoparticles)

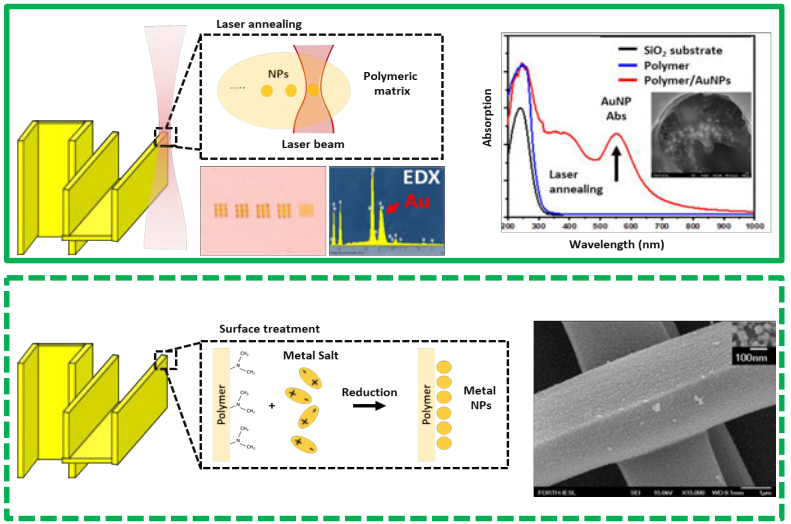

ACS Photonics 2, 287–294 (2015)
Adv. Opt. Mat. 5, 1700200 (2017)

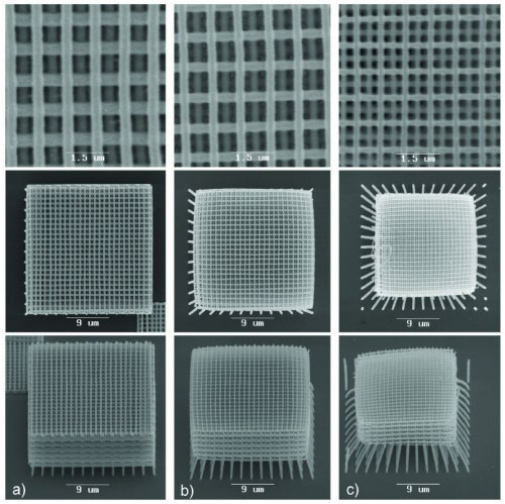

Increasing % of inorganic materia

Opt. Express 17, 2143 (2009)

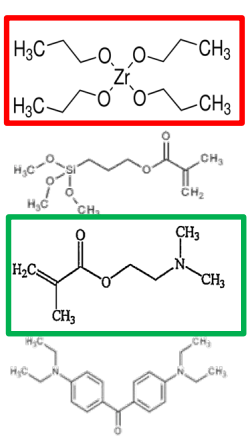

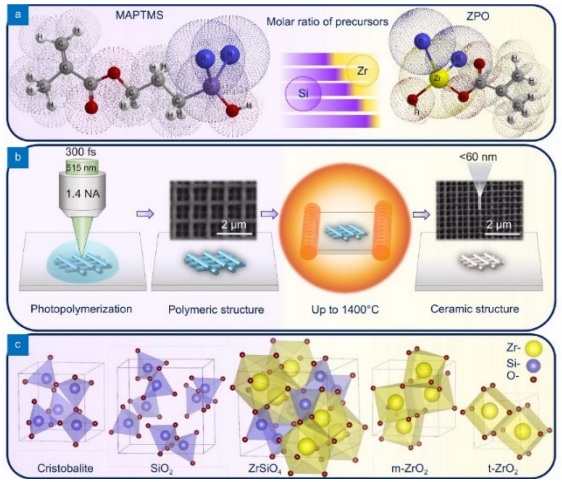

Hollow ceramic 3D structures

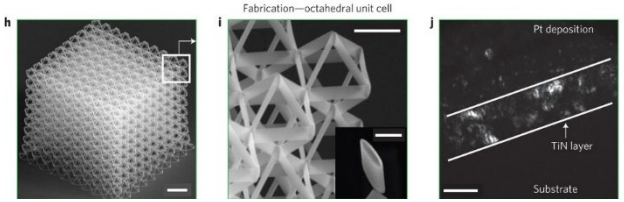

Nature Materials 12, 893 (2013)

From photo resist to ceramic
Opto-Electron Adv X, 210077 (2022)

Equipment & possibilities at Empa

High resolution 3D printer from Nanoscribe

Kelvin foam, advanced mechanical properties

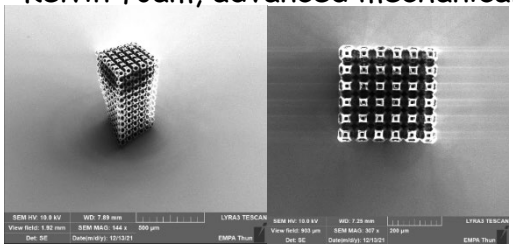

1mm tall
<1hr

ALD deposition to increase opto-mechanics

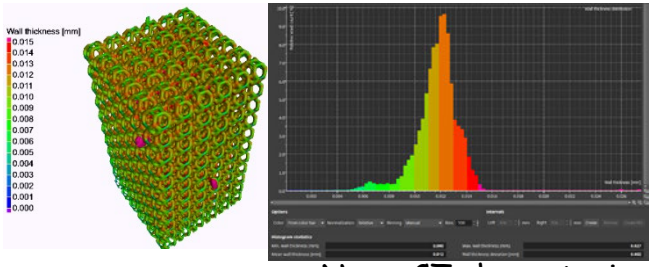

Nano-CT characterisation

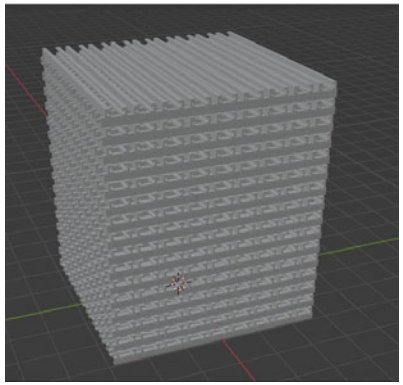

Scaling

Metamaterials with enhanced light-matter interactions

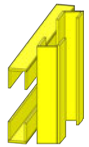

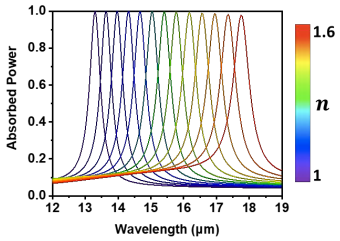

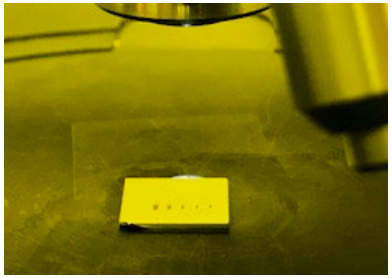

Nanoindentation

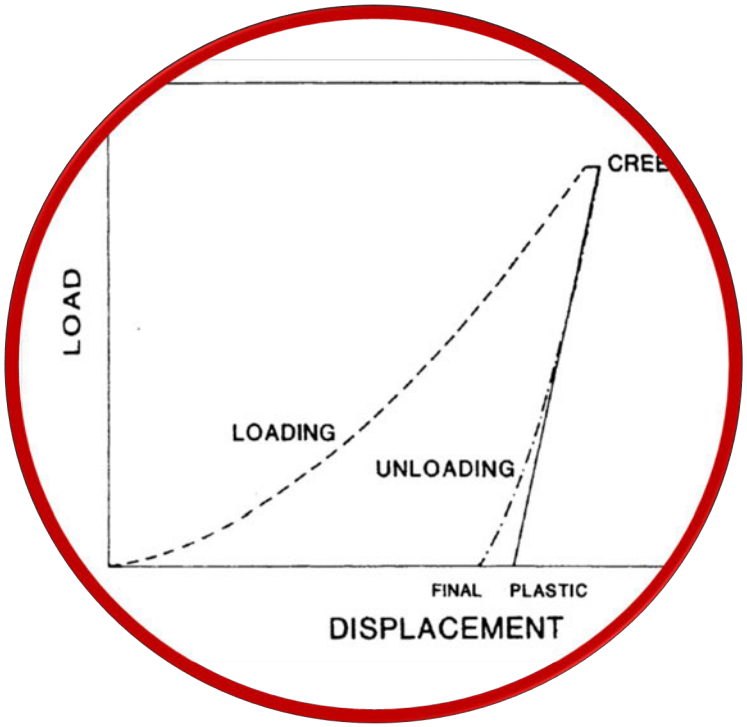

Nanoindentation

1. Definition of hardness

2. Principles of instrumented indentation

3. Load and displacement: actuation and measurement

4. What happens in the material?

5. Mechanical materials properties: beyond hardness and Youngs modulus

Hardness & Young's modulus

hardness: historical definition

Hardness	Mineral
1	Talc
2	Gypsum
3	Calcite
4	Fluorite
5	Apatite
6	Orthoclase
7	Quartz
8	Topaz
9	Corundum
10	Diamond

Mineralogist: resistance to scratching
Metallurgist: resistance to penetration
Machinist: resistance to cutting

Gypsum
Calcite
Fluorite
Apatite
Orthoclase
Quartz
Topaz
Diamond

1812:
Mohs scale of mineral hardness
(German mineralogist Frederich Mohs (1773-1839))

Selected the ten minerals because they were common or readily available.
The scale is not a linear scale, but somewhat arbitrary.

Vickers Hardness Test

Diamond indenter body
(Vickers pyramid)

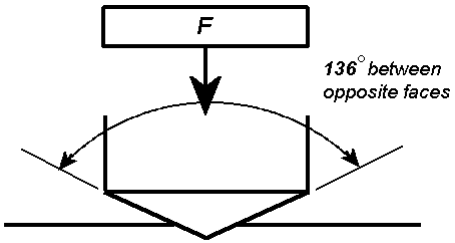

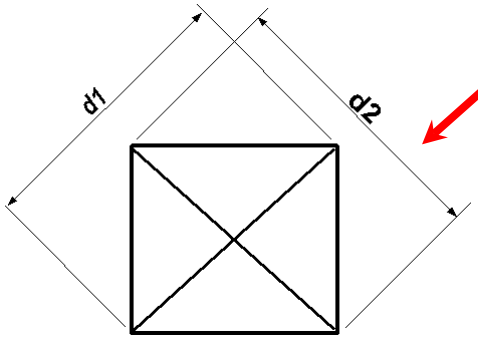

Residual impression
measured
by optical microscopy

$$HV = \frac{2F \sin\frac{136°}{2}}{d^2} \approx 1.854 \cdot \frac{F}{d^2}$$

Load in kgf
d in mm

1 kgf = 9.81 N

$$HV = 0.1891 \cdot \frac{F}{d^2}$$

Load in N
d in mm

Advantage:	„Easy"
Disadvantage:	Operator needed for optical measurement „NOT SUITED" FOR SMALL OBJECTS OR THIN FILMS

A nanoindenter

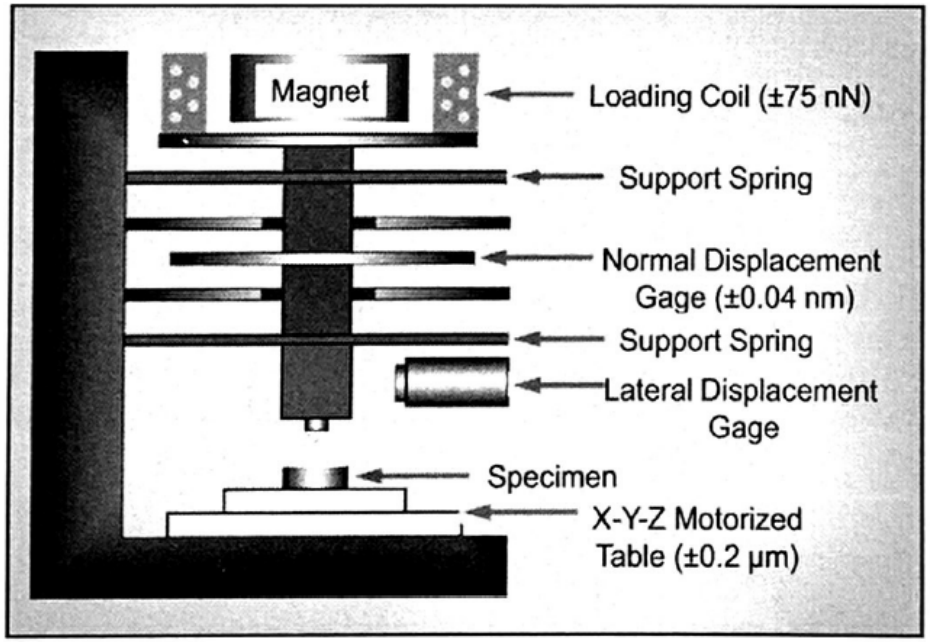

Indentation:

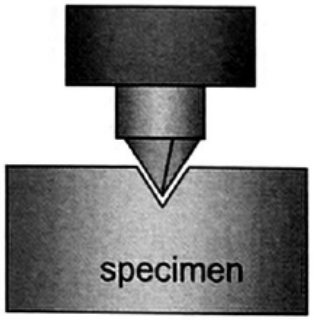

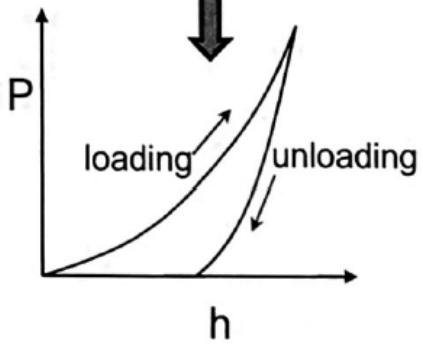

Pillar : Testing

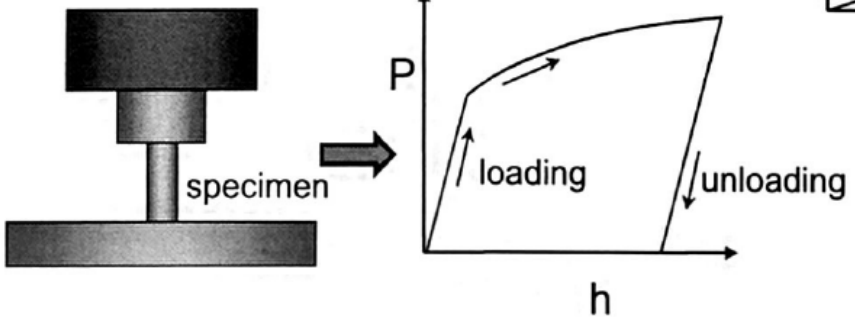

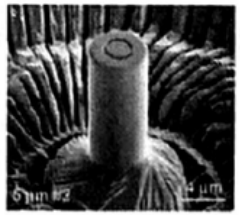

Courtesy GM Pharr, Univ. Texas

Load-Displacement curves: Typical shapes

Extreme cases:

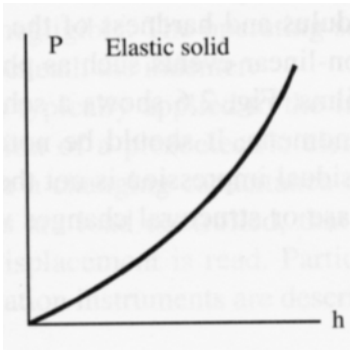

Elastic Solid

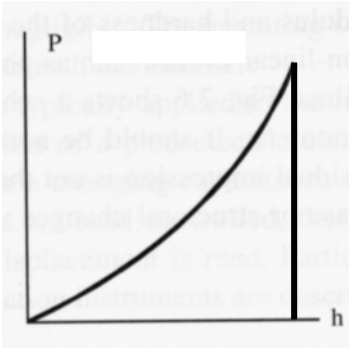

Fully plastic

Load-Displacement curves: Typical shapes

Extreme cases:

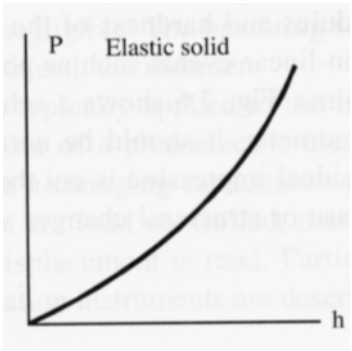

Elastic Solid

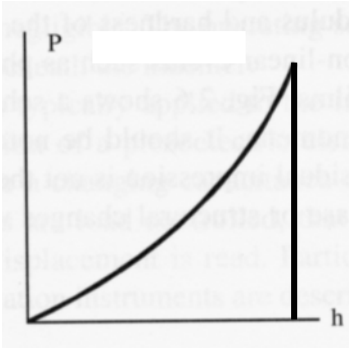

Fully plastic

Typical cases:

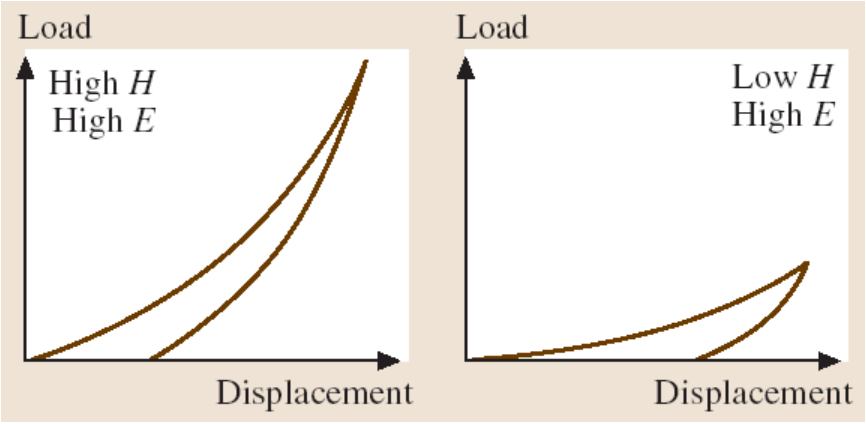

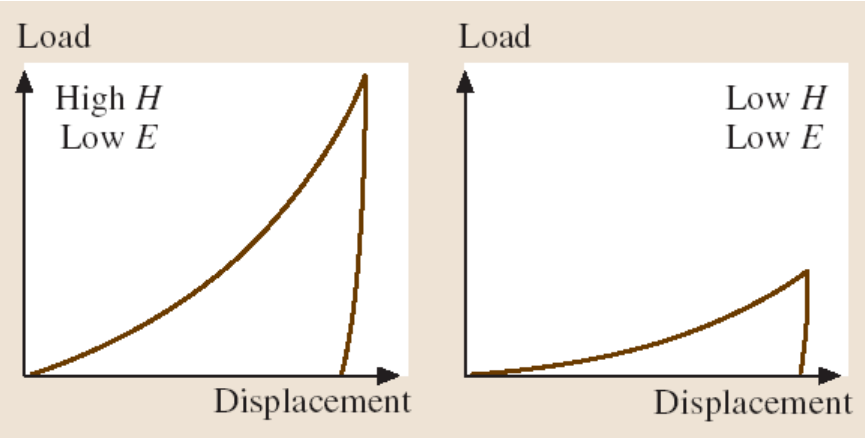

- High hardness ⇔ High load needed for a given displacement
- Young's modulus depends on the shape of the unloading curve

Load-Displacement curves: Typical shapes

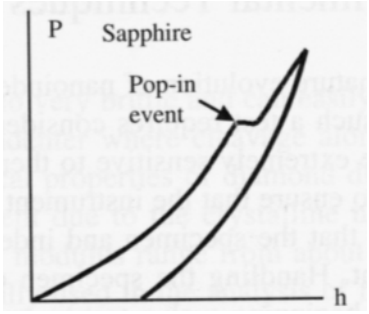

Brittle Solid
Cracking during loading

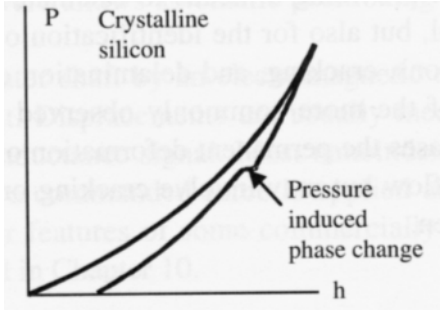

Pressure induced phase change
(Silicon)

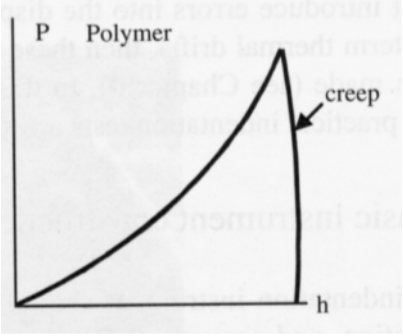

Polymer exhibiting creep

Principle of nanoindentation

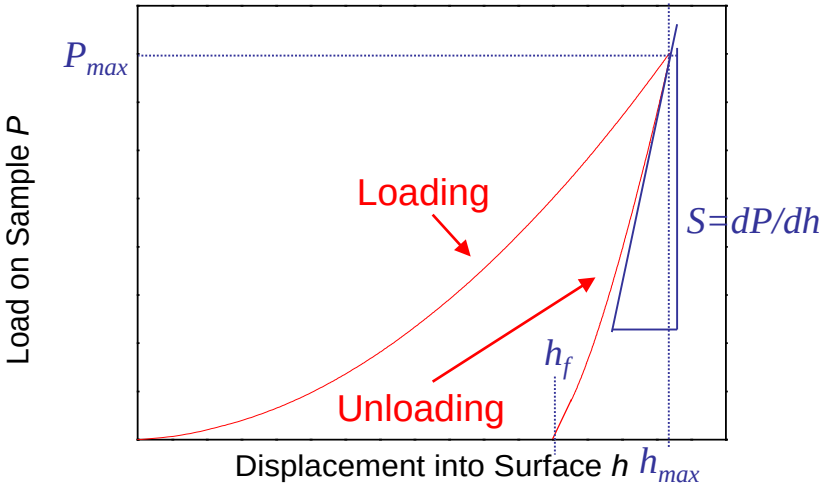

hardness:
Average contact pressure at maximum load (projected area)

Young`s modulus:
proportional to slope of unloading curve

Basic equations

$$E_r = \frac{\sqrt{\pi} \cdot S}{2 \cdot \sqrt{A}}$$

$$\frac{1}{E_r} = \frac{(1-\upsilon^2)}{E_{Indentation}} + \frac{(1-\upsilon_i{}^2)}{E_i}$$

$$H = P/A$$

What determines the contact area?

indenter geometries

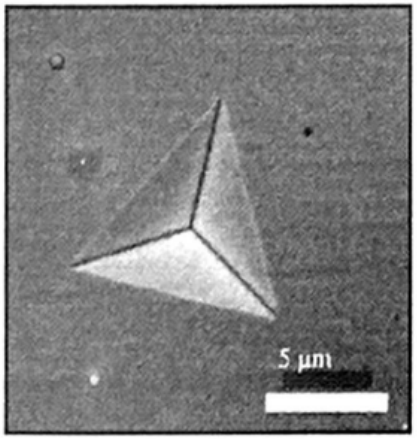

Berkovich

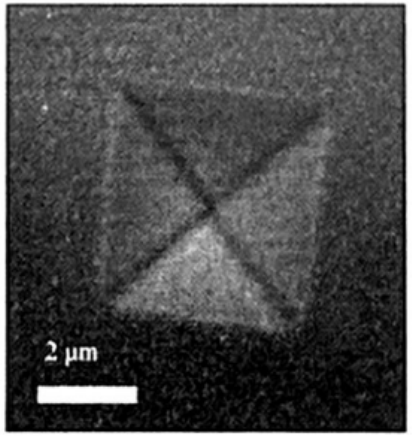

Vickers

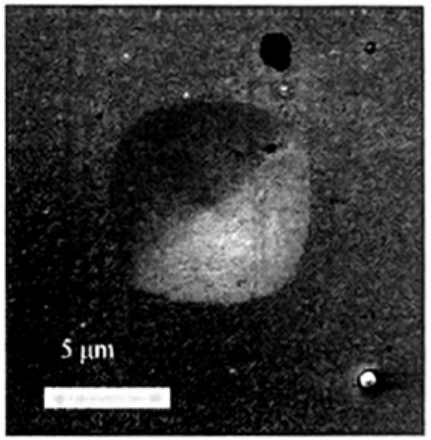

Conical

Berkovich indenter

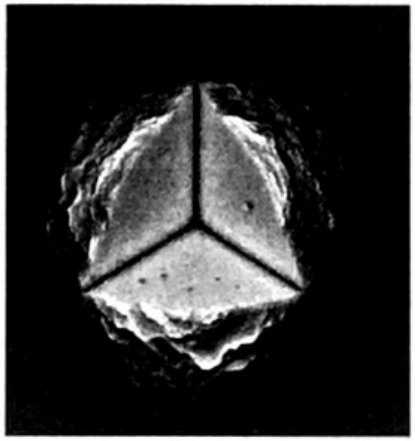

Cube-corner

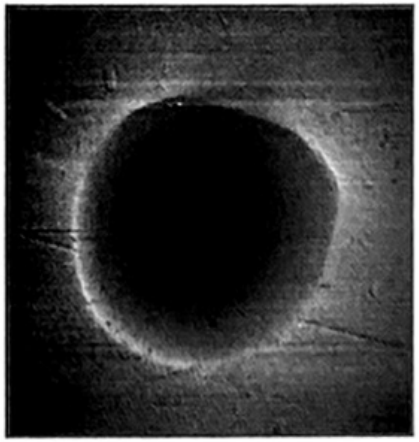

Spherical

Courtesy GM Pharr, Univ. Texas

Tip area function assuming ideal geometries

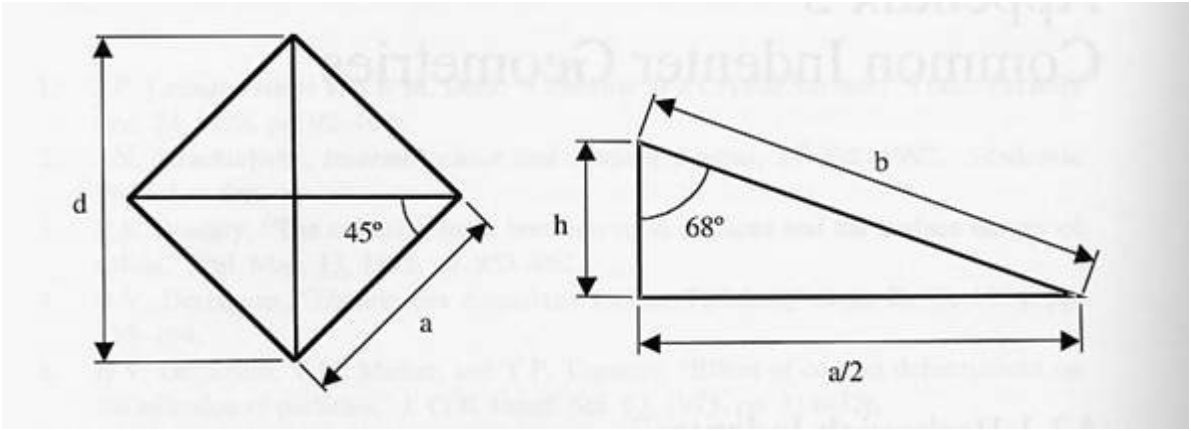

Vickers:

$A_{proj} = 24.504\ h^2$
$A_{surf} = 26.429\ h^2$

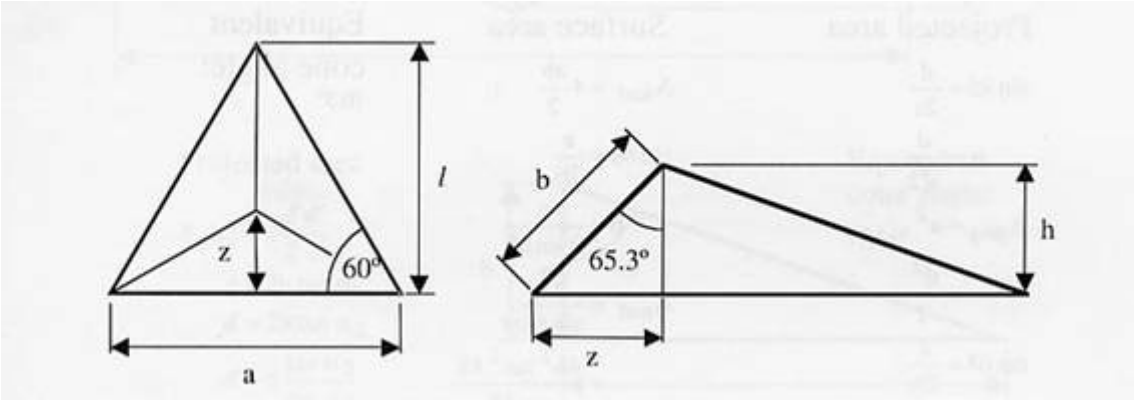

Berkovich:

$A_{proj} = 24.56\ h^2$
$A_{surf} = 27.05\ h^2$

Determination of the tip area function $A(h_c)$

Projected contact area needed for the determination of H and $E_{Indentation}$ is calculated using the displacement into the surface
Crucial point: Exact tip geometry has to be known for this procedure!!

For small indentation depths (<1μm) the assumption of having an ideal tip is not valid.

Berkovich: tip roundness between 20 and 100 nm

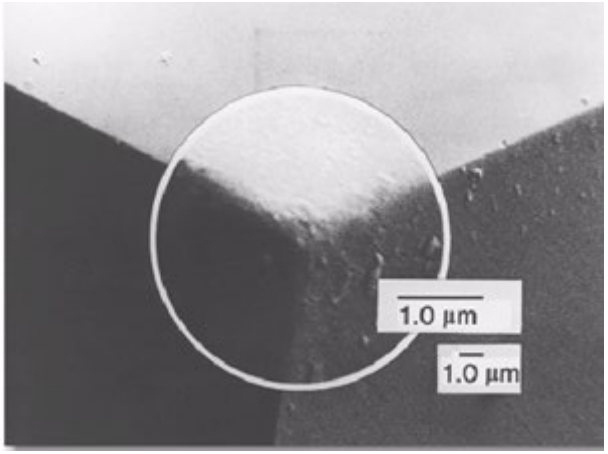

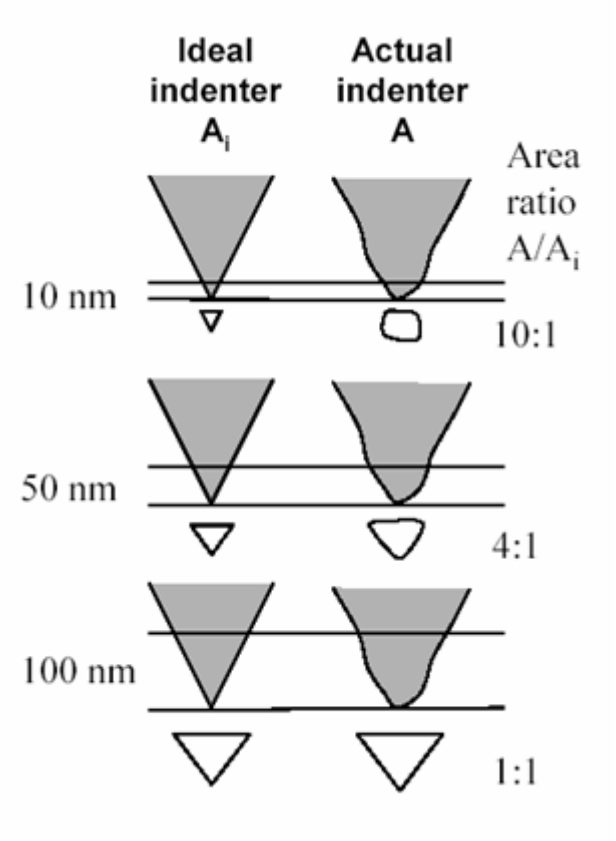

=> Tip area function $$A(h_c) = a_0 \cdot h_c^2 + \sum_{i=0}^{n} a_{i+1} \cdot h_c^{1/2^i}$$

Contact depth

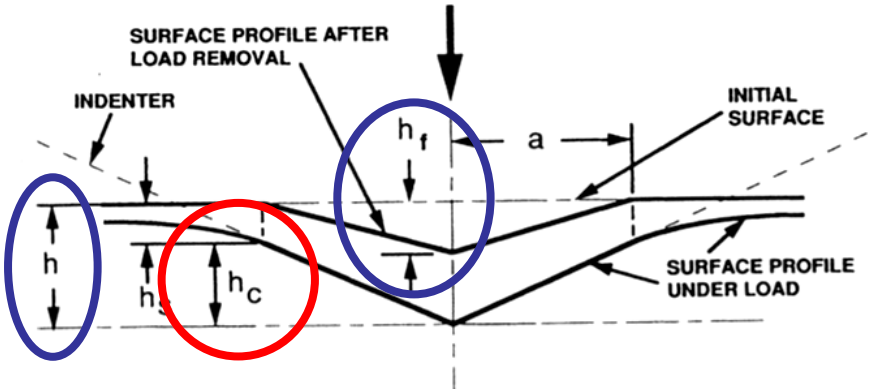

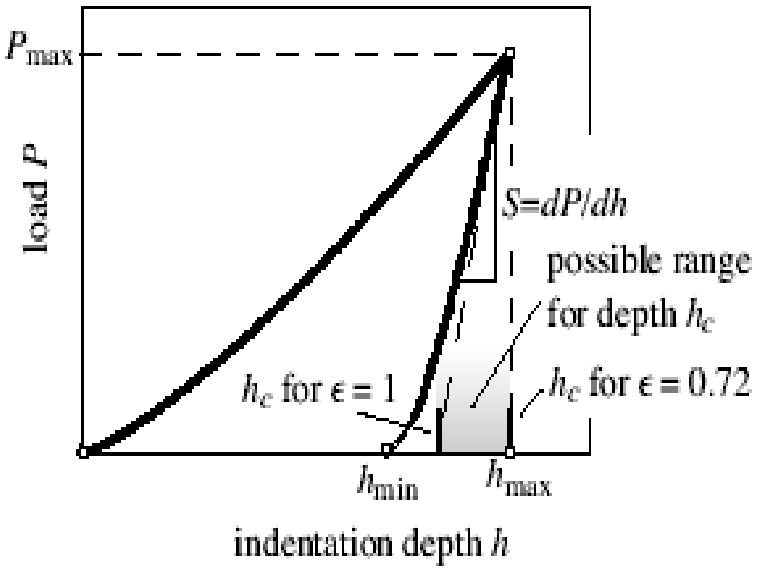

Take into account elastic sink-in!

h	maximum depth
h_f	residual depth
h_c	contact depth

$$h_c = h - \varepsilon \frac{P_{max}}{dP/dh}$$

ε is geometry factor to adapt "Flat Punch" model to Berkovic indenters

Limit of the model: Pile-up and Sink-in

Depending on strain hardening behavior,
pile-up or sink-in phenomena influence the contact depth value
=> errors in contact area => errors in hardness and modulus

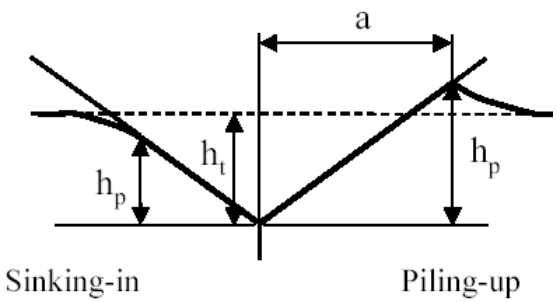

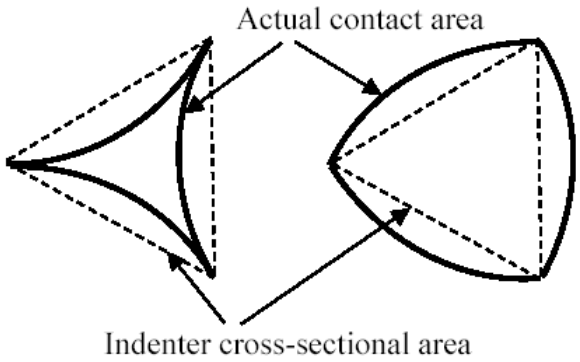

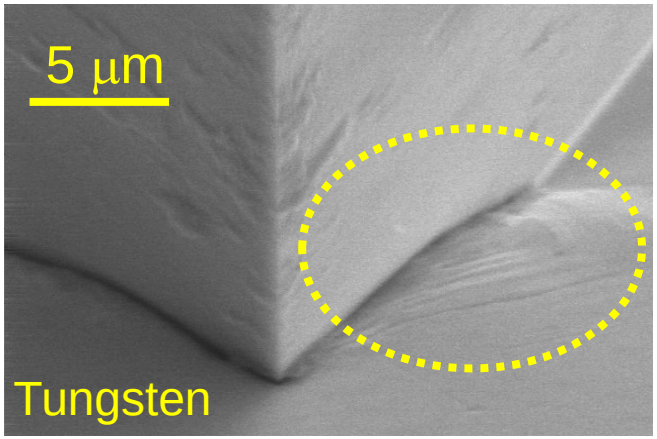

SEM image of cube corner
indent into tungsten

Summary: evaluation of load displacement curves

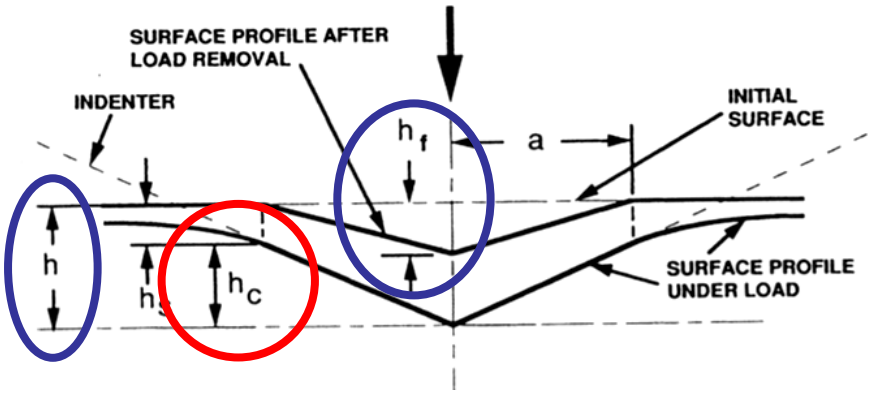

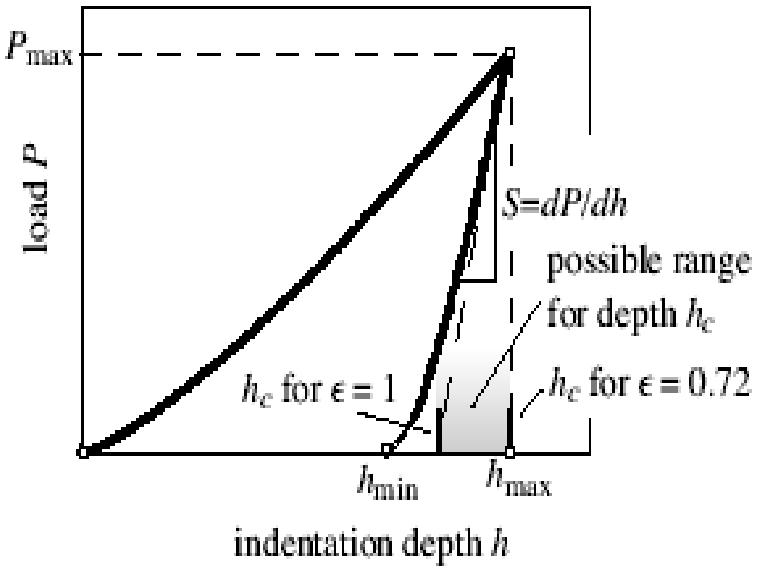

Fit unload curve

$$P = B(h - h_f)^m$$

$$S = dP/dh \longrightarrow S = Bm(h_{max} - h_f)^{m-1}$$

Projected contact area

$$h_c = h - \varepsilon P/S$$

$$A(h_c) = a_0 \cdot h_c^2 + \sum_{i=0}^{n} a_i \cdot h_c^{1/2^i}$$

a_i is determined from measurements on reference materials (Fused Silica)

Ideal Berkovich tip: a_0=24.5 / a_i=0 für i>0

Summary H and E

$$E_r = \frac{\sqrt{\pi} \cdot S}{2\beta \cdot \sqrt{A(h_c)}}$$

$$\frac{1}{E_r} = \frac{(1-\upsilon^2)}{E_{Indentation}} + \frac{(1-\upsilon_i^2)}{E_i}$$

$$H = P/A(h_c)$$

ε,β are geometry factors to adapt flat punch model to Berkovic geometry

Limit of the model: Pile-up and Sink-in

Pile-up or sink-in phenomena influence the contact depth value
=> errors in contact area => errors in hardness and modulus

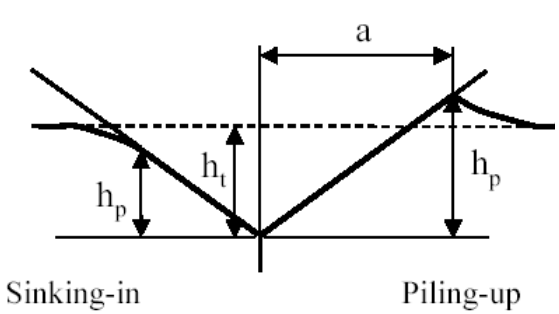

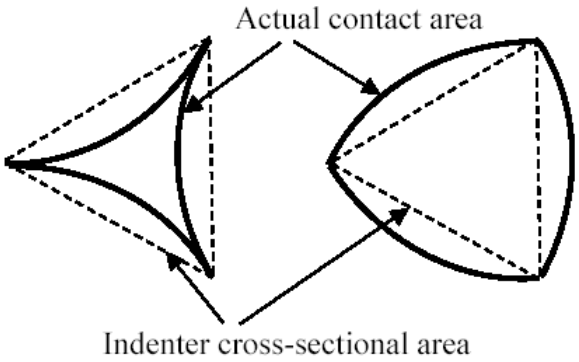

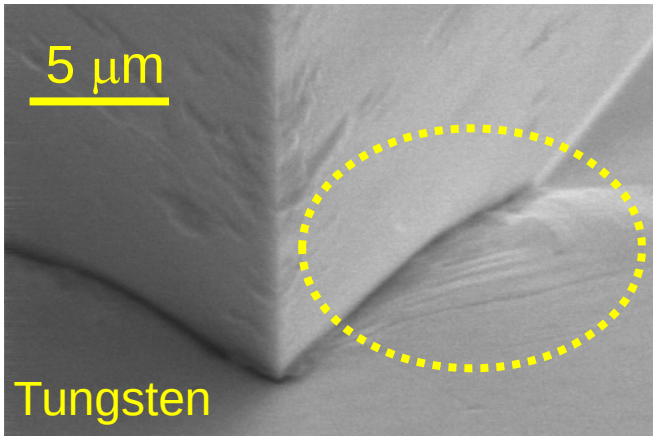

Limit of the model: Pile-up and Sink-in

Pile-up or sink-in phenomena influence the contact depth value
=> errors in contact area => errors in hardness and modulus

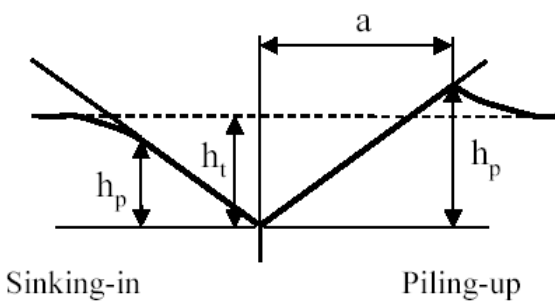

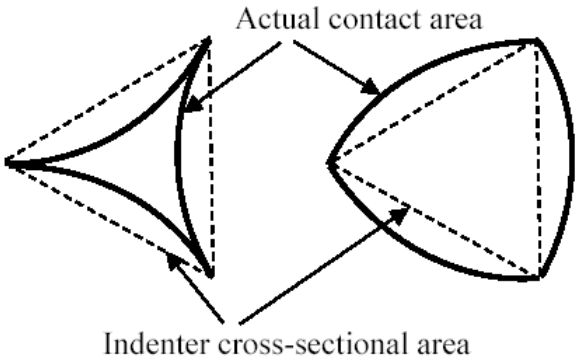

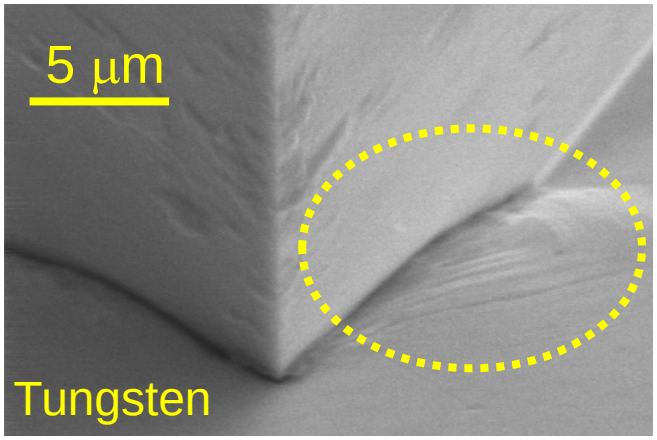

Correction factor: (from finite element simulations)

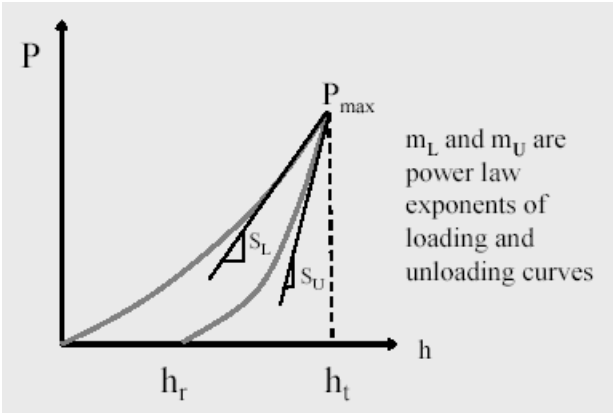

$$\frac{S_L}{S_U} = \frac{m_L}{m_U}\left(1 - \frac{h_r}{h_t}\right)$$

2 — m_L — h_r: Residual depth; h_t: Total depth; m_U: 1.35; S_L, S_U: Pile-up, Sink-in factor. Can be applied to calculated contact area to obtain true contact area.

in-situ measurement of contact area

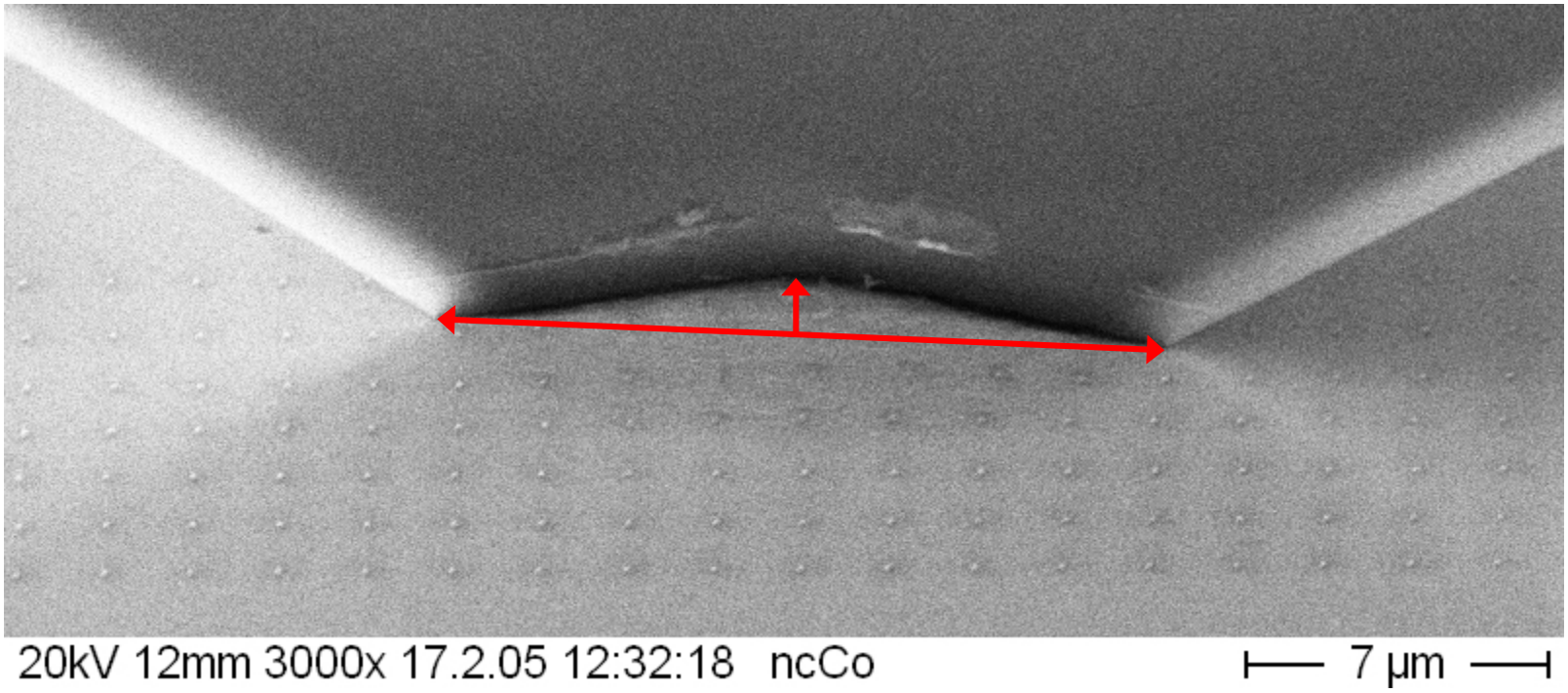

contact area of PDMS

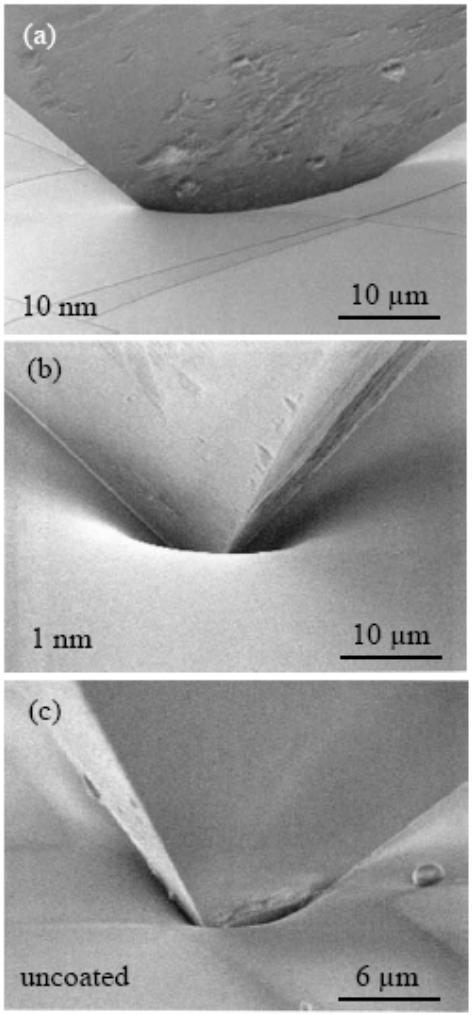

Figure 8

influence of gold layer

J. Deuschle (2008) J. Mater. Res.

contact area of glassy carbon

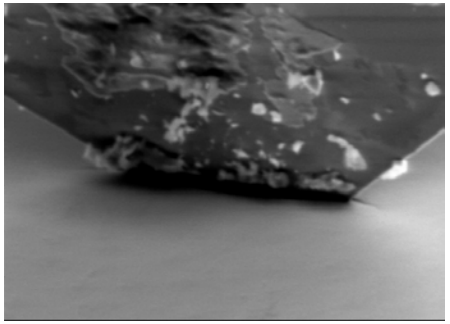

max.load

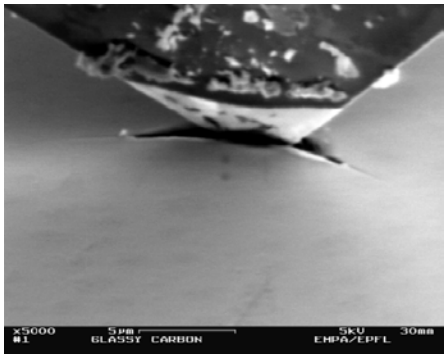

partial
unloading

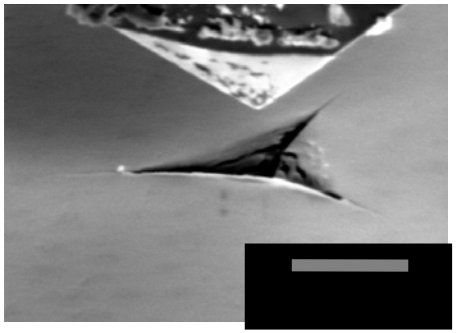

complete
unloading

Determination of tip area function $A(h_c)$

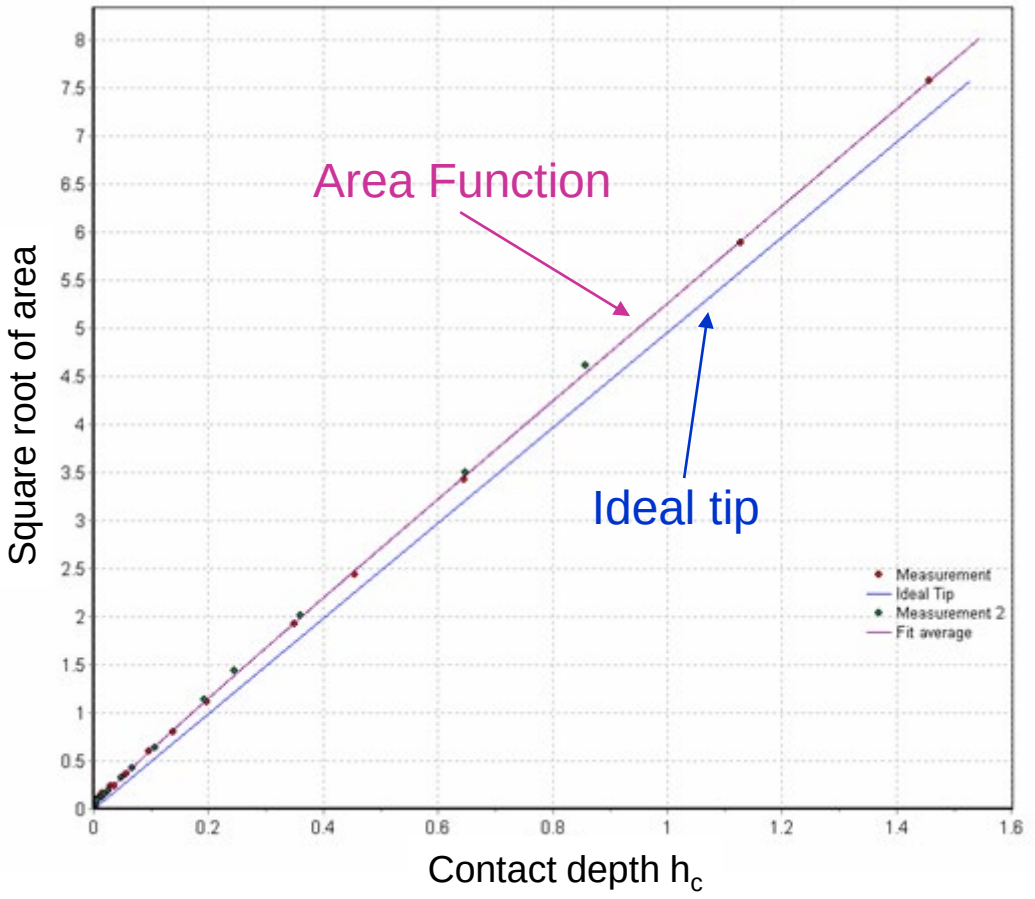

Reference Materials (typical):
Quartz E = 72 GPa
Sapphire E = 420 GPa

Load-Displacement curves on both materials are measured at different loads (500mN – 300μN)

Coefficents are adjusted to obtain the best modulus values for both reference values

$$\sqrt{A(h_c)} = a_0 + a_1 \cdot h_c^{0.25} + a_2 \cdot h_c^{0.5} + a_3 \cdot h_c + a_4 \cdot h_c^{1.5}$$

a1 = 0.0955987
a2 = -0.214813
a3 = 0.462383
a4 = 4.78958
a5 = 0.104144

Instrument stiffness

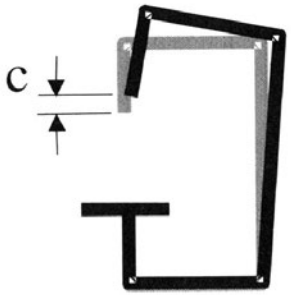

Problem: stiffness of the machine

$$\frac{dh}{dP} = \frac{1}{S} + C_f$$

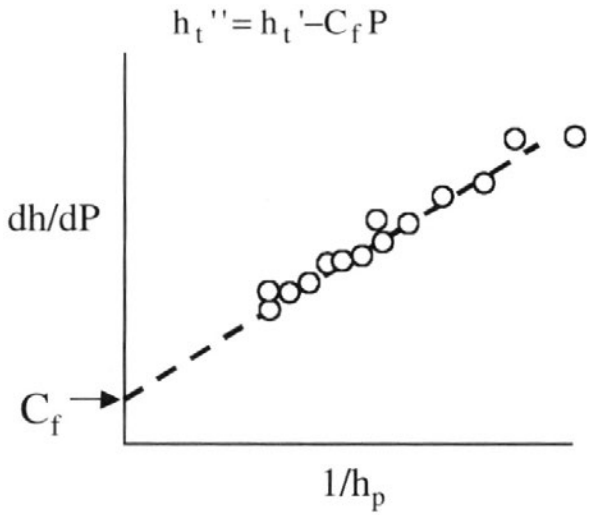

Use reference materials with known E

$$\frac{dh}{dP} = \sqrt{\frac{\pi}{24.5}} \frac{1}{2E^*} \frac{1}{h_p} + C_f$$

Surface Detection

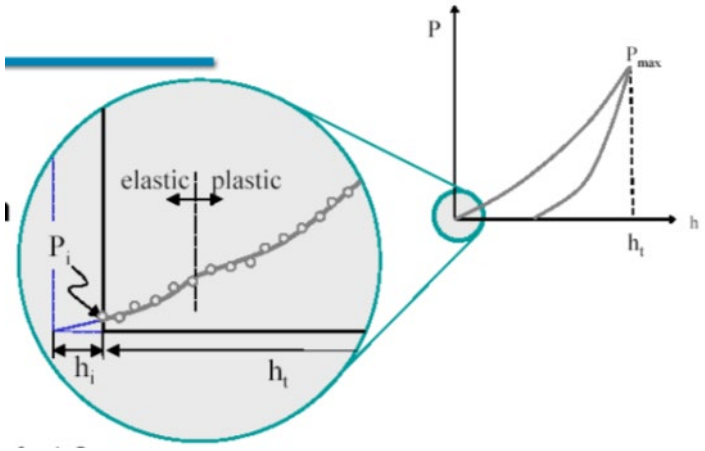

$$h' = h + h_i$$

corrected depth

initial depth h_i

measured depth (from instrument)

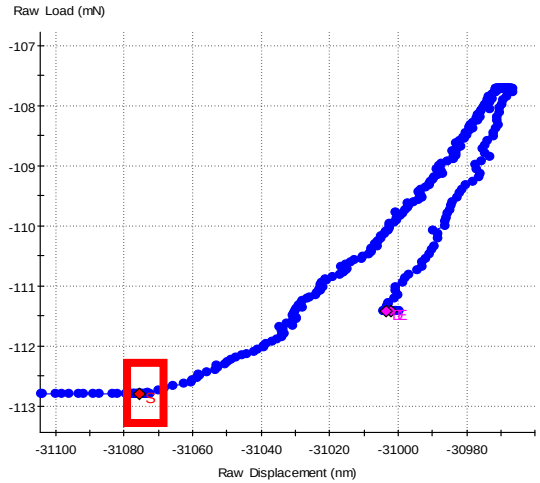

How to estimate h_i?

1. Estimate by eye the intercept with the depth axis
2. Fit a polynomial by least squares method to the initial loading data and extrapolate back to zero load.
3. Fit the Hertz equations for elastic contact to the initial loading data and extrapolate back to zero load.

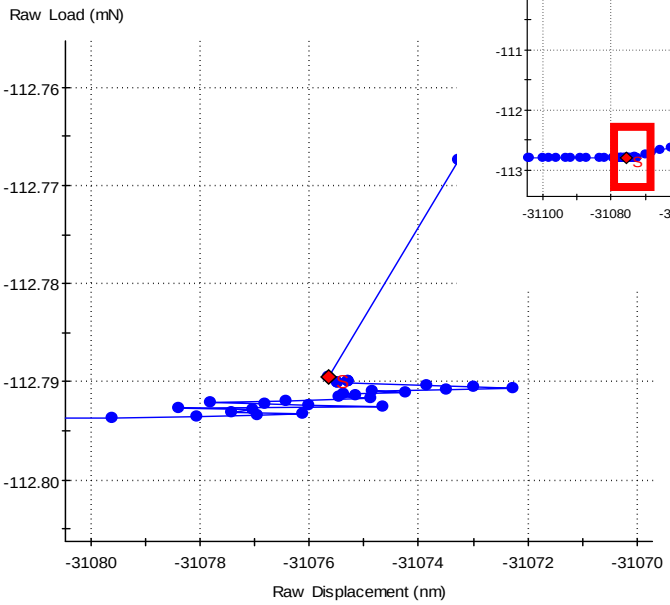

Surface Roughness

Low surface roughness

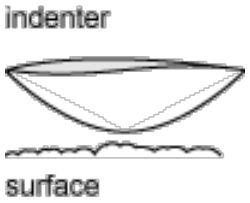

well-defined

Contact Area

High surface roughness

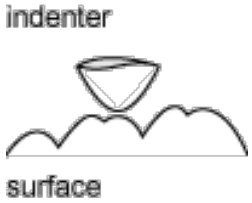

ill-defined

"Rule": $h_{max} > 20\ R_a$

Caution:
Polishing the sample surface results in a reduced roughness but considerable work hardening my occur

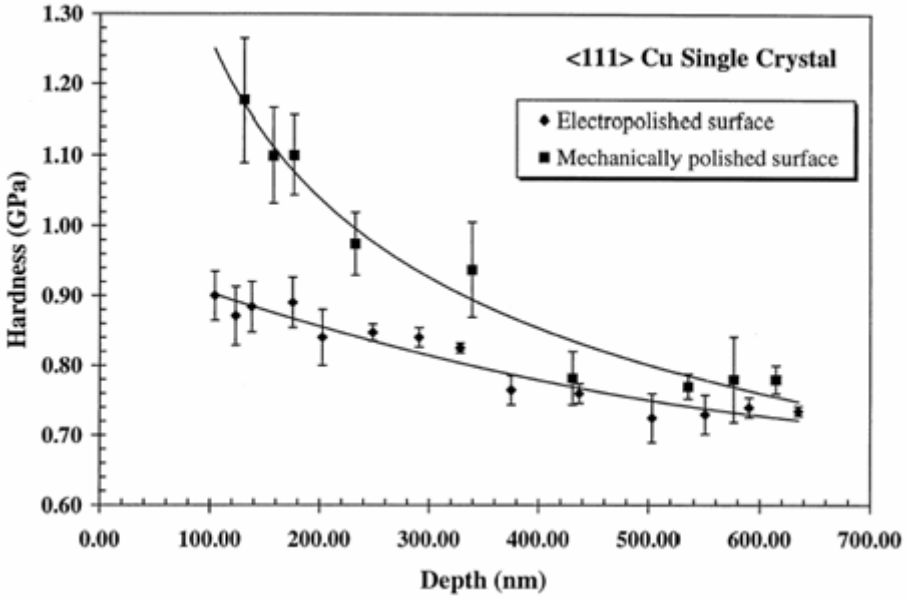

"A typical measurement"

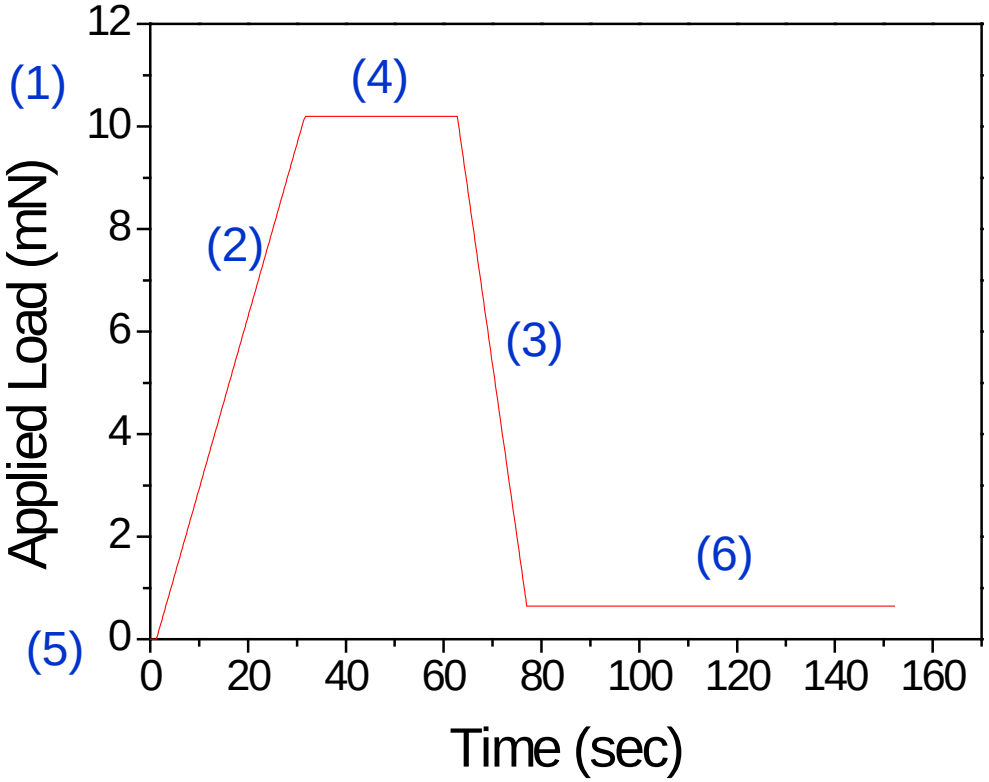

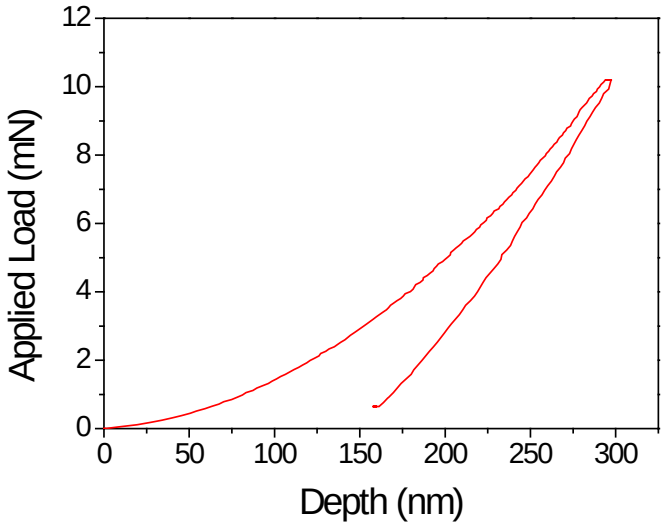

The loading - unloading cycle is load-controlled
Normally a constant load rate is used

Input Parameters:

(1) F_{max}
(2) Time to load / loading rate
(3) Time to unload / unloading rate
(4) Hold period @ F_{max}
(5) Load for 2nd hold period after partial unloading
(6) Period of 2nd hold period after partial unloading

Hold periods

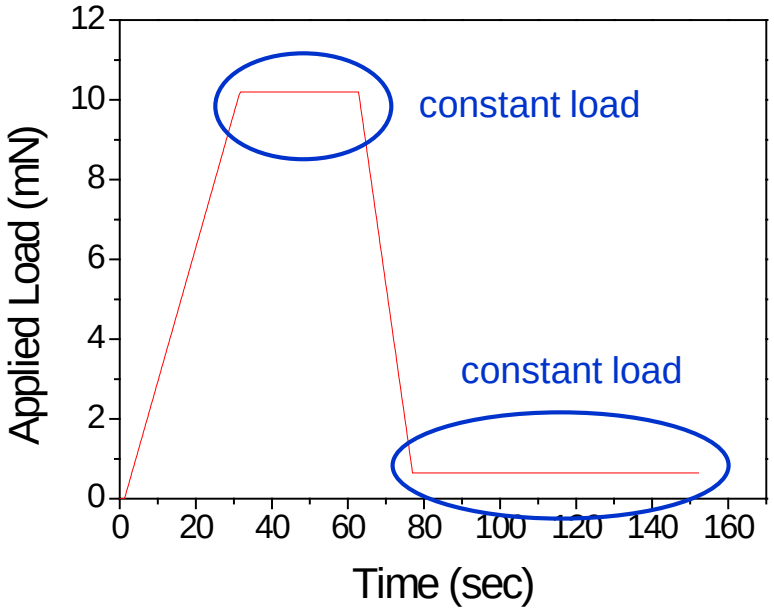

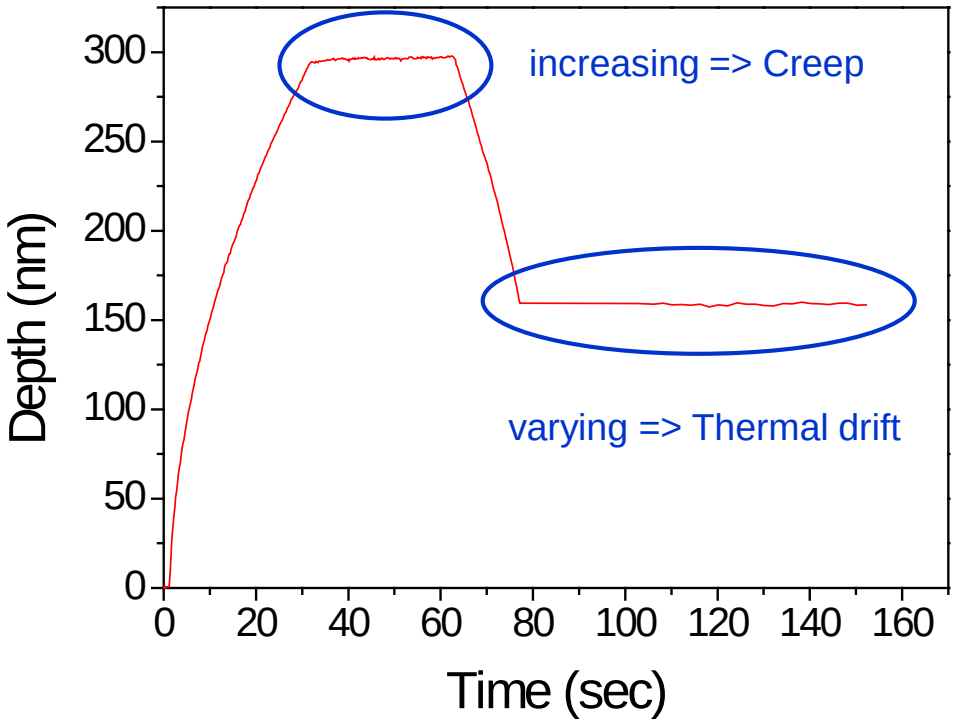

Thermal drift

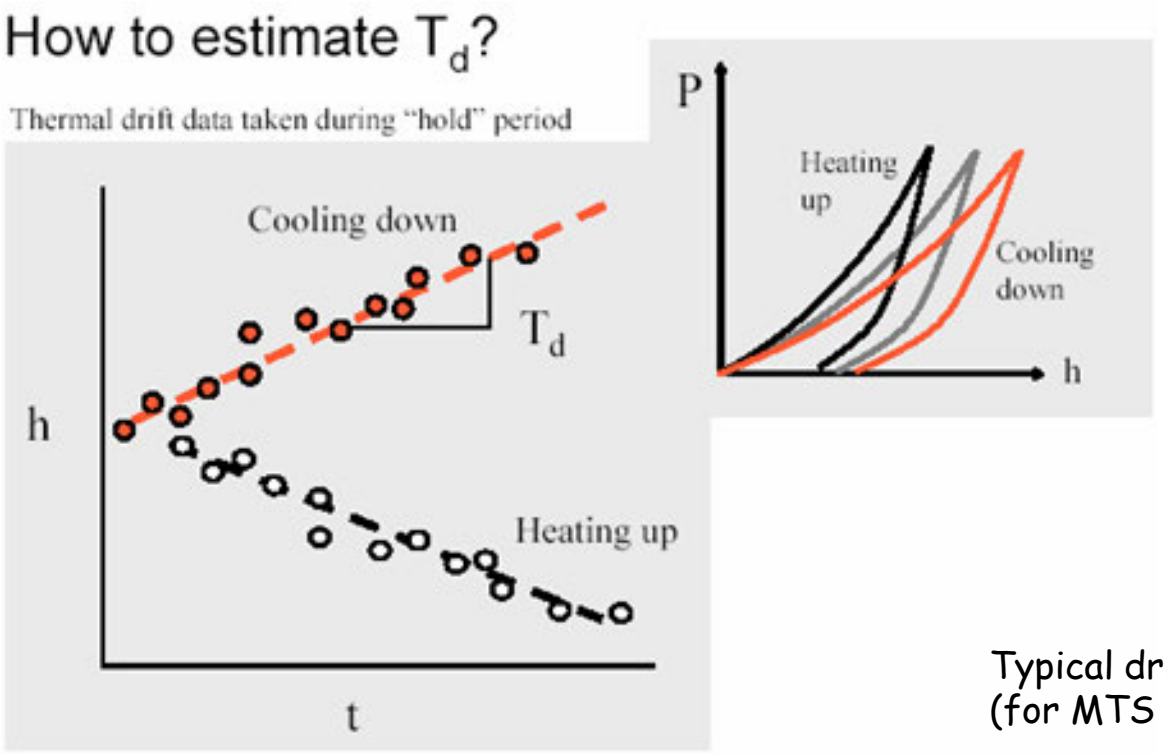

$$h' = h - T_d \cdot t$$

Typical drift values below 0.05 nm/sec
(for MTS Nanoindenter @ Empa Thun)

Strain rate in indentation tests

Tensile are normally performed with displacement-controlled machines at constant strain rate

With pyramidal indenters it is possible to perform constant strain rate experiments with load-controlled nanoindenters

$$\dot{\varepsilon} = \frac{\dot{P}}{P} = \frac{\dot{h}}{h} = const$$

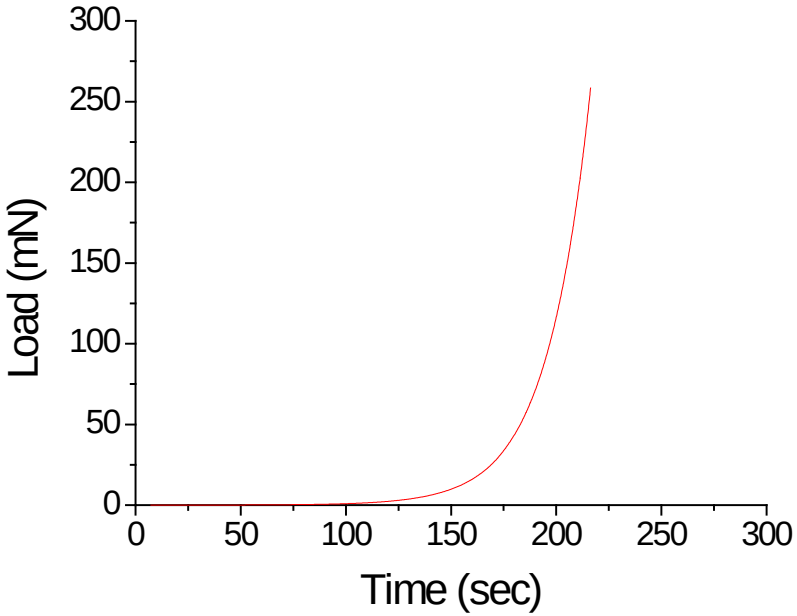

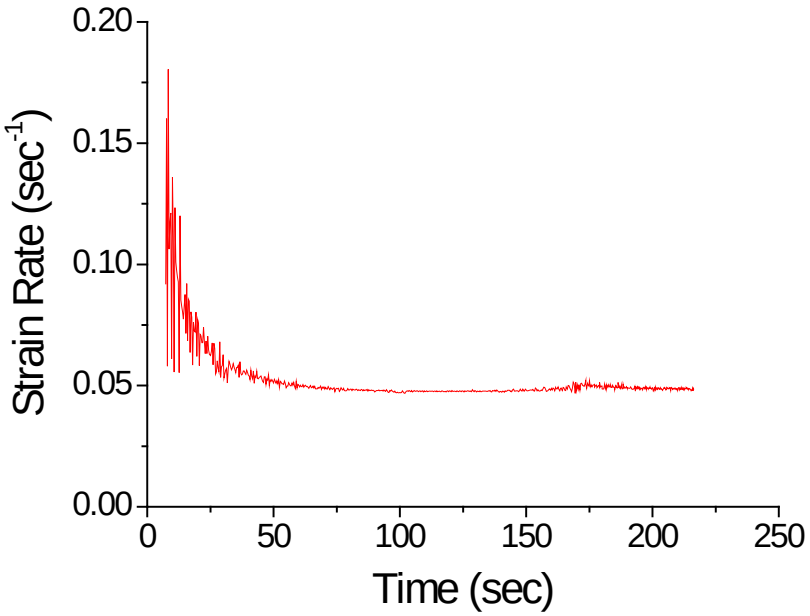

Surface Roughness

Low surface roughness

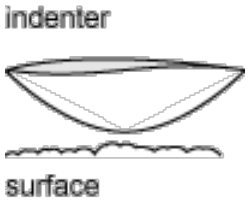

well-defined

Contact Area

High surface roughness

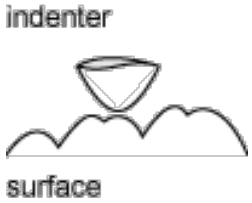

ill-defined

"Rule": $h_{max} > 20\ R_a$

Caution:
Polishing the sample surface results in a reduced roughness but considerable work hardening my occur

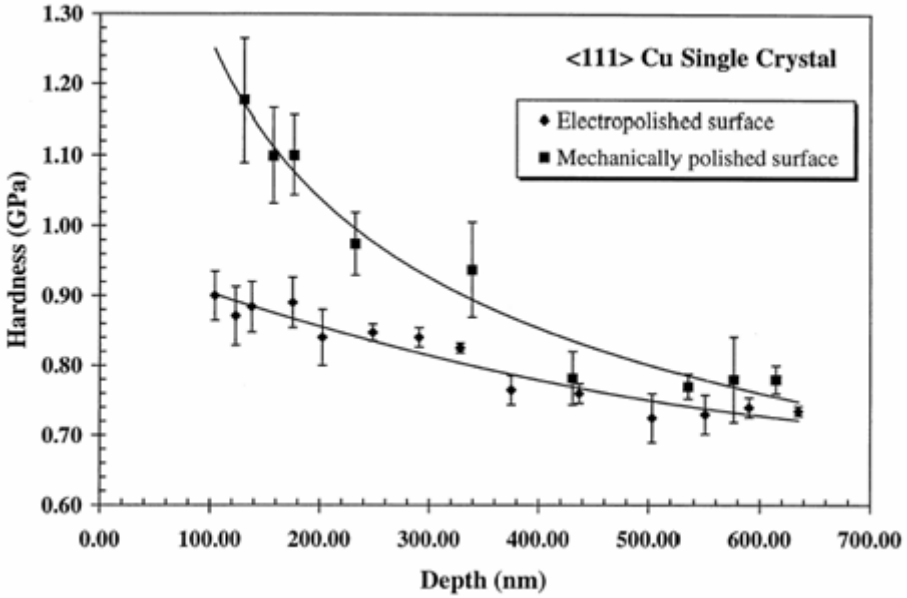

Indentation Size Effects (ISE)

Soft materials (Fe, Al, Cu) with surface contaminant layers (oxides, carbides)
=> dislocations pinned
=> higher hardness values @ small indentation depths

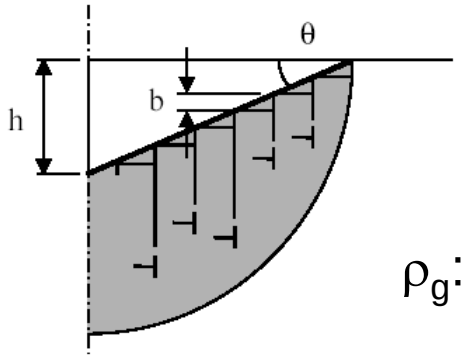

$$\rho_g = \frac{3}{2bh}\tan^2\Theta$$

ρ_g: dislocation density

circular dislocation loops serve to increase the effective yield strength

Nix & Gao, J. Mech. Phys. Solids 46(3) 1998, pp. 411-425

Other ISE effects:
- Real shape of indentation pyramid
- Sample surface roughness, surface polishing

Dynamic Contact Models

Principle:
A small AC load is superimposed to the DC load.
The contact stiffness S can be calculated throughout the complete indentation cycle.

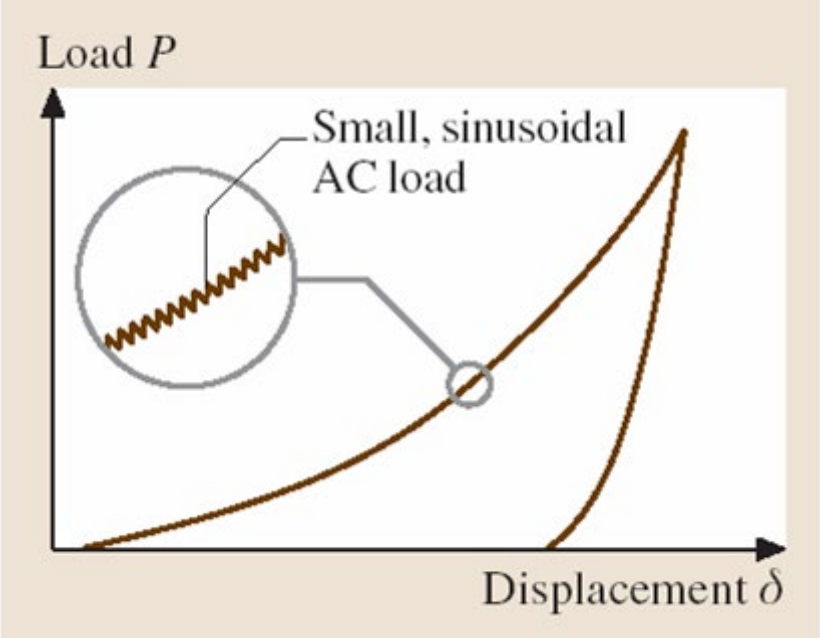

Typical frequency ≈ 60 Hz

The AC load creates a dynamic system with the sample acting as a spring with stiffness S (contact or unloading stiffness) and the nanoindentation system as a series of springs and dampers

Nanoindentation equipment: load actuation & displacement measurement

Load actuaction

Electromagnetic actuation:

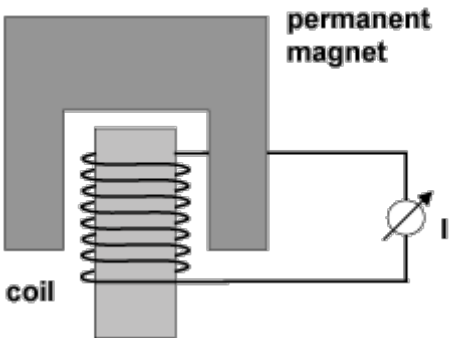

Advantages:

- long displacement range (up to mm)
- linear current-load behavior
- wide load range (mN to N)
- can be used to pick up the indenter as well as to push it down

Disadvantages:

- large (≈10cm) and heavy (order of kg)
- current in the coil => heat => thermal drift

By varying the current, *I*, through the coil, a magnetic field is generated that interacts with the magnetic field of the permanent magnet.

Calibration:
Hanging a series of weights to the indenter shaft and recording the load current to lift the shaft to the same position for each weight

Load actuaction

Electrostatic actuation:

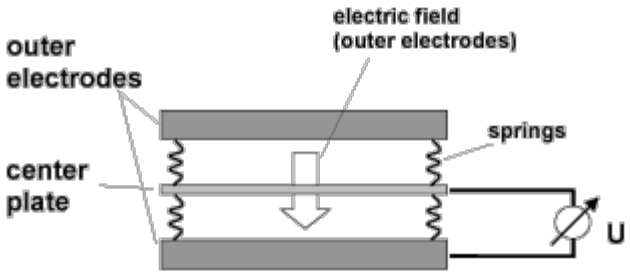

Advantages:

- small size of the system (in the order of tenths of mm)
- good temperature stability

Disadvantages:

- limited load range (in the order of tenths of mN)
- limited displacement range (in the order of tens of μm)
- usually only one possible direction of tip movement

The load is applied by an electrostatic force generated between the center plate and the upper or lower plate of a three-plate transducer system.

The applied load is proportional to the square of the voltage.

Load actuaction

Actuation through springs:

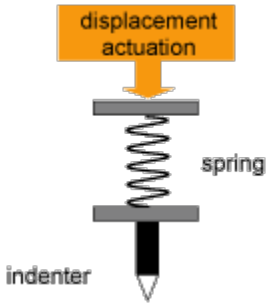

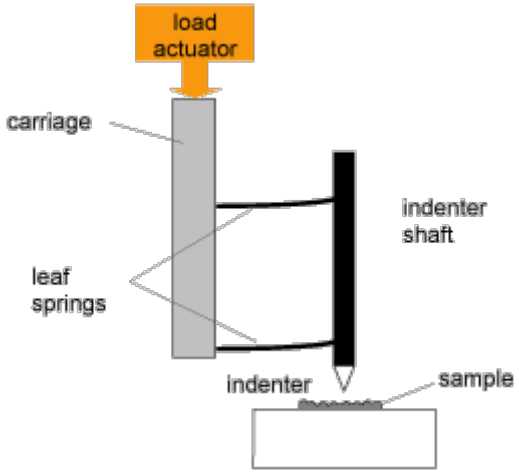

Range vs. resolution: In principle, very high force resolutions are possible. Cantilever based devices commonly report force resolutions in the pN range, or better. However, as resolution goes up, range goes down.

Geometric stability: One of the main disadvantages of using a cantilever is that the tip rotates as the load on it is increased.

Force response: The higher the force resolution, the greater are the displacements needed to change that force. The rate at which the force can be changed is limited in such machines.

Calibrations: Force calibration depends on accurate knowledge of the spring constant and the relative displacements.

Displacement measurement

Capacitive:

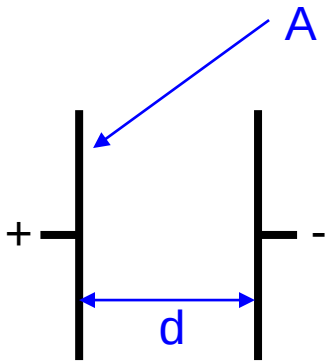

Paralell plate capacitor:

$$C = \frac{\varepsilon\varepsilon_0 A}{d}$$

Differential capacitor:

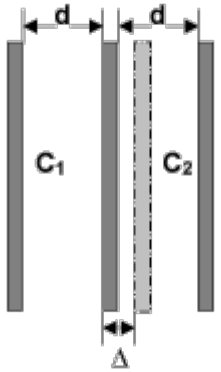

Difference between C_1 and C_2 is measured

Advantages:

- can be of very high precision (resolution below 1Å)
- small size

Disadvantages:

- total displacement range is relatively small

Displacement measurement

Linear Variable Differential Transducer (LVDT):

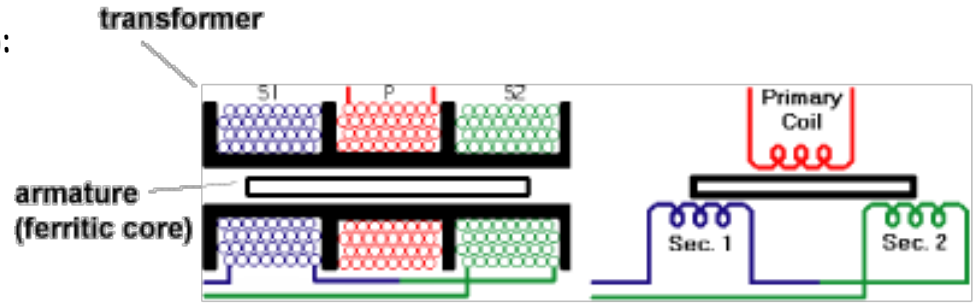

Advantages:

- relatively low cost due to its popularity
- solid and robust, capable of working in a wide variety of environments
- high signal to noise ratio
- negligible hysteresis
- no permanent damage to the LVDT if measurements exceed the designed range

Disadvantages:

- lower resolution compared to a capacitive displacement measurement
- core must be in contact (directly or indirectly) with the measured surface

Displacement measurement

Optical lever methods:

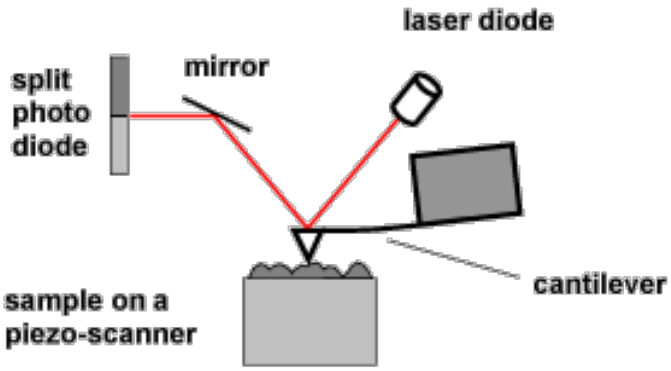

Used for example to measure the deflection of beams
Most of the Atomic Force Microscopes (AFM) use this principle

Very high sensitivity (below 1Å) is possible

Nanoindentation
other experimental aspects

Nanoindentation experiments on thin films

Advantage:
Film can be measured without removing it from the substrate
Spatial distribution in lateral & vertical direction

Chief difficulty:

Avoiding unintentional probing of substrate properties

1μm Al on glass (soft coating on hard substrate)

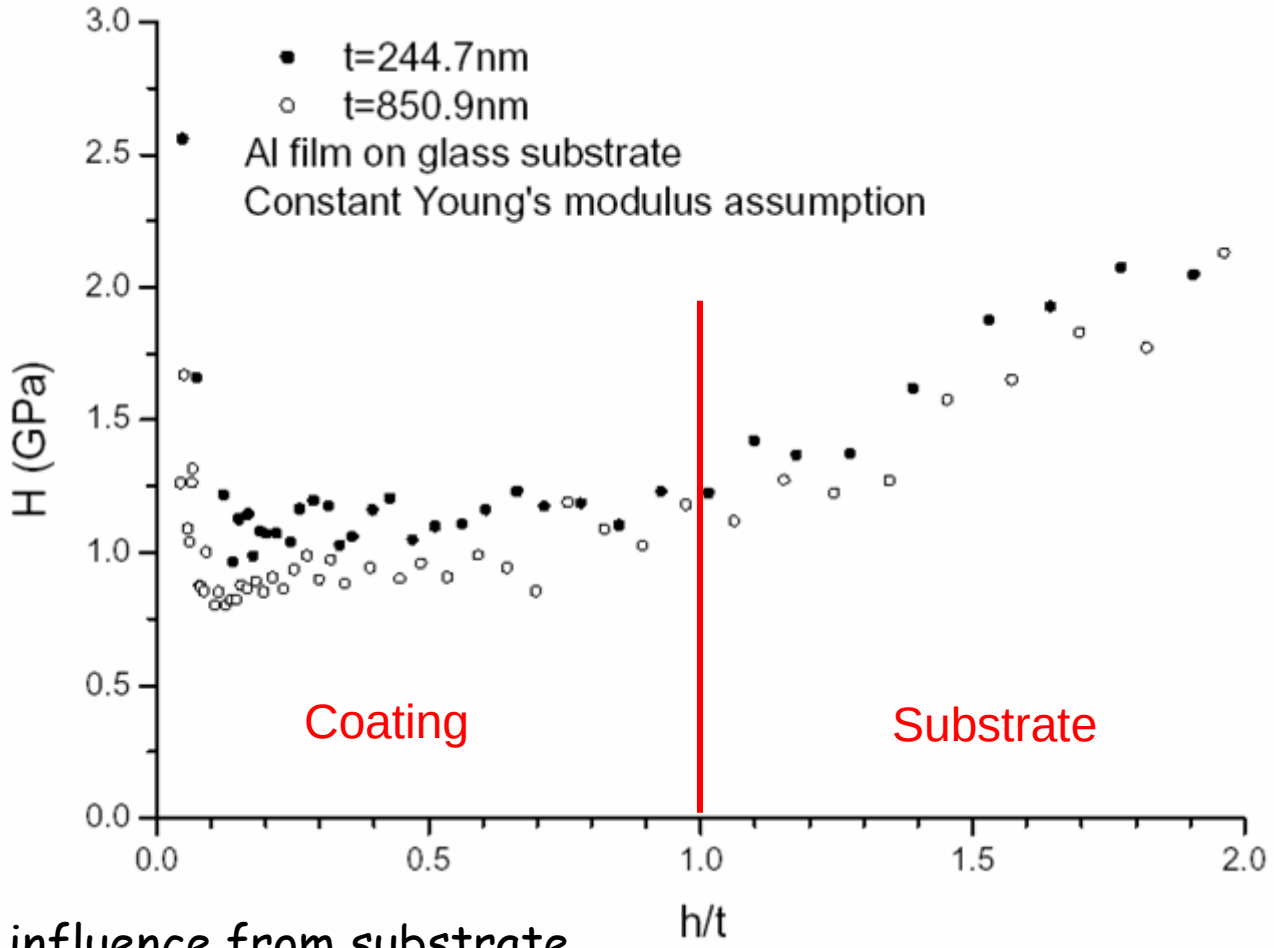

- almost no influence from substrate
- ISE observable

S. Chen, L. Liu, T. Wang, Acta Mater. 52 (2004), p. 1089

1μm Al on glass: effects of surface oxide layer

Surface oxide layer breaks under load resulting in "pop-in" features in the load-displacement curve
=> Evaluation of H and E is not possible at small penetration depths

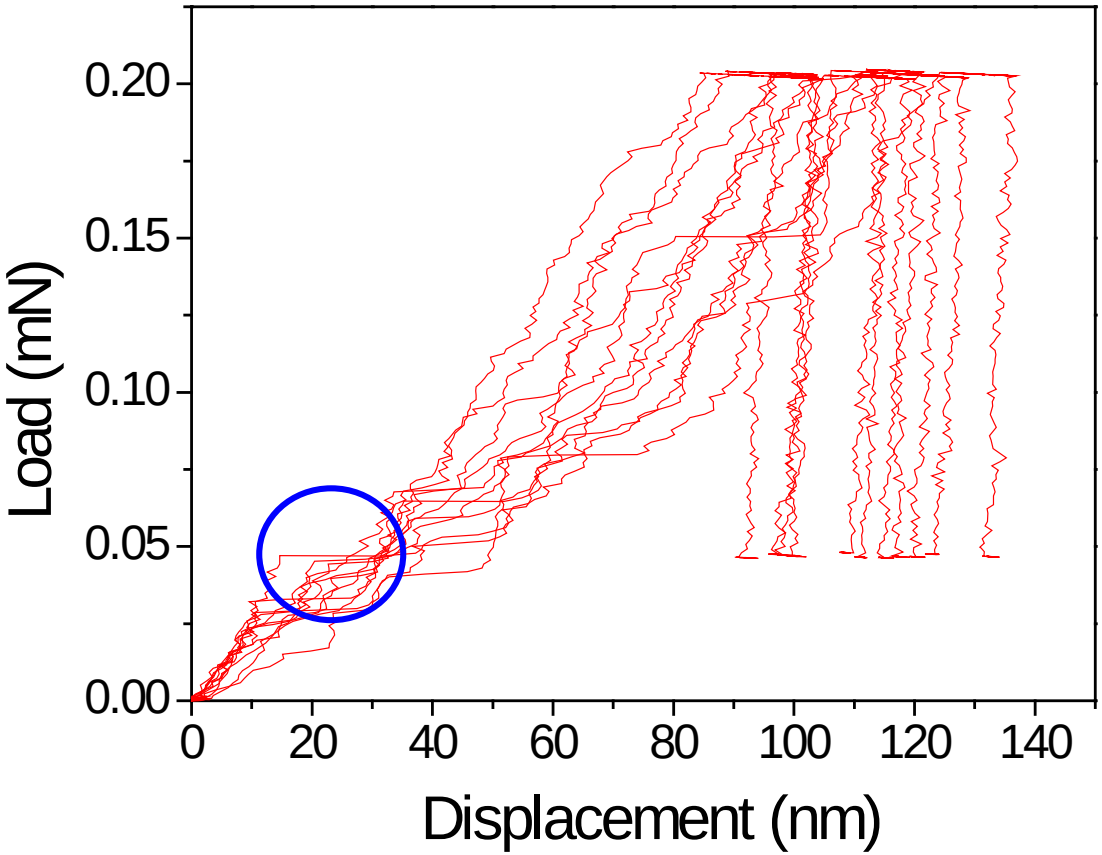

Considering the substrate properties

Soft film on hard substrate:

$$H_{eff} = H_S + (H_f - H_s) \cdot \exp\left\{ -\frac{Y_f}{Y_S} \frac{E_S}{E_f} \left(\frac{h}{t} \right)^2 \right\}$$

Hard film on soft substrate:

$$H_{eff} = H_S + (H_f - H_s) \cdot \exp\left\{ -\frac{H_f}{H_S} \frac{Y_S}{Y_f} \sqrt{\frac{E_S}{E_f}} \frac{h}{t} \right\}$$

H_{eff}: hardness of film-substrate combination
Y : Yield stress
h: penetration
t: film thickness

„Finite element simulation of indentation experiments"
Bhattacharya and Nix, Int. J. Solids Structures 24, 1988, 1287-1298

BUT:
There is no one relationship which covers a wide range of materials behaviour

Young's modulus

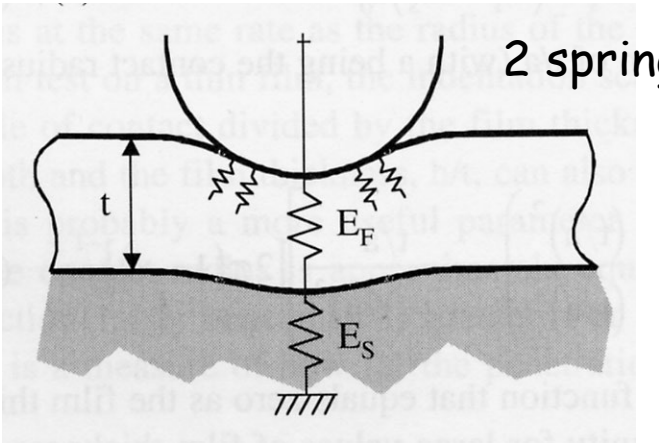

2 springs in series

Evaluating E for different a/t values
=> extrapolating to E_f

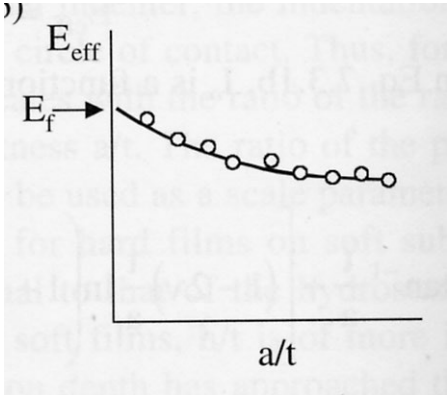

$$\frac{dP}{dh} = \beta \frac{2}{\sqrt{\pi}} E_{eff} \sqrt{A} \left[\frac{\frac{(1-\upsilon_s^2)}{E_s} + \frac{(1-\upsilon_i^2)}{E_i}}{\frac{(1-\upsilon_f^2)}{E_f}(1-e^{-\alpha t\sqrt{A}}) + \frac{(1-\upsilon_s^2)}{E_s}(1-e^{-\alpha t\sqrt{A}}) + \frac{(1-\upsilon_i^2)}{E_i}} \right]$$

a: penetration depth
β: depends on the indentation tip geometry

t: coating thickness
α: empirical constant, determined from a series of experiments

R.B. King, Int. J. Solids Structures 23(12), 1987, pp. 1657-1664

"1/10-rule of thumb"

Rule of thumb by H. Bückle:
(h_{max} = maximal depth; d_{Film} = film thickness)

$$h_{\max} \leq 0.1 \cdot d_{Film}$$

For the "extreme" cases of a hard film on a soft substrate (Nanocomposite coatings) or for a soft coating on a hard substrate (Al on glass)
this rule may be too lax or to strict

H. Bückle, VDI Berichte, Vol. 41, p. 14, 1961

Choice of applied maximal load / maximal displacement

Rules:
- Displacement > 20 R_a
- Displacement ≤ 10% of coating thickness

Nanoindentation equipment: Commercial Nanoindenters

MTS Nanoindenter XP / KLA Tencor NanoIndenter G200

(1) Inductive Force Generation
(2) Capacititive Displacement Measurement

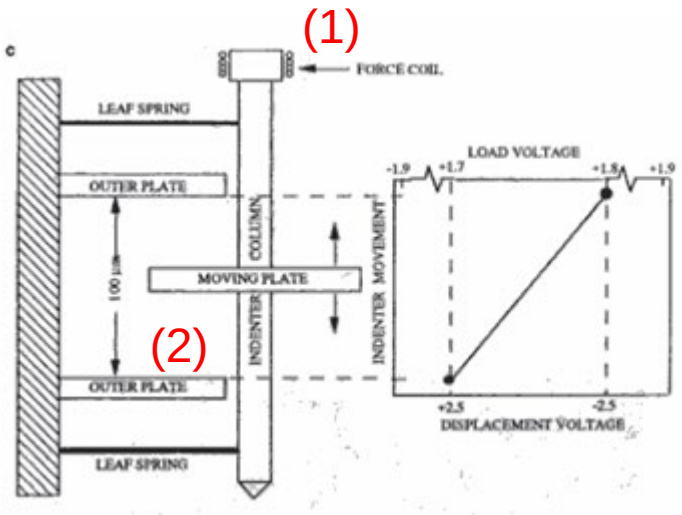

MTS Nanoindenter XP installed @ Empa in Thun:

Displacement resolution	< 1 nm
Maximum indentation depth	500 µm
Minimal peak load	100 µN
Maximum load	500 mN
Load resolution	50 nN
Lateral position accuracy	± 1µm

Scratch option with lateral force measurement
(Measurement of Friction Coefficient)

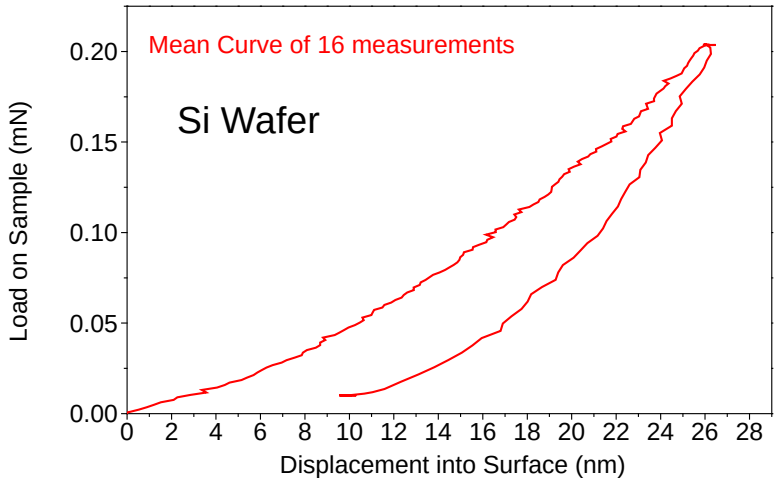

Hysitron Tribo-Scope / Ubi

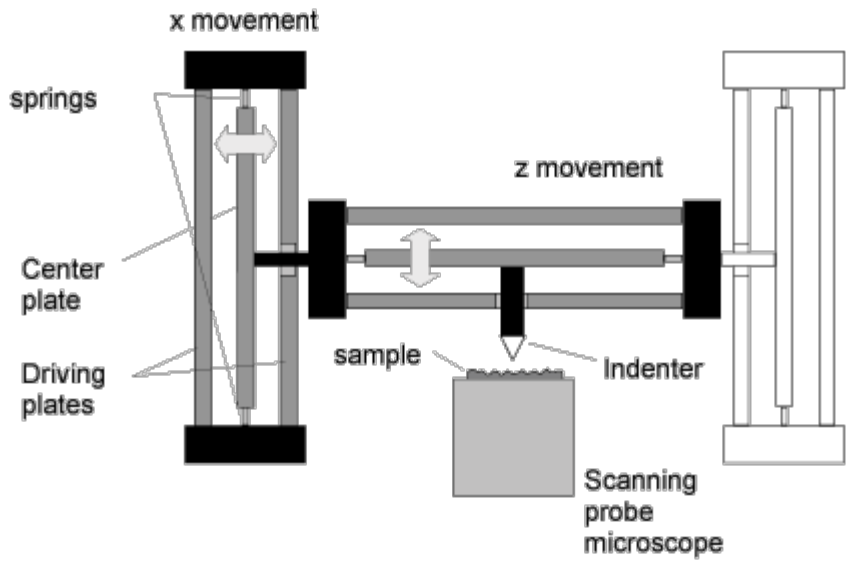

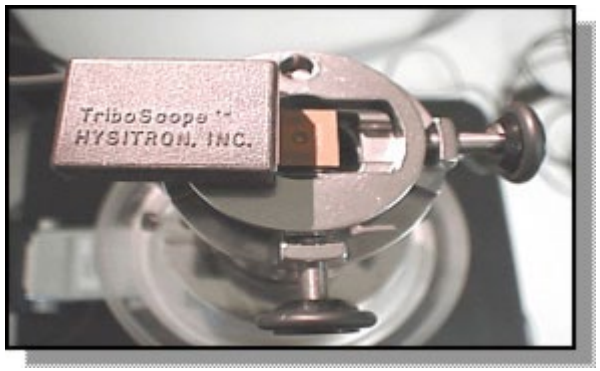

Transducer Specifications

· Load
Resolution: <1nN
Noise Floor: 100nN

· Displacement
Resolution: 0.0002nm
Noise Floor: 0.2nm
Drift: <0.05nm/sec

CSM Instruments Nano-Hardness Tester

Indentation Testers Specifications		
	Micro	Nano
Maximum Load	10 N (30 N Optional)	500 mN
Load Resolution	100 µN	0.04 µN
Maximum Depth	0-20 & 0-200 µm (1 mm optional)	0-20 & 0-200 µm
Depth Resolution	0.04 & 0.3 nm	
XY stages (*)	120 mm x 20 mm	
XY resolution	0.25 µm	

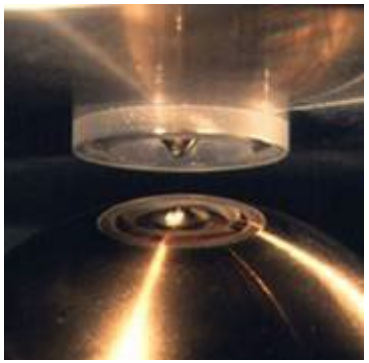

Surface reference by contact with a ring

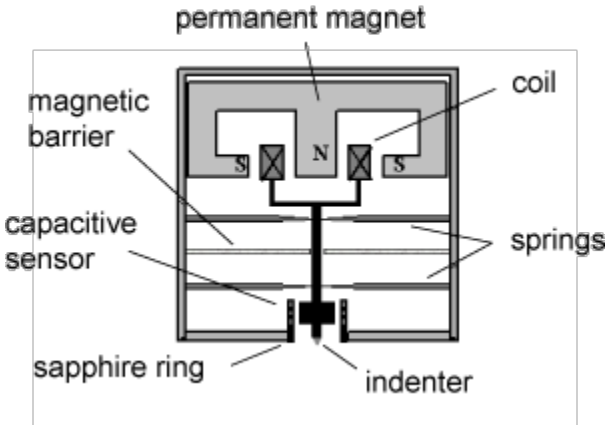

Alemnis in situ indenter

- In situ experiments inside the SEM
- Actuation: Piezo
- Load, displacement measurement: Strain gauges
- Load range: Up to 2.5N
- Load noise: 4 µN
- Displacement range: 40 µm
- Displacement noise: 0.2 nm

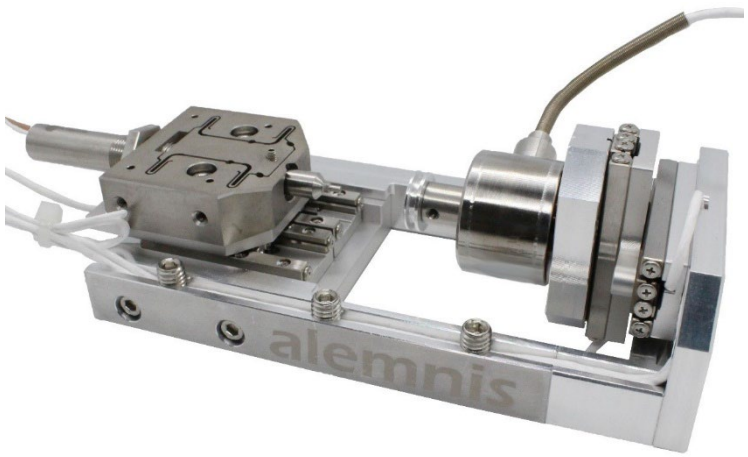

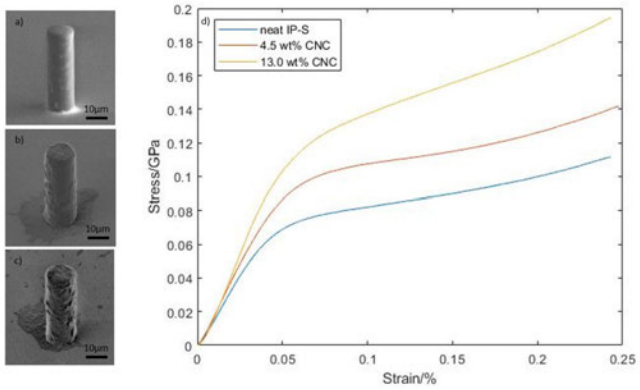

- Variable temperature modules (-150°C to 1000°C)
- High strain rate module (up to 1000/s)

What happens in the material?

- Sink-in and pile-up around the tip (a-Me)
- Densification and phase transformation (Remy)
- Dislocation nucleation and grain boundary sliding (Sid etc.)
- Creep
- Crack propagation

Pop-in and defect microstructure

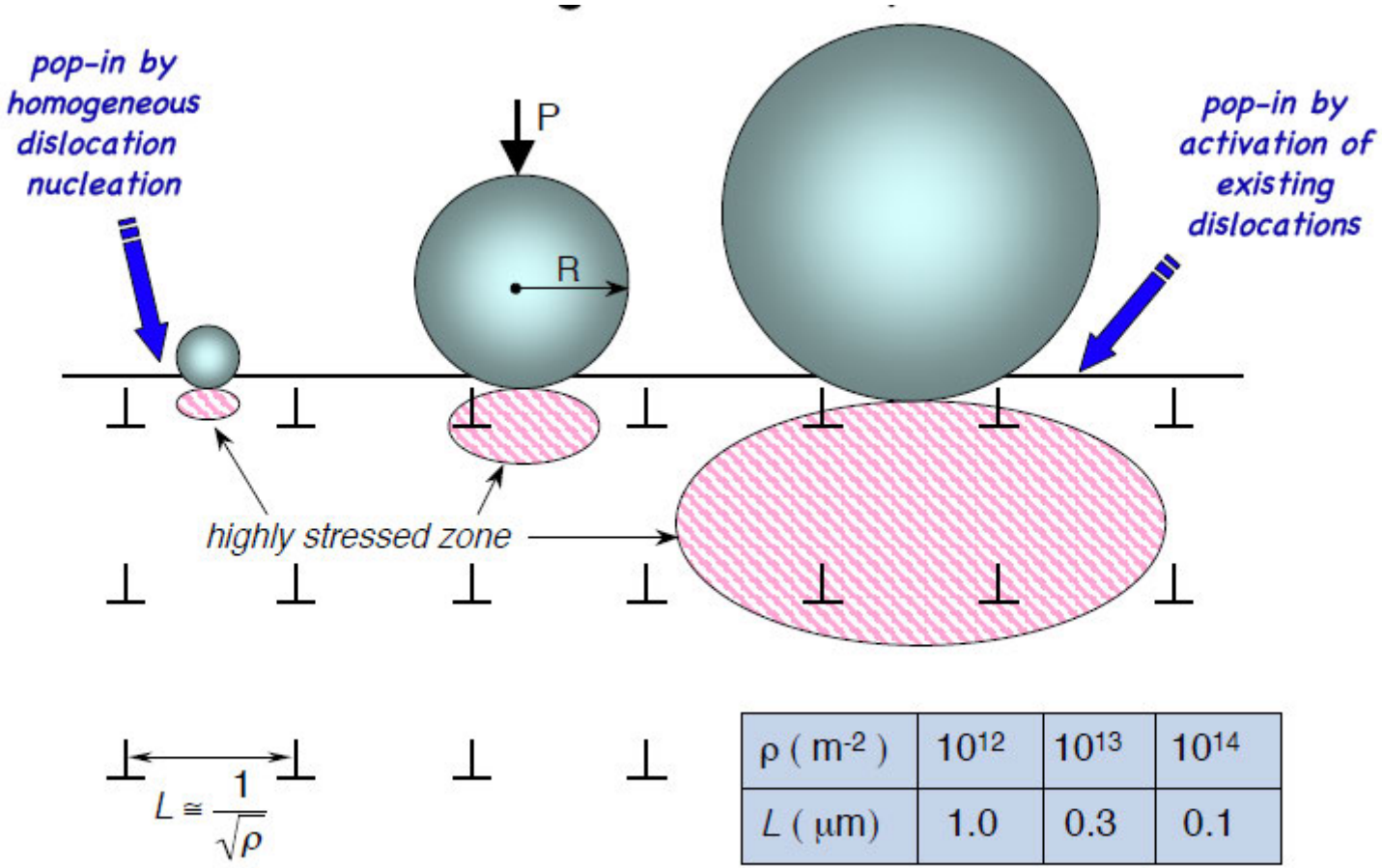

ρ (m^{-2})	10^{12}	10^{13}	10^{14}
L (μm)	1.0	0.3	0.1

40

Typical load displacement curves

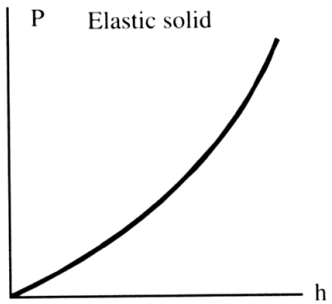

Elastic Solid

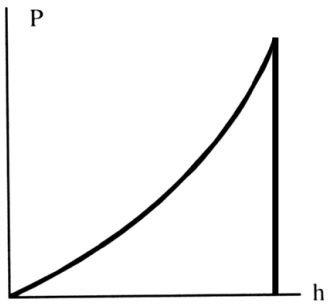

Fully plastic

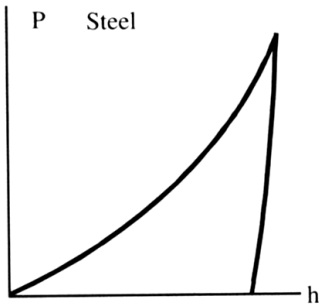

Ductile Solid
(Steel)

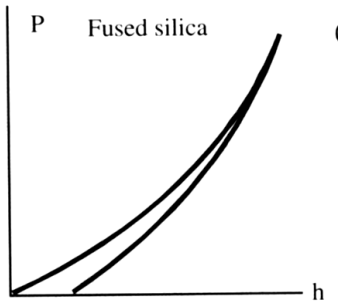

Brittle Solid
(Fused Silica)

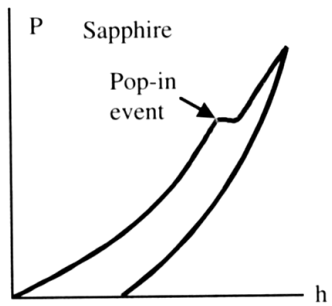

Brittle Solid
Cracking during
loading

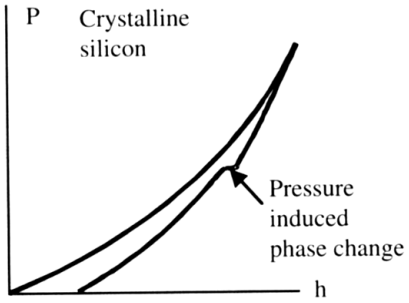

Pressure induced
phase change
(Silicon)

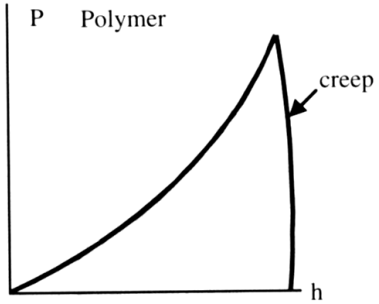

Polymer exhibiting
creep

phase transformations in silicon

slow (<1μm/s)

fast (>100μm/s)

intermediate

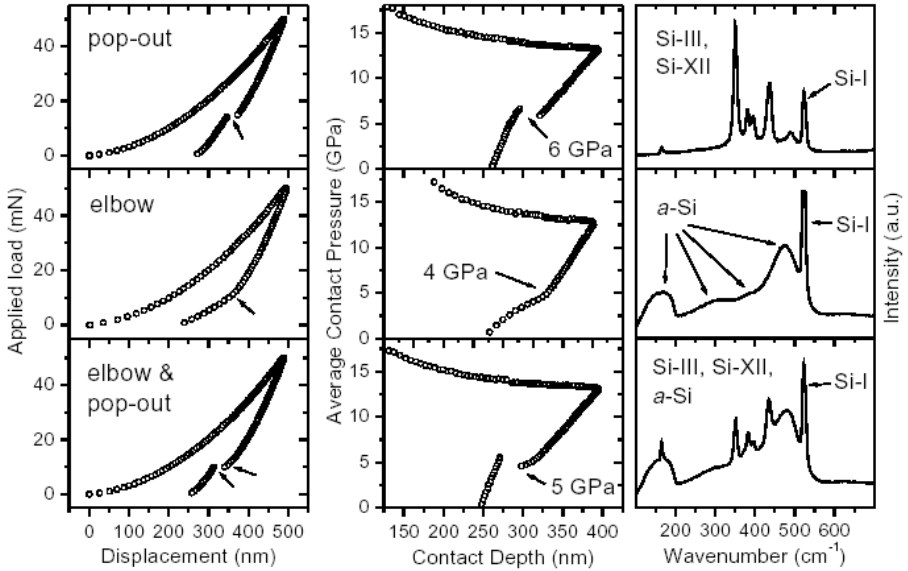

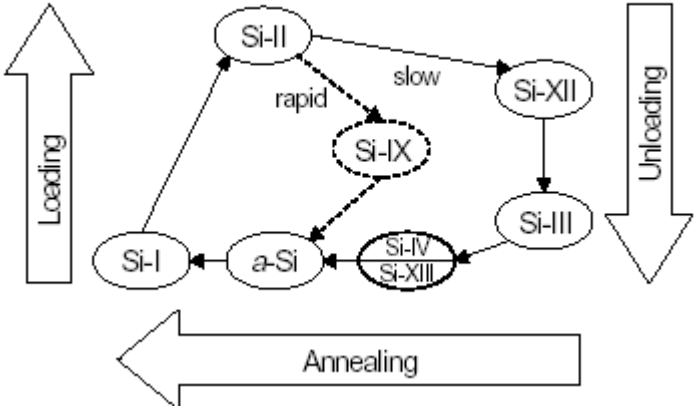

Fracture toughness

Determine K_{Ic} : measure size of residual impression a and crack length c

Palmqvist (radial)

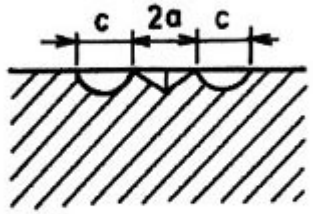

$$K_{Ic} = 0.035\left(\frac{kE}{H_V}\right)^{2/5}\left(\frac{a}{c}\right)^{1/2}\frac{H_V a^{1/2}}{k}$$

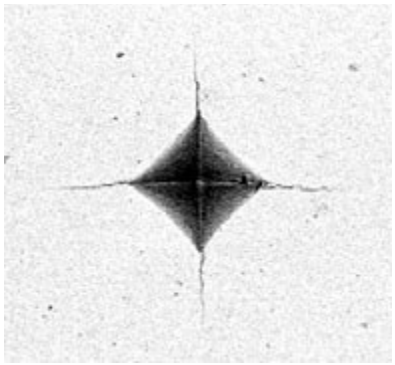

Half-penny (median)

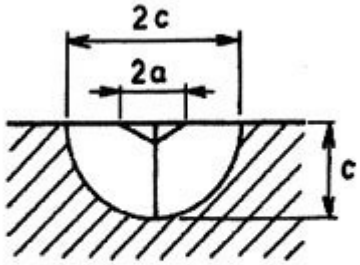

$$K_{Ic} = 0.129\left(\frac{kE}{H_V}\right)^{2/5}\left(\frac{a}{c}\right)^{3/2}\frac{H_V a^{1/2}}{k}$$

Probleme:
- precision of length measurement
- Crack morphology
- When is crack generated?
- Model is material specific

Fracture toughness

Possible crack modes

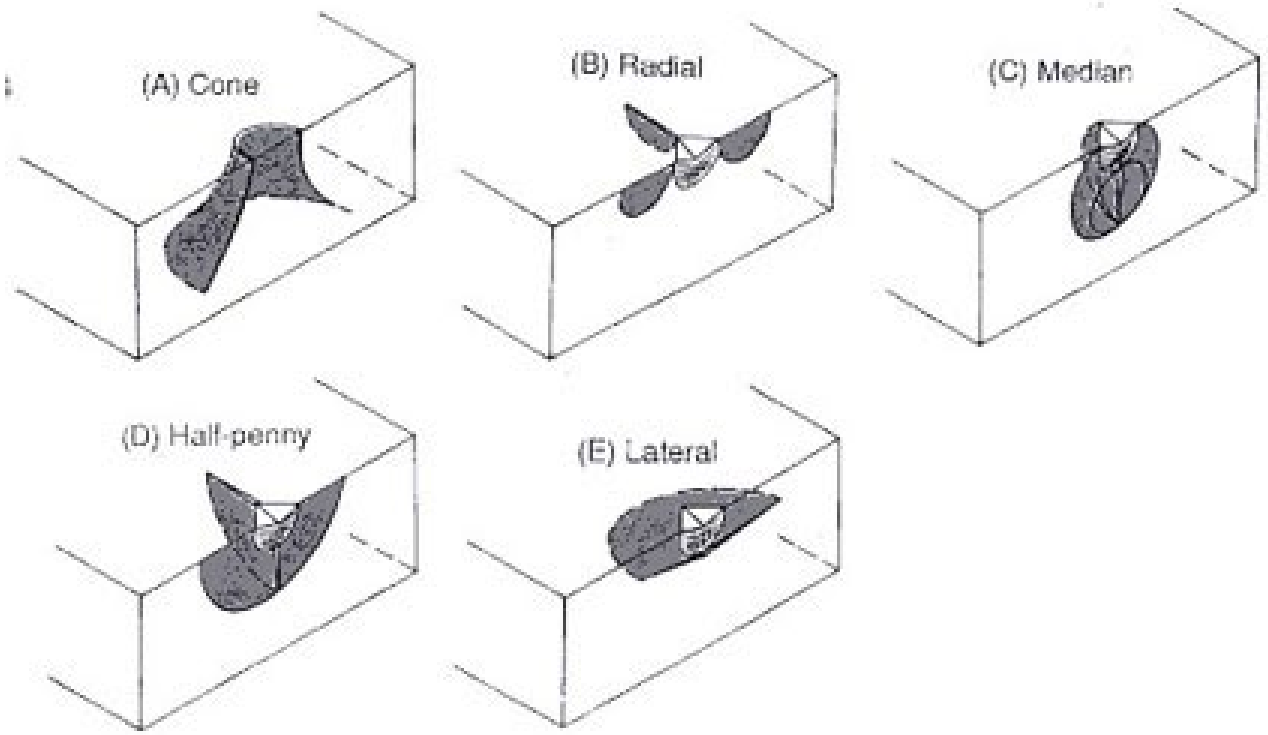

Example: fracture toughness

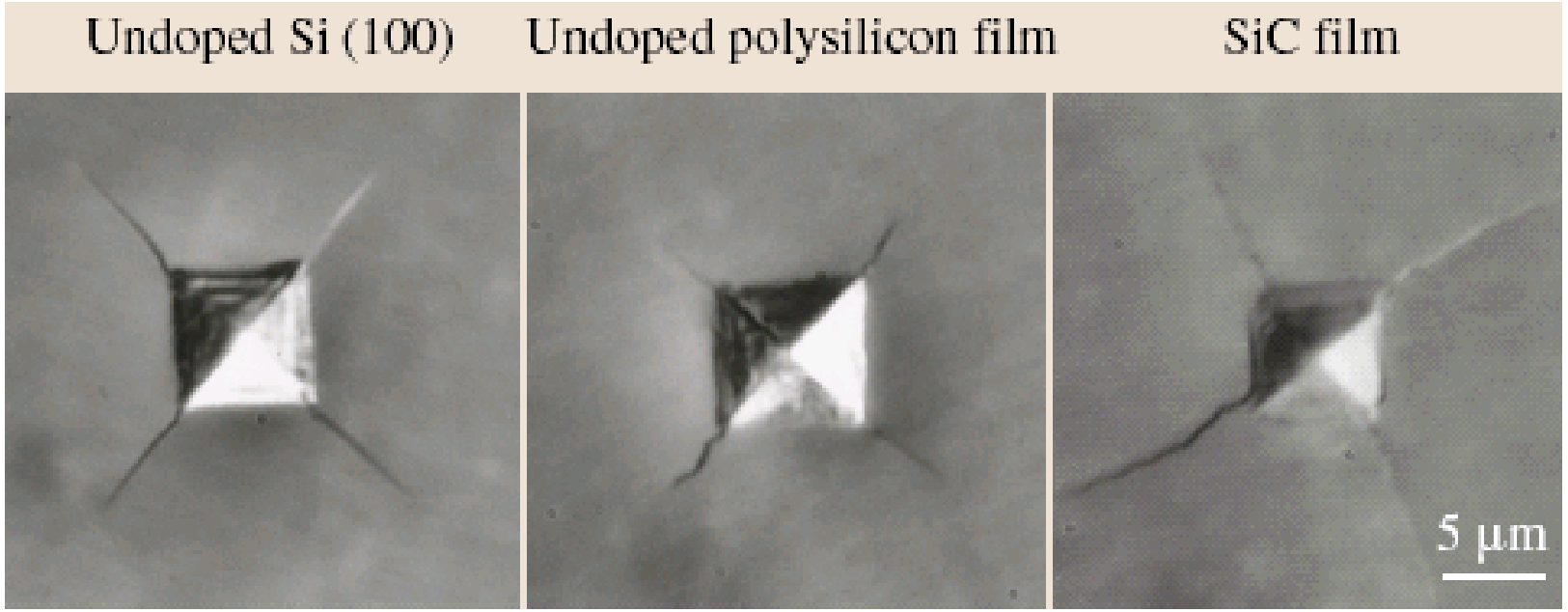

Kc/MPa $m^{0.5}$	0.75	1.11	0.78

(Half- penny crack model)

Example: fracture toughness

Indenter:
cube corner

coating:
a-C:H mit 20at% Si
3.5 μm thickness
H=8GPa

Substrate:
(X155CrMoV121)

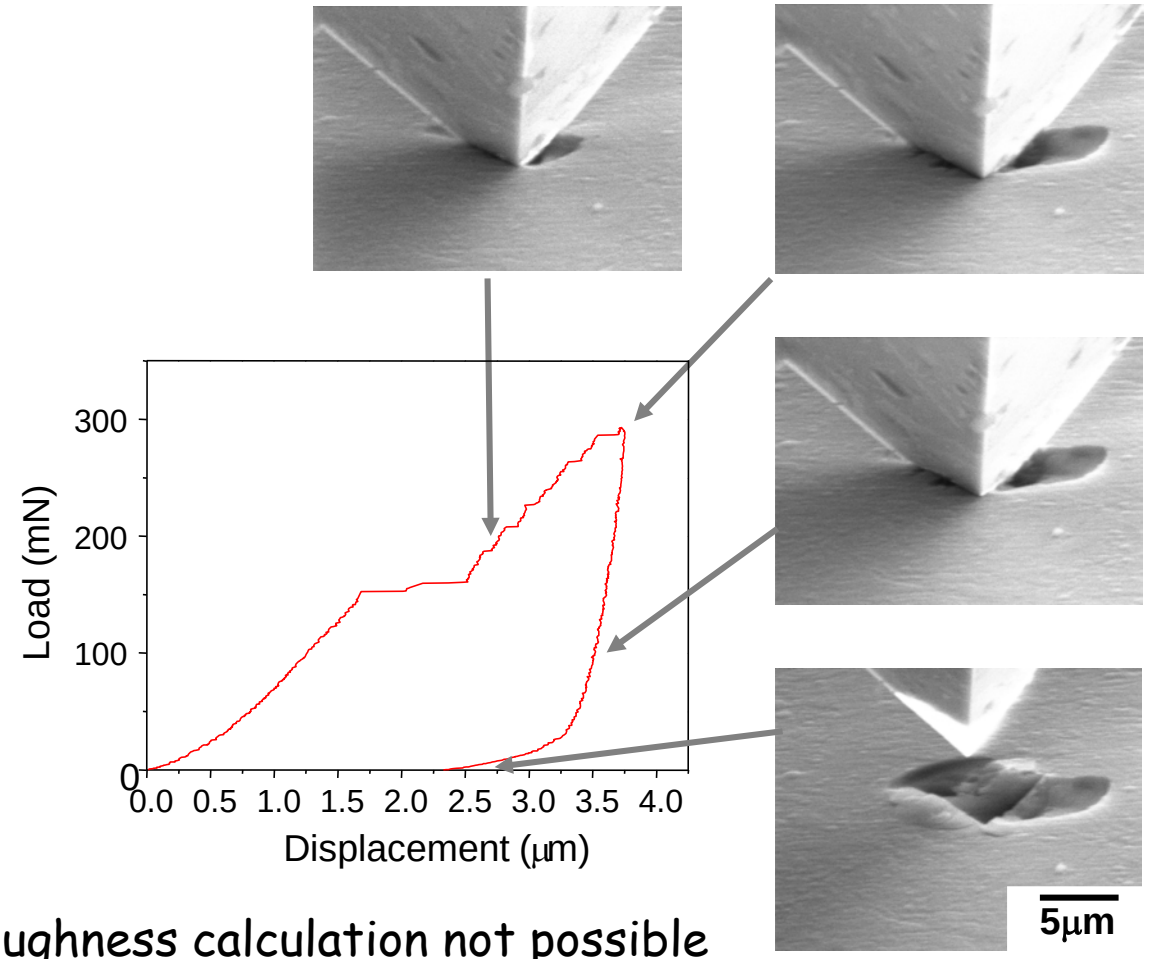

Lateral cracks form: toughness calculation not possible

Stress-strain curves from indentation

?

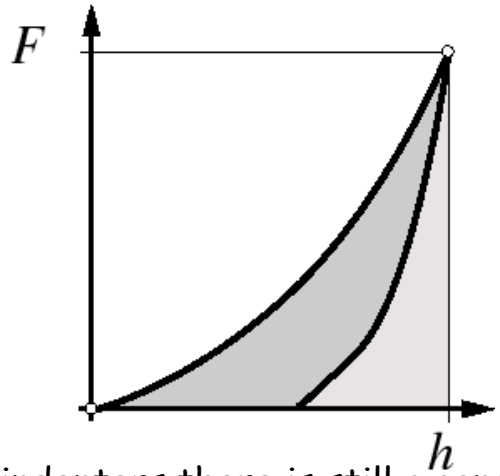

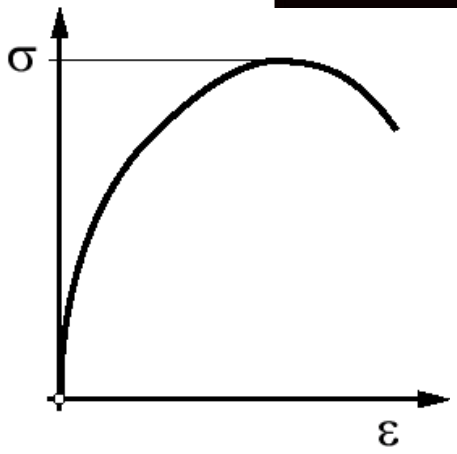

For conical type indenters,there is still a considerable debate about the feasability:
Cheng YT, Cheng CM (1999) J Mater Res 19, 3493.
Venkatesh TA, Van Vliet KJ, Giannakopoulos AE, Suresh S. (2000) Scripta Mater 42, 833

Can we at least develop a robust practical method by pure numerical methods?

idea: combination of experiments

Conical tips

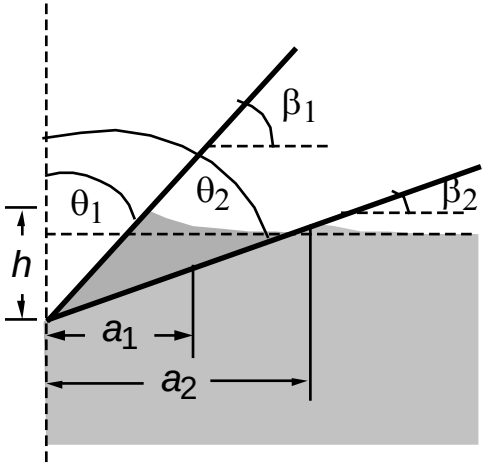

$$\varepsilon \sim \frac{h}{a} \sim \cot\Theta$$

Johnson, K.L.: Contact Mechanics, 1985.

Spherical tip

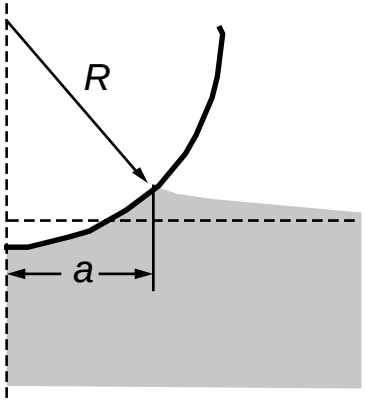

$$\varepsilon \sim \frac{a}{R}$$

Tabor, D.: The Hardness of Metals, 1951

combine several experiments with varying cone angle

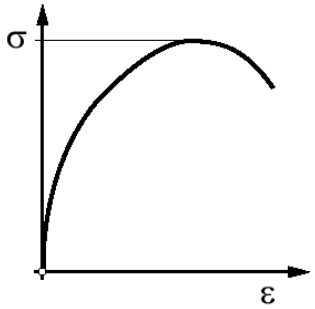

combine load displacement data with residual profile

some definitions

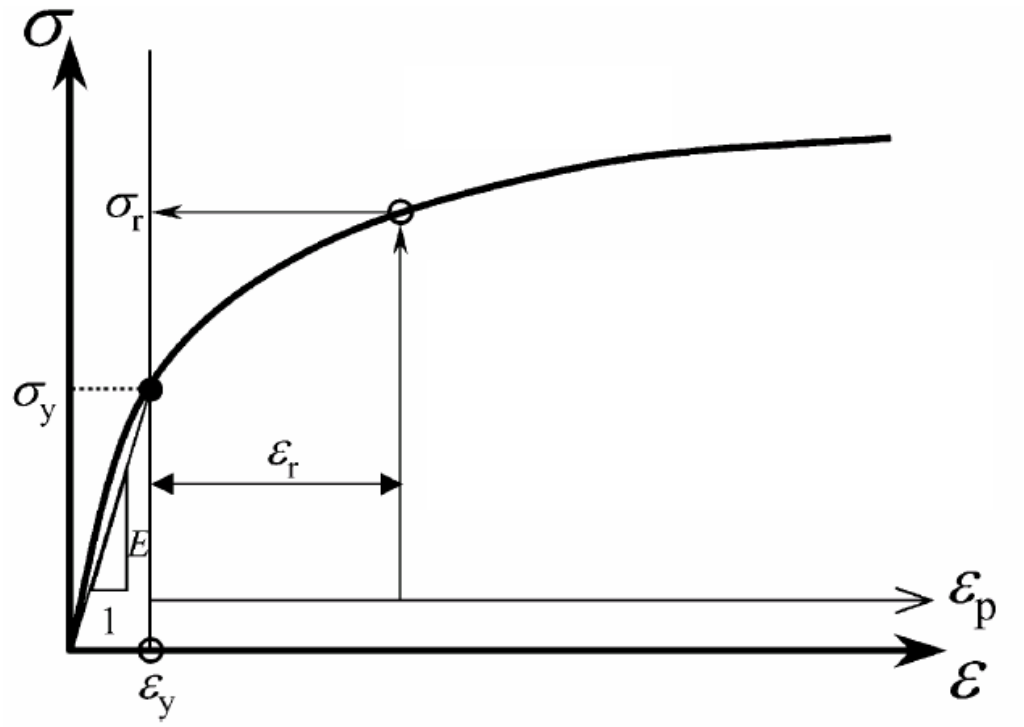

$$\sigma = \begin{cases} E\varepsilon & \varepsilon < \varepsilon_y \\ \sigma_y\left(1+\frac{E}{\sigma_y}\varepsilon_{pl}\right)^n & \varepsilon > \varepsilon_y \end{cases}$$

$\varepsilon = true\ strain, \sigma = true\ stress$

We can describe the elastic behavior by E (ν) and the plastic behavior by σ_y and n

conical tips: algorithm I

parametric finite element calculations of a large set of typical E, σ_y , n and θ

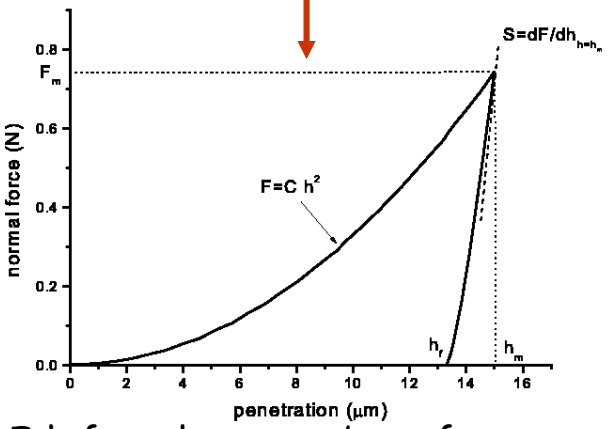

F-h for a large number of combinations of σ_y, n, θ

modeling of loading: $F = Ch^2$

for a given θ find representative ε_r for that all C/σ_r and E^*/σ_r are superimposed on one curve (Dao, Acta Mater. (2001),
-> average total strain independent on strain hardening

example θ=50°

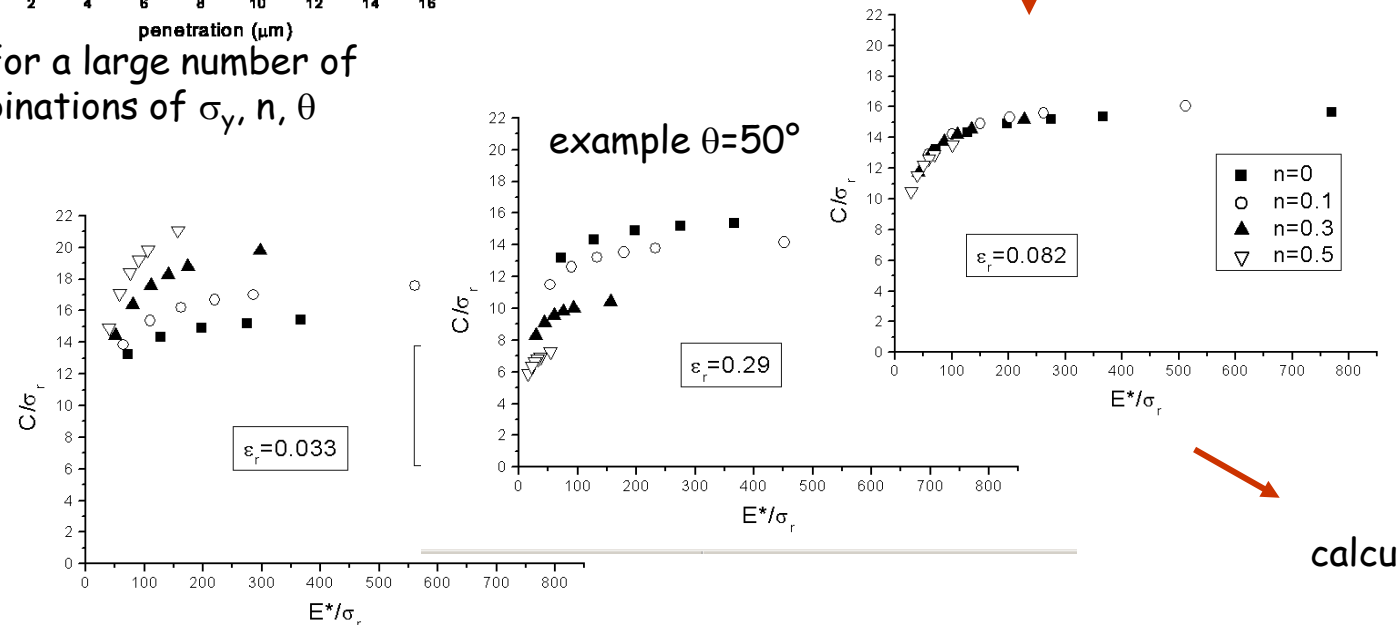

calculate back σ_y , n

Dao, Acta Mater. (2001)

conical indenters: algorithm II

normalized dimensionless functions

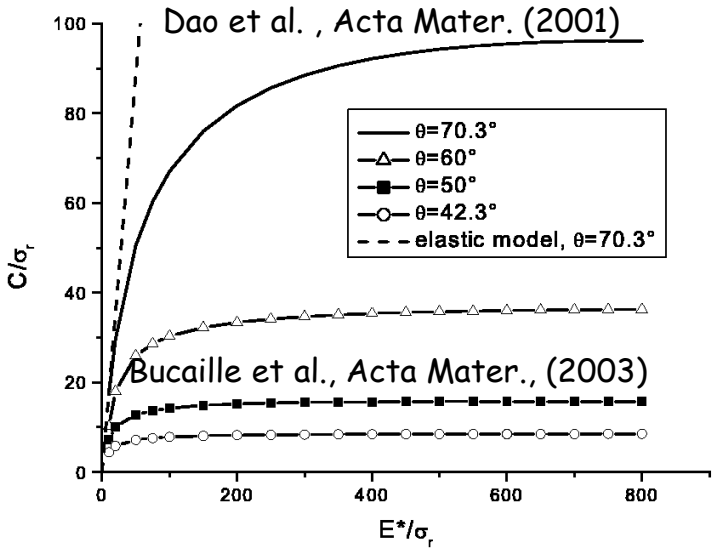

master curve:
relation between C and E, σ_r for any value of θ

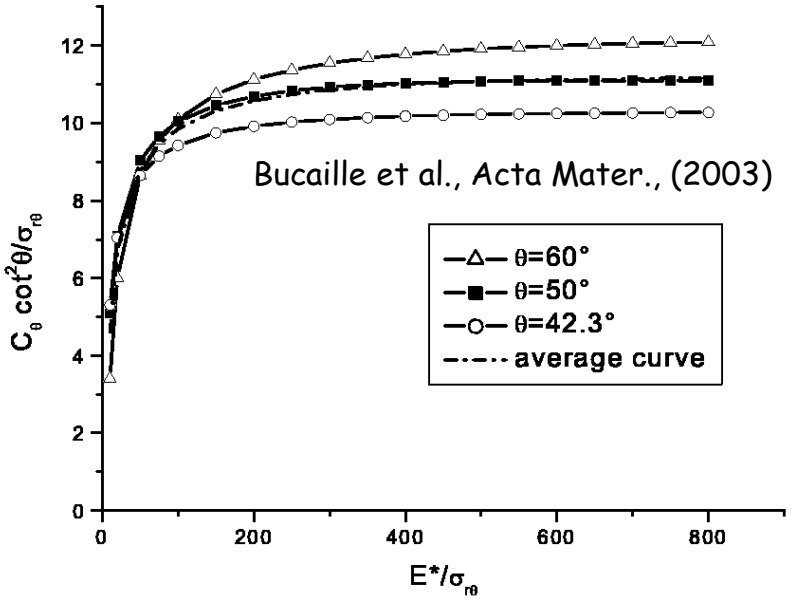

representative **strain**

$$\varepsilon_r = 0.105 \cot\theta$$

and the corresponding **stress** computed with the Π_1 function below:

$$\Pi_{1\theta} = \frac{C_\theta}{\sigma_{r\theta}} = \tan^2\theta\{0.02552[\ln(\frac{E*}{\sigma_{r\theta}})]^3 - 0.72526[\ln(\frac{E*}{\sigma_{r\theta}})]^2 + 6.34493[\ln(\frac{E*}{\sigma_{r\theta}})] - 6.47458\}$$

-> two simple formula based on E*, C_θ from experimental load-displacement data

conical indenters: experiment

Material:
CuCo2Be

Indentation tests:
Zwick Universal
hardness tester

Diamond tip geometries
38.6°, 47.0°, 50.0°, 51.0°, 61.7°
62.8°, 63.3°, 67.7°, 68.6°

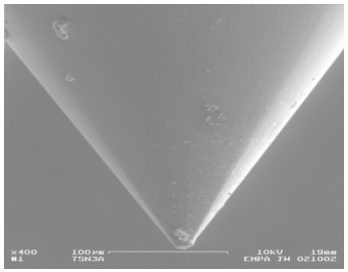

& Vickers (70.3°)

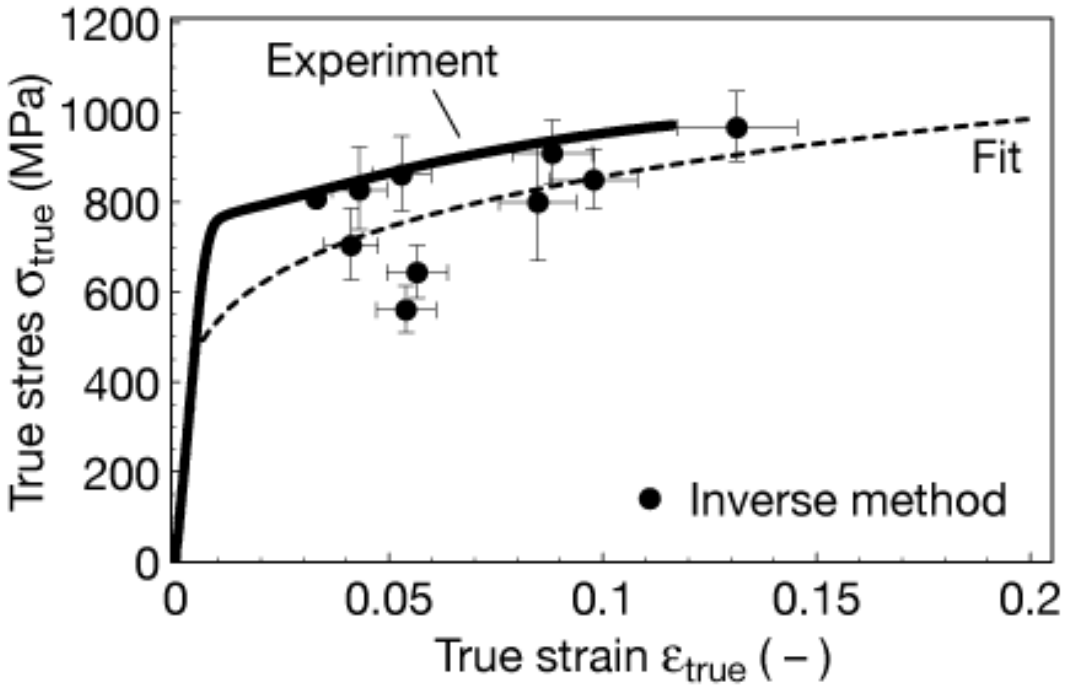

spherical indentation: algorithm I

idea: optimize FE calculation until calculated data fit experimental topography and load-displacement data

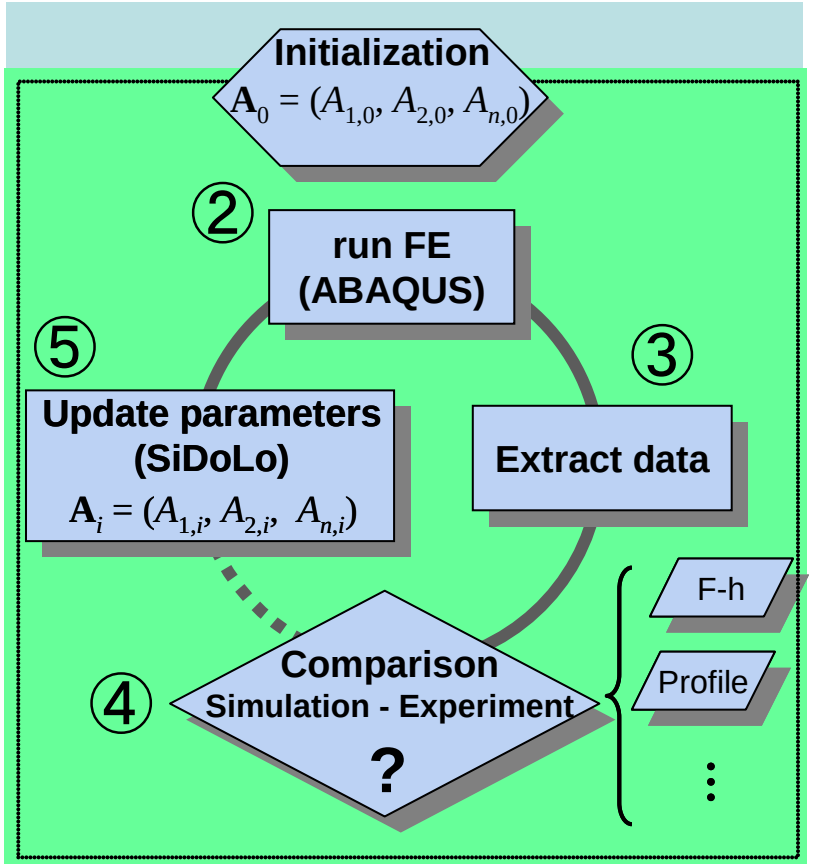

FE meshing scheme optimized for minimizing computing time; combination of finite and infinite axisymmetric elements (to eliminate boundary effects (i.e. $u_i = 0$) on numerical solution)

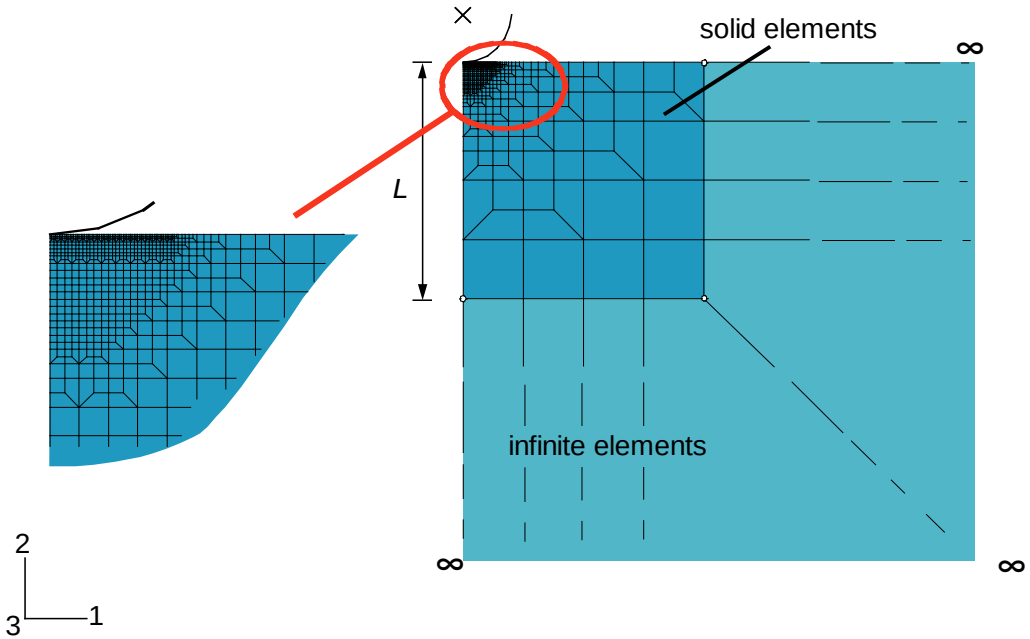

spherical indentation: algorithm II

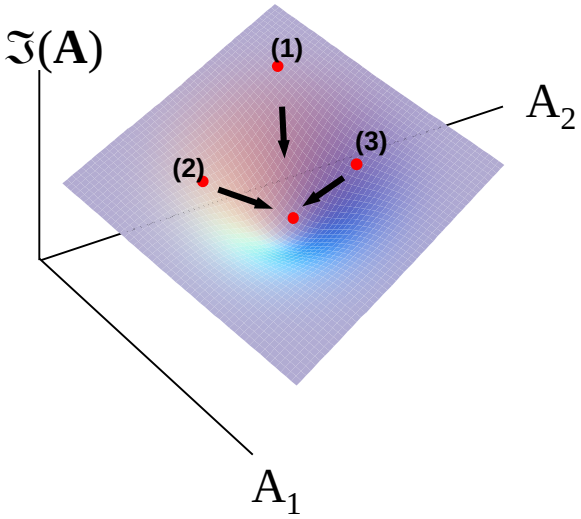

Fitting: Vary systematically parameters around starting point and "go a step in direction of the deepest gradient" to minimize the difference $\mathfrak{I}(\boldsymbol{A})$ between simulated and experimental data

But: Ill conditioned problem?

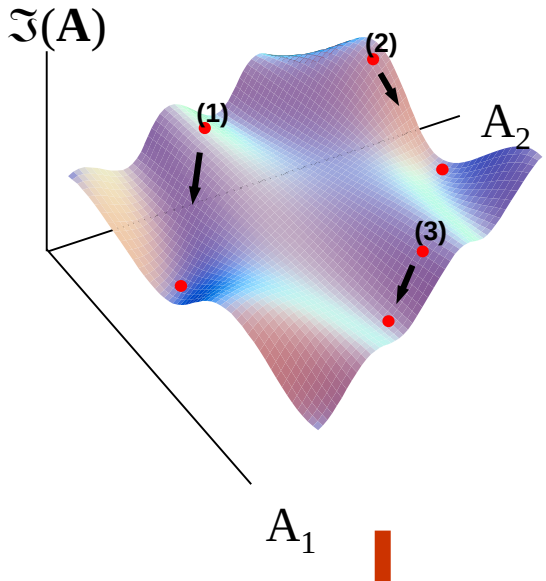

Practical guideline: Good estimation of initial values and stabilization of the solution by increasing the number of fitted parameters

spherical indentation: model calculation

Validation: Fit back a finite element calculation after starting from 10% perturbation

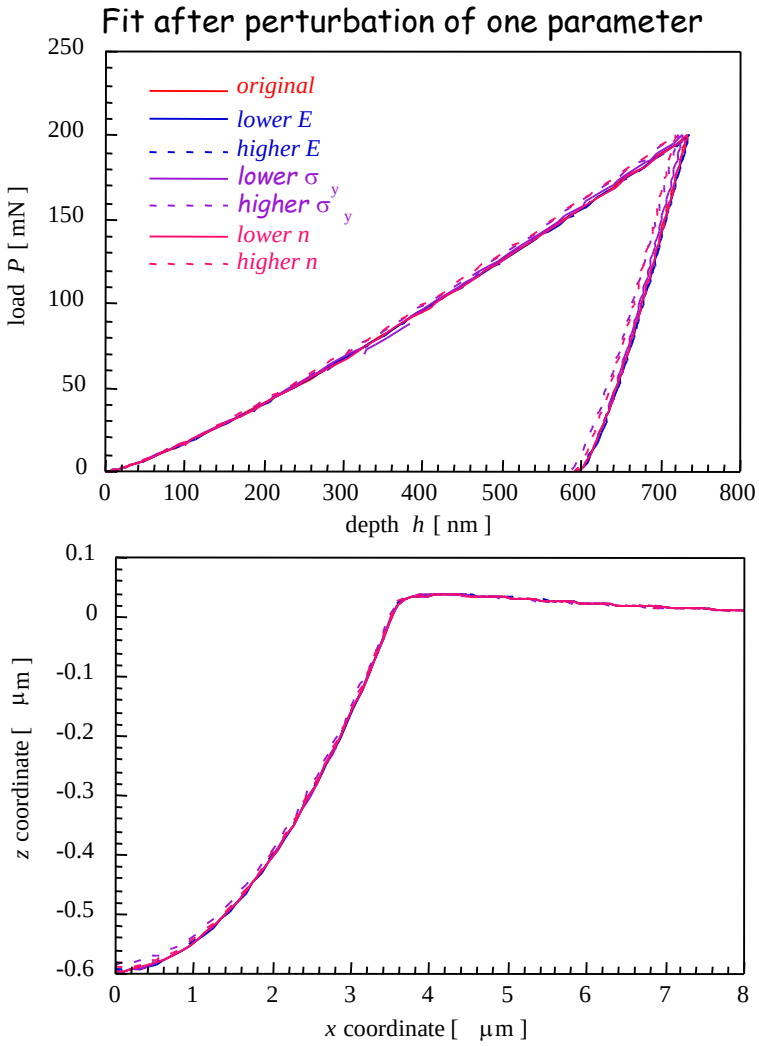

Material model:

$$\sigma = \begin{cases} E\varepsilon \\ \sigma_y \left(1 + \dfrac{E}{\sigma_y}\varepsilon_{pl}\right)^n \end{cases}$$

Example calculation (perturbation of all param.):

	E [GPa]	σ_y [MPa]	n [ ]
Original	**210**	**500**	**0.3**
Start	189	450	0.27
Fit	**208**	**494**	**0.30**

spherical indenters: experiment

material:
CuCo2Be

indentation tests:
universal
hardness tester

topography measurements:
laser profilometer

tip geometry:
WC sphere R=0.5mm

fit:
perturbation of
all parameters
by 10%

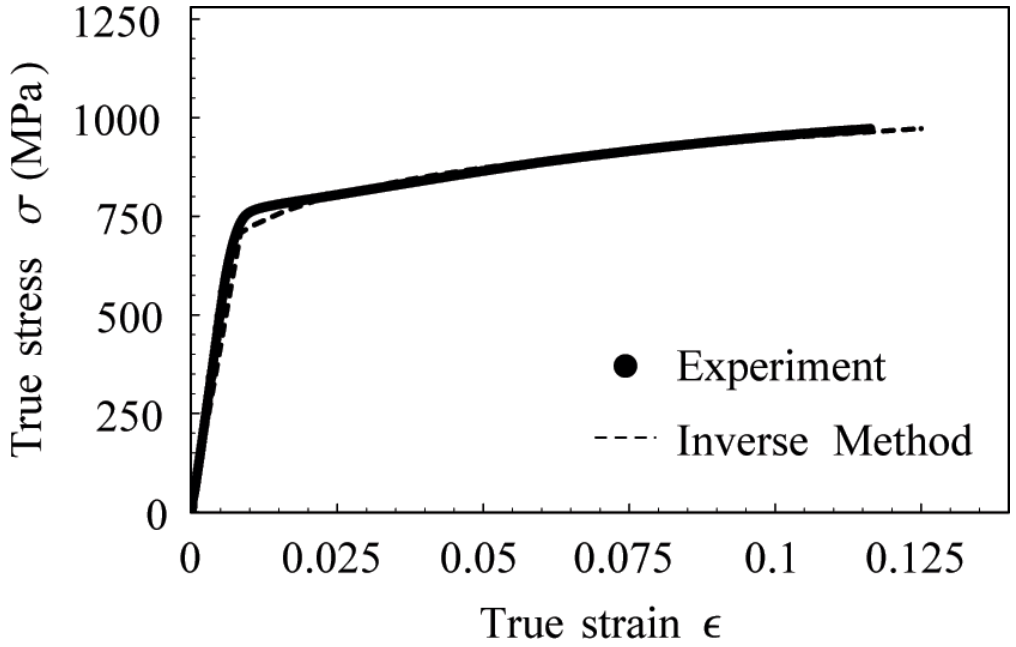

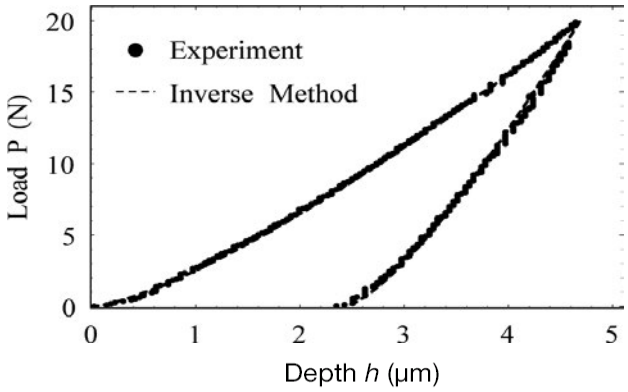

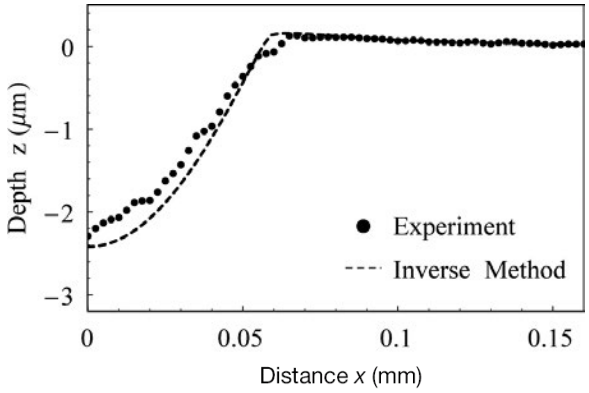

comparison of "conical" and "spherical" indentation methods

sphere & residual imprint

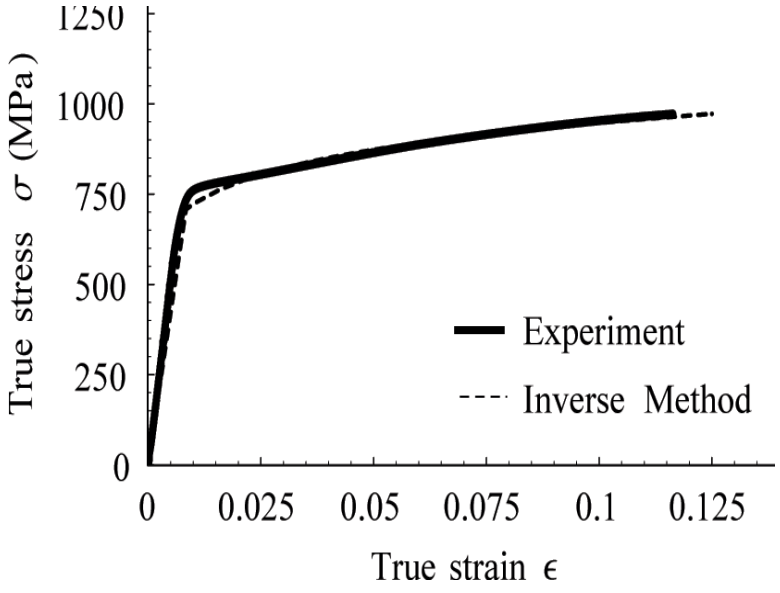

multiple cones

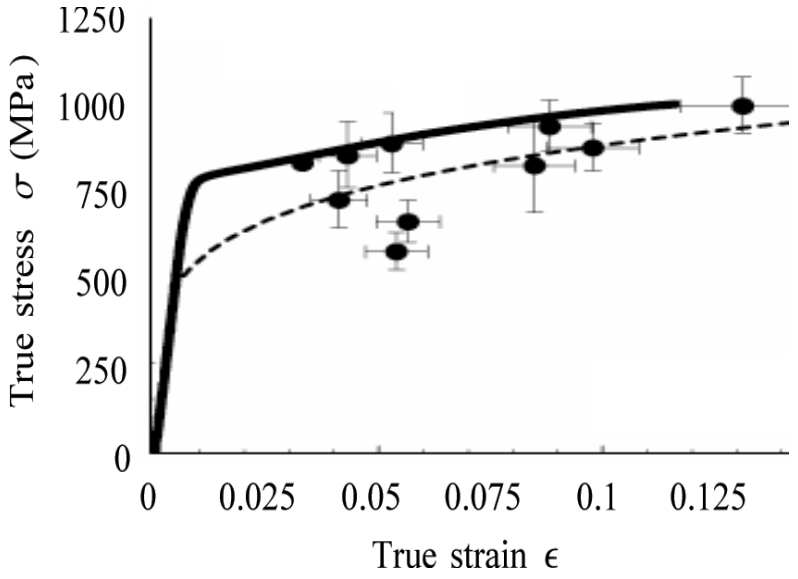

outlook: application to coatings

material:
NiCo electrodeposited coating

tensile tests:
UV-Liga tensile test bars

indentation tests:
MTS nanoindenter XP

topography measurements:
AFM

tip geometry:
diamond
spherical R=10μm

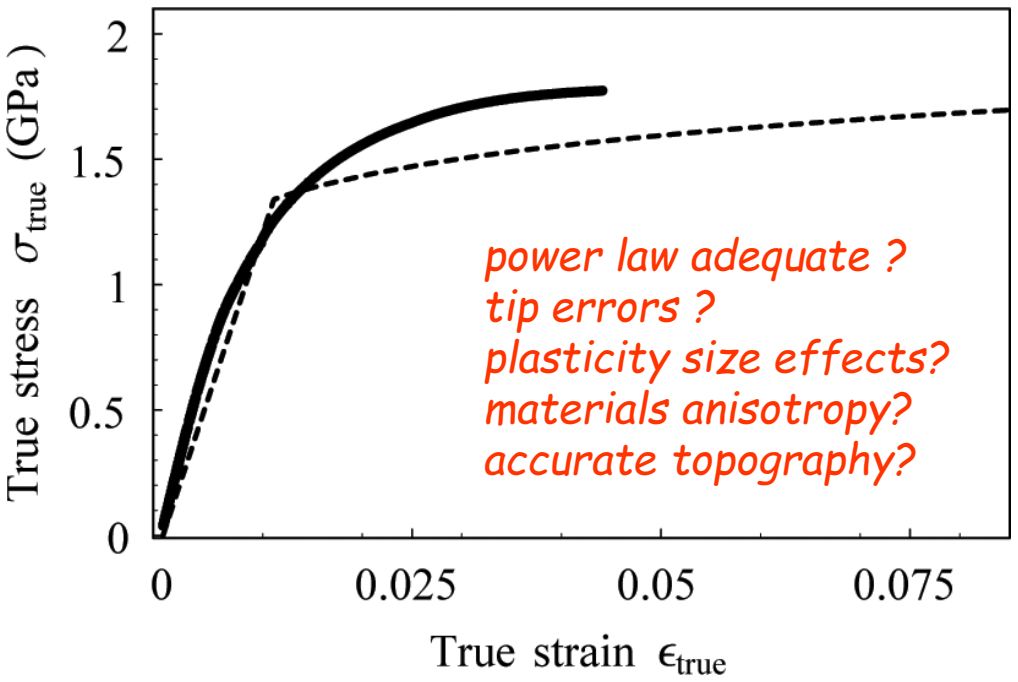

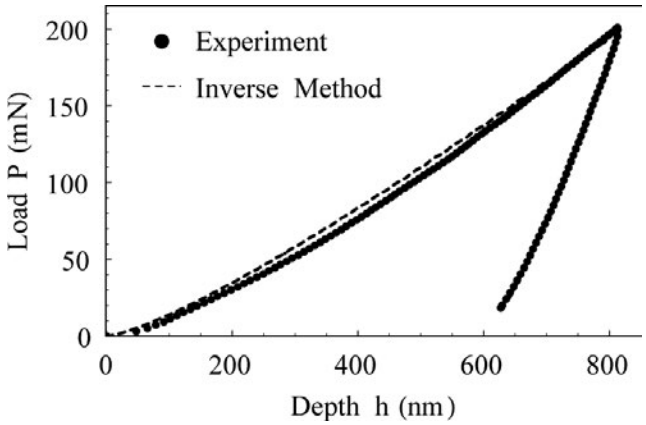

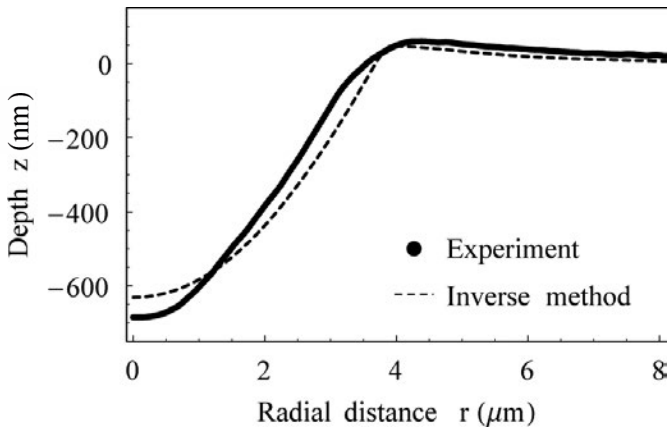

Microscale tensile testing

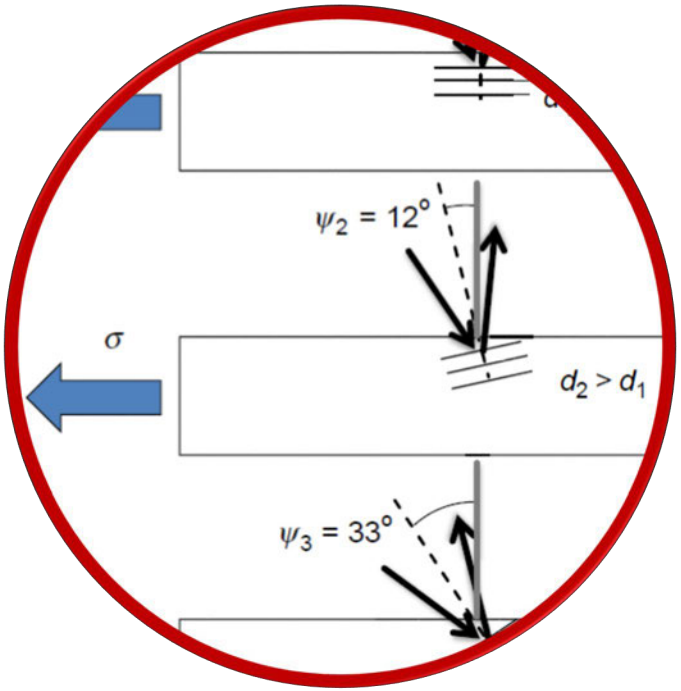

Challenges of small scale tension

Possible issues in small scale tensile experiments:

Specimen design

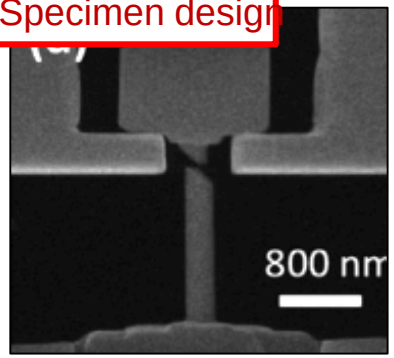

Liontas et al. *Acta Mater.* (2016)

Misalignment

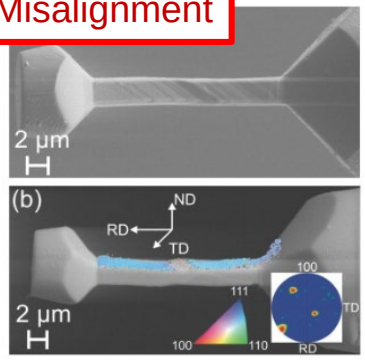

Kiener et al. *Acta Mater.* (2008)

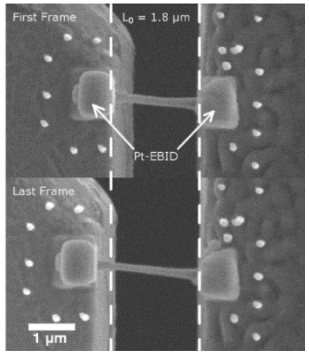

Magagnosc et al. *Sci. Rep.* (2015)

Fabrication artifacts

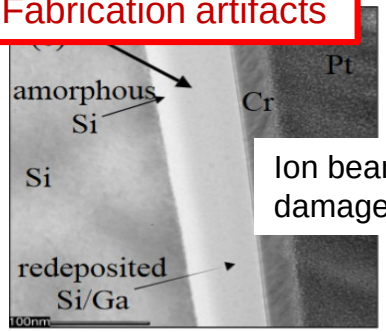

Ion beam damage

Rajsiri et al. *Microsc Microanal* (2002)

Complex setup and sample handling

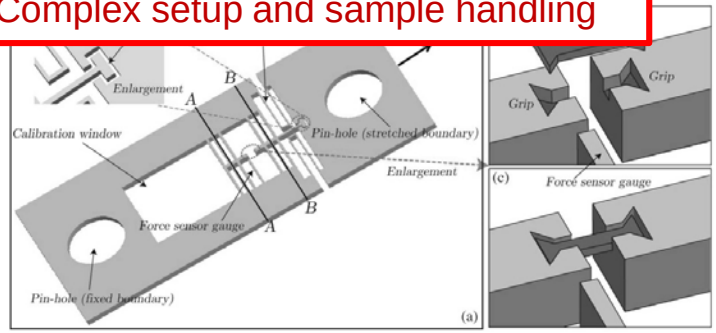

Kang et al. *J. Microelectromech. Syst.* (2010)

Requirements for the new methodology:

1. Minimise stress concentrations.
2. Optimise specimen fabrication via FIB.
3. Ensure alignment.
4. Avoid complex and tedious manipulations. No single use setups.

In situ tension: single-crystal copper samples

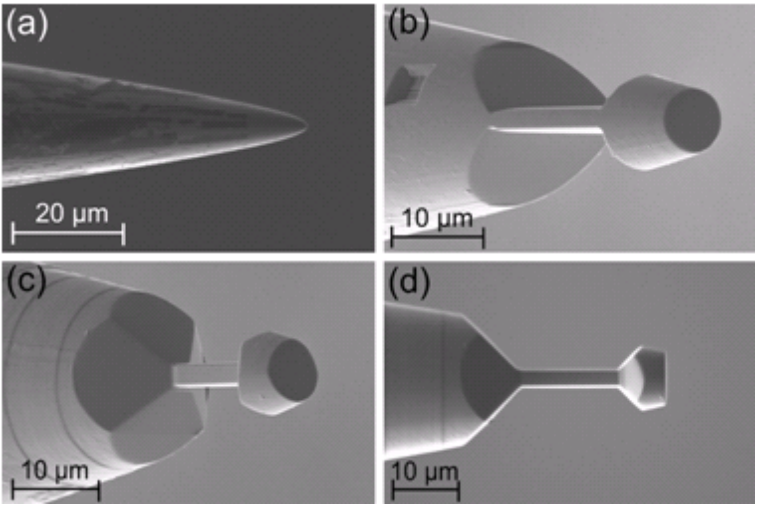

Fig. 1

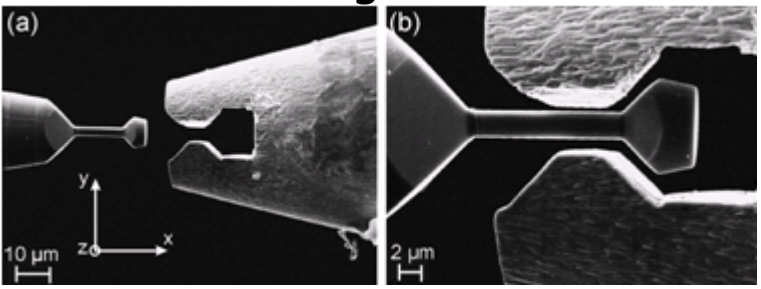

Fig. 2

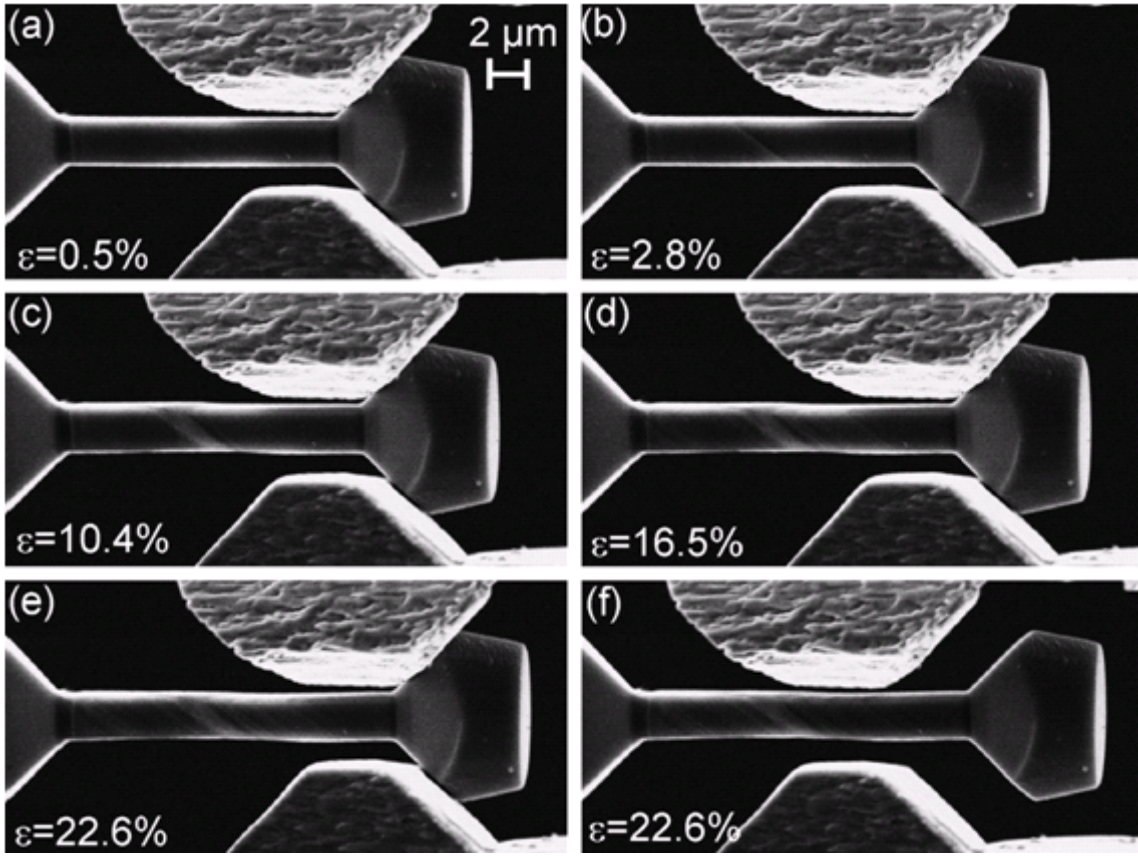

Fig. 3

Compression versus tension

Cu(100) oriented tensile and compression sample

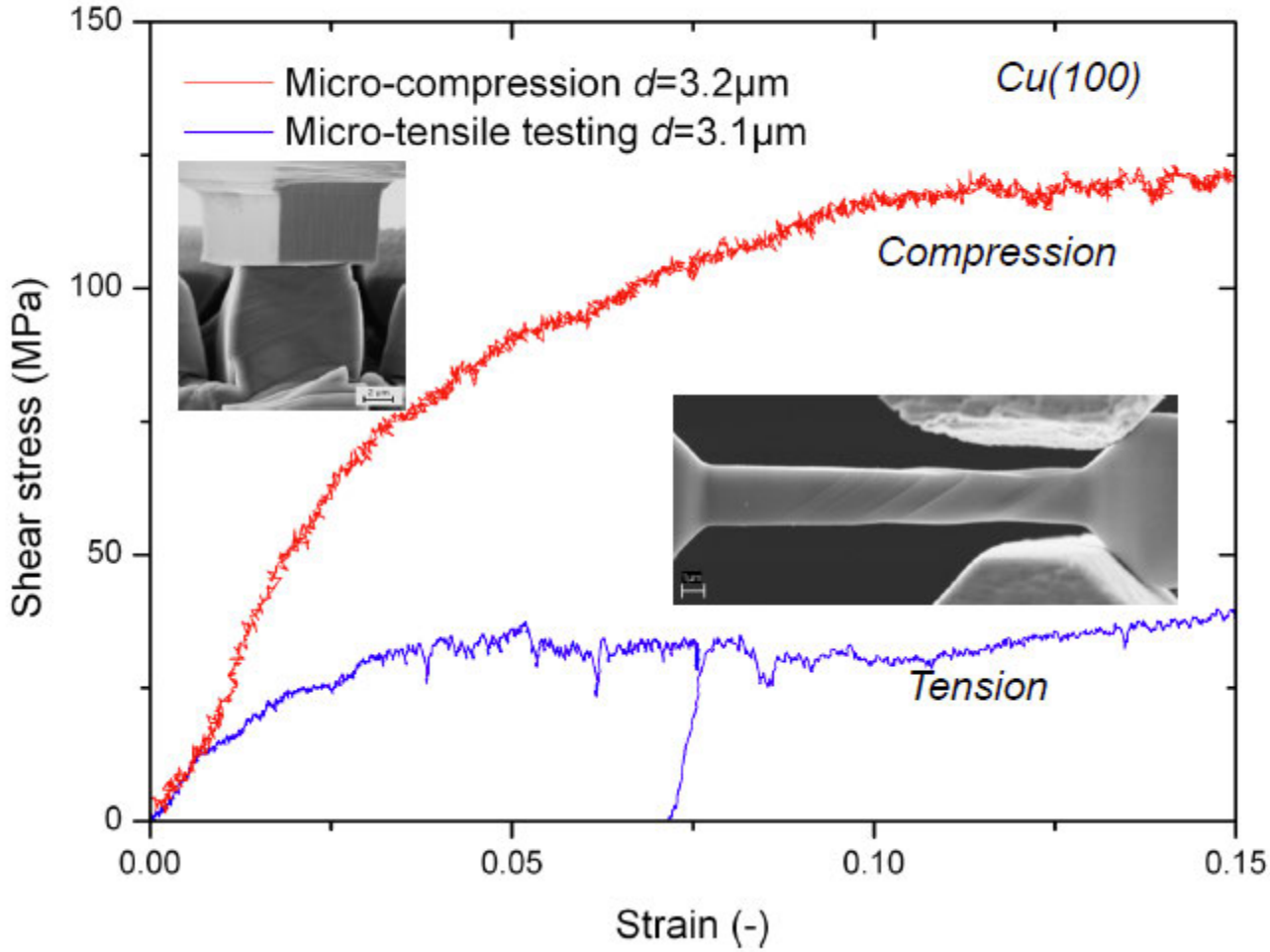

Rotation of the Crystal Lattice

The slip direction rotates towards the tensile axis

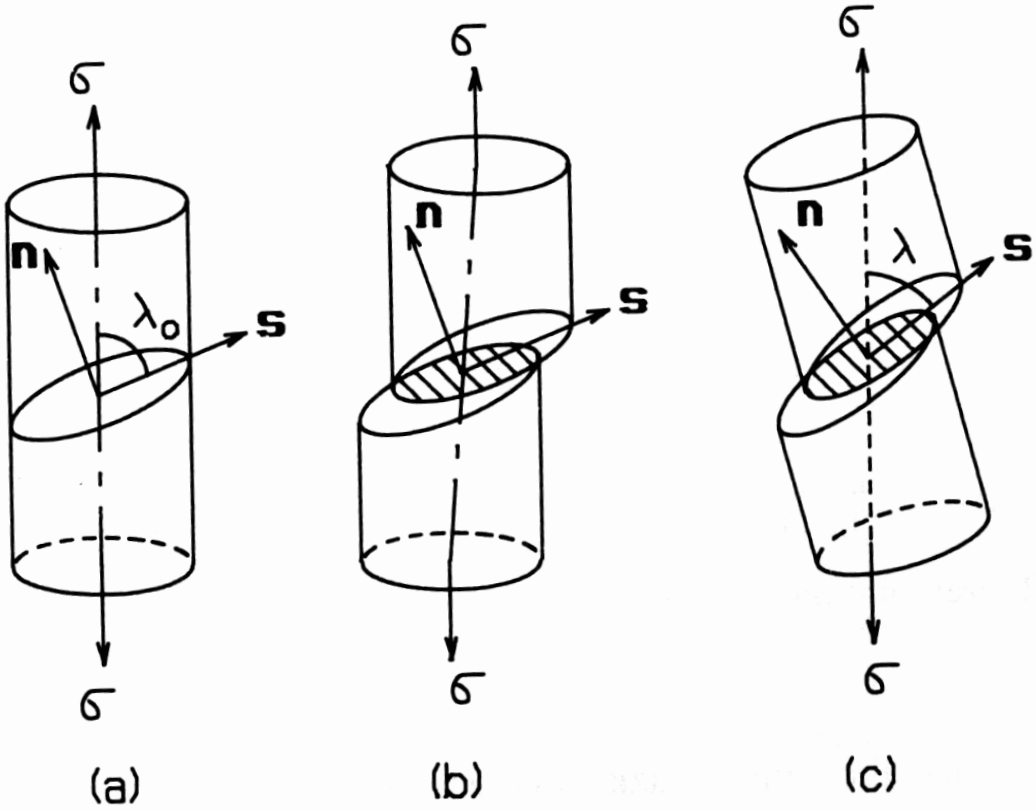

Fig. 10.5 Rotation of crystal lattice in tension

Standard testing at the microscale?

Macroscale

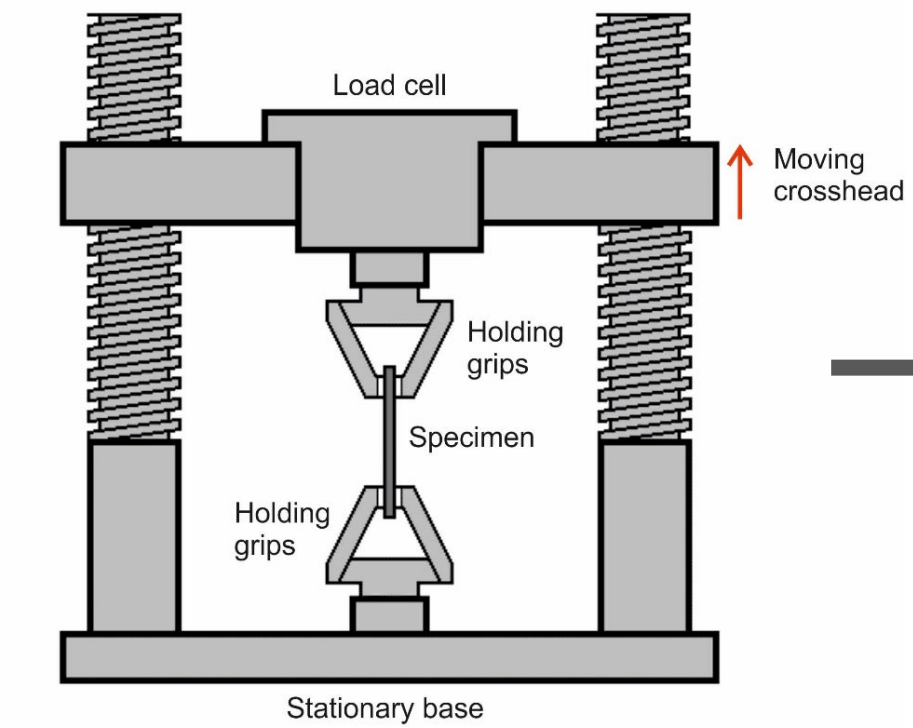

Microscale

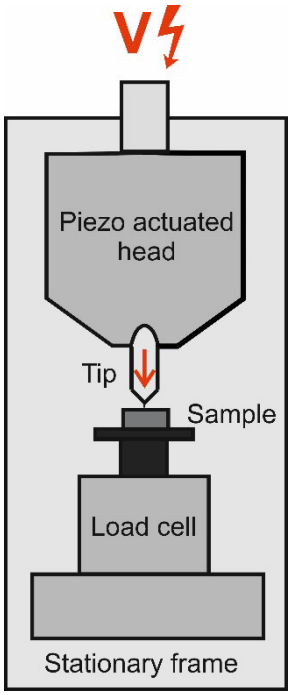

Standard testing at the microscale?

Macroscale

ASTM 638 Type V

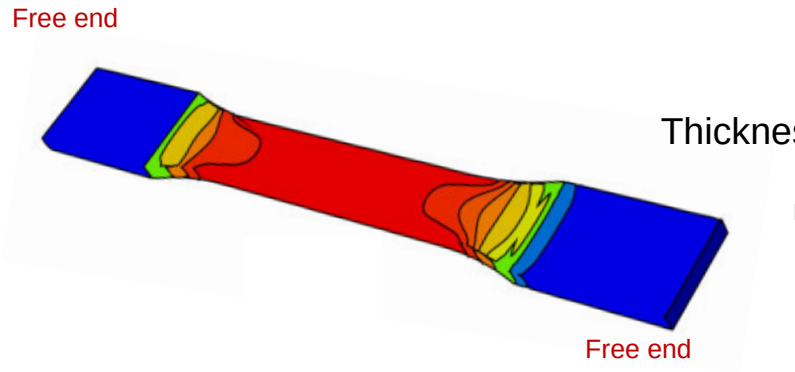

Variables

Thickness, width, radius, head shape

Microscale

New specimen geometry

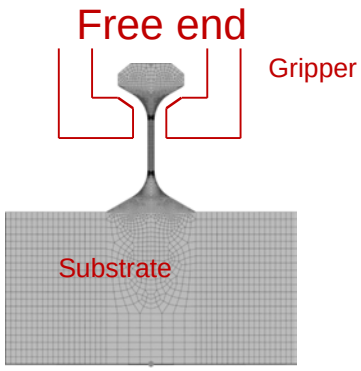

Goals

Homogeneous stress in the gauge section

Low stress concentration at the radius (<5%)

Constrains

Maximum gauge dimensions = 10 µm (**lamell**

On bulk substrate (**no micromanipulation**)

FIB milling fabrication

Specimen design

- **Finite elements analysis using Abaqus/Standard:**
  - ¼ Symmetry, C3D8R (no bending).
  - Linear elastic material properties.
  - Hourglassing controlled and checked with ALLAE/ALLIE < 1%.

Variables: thickness, width, radius, head;
Fixed: gauge length = 10 μm

Output: stress profile and stress concentrations

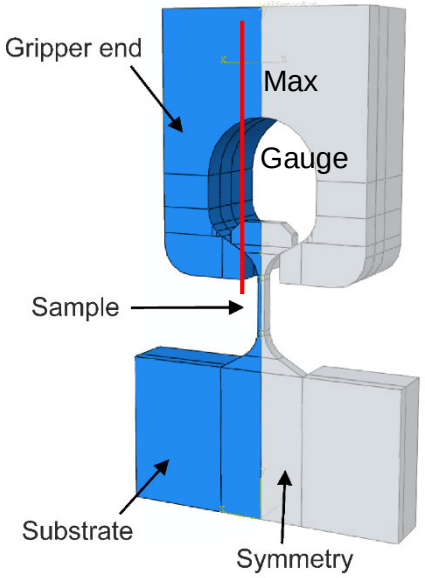

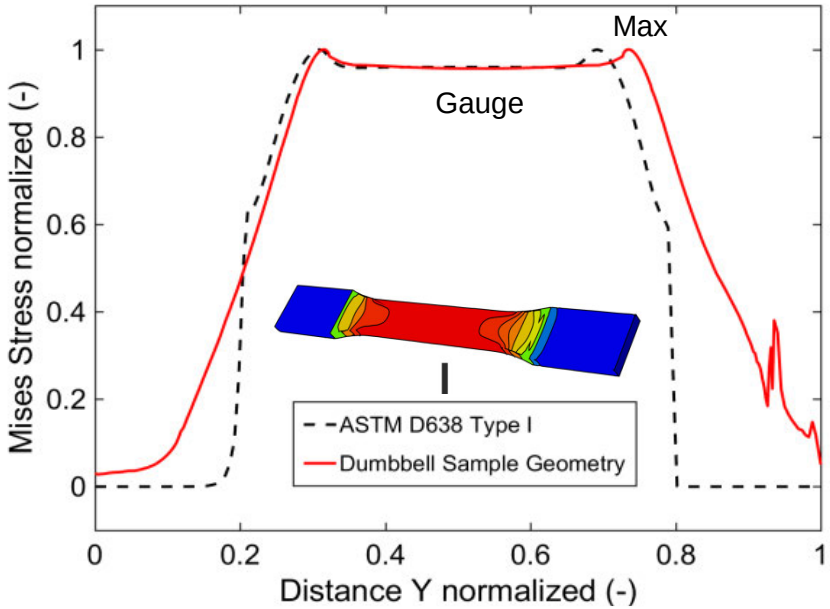

Specimen design

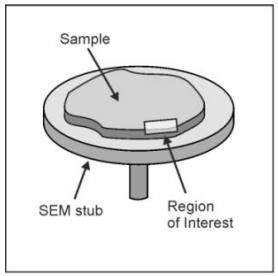

0. Sample on a SEM stub

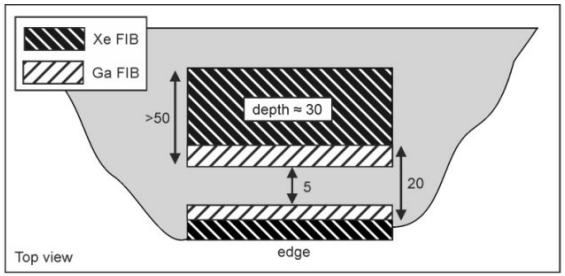

1. Xe plasma-FIB milling (30kV, 30 nA) and Ga FIB (30kV, 4.5nA and 0.7nA)

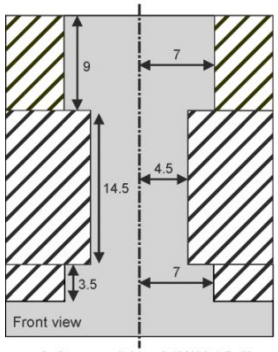

2. Coarse polishing A (30kV, 4.5nA)

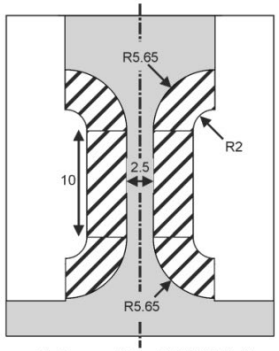

3. Coarse polishing B (30kV, 4.5nA)

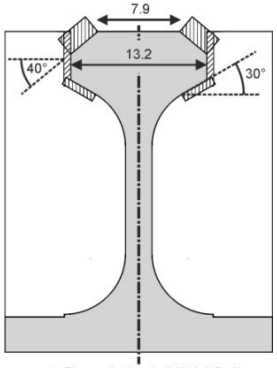

4. Fine polishing A (30kV, 0.7nA)

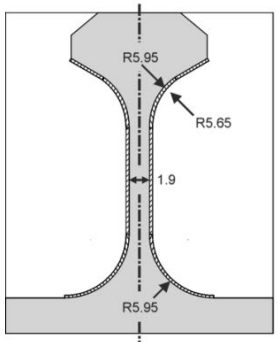

5. Fine polishing B (30kV, 0.7nA)

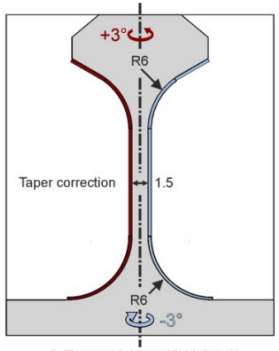

6. Taper polishing (15kV, 0.4nA)

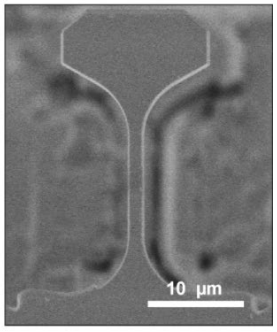

Final geometry

Homogeneous stress profile in the gauge

Gauge section length ≥ 4w.

Low stress concentration at the radius

$$K_c = \frac{\sigma_{max}}{\sigma_{gauge}}$$

Maximise geometry ratio r/w (r/w ≥ 4 → K_c < 1.05).

K_c independent of thickness.

Fabrication via FIB possible

Optimized FIB Milling protocol

Microtensile gripper

Requirements: **Solutions:**

Mounting
Handling
} **Large base**

No creep
Reproducible
} **Silicon**

Alignment
Gripping
} **Needle shaped**

Lateral compliance
↓
Self-aligning

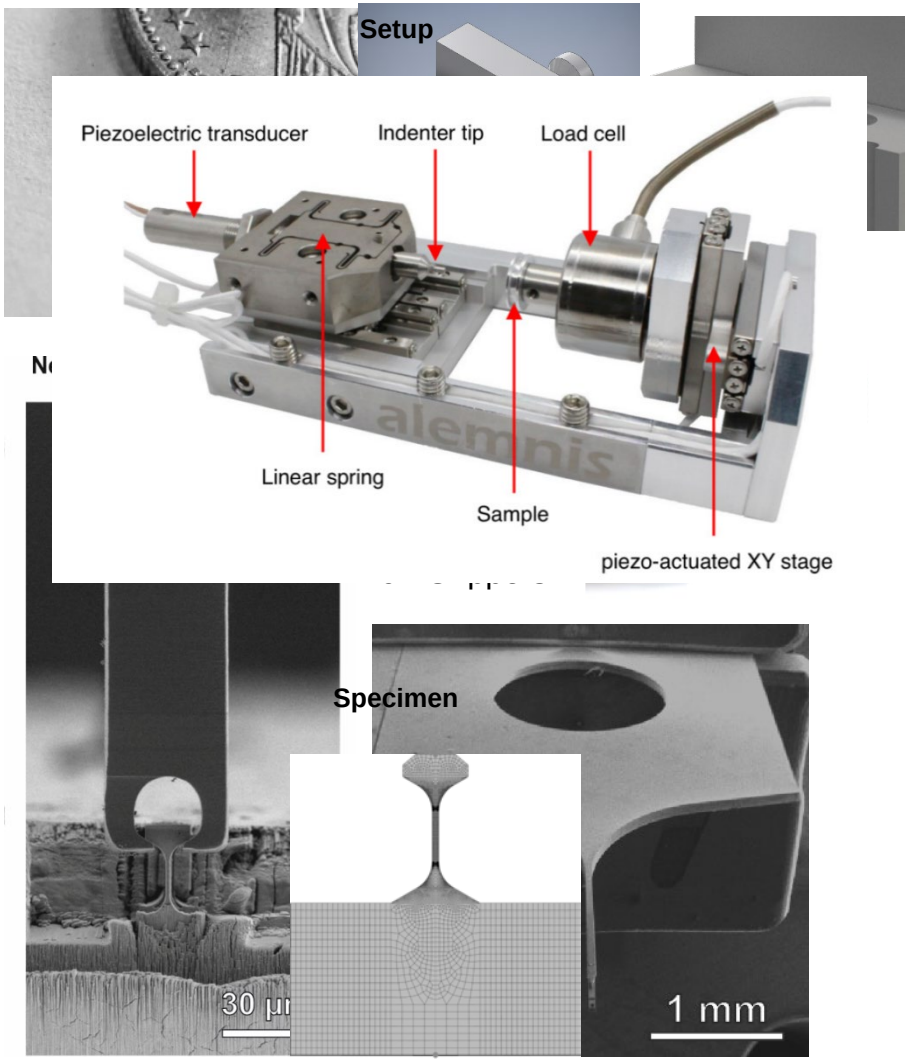

Misaligment tolerance

Mathematic a

Abaqus/Standa rd

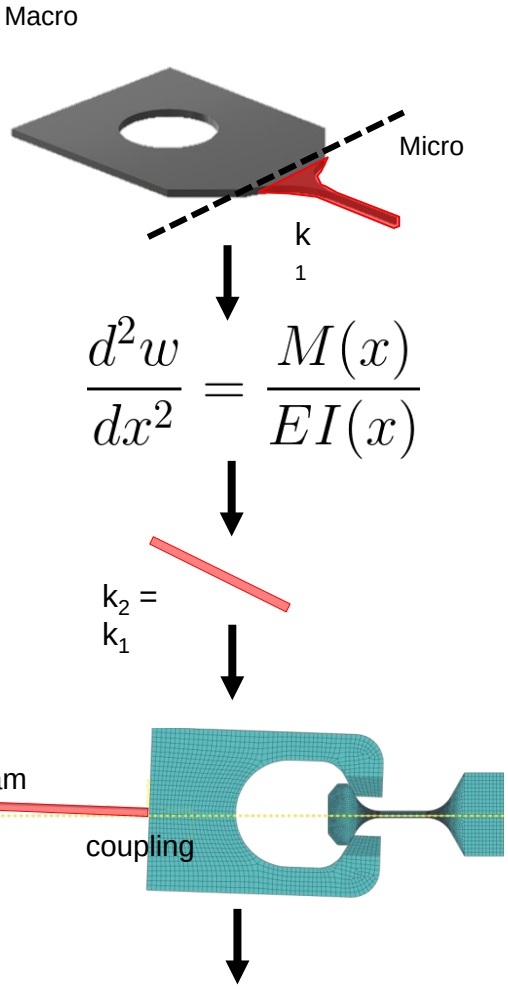

Which needle shape is bette

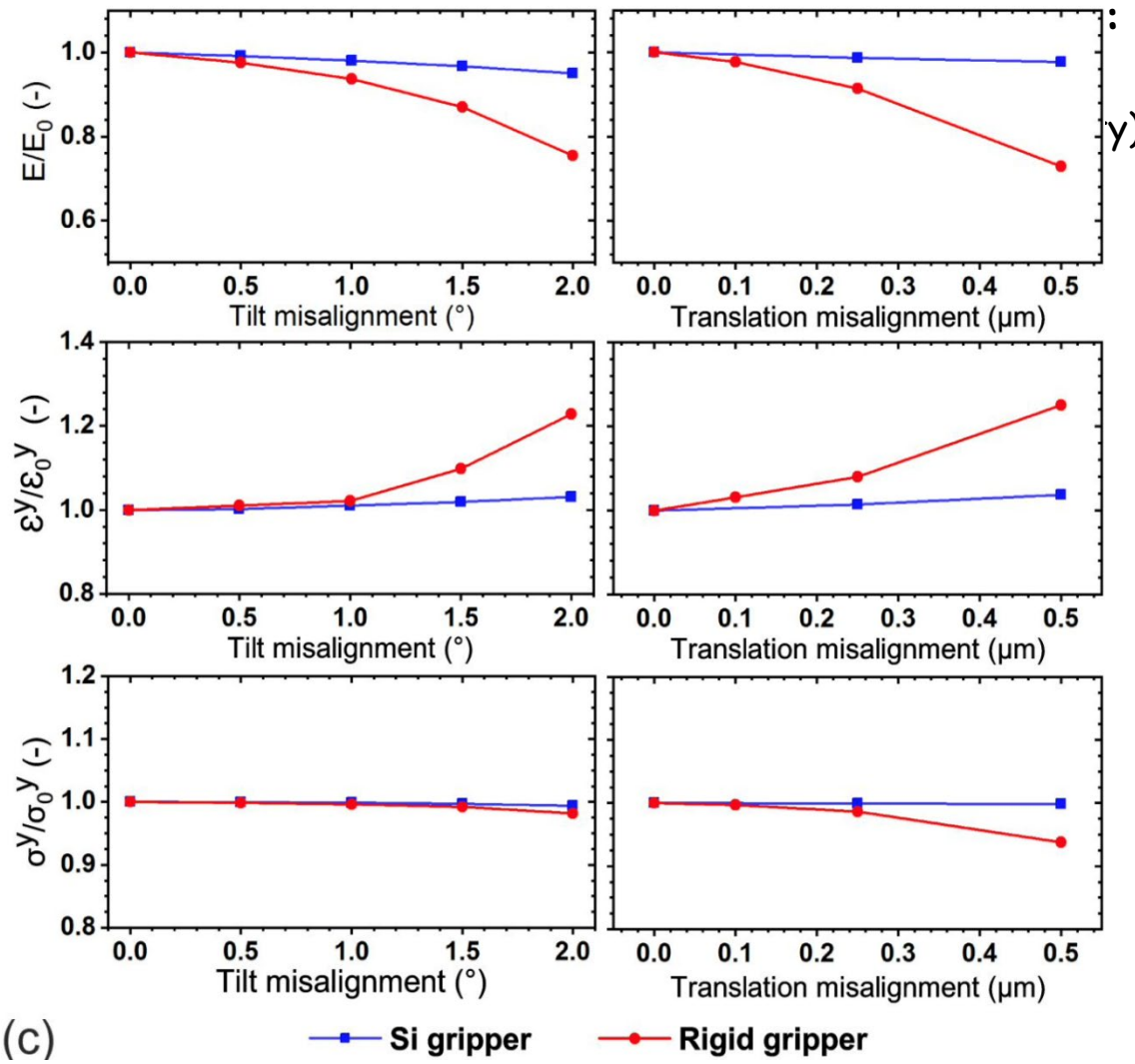

Misaligment tolerance

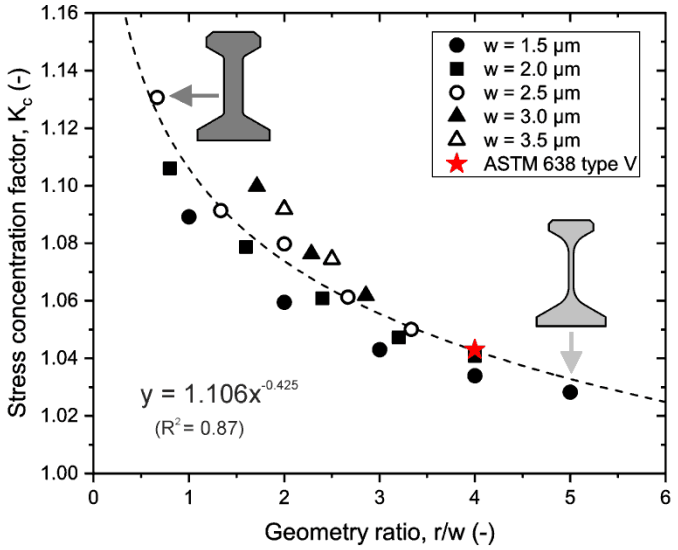

(a)

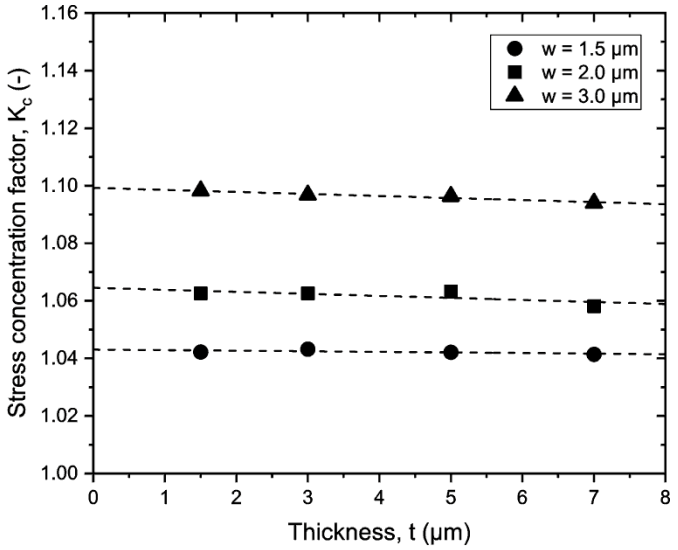

(b)

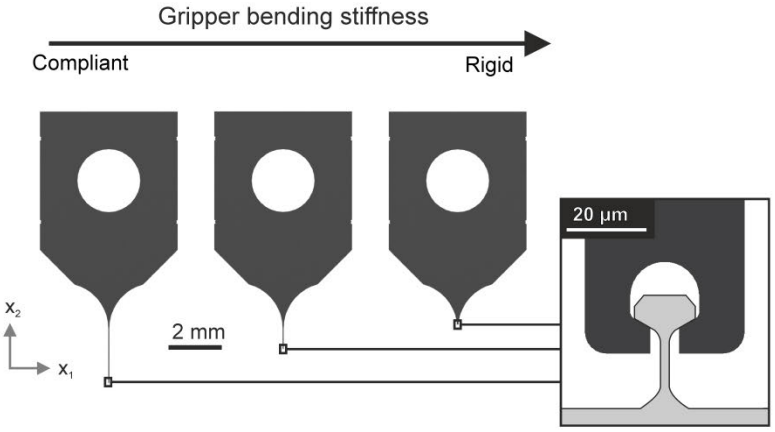

(a)

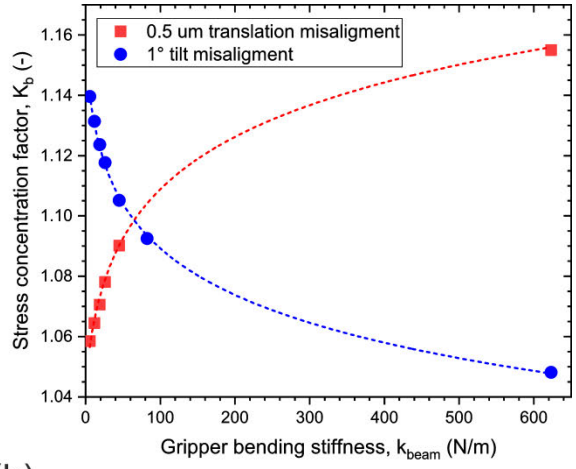

(b)

Microtensile setup

Setup components

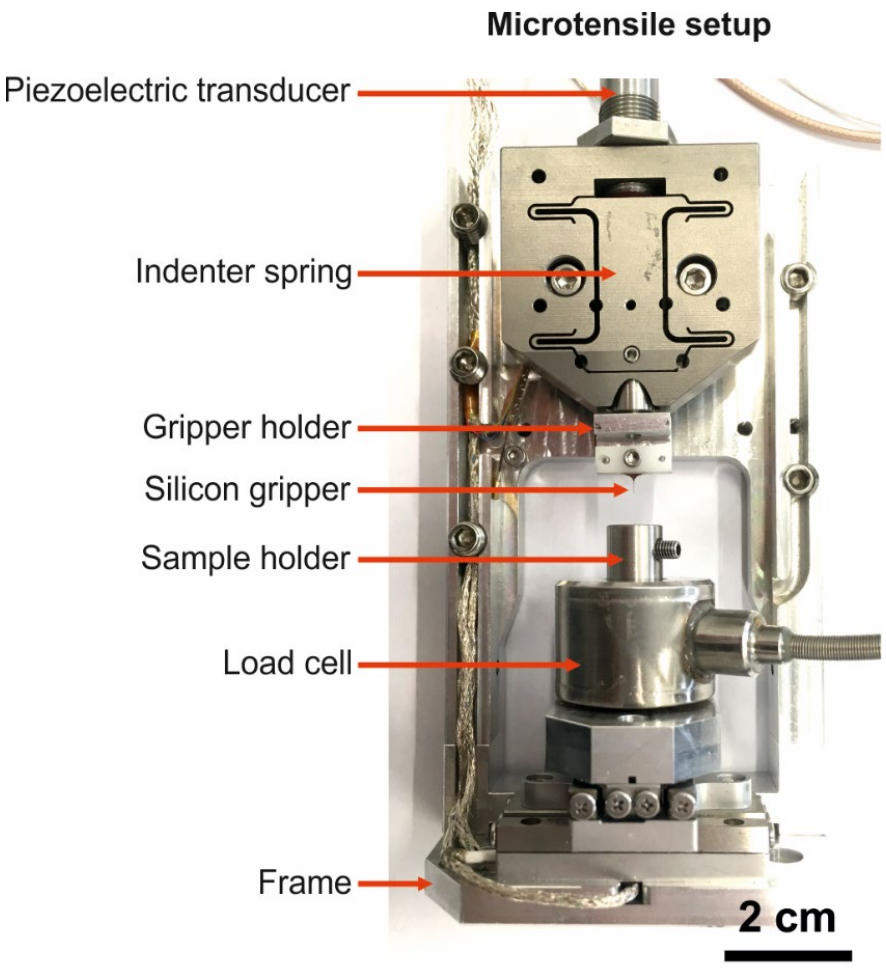

Misalignment tolerance

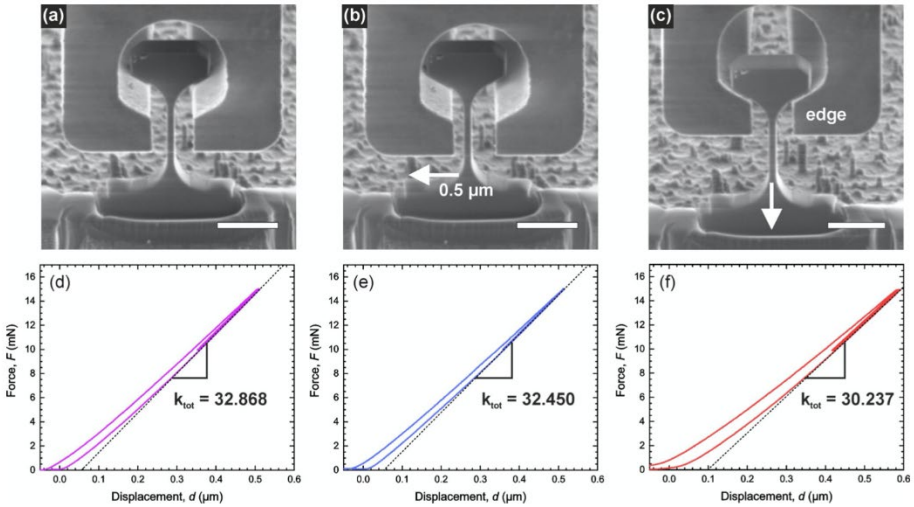

Compliance correction

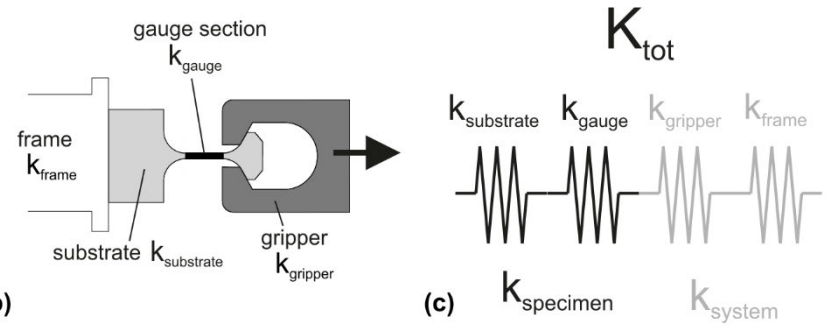

Validation and application

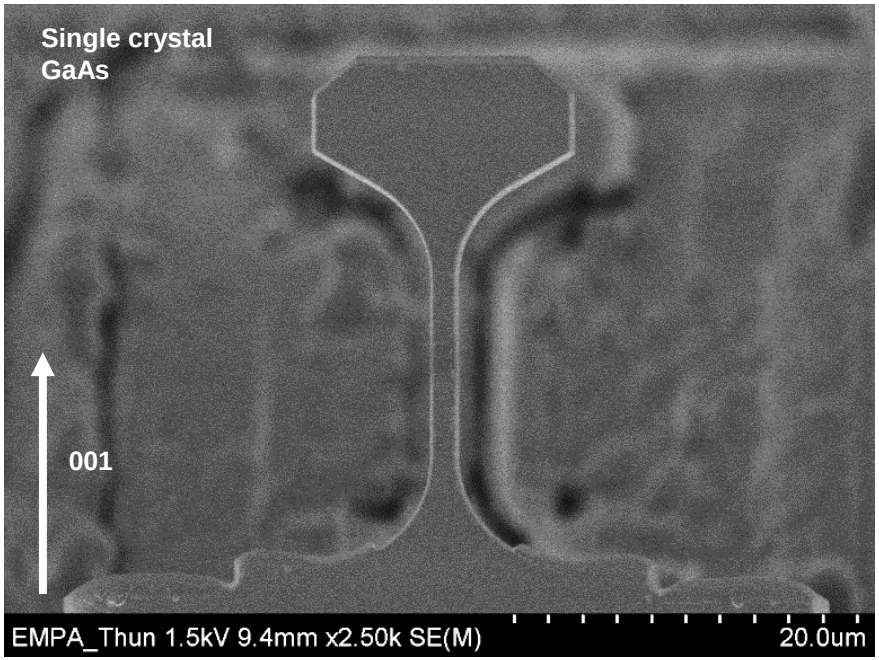

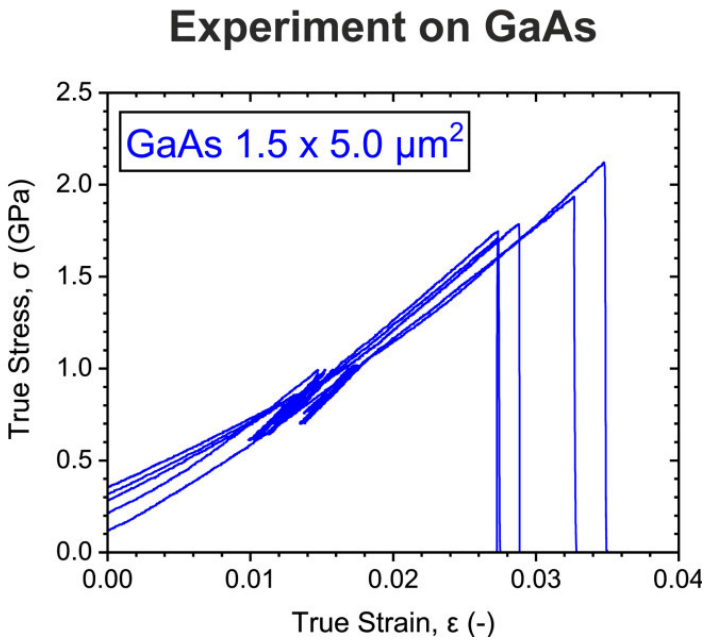

Property	Literature value (GPa)	Measured (N = 5) (GPa)	Relative difference (%)
Elastic modulus E_{001}	**85.5**		

More information in: A self-aligning microtensile setup: application to single-crystal GaAs microscale tension–compression asymmetry, *Journal of Material Research, **34,*** 2019

Case study: Microtensile properties of bone

Tension-compression asymmetry

Structural hierarchy of bone

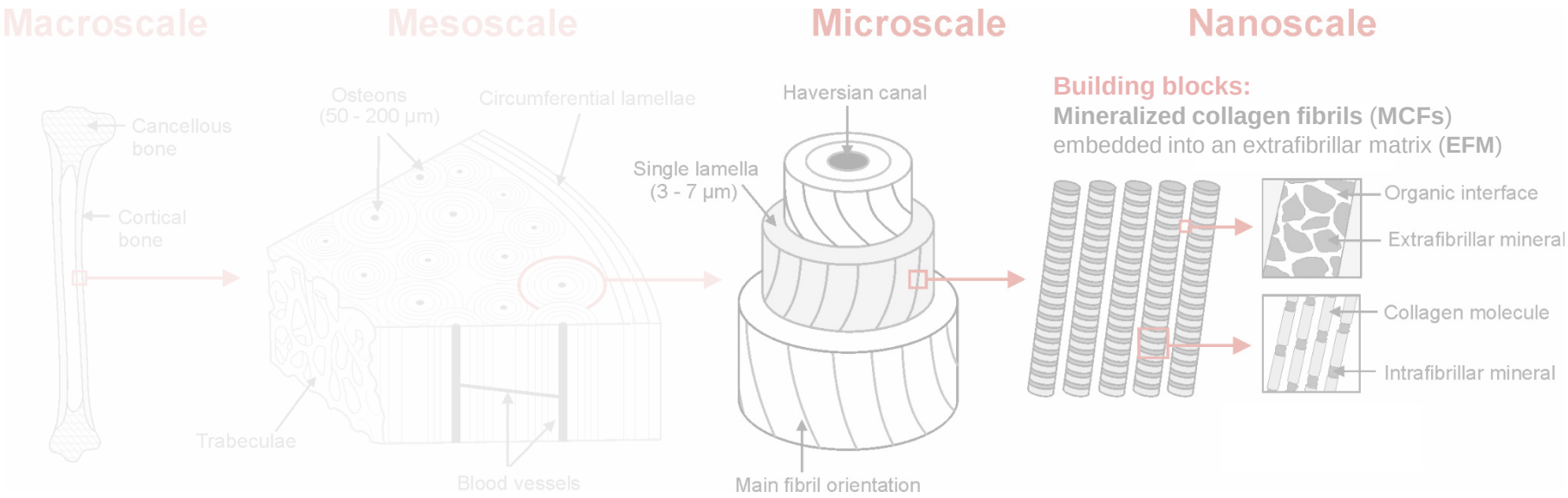

Limited selection constituents: collagen, hydroxyapatite minerals, water and non-collagenous proteins

Lamellar bone: most abundant type of bone, MCFs arrays oriented within each lamella.

Properties: lightweight, stiff, strong and tough.

Microscopic cracks, blood vessels, cells network **BUT** **Tolerance to flaws** (healthy)

How? Several **weak interfaces** at different length scales create different toughening mechanisms.

Toughening mechanisms

Several toughening mechanisms in bone

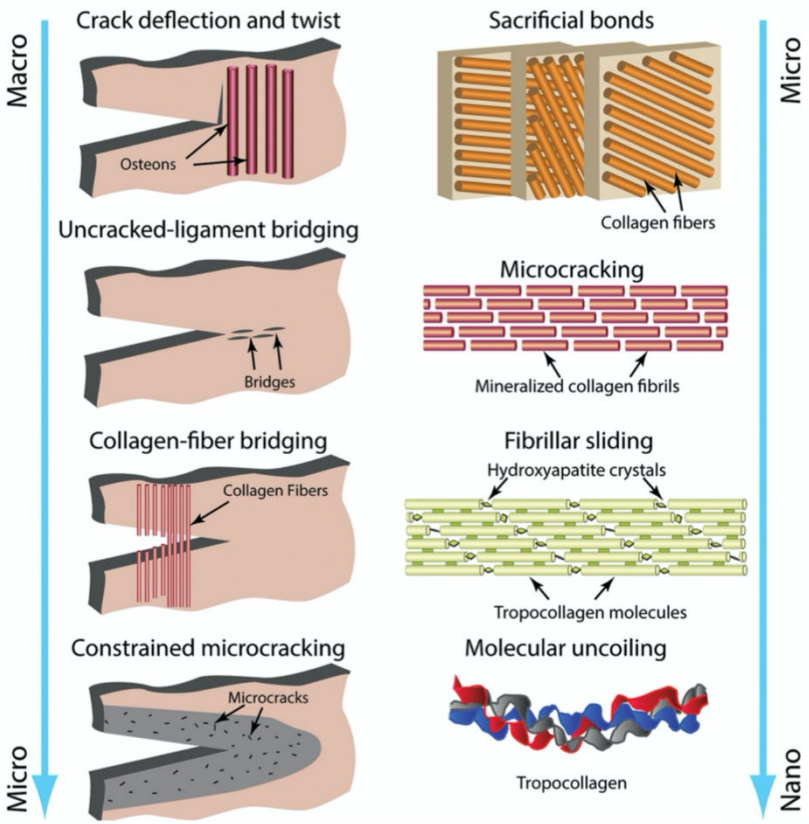

Zimmerman & Ritchie, *Adv. Healthc. Mater.* (2015)

Bone exhibits **two types** of toughening mechanisms

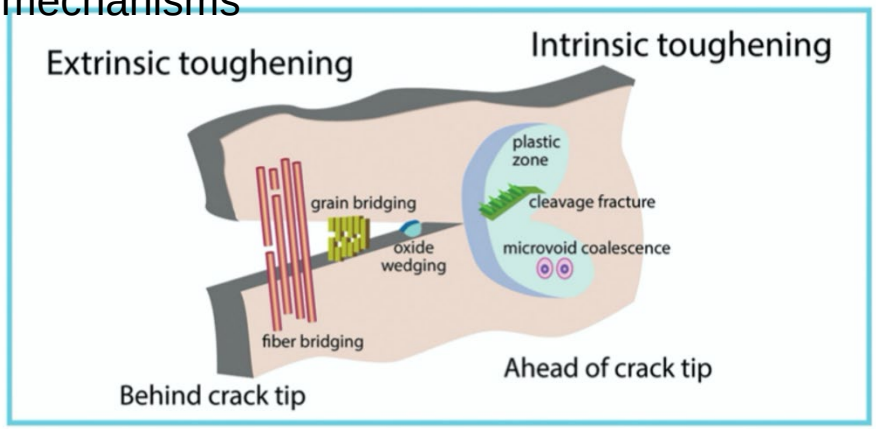

Zimmerman & Ritchie, *Adv. Healthc. Mater.* (2015)

Intrinsic mechanisms:
prevent crack initiation (and growth).

Extrinsic mechanisms:
resist propagation of an existing crack.

The **hierarchical** organization of simple **building blocks** and **interfaces** allows bone to resist fracture.

Macroscale mechanical properties

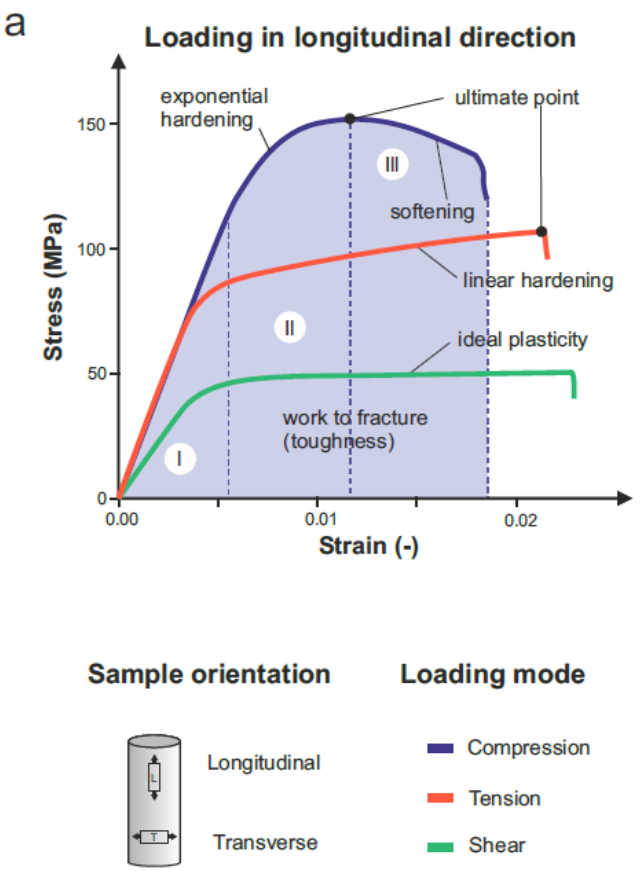

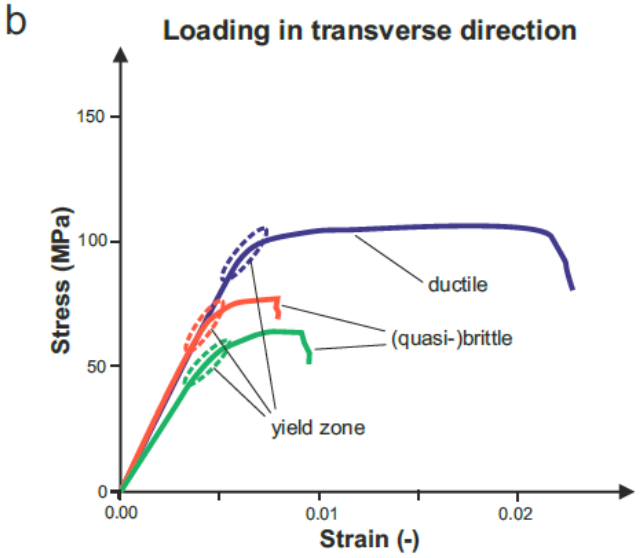

Loading mode dependent

Anisotropic

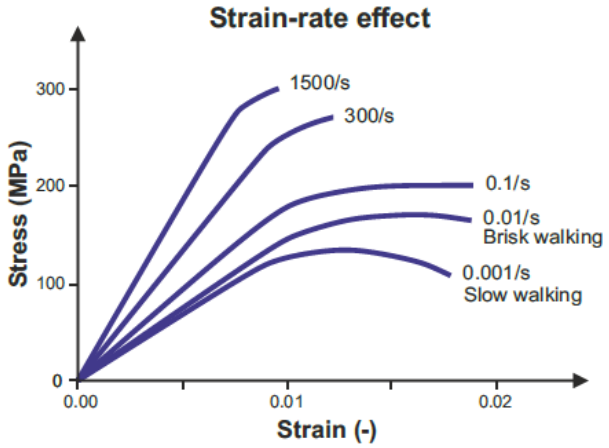

Viscoelastic

(a,b) adapted from Wolfram & Schwiedrzik, *BoneKEy reports* (2016)
(c) adapted from McElhaney *J. Appl. Physiol.* (1966)

Degradation and osteoporosis

Decrease in bone strength and toughness with age

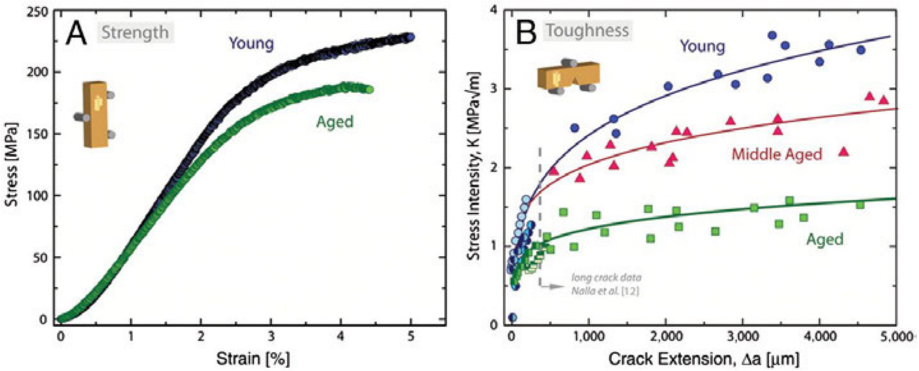

Strength: - 2% every decade*

Toughness: - 4% every decade*

Zimmerman et al. *PNAS* (2011)

*from 40 years old

Increase in porosity (bone quantity)

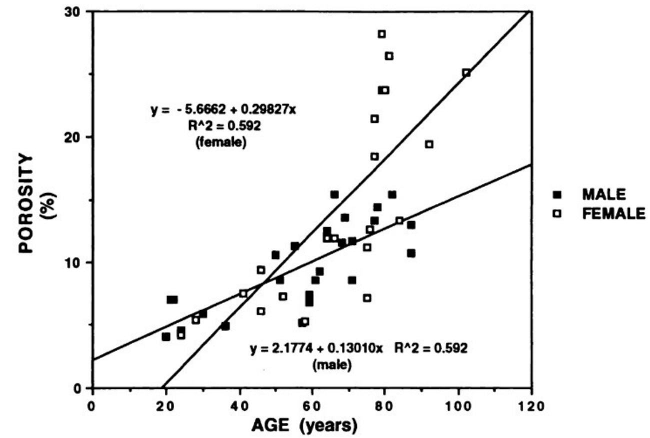

McCalden et al. *JBJS* (1993)

Microdamage accumulation (bone quality)

Osteoporosis: conventional diagnosis via dual-energy X-ray absorptiometry (DXA)

Changes in composition (bone quality)

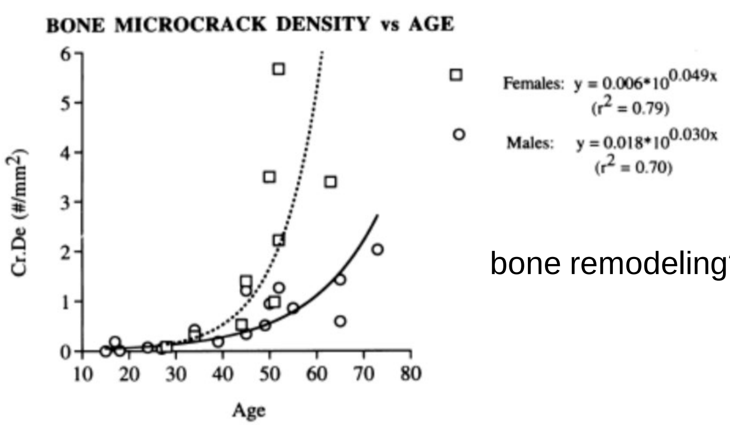

Schaffler et al. *Bone* (1995)

bone remodeling?

Increased **collagen cross-linking** inhibits collagen slip

Snedeker et al. *MLTJ*, 2014

Changes in **interfaces**?

Higher fraction of weak cement lines

Smaller osteons: reduced crack deflection

Zimmerman et al. *PNAS* (2011)

crite

Empa
Materials Science and Technology

Sample preparation

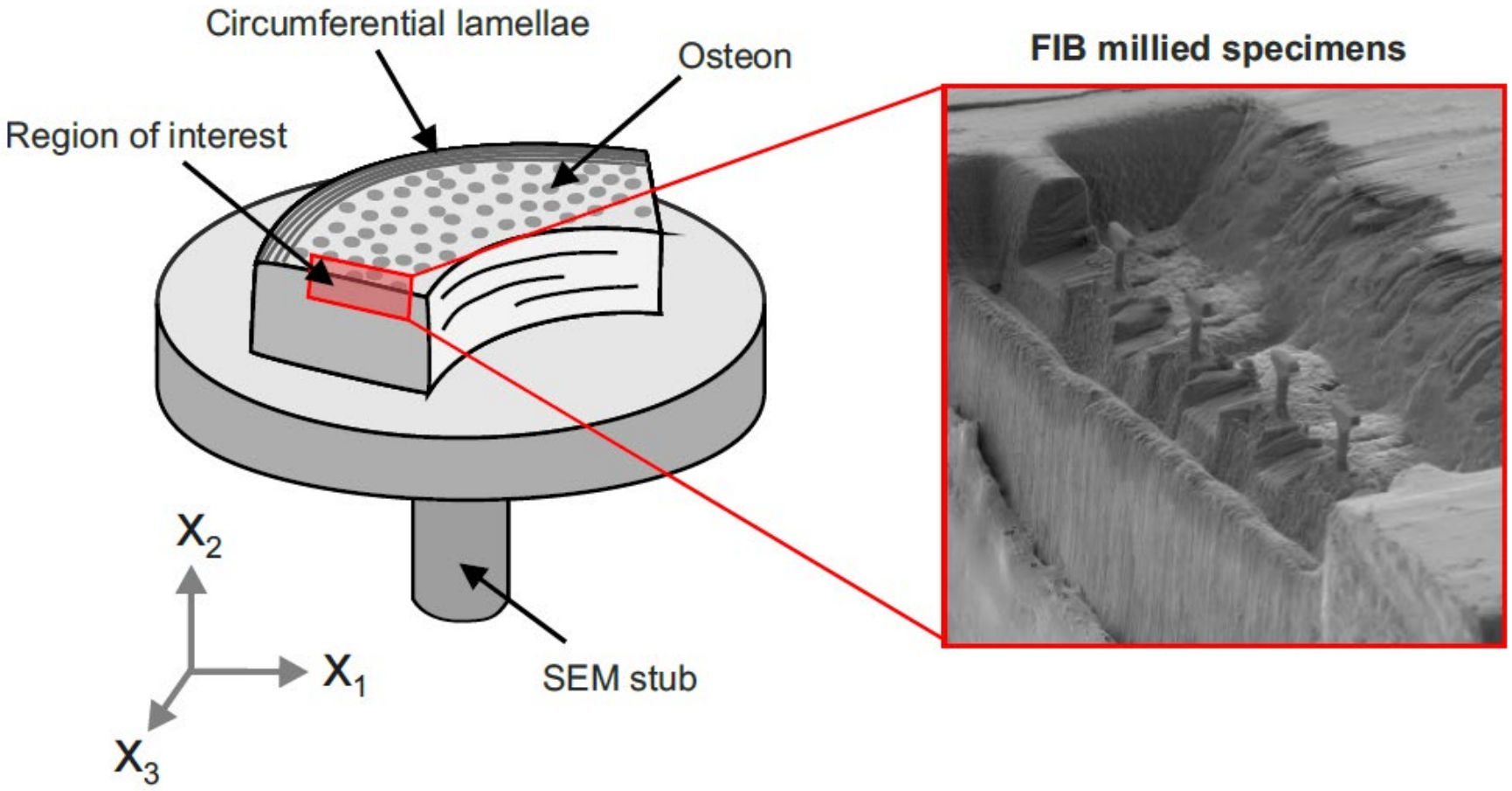

Microtensile experiments

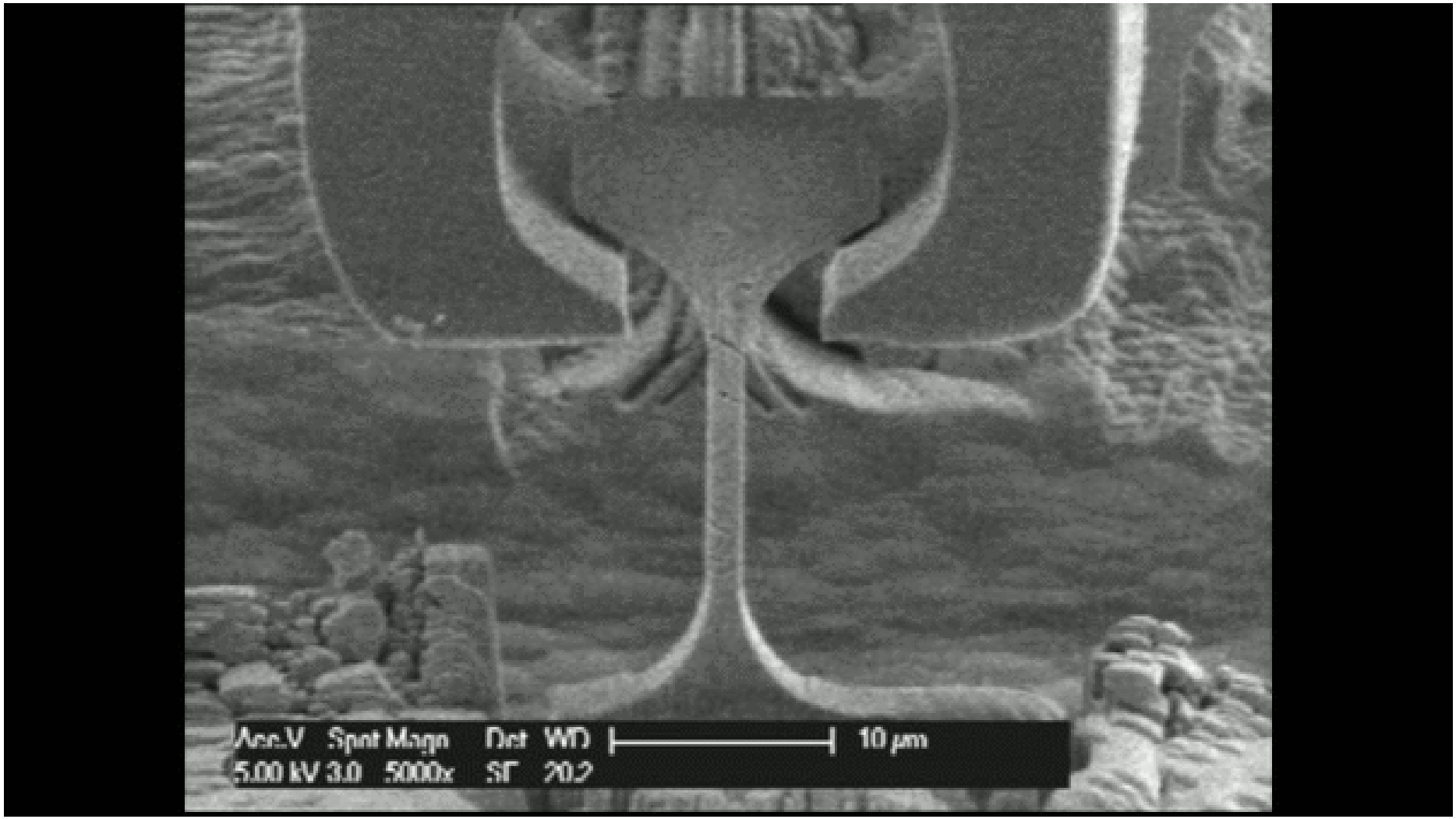

Tension-compression asymmetry

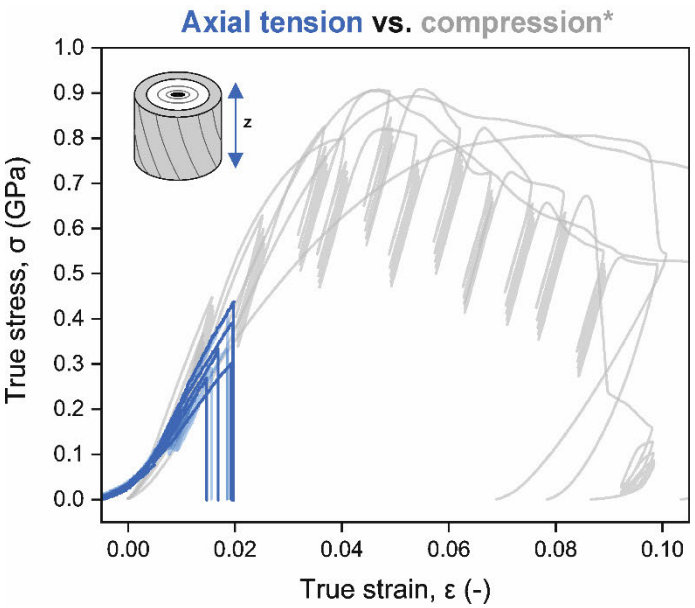

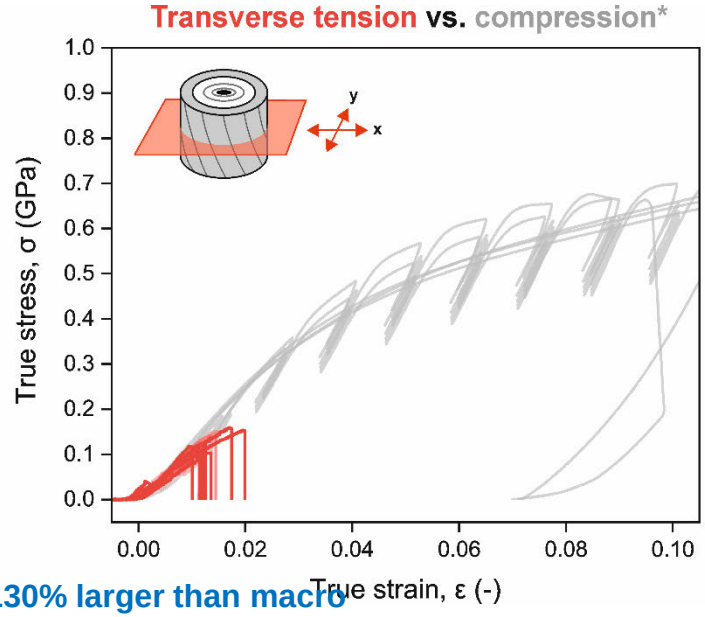

130% larger than macro

Sample Orientation	Loading mode	E (GPa)	σ^{max} (GPa)	$\varepsilon(\sigma^{max})$ (%)	σ^{y} (GPa)
Axial	Compression*	31.1 ± 6.5	0.75 ± 0.06	5.4 ± 1.7	0.49 ± 0.10
	Tension	28.9 ± 3.4	0.35 ± 0.05	1.8 ± 0.2	-
Transverse	Compression*	16.5 ± 1.5	0.59 ± 0.04	12.1 ± 2.5	0.30 ± 0.02
	Tension	13.6 ± 1.2	0.13 ± 0.02	1.3 ± 0.3	-

1.3

2.7

* data obtained from Schwiedrzik et al. *Nat. Mat.* (2014)

- **Elastic properties are similar** between loading mode and depend on sample orientation.
- Bone is **stronger at the microscale** (2.3 fold increase, similarly to compression).
- **Strength anisotropy** is much higher in **tension** than in compression.

Post-test analysis

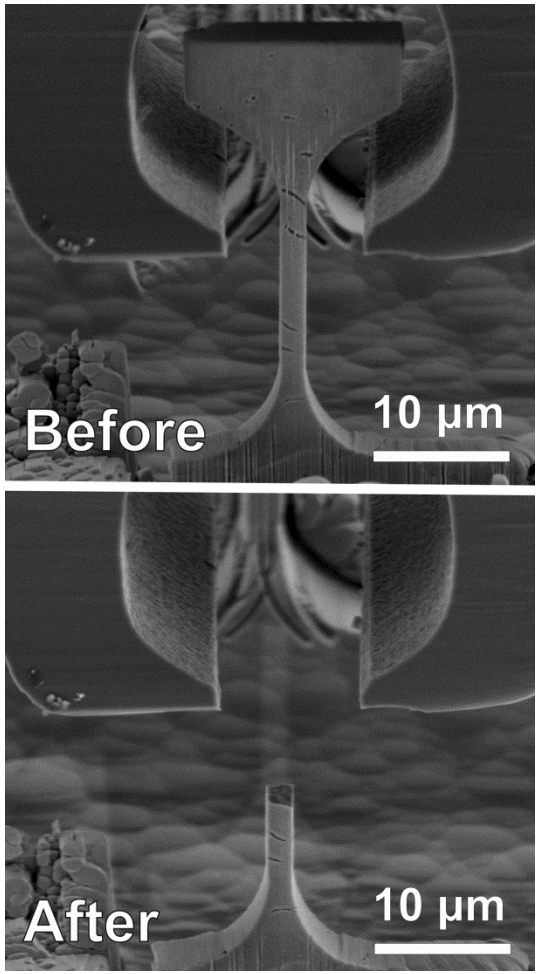

SEM

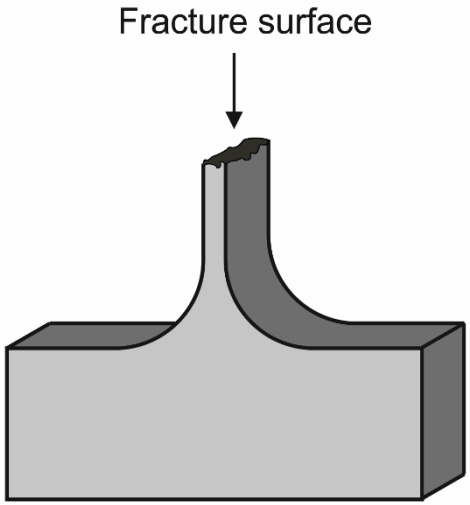

+ Quick, no further modification
+ Failure information
- Only surface information

STEM

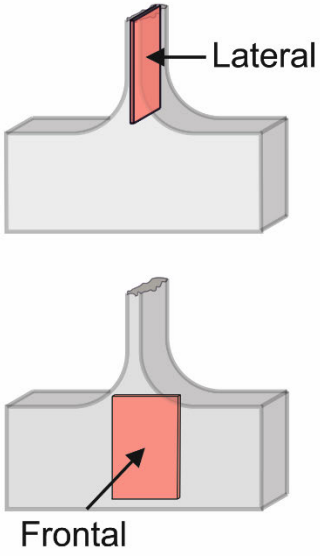

- Tedious process
- Information on 200 nm in thickness
+ Crack dynamics (lateral section)
+ Microstructure (MCF organization)

Failure mode: fracture surfaces

Contrarily to compression, **change in failure mode** between axial and transverse direction.
→ increase in strength anisotropy compared to compression.

Axial fracture (top view)

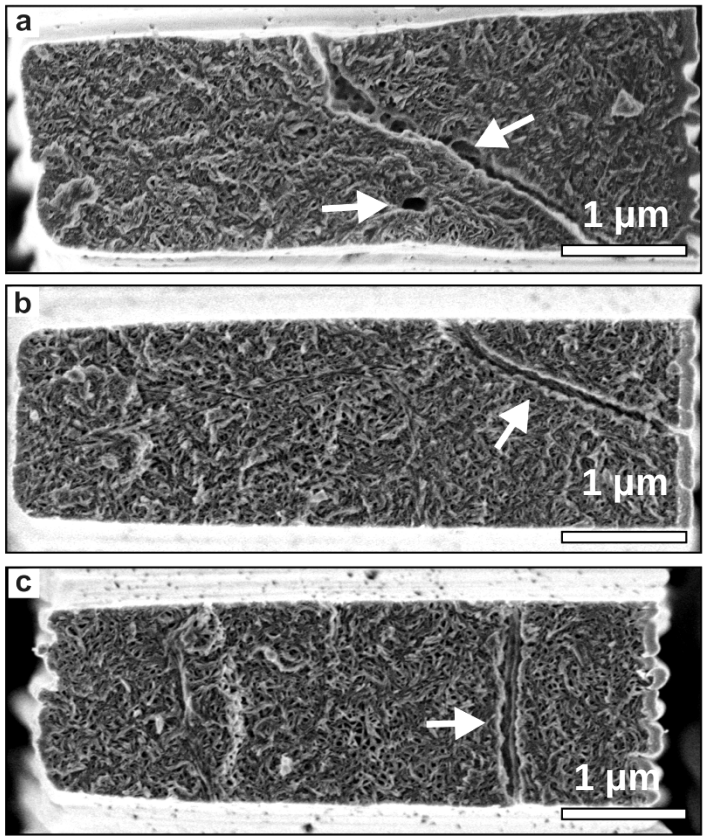

fibril-matrix **interfacial shearing**

Transverse fracture (top view)

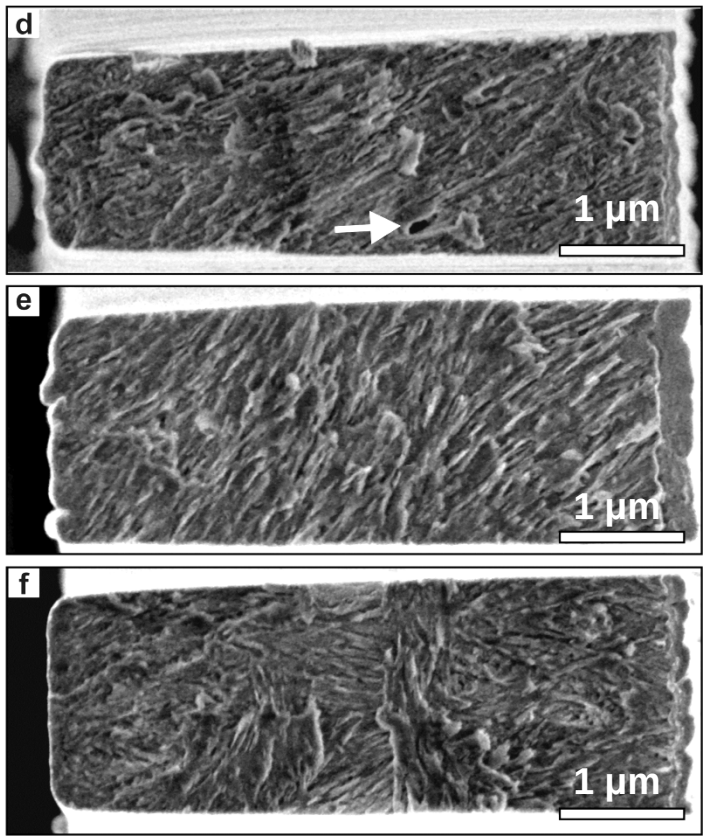

fibril-matrix **tensile debonding**

Axial specimens failure (STEM)

Canaliculi: stress concentrators

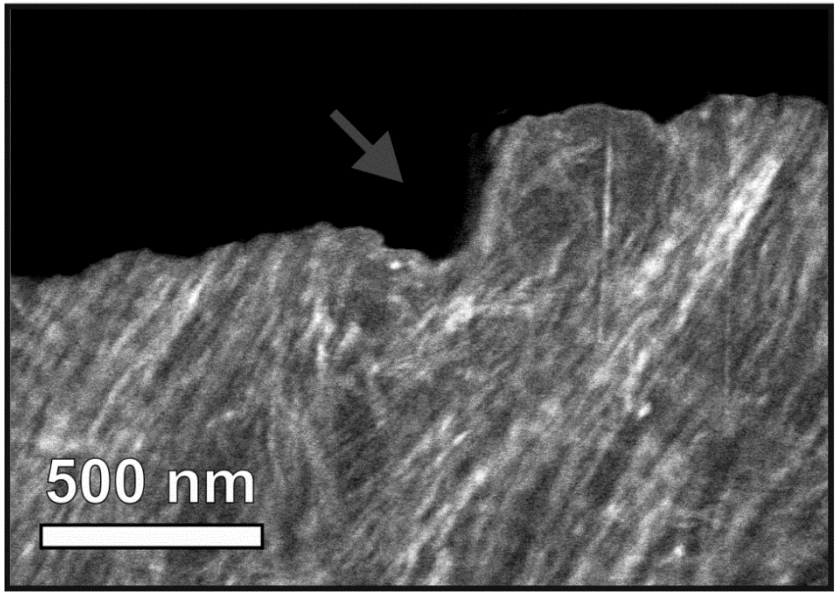

- Canaliculi act as **stress concentrators**.
- Oriented at high angles vs loading directi
- Fracture toughness (LEFM): K_{IC} = 0.17 ± 0.03 MPa(
  1 order of magnitude **smaller than macroscale.**

$$K_I = \sigma\sqrt{\pi a}\left[\sec\left(\frac{\pi a}{2W}\right)^{1/2}\right]\left[1 - 0.025\left(\frac{a}{W}\right)^2 + 0.06\left(\frac{a}{w}\right)^4\right]$$

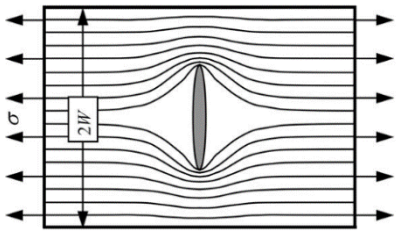

T.L. Anderson, Fracture Mechanics: Fundamentals and Applications, *CRC Press* 3rd ed. (2005)

Transverse specimens failure (STEM)

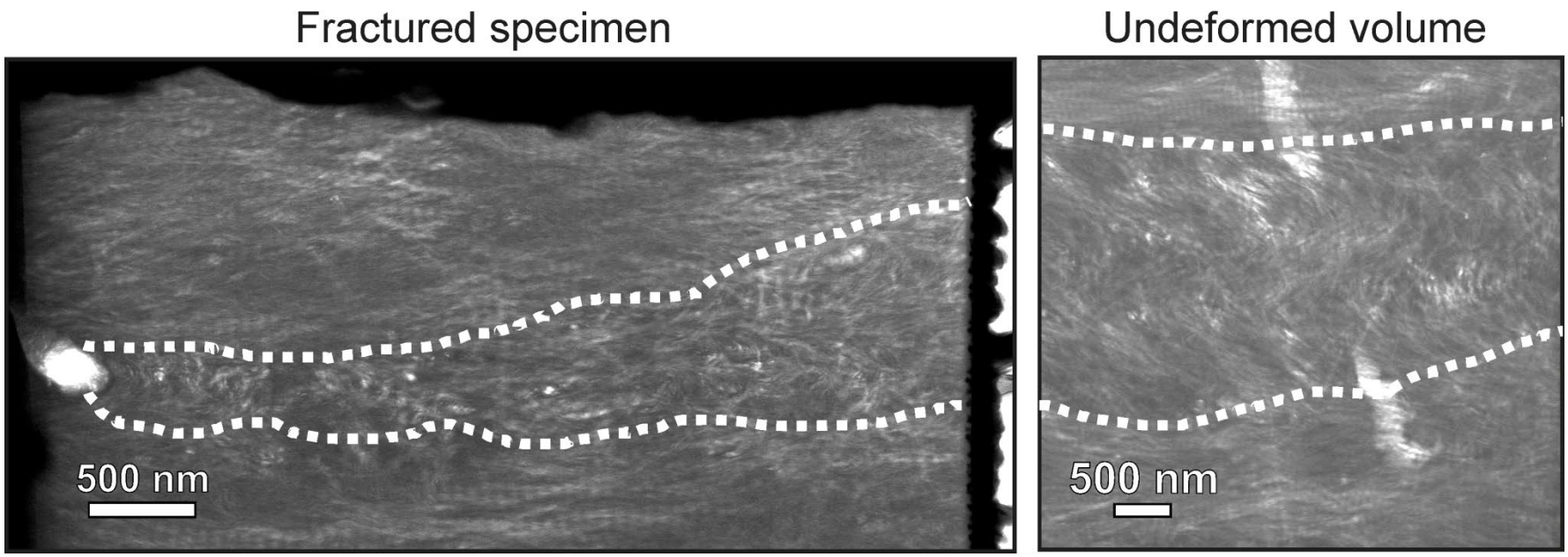

- Crack always perpendicular to loading direction (<3°) even without canaliculi (in 58% cases).
- Fracture toughness when **canaliculi** is present: $K_{IC} = 0.07 \pm 0.01$ MPa(m) $^{1/2}$
- The **disordered phases** act as **weak interfaces** → crack deflection.
- These weak interfaces are not resulting from the tests, but are present in the material.

MCF orientation (STEM + ImageJ)

Can we correlate **MCF orientation** and distribution with bone strength?

Region of interest

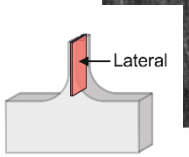

Vector Field (OrientationJ)

Normal distribution

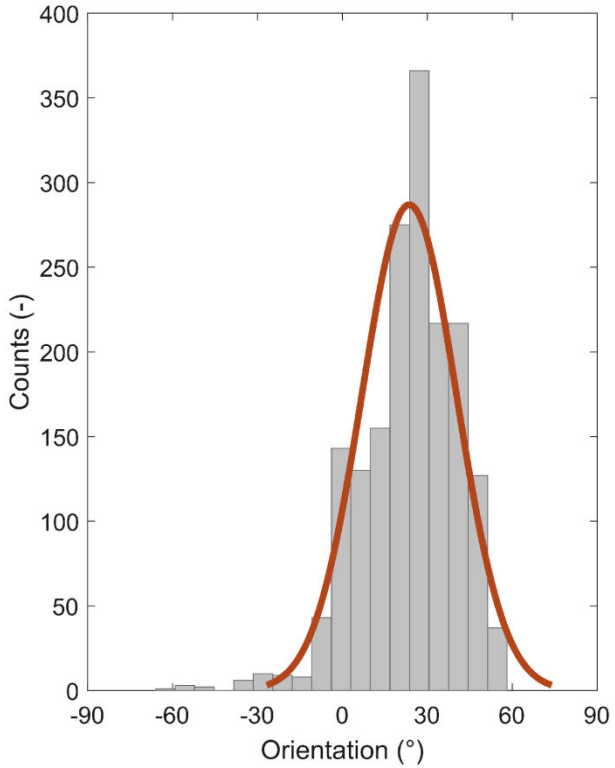

Finite difference gradient over Gaussian window of 150 nm (since banding pattern 67 nm).

ImageJ (NIH, Bethesda, Maryland, USA).
OrientationJ plugin (Biomedical Imaging Group, EPFL, Switzerland, http://bigwww.epfl.ch/demo/orientation/)

Single lamella: orientation vs. strength

Uniaxial microtensile

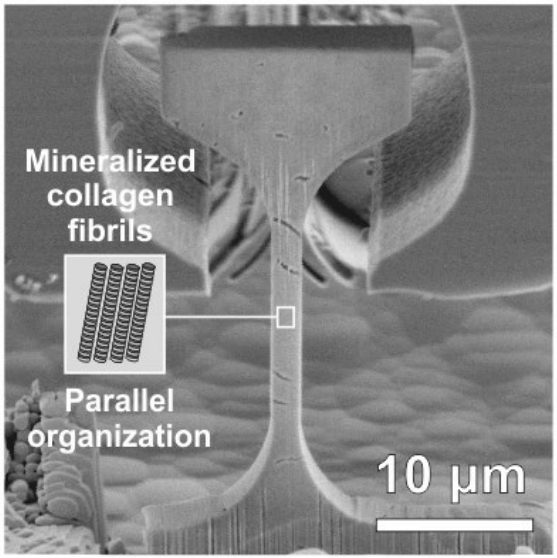

Composite failure model

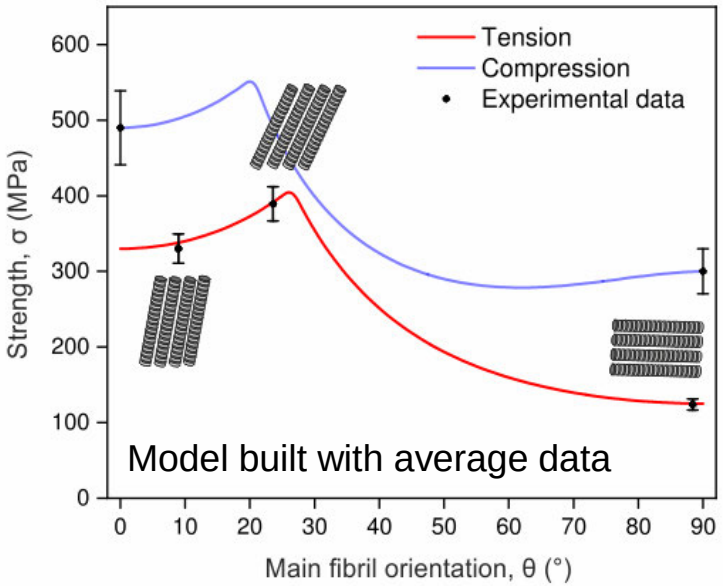

X-ray diffraction

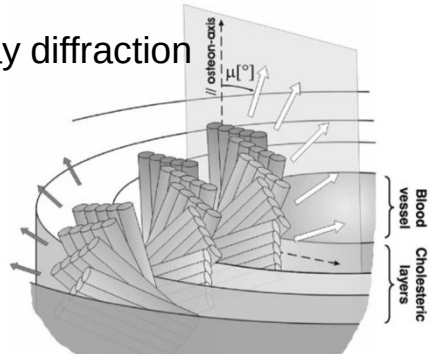

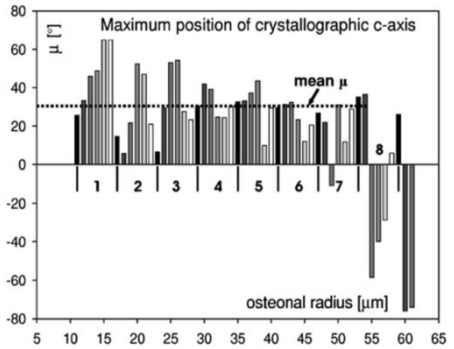

Wagermaier et al. *Biointerphases* 2006.

- Hashin based composite failure model + mechanical and STEM data.
  Gu et al. *Compos. Struct.* (2017)
- Predicts **counterintuitive behavior** yet agreement with experime
- High mineral content in the EFM → **high shear strength**
- High **tolerance** with respect to MCF main orientation.

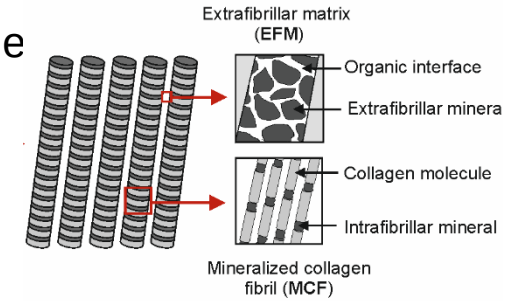

Microcompression testing

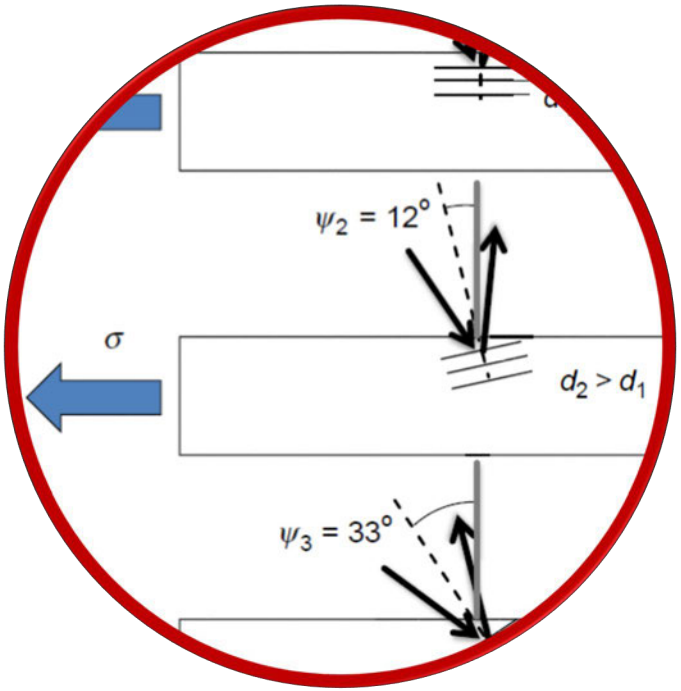

Micropillar Compression

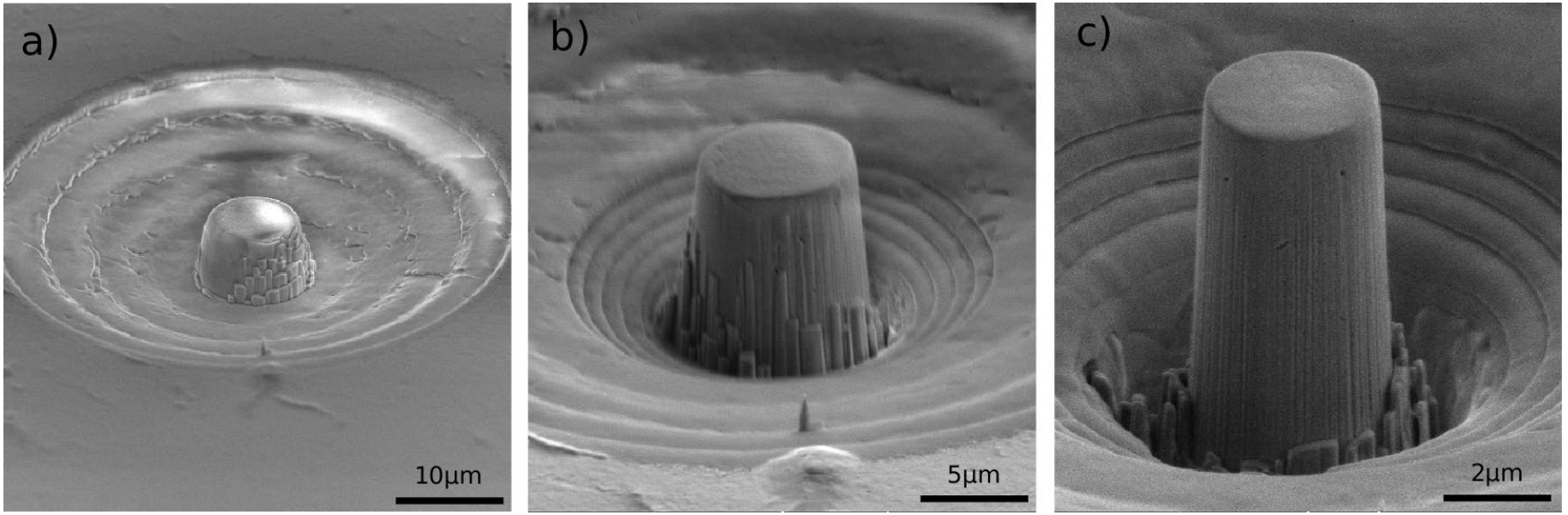

- Micropillars machined using focused ion beam
- Compression with flat punch diamond indenter
- Uniaxial stress state → straightforward interpretation

Micropillar Compression

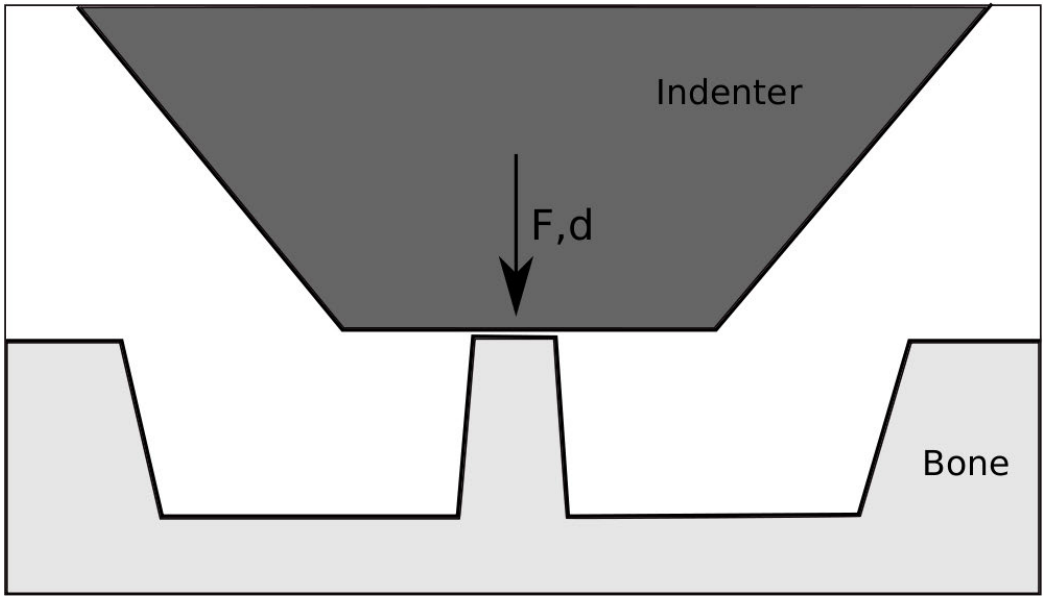

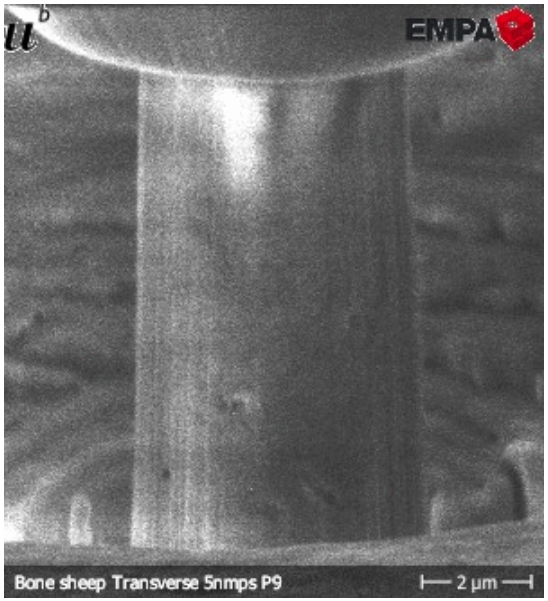

Schwiedrzik et al., Nat. Mat. (2014)

- Micropillars machined using focused ion beam
- Compression with flat punch diamond indenter
- Uniaxial stress state → straightforward interpretation

Micropillar compression (and analysis)

Focused ion beam (FIB) milling

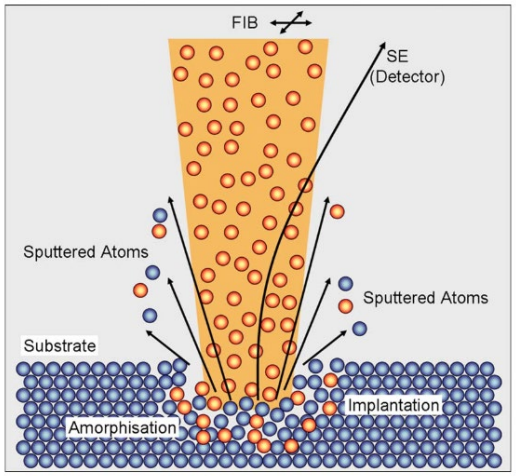

Utke et al. *J. Vac. Sci. Technol. B* (2008)

Different types of FIB

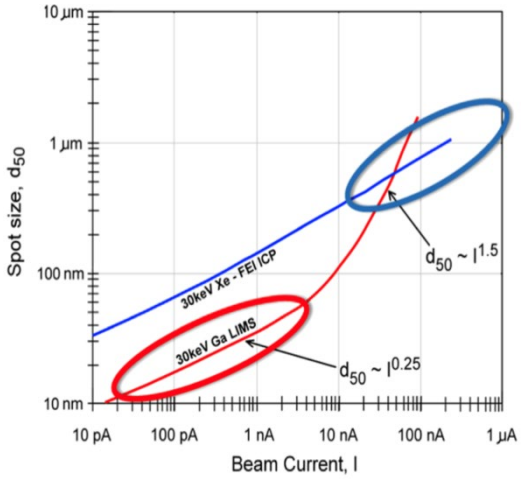

Smith et al. *J. Vac. Sci. Technol. B* (2006)

Compression sample

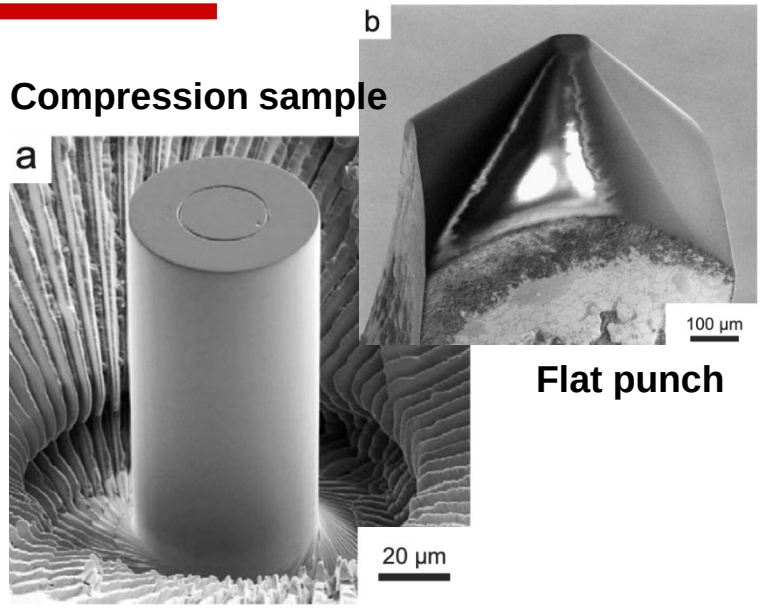

Flat punch

Uchic et al. *Science* (2004)

FIB induced deposition

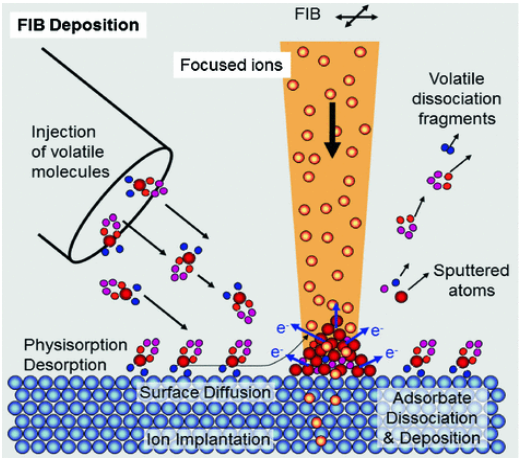

Shorubalko et al.. Helium Ion Microscopy, *Springer* (2016)

Transmission electron microscopy (TEM) lamella preparation

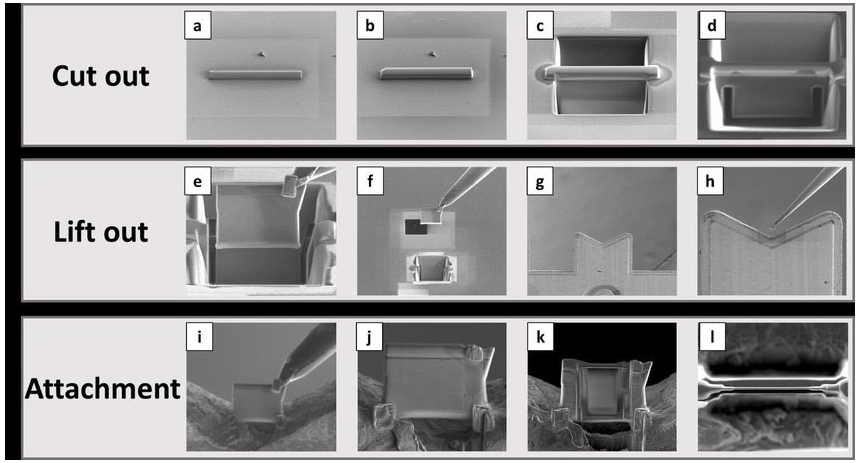

Abed, MSc thesis, University *of Toronto* (2007)

Micropillar Compression
Straightforward
Post-yield behaviour

TEM
Microstructure
Deformation mechanisms

Powerful combination for micro-nanoscale

Micro compression tests

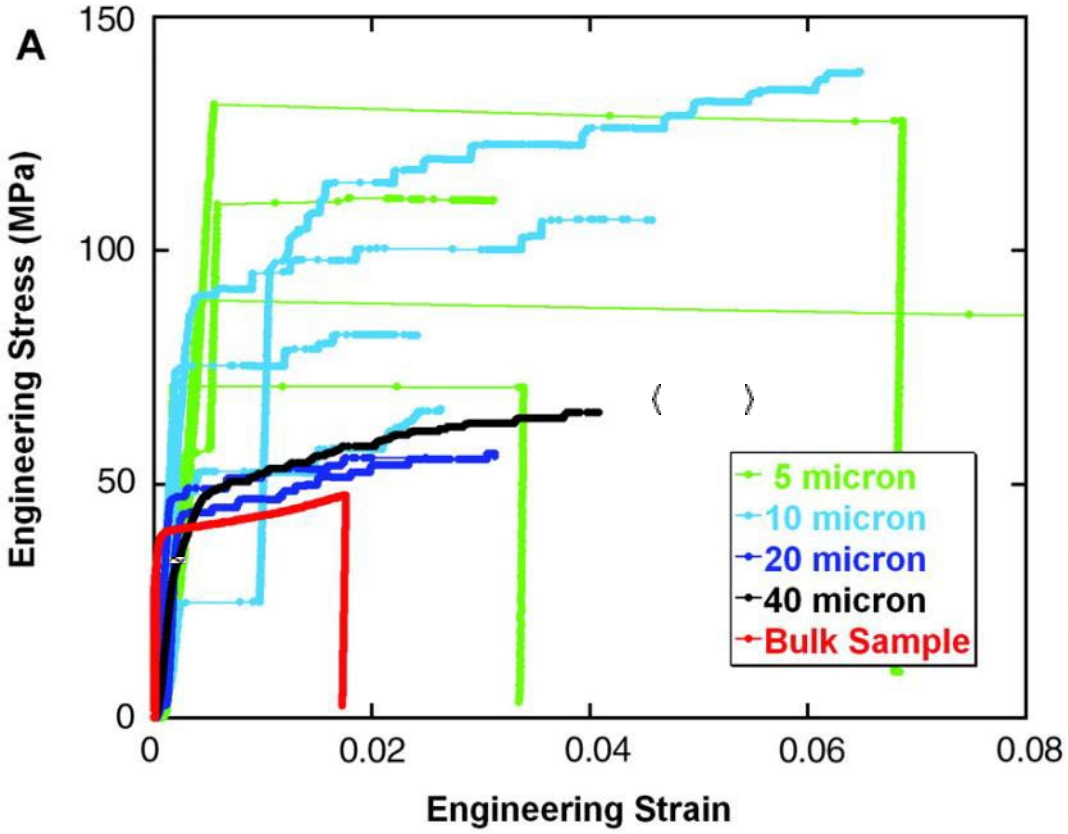

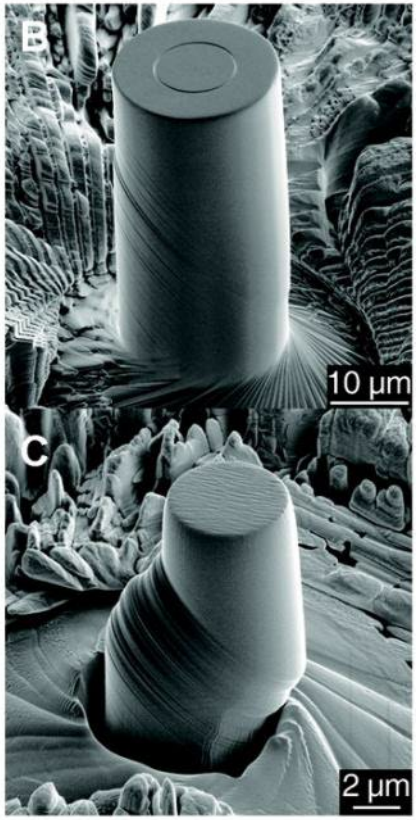

MD Uchic, DM Dimiduk, JN Florando, WD Nix (2004) Sample dimensions influence strength and crystal plasticity, SCIENCE 305, 986-989

Smaller is stronger

Smaller is stronger

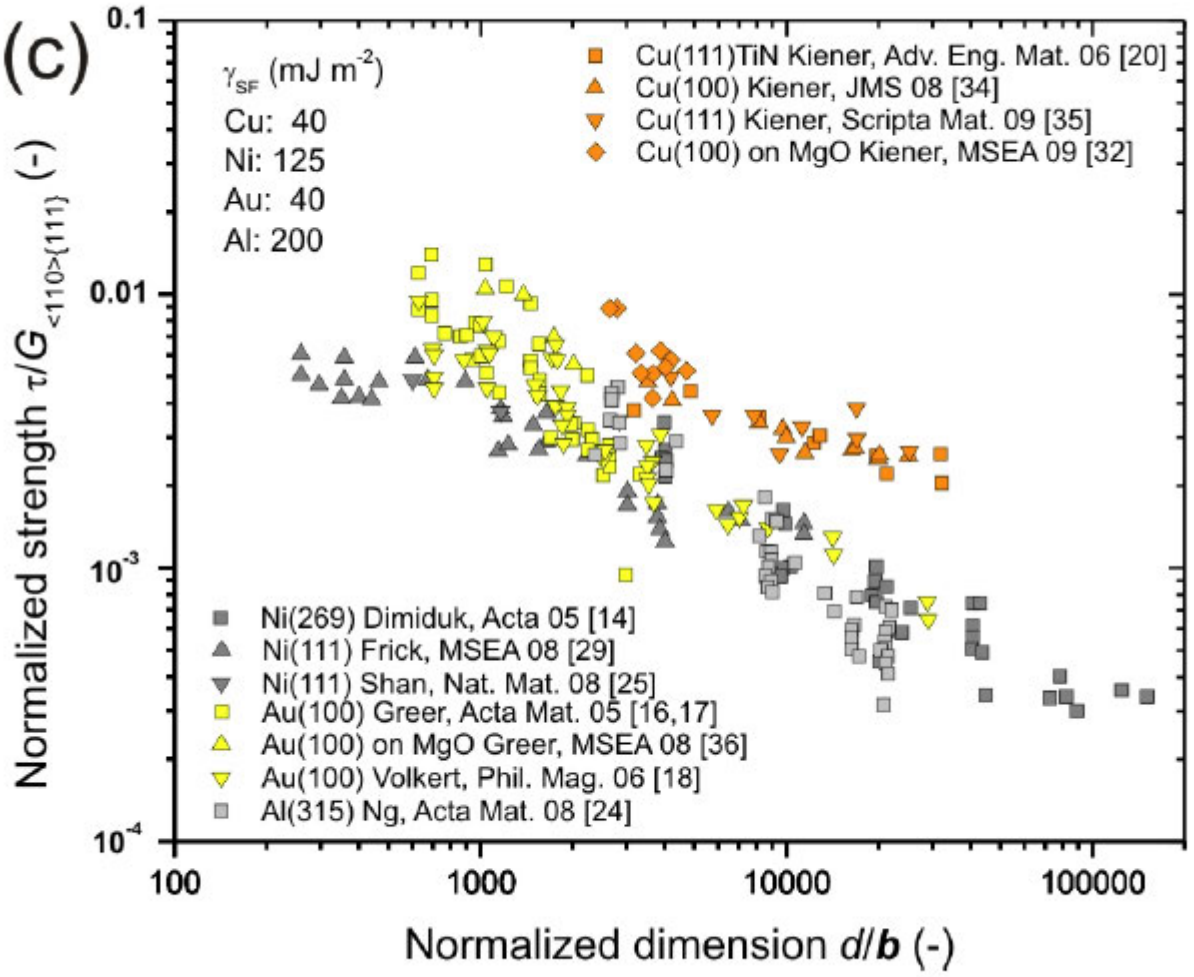

Kiener D, Motz C, Dehm G, Pippan R. Int. J. Mat. Res. 2009;100.

Micro compression tests

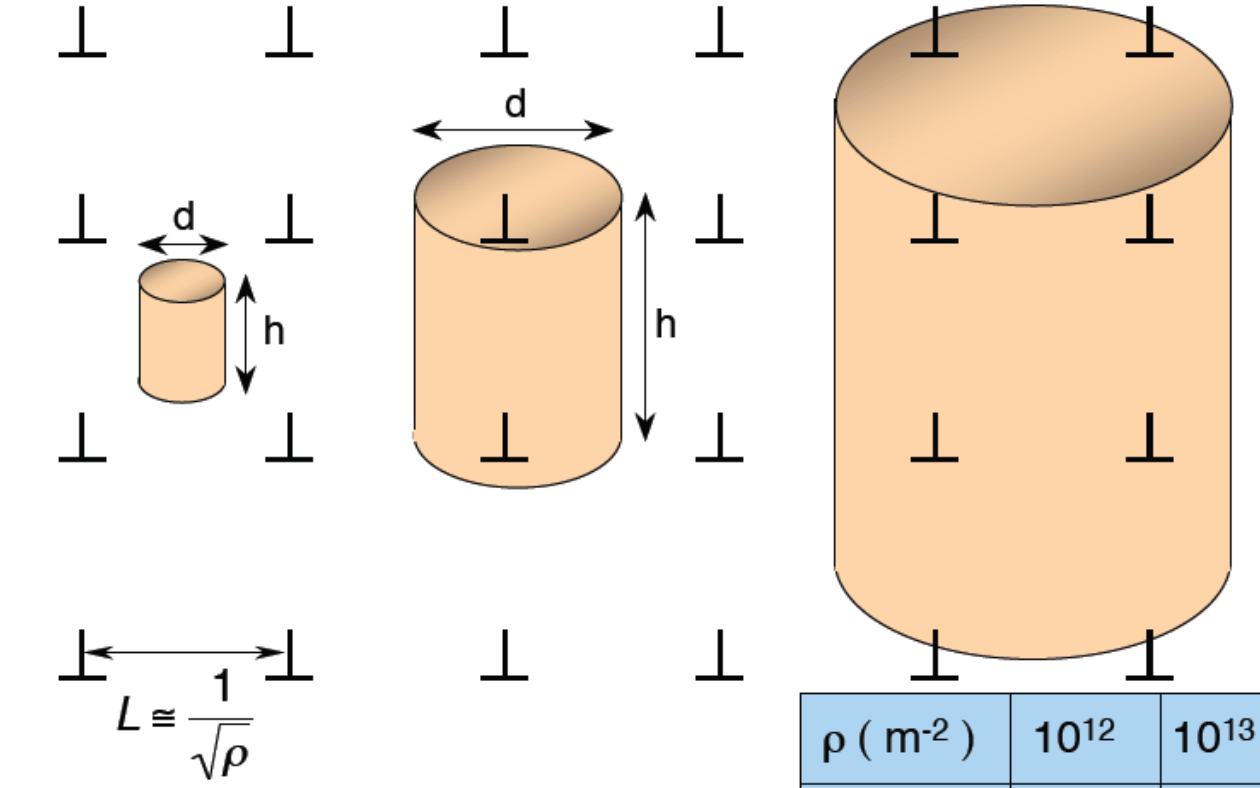

ρ (m^{-2})	10^{12}	10^{13}	10^{14}
L (μm)	1.0	0.3	0.1

Extrinsic influences of FIB milling on pillar strength

Kiener et al, *Mater. Sci. Eng. A* **459**, 262 (2007)

TEM of polycrystalline Cu

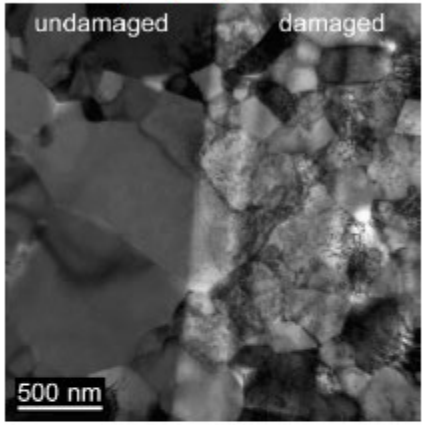

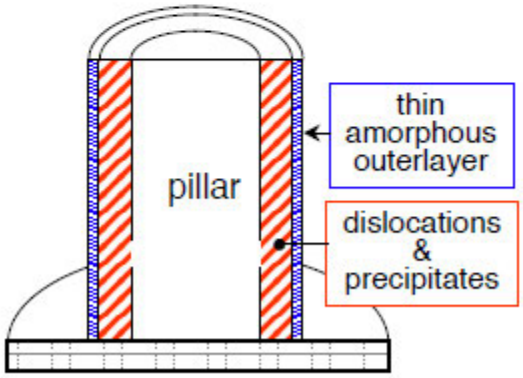

Important parameters

- beam incidence (normal/grazing)
- accelerating voltage (5-30 kV)
- current (10-2000 pA)

Strengthening mechanisms

- hard amorphous film formation
- dislocations
- precipitation

Conclusions

- FIB damage reduced at smaller accelerating voltages & grazing incidence
- even for grazing incidence, effects on strength may be significant for submicron pillars

20

Influence of lateral stiffness

Micro-compression of a Cu(100) sample with reduced lateral stiffness

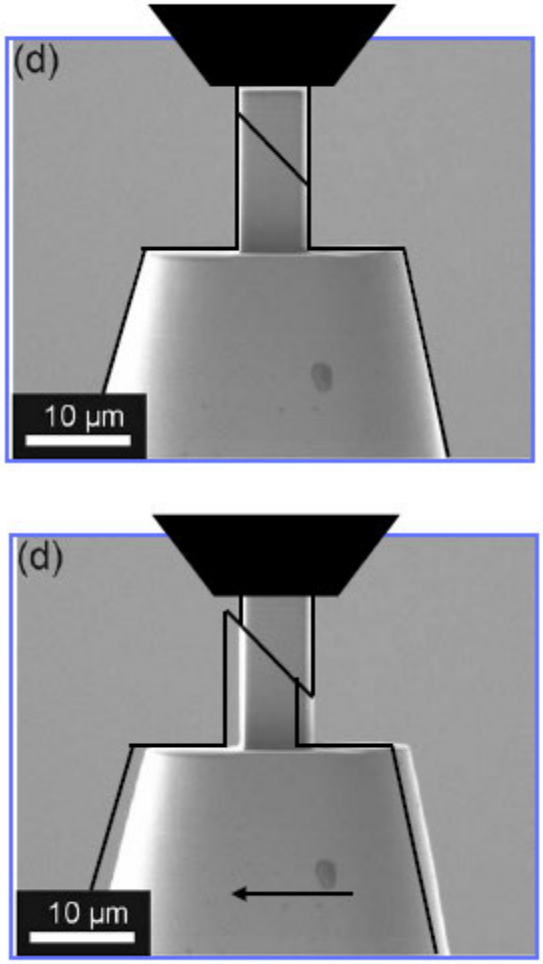

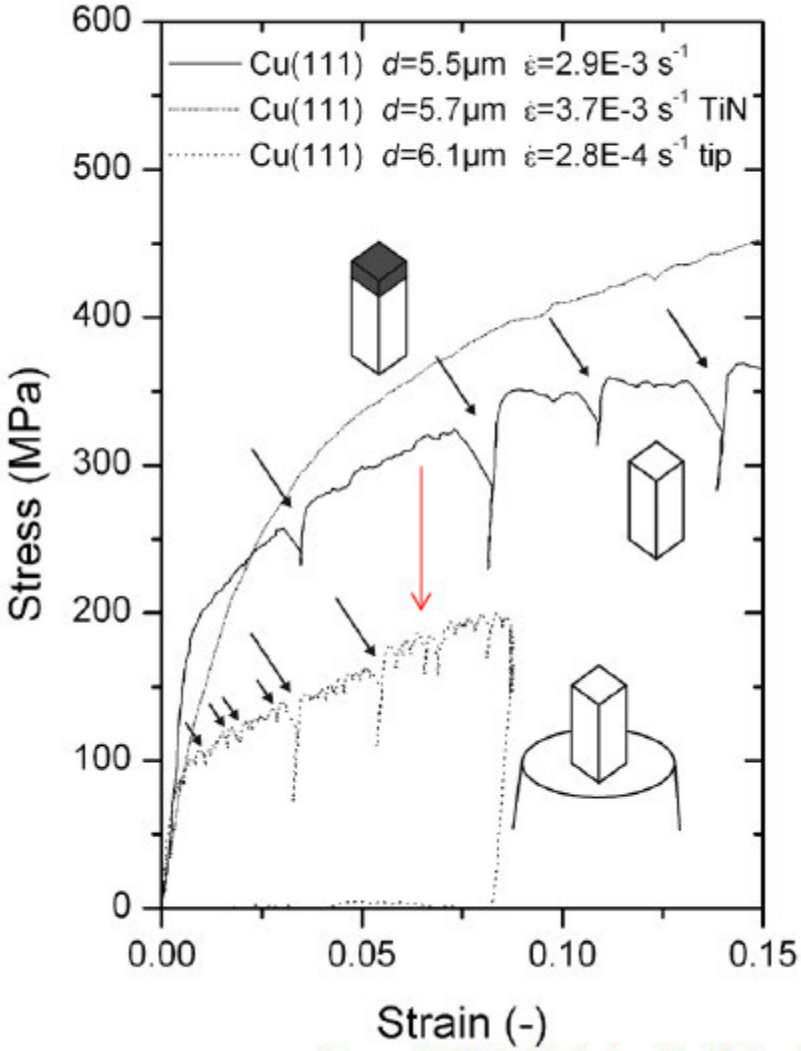

Kiener D, Motz C, Dehm G. Mater. Sci. Eng. A 2009;505:79.

the pain with the strain (-measurement)

Comparison of Modulus values from 200°C, 6.8µm diameter pillar with various corrections:

- Indenter frame compliance
- Pillar sink-in into substrate

$$\frac{D_{Sink-In}}{D_{Total}} = \left(1 + \frac{2}{\pi(1-\nu^2)}\left(\frac{h}{a_c}\right)\right)^{-1}$$

- Correction for fillet on pillar base

$$a_c = \eta\left(r_{pillar} + r_{fillet}\right)$$

- Correction for contact thermal drift

  (60 second, constant-load hold period at 1/20th of maximum load during unloading)

- Effective modulus correction using high temperature indenter modulus

$$E^* = \left(\frac{1-\nu_i^2}{E_i} + \frac{1-\nu_s^2}{E_s}\right)^{-1}$$

Values converge towards ideal single crystal [100] value. Micro-pillars are not an ideal geometry for Young's modulus measurements, but it is possible.

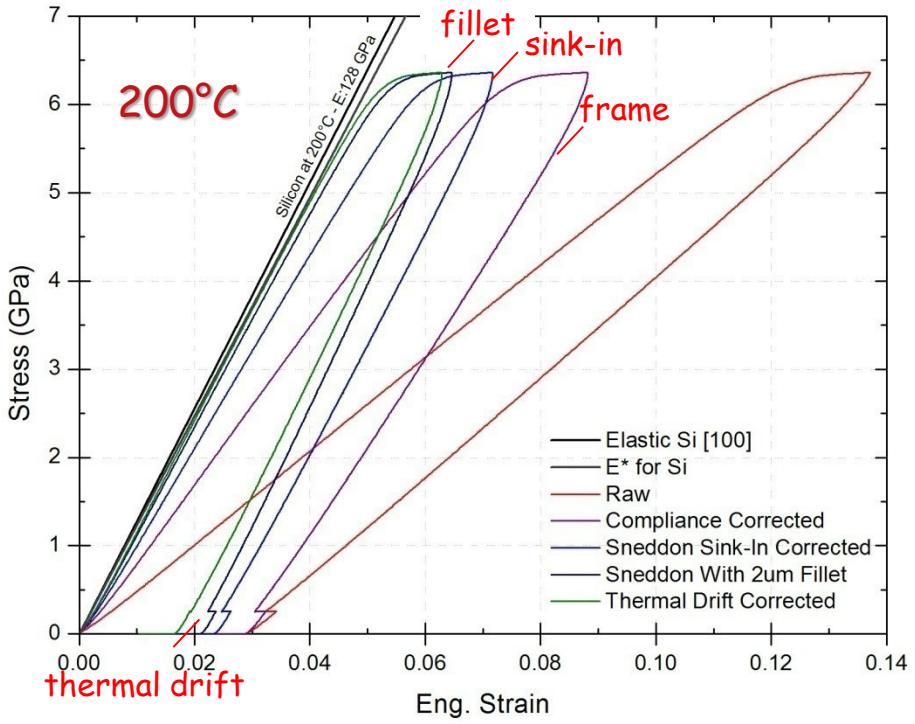

Alternative: Digital image correlation

"Flat Punch"-Model

Elastc-plastic contact cylinder on flat

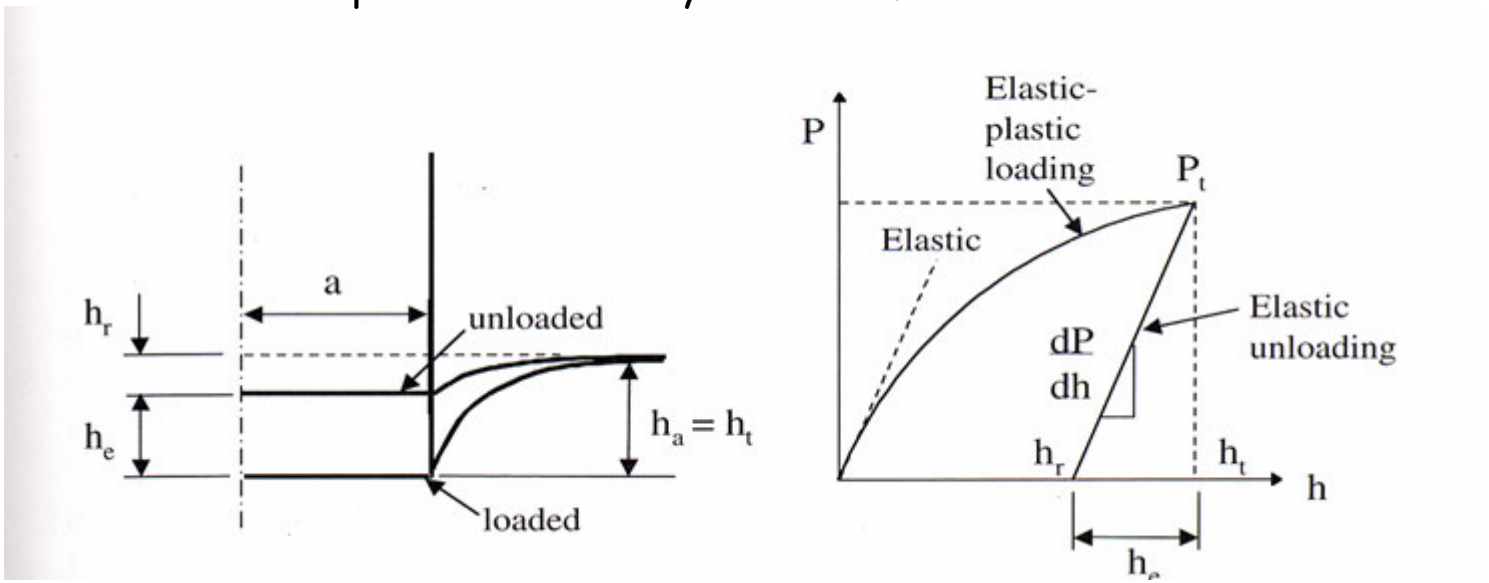

In elastic case:

$$\frac{dP}{dh} = 2aE_r = 2E_r \frac{\sqrt{A}}{\pi}$$

i.e. Young's modulus can be derived from slope of unloading curve:

$$E_r = \frac{dP}{dh} \frac{\pi}{2\sqrt{A}}$$

Example: microcompression of silicon <001>

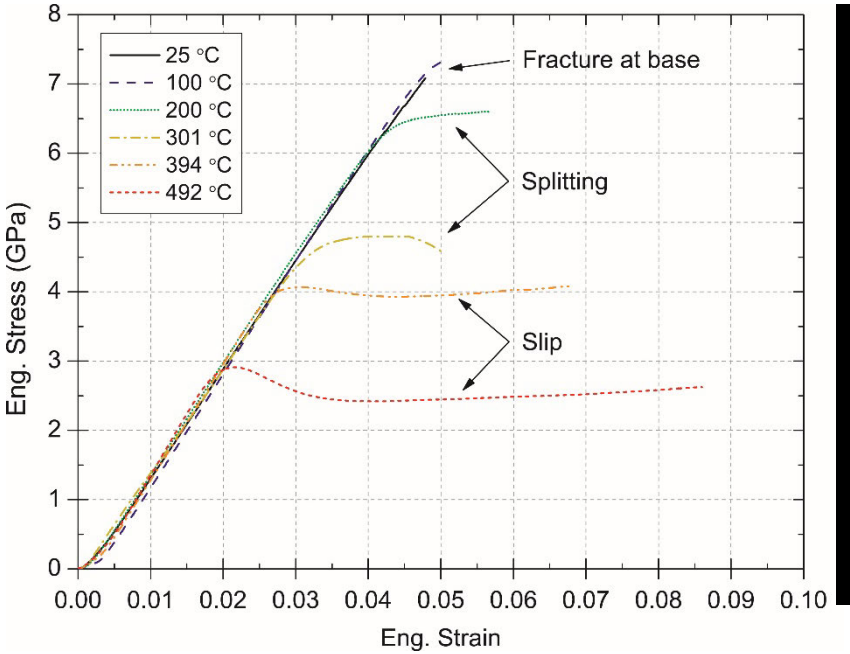

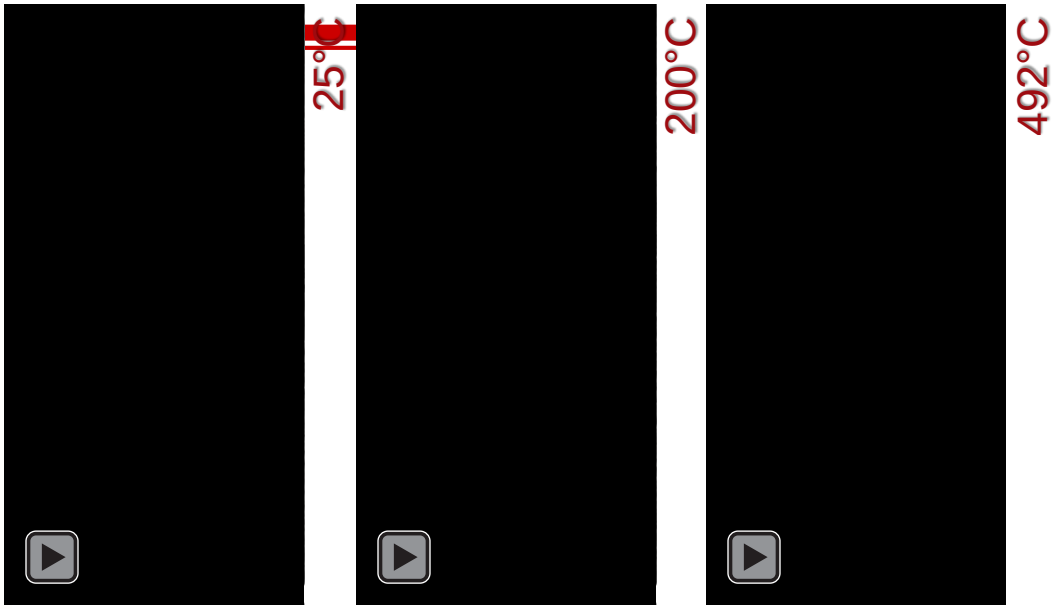

- Transitions between in deformation mechanisms between fracture, splitting, and plasticity directly observed.
- At a diameter of 6.7 μm, the brittle-ductile transition is seen at ~400°C – significantly lower than bulk silicon.
- Classic upper yield point consistent with dislocation nucleation observed during plastic deformation due to system's intrinsic displacement control.

EMPA

*J.M. Wheeler & J. Michler, *Rev Sci Instrum* (2013)

strain rate jump tests

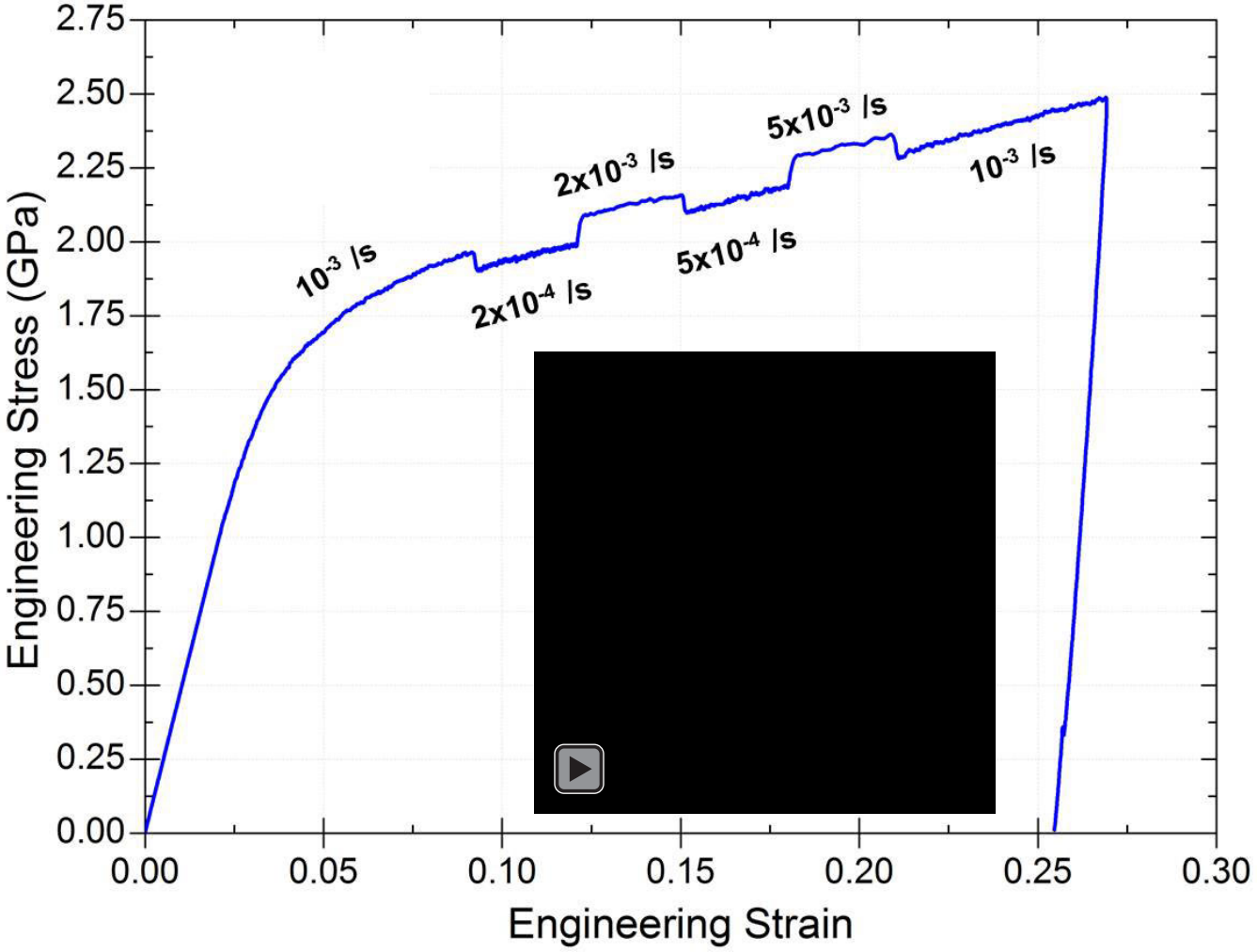

the strain rate sensitivity exponent

$$m = \frac{d(\ln \sigma_f)}{d(\ln \dot{\varepsilon})}$$

the activation volume

$$V = \frac{\sqrt{3} k_B T}{m \cdot \sigma_f}$$

strain rate jump tests are straightforward to perform using a displacement control.

strain rate sensitivity values are obtained by linear extrapolation to the elastic limit.

EMPA

Microscale fracture testing

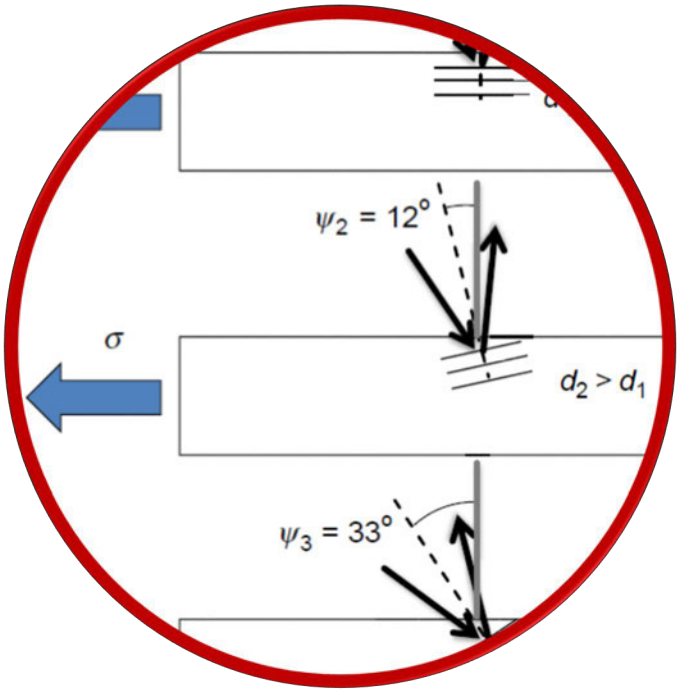

Why fracture mechanics?

Ideal

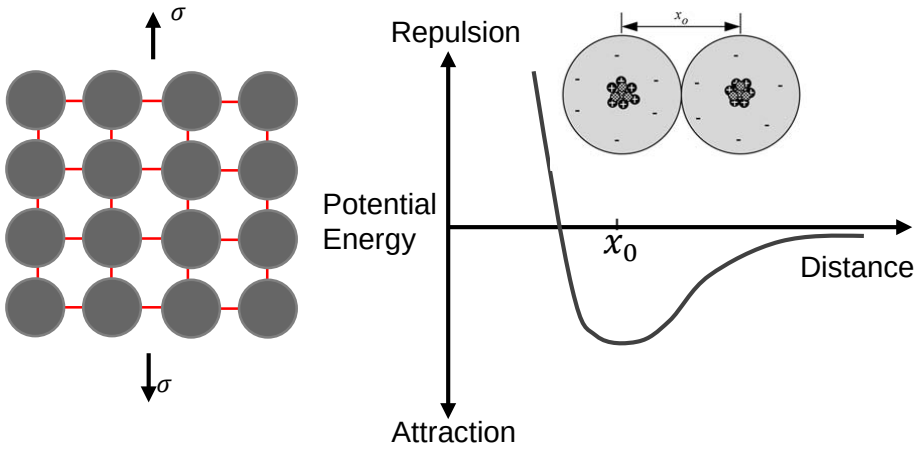

- Perfect material
- σ equal to cohesive stress σ_c to break bonds

Theoretical fracture stress:

$$\sigma_f = \sigma_c \approx \frac{E}{\pi}$$

Real

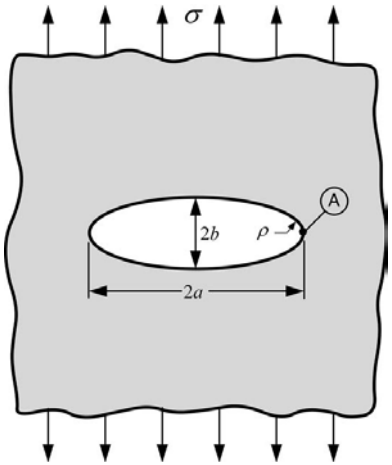

Sources of flaws:

Casting;
Particle decohesion;
Plastic deformation
…

- Material with flaw
- Stress concentration at flaws
- σ much smaller than σ_c

Fracture stress with a flaw:

$$\sigma_f \approx \sigma_c \cdot \sqrt{\frac{x_0}{4a}}$$

$\sim 10^{-10}m$

$\sim 10^{-6}m$

$\sim 0.01\sigma_c$

Study the material resistance to preexisting crack propagation

Anderson, Ted L. Fracture mechanics: fundamentals and applications. CRC press, 2017.

Two ways to understand fracture toughness

- Energy balance: *G*

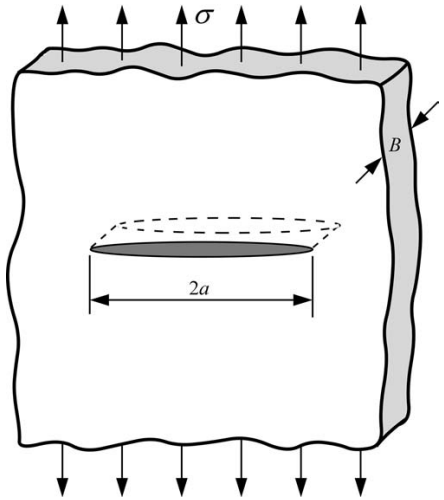

Crack can only grow when this process causes the total energy to decrease or remain constant.

Unit: J/m^2

$$-\frac{d\Pi}{dA} \geq 2\gamma_s$$

$$-\frac{d\Pi}{dA} = G$$

energy release rate;

$G_c \geq 2\gamma_s$

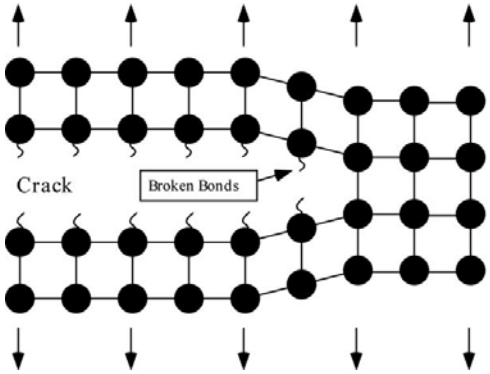

Griffith's theory
*Ideal elastic brittle material

$$G_c = 2\gamma_s$$

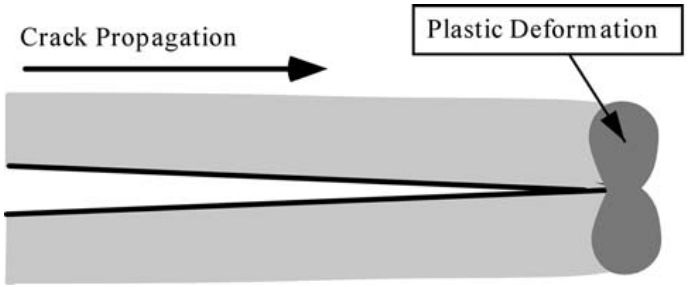

Irwin and Orowan theory
*Metals with plastic zone

$$G_c = 2(\gamma_s + \gamma_\rho)$$

Anderson, Ted L. Fracture mechanics: fundamentals and applications. CRC press, 2017.

Two ways to understand fracture toughness

- Stress distribution: *K* & *J*

Linear elastic material:

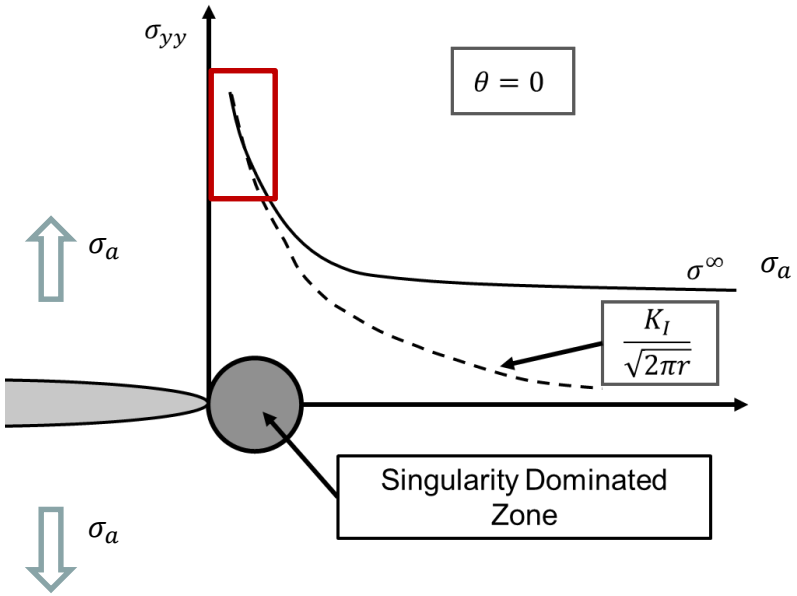

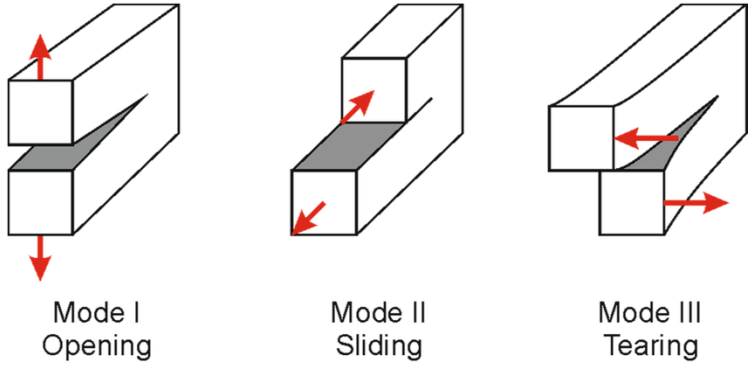

Elastic Plastic Material:

$$\sigma_{ij}(r,\theta) = c\left(\frac{J}{r}\right)^{\frac{1}{1+n}} s_{ij}(\theta)$$

$$\sigma_{ij}(r,\theta) = \frac{K_{I,II,III}}{\sqrt{2\pi r}} f_{ij}(\theta)$$

$$J_{pl} = \frac{\eta A_{pl}}{B b_0}$$

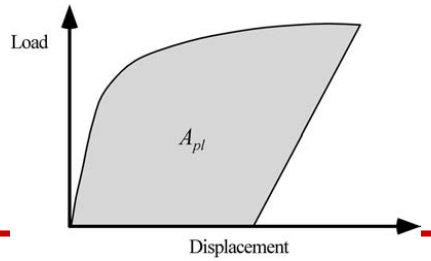

$K_{I,II,III}$: stress intensity factor Unit: $\mathrm{MPa}.m^{0.5}$ Unit: J/m^2

Anderson, Ted L. Fracture mechanics: fundamentals and applications. CRC press, 2017.

Two ways to understand fracture toughness

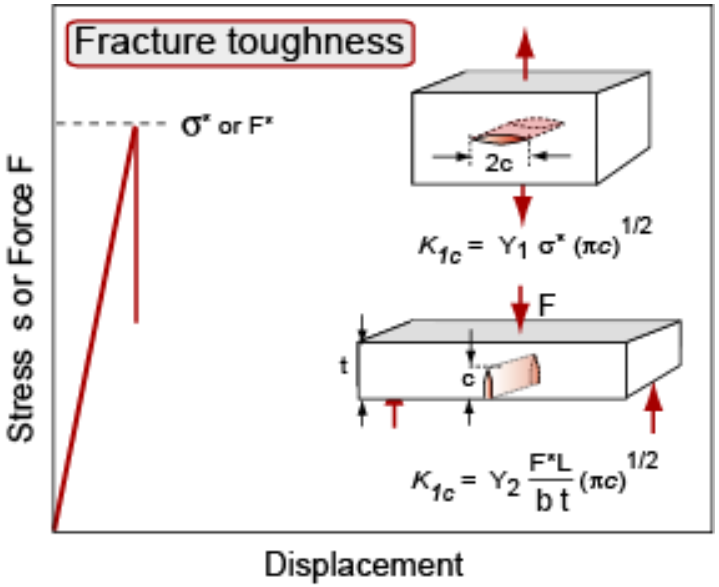

Definition:

Fracture toughness $K_{1c} = Y_1 \sigma^* \sqrt{\pi c}$

Fracture energy or toughness $G = \frac{K_c^2}{E}$

Plane stress: $E' = E;$

Plane strain: $E' = \frac{E}{1 - \nu^2}$

Range of fracture toughness:

0.3 MPa $m^{1/2}$ (glass) to 200 MPa $m^{1/2}$ GPa (steel)

Anderson, Ted L. Fracture mechanics: fundamentals and applications. CRC press, 2017.

Why microscale fracture testing?

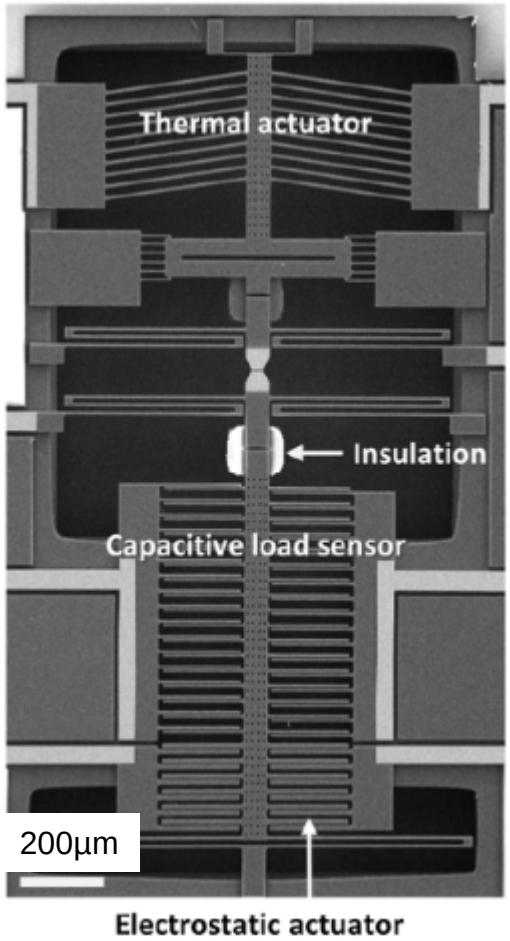

MEMS actuator/sensor

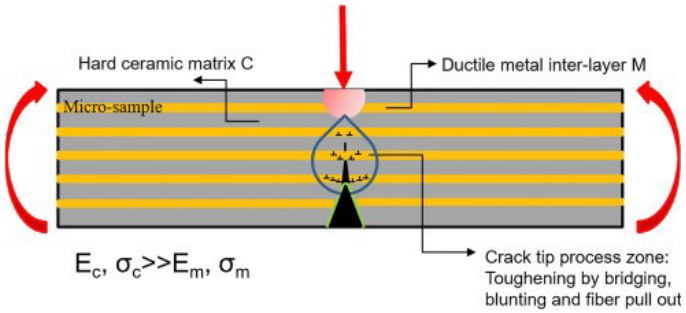

Thin film coating

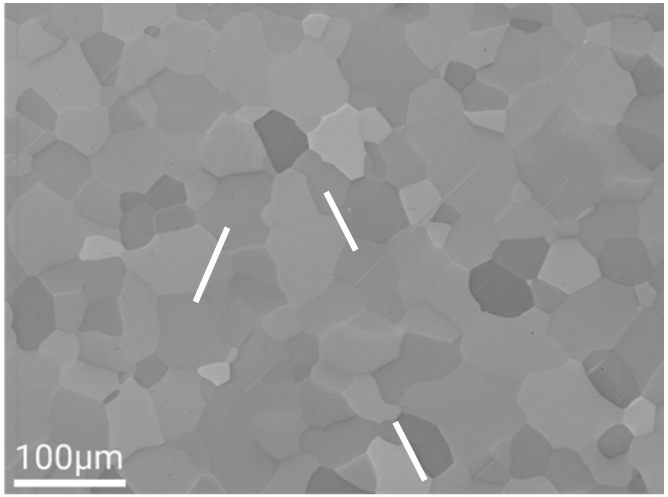

Interface/boundary brittleness

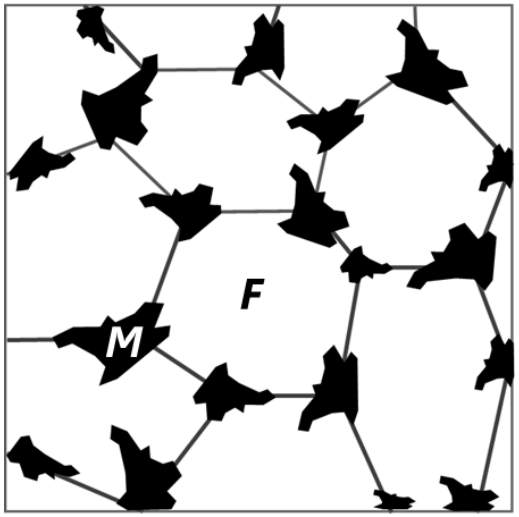

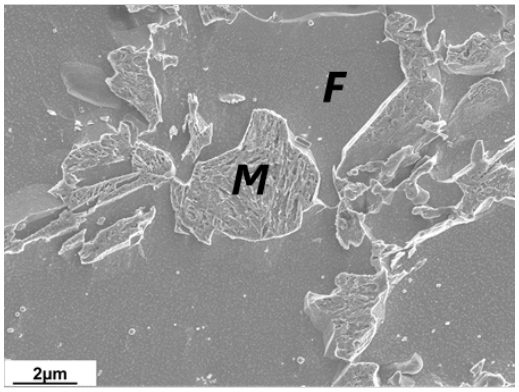

Damage sensitive phase

Pantano, et al., Meccanica, 2015.

Dehm et al. Acta Materialia (2017)